Probing the electroweak sector of the $\mu\nu$SSM at the LHC

Memoria de Tesis Doctoral realizada por

Iñaki Lara Pérez

presentada ante el Departamento de Física Teórica
de la Universidad Autónoma de Madrid
para optar al título de Doctor en Física Teórica.

Tesis dirigida por el **Prof. Carlos Muñoz López**

Instituto de Física Teórica
UAM-CSIC

Cincuenta Aniversario
UAM Universidad Autónoma de Madrid

Departamento de Física Teórica
Universidad Autónoma de Madrid
Instituto de Física Teórica UAM-CSIC

November 2, 2018

This thesis is based on the following scientific articles:

1 P. Ghosh, I. Lara, D. E. López-Fogliani, C. Muñoz, and R. Ruiz de Austri, "Searching for left sneutrino LSP at the LHC,"*Int. J. Mod. Phys.* **A33** no. 18n19, (2018) 1850110, arXiv:1707.02471 [hep-ph]

2 I. Lara, D. E. López-Fogliani, C. Muñoz, *et al.*, "Looking for the left sneutrino LSP with displaced-vertex searches,"*Phys. ReV.* D98 no. 7, (2018) 075004 arXiv:1804.00067 [hep-ph]

3 I. Lara, D. E. López-Fogliani, C. Muñoz, "Electroweak superpartners scrutinized at the LHC in events with multi-leptons," *To be published in Phys. Lett. B*, arXiv:1810.12455 [hep-ph]

A Ana, la persona más importante de mi vida.
A Asier, Javi y Gemma, por ellos he llegado hasta aqui.

Agradecimientos

Escribir esta tesis han sido 4 años de enorme esferzo y trabajo. Durante este tiempo ha habido momentos en los que todo parecía ir cuesta abajo, pero tambien los más en los que todo parecia a punto del desastre. Quiero pararme aqui a agradecer a todas las personas que me han acompañado en este proceso, y sin los cuales esto habría sido imposible.

En primer lugar al Prof. Carlos Muñoz. Sin conocerme me dió la oportunidad de entrar en este mundo. Sus amplios conocimientos de física y su atención a los detalles han sido una gran guía para mi. Quiero agradecer también sus consejos más allá de la física, que me han enseñado cómo funciona este mundillo. En último lugar, quiero agradecer la oportunidad que he tenido de experimentar la docencia a su lado, la cual me ha resultado profundamente gratificante.

Durante estos años he tenido la oportunidad de trabajar con grandes científicos. Es dificil condensar todo lo que he aprendido del Dr. Pradipta Ghosh, nunca habría aprovechado mi primer año tanto sin todo lo que él me ha enseñado. Gracias al Dr. Daniel López-Fogliani, sin el todo este proyecto habría sido imposible. Quiero agradecer también al Dr. Roberto Ruiz de Austri, al Dr. Hidetoshi Otono y al Dr. Natsumi Nagata, por todo lo que he aprendido de ellos. Quiero agradecer en especial la hospitalidad del Dr. Natsumi Nagata, del Prof. Hamaguchi Koichi, del Prof. Takeo Moroi y del resto del grupo de Altas Energías de la Universidad de Tokio. Me acogieron como uno más los meses que estuve de visita allí.

No quiero dejar de mencionar a mis compañeros del Insituto de Física Teórica, a todos ellos les deseo que tengan tanta suerte como yo. A Thomas Biekötter, Jorge Fernández y Raoul Letschka por todas las discusiones cientícias en el despacho, y tambien por las no científicas, no habría aprendido tanto sin vosotros. A Donald Kpatcha, compañeros de camino desde el primer día. Quiero agradecer tambien a Franco Albareti el tiempo compartido preparando las clases, ha sido un placer compartir la docencia contigo.

A Diego, Elias y Adrián, los años que hemos vivido juntos convertisteis nuestra casa en un oasis donde siempre recobraba fuerzas. A mis padres Javi y Gemma, y a mi hermano Asier, ellos siempre han creido en mi y me han apoyado. Cuando más lejos me he sentido del la meta más fuerte me han animado.

Y por encima de todo a Ana. Porque ha estado a mi lado cada segundo, apoyandome, dándome fuerzas y escuchándome, y cuando lo necesitaba prohibiendome hablar de física. Porque ha sido la mejor compañera que jamás podría tener. En resumen, por todo.

Contents

Resumen

El descubrimiento del boson de Higgs en El Gran Colisionador de Hadrones (LHC) constituye la confirmación de la existencia de la ultima pieza del Modelo Estándar de la física de partículas. Sin embargo, existen aun problemas importantes que dicho marco teórico no pude responder, tales como el origen de la masa de los neutrinos, la naturaleza de la materia oscura, el origen de la asimetría bariónica del universo o el problema CP de las interacciones fuertes. Han aparecido diversas propuestas en las últimas décadas para responder a estas preguntas, con la característica común de que todas estas extensiones a energías más allá del Modelo Estándar deben mostrarse de algún modo a energías no mucho mas elevadas que la Escala Electrodébil. Esto constituye una invitación a explorar experimentalmente la física a energías del orden del Teraelectrónvoltio (TeV). El número de posibilidades para extender el Modelo Estándar es enorme, con cada caso motivado por diferentes ideas teóricas o diferentes indicios experimentales.

El plan de investigación experimental a energías por encima de la Escala Electrodébil para las próximas décadas utiliza el aprovechamiento exhaustivo de las posibilidades del LHC, incluyendo la fase de Alta Luminosidad (HL), y la incorporación de nuevos detectores centrados en señales específicas, difíciles de medir con los experimentos actuales, tal como las búsquedas de partículas con vida media larga. Así mismo, hay planes para construir el Colisionador Lineal Internacional (ILC) en Japón, un colisionador de electrones-positrones con energías de 500 GeV. Por lo tanto, en la actualidad y en el futuro próximo, las posibilidades de probar cualquier teoría más allá del Modelo Estándar en términos de su efecto sobre la fenomenología de partículas están restringidas a experimentos alrededor del TeV de energía. Afortunadamente esto es suficiente para analizar gran cantidad de modelos capaces de resolver algunos de los problemas del Modelo Estándar y a la vez producir señales en los aceleradores, tanto directas como indirectas. Por ello es crucial hacer un análisis detallado de cada modelo, que permita diseñar los experimentos para tener una cobertura óptima y a la vez tenga la capacidad de diferenciar entre distintos modelos.

La supersimetría a la escala del TeV ha sido quizás la teoría más aceptada en las últimas décadas para extender el Modelo Estándar a la escala Electrodébil. Las extensiones supersimétricas del Modelo Estándar resultan útiles resolviendo el denominado *problema de las jerarquías* y proporcionando un buen candidato a materia oscura. Las teorías supersimétricas tienen además propiedades interesantes como la unificación de las interacciones gauge tras incluir su efecto en las ecuaciones del grupo de renormalización.

La supersimetría predice la existencia de una partícula nueva asociada a cada una de las del Modelo Estándar con los mismos número cuánticos, exceptuando el espín. Por lo tanto predice la existencia de un compañero escalar por cada fermión y un compañero fermiónico por cada bosón. Además hay buenas razones para predecir la masa de estas partículas alrededor de la escala del TeV. De este modo, la supersimetría predice la existencia de un gran número de partículas que estarían dentro del rango de energías accesible para el LHC o la siguiente generación de aceleradores.

A lo largo de la presente tesis se discuten los aspectos fenomenológicos del modelo supersimétrico denominado $\mu\nu$SSM relevantes para el LHC. Además de las propiedades atractivas de los modelos supersimétricos, el $\mu\nu$SSM permite solucionar el denominado problema μ del *Minimal Superymmetric Standard Model* (MSSM) y explicar al mismo tiempo el origen de la masa de los neutrinos. Dentro de este modelo, el gravitino es un buen candidato a materia oscura.

En extensiones supersimétricas del Modelo Estándar, el número bariónico ya no es una simetría accidental y ha de ser obtenida imponiendo algún tipo de simetría discreta. De otro modo los modelos predirían una vida media para el protón inaceptablemente baja. Generalmente este rol lo juega la simetría discreta denominada R-paridad, que fuerza a cada partícula supersimétrica a ser producida a pares. La consecuencia directa de esta simetría es que la partícula supersimétrica más ligera (LSP) será estable. En ese caso existen fuertes límites cosmológicos a las propiedades que ha de tener dicha partícula, que por otro lado la convierten en un candidato a materia oscura ideal. En los aceleradores, la familia de modelos supersimétricos que respetan la R-paridad predice la producción de eventos con una gran cantidad de momento transversal desaparecido (MET).

En su lugar, el $\mu\nu$SSM incluye términos en el lagrangiano que no permiten asignar de forma consistente cargas bajo R-paridad a todas las partículas y por lo tanto esta simetría está explícitamente rota. Dado que las partículas supersimétricas pueden decaer a partículas del Modelo Estándar, la fenomenología del modelo es más rica y debe ser estudiada detalladamente. Aunque existen otros modelos que rompen R-paridad, la estructura del $\mu\nu$SSM es compleja y da lugar a señales únicas.

El objetivo de ésta tesis es llevar a cabo un estudio de las posible señales a las que podría dar lugar el $\mu\nu$SSM en el LHC . En concreto nos enfocamos en el sector electrodébil del modelo, el cual en principio puede ser comprobado con una cierta facilidad en un acelerador de hadrones, de forma que identificamos las señales que pueden aparecer en la producción de los supercompañeros electrodébiles en el LHC. El texto está organizado como se explica a continuación: El capitulo 1 es una breve introducción a la supersimetría, presentando las características mas importantes del marco teórico y presentando los modelos más populares, con sus limitaciones. En el capítulo 2 introducimos el modelo $\mu\nu$SSM, describiendo sus características mas importantes y resumiendo los análisis fenomenológicos previos. El capítulo 3 está dedicado al análisis pormenorizado de las características fenomenológicas más importantes del *left sneutrino*, cuando ésta es la partícula supersimétrica más ligera. Allí mostramos las posibles señales a las que podría dar lugar en el LHC, cuando la desintegración es inmediata. En el capítulo 4 hacemos uso de una serie de puntos representativos del espacio de parámetros del *left-sneutrino*, que pueden producir señales detectables en el LHC. En capítulo 5 se usan las búsquedas de ATLAS de partículas con una vida media larga para poner límites al espacio de parámetros del modelo cuando el *left-sneutrino* es la partícula supersimétrica más ligera y decae a una distancia significativa del punto de interacción primaria, produciendo vértices desplazados. En el capítulo 6 se utilizan las búsquedas de ATLAS de partículas supersimétricas Electrodebiles en espectros comprimidos para poner límites a la masa del *left-sneutrino*, cuando la partícula más ligera es un neutralino tipo bino y el sneutrino es la partícula siguiente. Adicionalmente, en este capítulo explicamos que el proceso descrito es compatible con un exceso local presentado recientemente por la colaboración ATLAS.

El capítulo 7 concluye la tesis resumiendo los principales resultados y perfilando los proyectos futuros que se abren.

Summary

The discovery of the Higgs boson at the Large Hadron Collider (LHC) constitutes the confirmation of the existence of the last building block of the Standard Model (SM) of particle physics. However, there are still important questions unanswered by this theoretical framework, such as for example the origin of neutrino masses, the nature of dark matter, the origin of the baryon asymmetry of the Universe or the strong CP problem. Many proposals have appeared in the last decades to address some of these questions, with the general feature that the extensions Beyond the Standard Model (BSM) should somehow manifest at energy scales no too far from the Electroweak Scale (EW). This constitutes an invitation to explore experimentally the physics at the TeV scale. Nevertheless, the range of possibilities to extend the standard model is huge, each of them motivated by different theoretical paradigms or experimental hints.

The experimental road-map at energies above the EW scale for the next decades consists of the exploitation of the full capabilities of the LHC, including the High Luminosity (HL) phase, and the addition of new detectors focused on specific signals hard to measure by the actual experiments, such as very long-lived particles. Also there are plans to build the International Linear Collider (ILC) in Japan, an electron-positron collider with energies of 500 GeV. Therefore, in the present and in the nearest future, the possibilities to test any BSM theory in terms of its influence on particle phenomenology are constrained to collider experiments around few TeV scale. Nevertheless, this is enough to reach a plethora of models capable of solving problems of the SM and leave a signal in collider experiments, both direct and indirect. Thus each model deserves a detailed analysis of the expected phenomenology, in order to be able to design efficient searches covering the most of the models and to differentiate between them in the case that a signal is finally detected.

TeV scale supersymmetry (SUSY) has been perhaps the most popular choice in the past decades to extend the SM at the EW scale. Supersymmetric extensions of the SM have proven themselves very useful solving the hierarchy problem and providing also a Dark Matter (DM) candidate. SUSY theories are in addition quite appealing since they make the gauge couplings become unified at some high energy scale after the inclusion of the effects of SUSY on the renormalization group equations.

SUSY predicts the existence of a new particle for each one in the Standard Model, with the same quantum numbers excepting the spin. Thus it predicts a scalar partner for each fermion, and a fermionic partner for each boson, and the masses of these particles are highly motivated to be around the TeV scale. Consequently, it predicts a large number of new particles that could be within the experimental reach of the LHC or the next generation of colliders.

In this thesis we discuss the phenomenological aspects of a SUSY model, the so-called called $\mu\nu$SSM, at the LHC. Besides the good common properties of the SUSY models, the $\mu\nu$SSM can provide a solution of the μ-problem of the Minimal Supersymmetric Standard Model (MSSM) and simultaneously explain the origin of the measured properties of

neutrinos. In addition, the Gravitino in the $\mu\nu$SSM is a good DM candidate also.

In the SUSY extensions of the SM the baryon number is no longer an accidental symmetry and should be achieved imposing a discrete symmetry to prevent fast decay of the proton. This role is usually played by *R-parity* conservation (RPC), which forces each superpartner to be pair produced. The direct consequence of this is that the *lightest supersymmetric particle* (LSP) would be stable. There exist cosmological constraints which bound this particle to be neutral, and play the role of the dark matter. At colliders, this family of models would produce events with neutral stable particles which manifest themselves as events with large missing transverse momentum (MET).

Instead, the $\mu\nu$SSM includes terms in the Lagrangian which do not allow for a proper assignment of *R-parity* charges and thus this symmetry is explicitly *violated* ($\not{R}_p$). Since the superpartners can decay to SM particles, the expected phenomenology is richer and should be carefully studied. Altough there exist other $\not{R}_p$ models, the structure of the $\mu\nu$SSM is complex and leads to unique signals.

The objective of this thesis is to make an exhaustive exploration of interesting signals within the $\mu\nu$SSM framework. In particular, we focus on the electroweak sector of the model, which in principle can be explored with a certain ease in a hadron collider, and identify the signatures that can appear in the production of electroweak superpartners at the LHC. The text is organized as follows. Chapter 1 is a brief introduction to SUSY, discussing the most important characteristics of the theoretical framework and presenting the most popular models, with its limitations. In chapter 2, we introduce the $\mu\nu$SSM, describing its most important features and summarizing the previous phenomenological studies. Chapter 3 is devoted to an analysis of the most important phenomenological aspects of the left-handed neutrino superpartner, the left sneutrino, when it is the LSP. There we show the possible signals that can be generated at colliders when producing this particle. In chapter 4, we choose a selection of benchmark points representative of the left sneutrino phenomenology, that can produce detectable prompt signals at the LHC. In chapter 5, we use some of the current ATLAS searches for long lived particles to constrain the parameter space of the model, when the left sneutrino is the LSP and decays at significant distance of the interaction point, producing displaced vertices. In chapter 6, we utilize the ATLAS searches for electroweak production of SUSY particles in compressed scenarios, to obtain limits on the sneutrino mass, when the LSP is a bino-like neutralino and the sneutrino is the NLSP. In addition, we explain that the process described is compatible with the local excess of three leptons recently reported by the ATLAS collaboration. Chapter 7 concludes the thesis summarizing the main results and outlining the future prospects of research.

Chapter 1

Introduction

The discovery of the Higgs boson at the Large Hadron Collider (LHC) [1, 2] constitutes the confirmation of the existence of the last building block of the Standard Model (SM) of particle physics. However, there are still important questions unanswered by this theoretical framework, such as for example the origin of neutrino masses, the nature of dark matter, the origin of the baryon asymmetry of the Universe or the strong CP problem. Many proposals have appeared in the last decades to address some of these questions, with the general feature that the extensions Beyond the Standard Model (BSM) should somehow manifest at energy scales no too far from the Electroweak Scale (EW). This constitutes an invitation to explore experimentally the physics at the TeV scale. Nevertheless, the range of possibilities to extend the standard model is huge, each of them motivated by different theoretical paradigms or experimental hints.

The experimental road-map at energies above the EW scale for the next decades consists of the exploitation of the full capabilities of the LHC, including the High Luminosity (HL) phase, and the addition of new detectors focused on specific signals hard to measure by the actual experiments, such as very long-lived particles. Also there are plans to build the International Linear Collider (ILC) in Japan, an electron-positron collider with energies of 500 GeV. Therefore, in the present and in the nearest future, the possibilities to test any BSM theory in terms of its influence on particle phenomenology are constrained to collider experiments around few TeV scale. Nevertheless, this is enough to reach a plethora of models capable of solving problems of the SM and leave a signal in collider experiments, both direct and indirect. Thus each model deserves a detailed analysis of the expected phenomenology, in order to be able to design efficient searches covering the most of the models and to differentiate between them in the case that a signal is finally detected.

TeV scale supersymmetry (SUSY) has been perhaps the most popular choice in the past decades to extend the SM at the EW scale. Supersymmetric extensions of the SM have proven themselves very useful solving the hierarchy problem and providing also a Dark Matter (DM) candidate. SUSY theories are in addition quite appealing since they make the gauge couplings become unified at some high energy scale after the inclusion of the effects of SUSY on the renormalization group equations.

SUSY predicts the existence of a new particle for each one in the Standard Model, with the same quantum numbers excepting the spin. Thus it predicts a scalar partner for each fermion, and a fermionic partner for each boson, and the masses of these particles are highly motivated to be around the TeV scale. Consequently, it predicts a large number of new particles that could be within the experimental reach of the LHC or the next generation of colliders.

In this thesis we discuss the phenomenological aspects of a SUSY model, the so-called

called $\mu\nu$SSM, at the LHC. Besides the good common properties of the SUSY models, the $\mu\nu$SSM can provide a solution of the μ-problem of the Minimal Supersymmetric Standard Model (MSSM) and simultaneously explain the origin of the measured properties of neutrinos. In addition, the Gravitino in the $\mu\nu$SSM is a good DM candidate also.

In the SUSY extensions of the SM the baryon number is no longer an accidental symmetry and should be achieved imposing a discrete symmetry to prevent fast decay of the proton. This role is usually played by *R-parity* conservation (RPC), which forces each superpartner to be pair produced. The direct consequence of this is that the *lightest supersymmetric particle* (LSP) would be stable. There exist cosmological constraints which bound this particle to be neutral, and play the role of the dark matter. At colliders, this family of models would produce events with neutral stable particles which manifest themselves as events with large missing transverse momentum (MET).

Instead, the $\mu\nu$SSM includes terms in the Lagrangian which do not allow for a proper assignment of *R-parity* charges and thus this symmetry is explicitly *violated* ($\not{R}_p$). Since the superpartners can decay to SM particles, the expected phenomenology is richer and should be carefully studied. Altough there exist other $\not{R}_p$ models, the structure of the $\mu\nu$SSM is complex and leads to unique signals.

The objective of this thesis is to make an exhaustive exploration of interesting signals within the $\mu\nu$SSM framework. In particular, we focus on the electroweak sector of the model, which in principle can be explored with a certain ease in a hadron collider, and identify the signatures that can appear in the production of electroweak superpartners at the LHC. The text is organized as follows. Chapter 2 is a brief introduction to SUSY, discussing the most important characteristics of the theoretical framework and presenting the most popular models, with its limitations. In chapter 3, we introduce the $\mu\nu$SSM, describing its most important features and summarizing the previous phenomenological studies. Chapter 4 is devoted to an analysis of the most important phenomenological aspects of the left-handed neutrino superpartner, the left sneutrino, when it is the LSP. There we show the possible signals that can be generated at colliders when producing this particle. In chapter 5, we choose a selection of benchmark points representative of the left sneutrino phenomenology, that can produce detectable prompt signals at the LHC. In chapter 6, we use some of the current ATLAS searches for long lived particles to constrain the parameter space of the model, when the left sneutrino is the LSP and decays at significant distance of the interaction point, producing displaced vertices. In chapter 7, we utilize the ATLAS searches for electroweak production of SUSY particles in compressed scenarios, to obtain limits on the sneutrino mass, when the LSP is a bino-like neutralino and the sneutrino is the NLSP. In addition, we explain that the process described is compatible with the local excess of three leptons recently reported by the ATLAS collaboration. Chapter 8 concludes the thesis summarizing the main results and outlining the future prospects of research.

Introducción

El descubrimiento del boson de Higgs en El Gran Colisionador de Hadrones (LHC) [1, 2] constituye la confirmación de la existencia de la ultima pieza del Modelo Estándar de la física de partículas. Sin embargo, existen aun problemas importantes que dicho marco teórico no pude responder, tales como el origen de la masa de los neutrinos, la naturaleza de la materia oscura, el origen de la asimetría bariónica del universo o el problema CP de las interacciones fuertes. Han aparecido diversas propuestas en las últimas décadas para responder a estas preguntas, con la característica común de que todas estas extensiones a energías más allá del Modelo Estándar deben mostrarse de algún modo a energías no mucho mas elevadas que la Escala Electrodébil. Esto constituye una invitación a explorar experimentalmente la física a energías del orden del Teraelectrónvoltio (TeV). El número de posibilidades para extender el Modelo Estándar es enorme, con cada caso motivado por diferentes ideas teóricas o diferentes indicios experimentales.

El plan de investigación experimental a energías por encima de la Escala Electrodébil para las próximas décadas utiliza el aprovechamiento exhaustivo de las posibilidades del LHC, incluyendo la fase de Alta Luminosidad (HL), y la incorporación de nuevos detectores centrados en señales específicas, difíciles de medir con los experimentos actuales, tal como las búsquedas de partículas con vida media larga. Así mismo, hay planes para construir el Colisionador Lineal Internacional (ILC) en Japón, un colisionador de electrones-positrones con energías de 500 GeV. Por lo tanto, en la actualidad y en el futuro próximo, las posibilidades de probar cualquier teoría más allá del Modelo Estándar en términos de su efecto sobre la fenomenología de partículas están restringidas a experimentos alrededor del TeV de energía. Afortunadamente esto es suficiente para analizar gran cantidad de modelos capaces de resolver algunos de los problemas del Modelo Estándar y a la vez producir señales en los aceleradores, tanto directas como indirectas. Por ello es crucial hacer un análisis detallado de cada modelo, que permita diseñar los experimentos para tener una cobertura óptima y a la vez tenga la capacidad de diferenciar entre distintos modelos.

La supersimetría a la escala del TeV ha sido quizás la teoría más aceptada en las últimas décadas para extender el Modelo Estándar a la escala Electrodébil. Las extensiones supersimétricas del Modelo Estándar resultan útiles resolviendo el denominado *problema de las jerarquías* y proporcionando un buen candidato a materia oscura. Las teorías supersimétricas tienen además propiedades interesantes como la unificación de las interacciones gauge tras incluir su efecto en las ecuaciones del grupo de renormalización.

La supersimetría predice la existencia de una partícula nueva asociada a cada una de las del Modelo Estándar con los mismos número cuánticos, exceptuando el espín. Por lo tanto predice la existencia de un compañero escalar por cada fermión y un compañero fermiónico por cada bosón. Además hay buenas razones para predecir la masa de estas partículas alrededor de la escala del TeV. De este modo, la supersimetría predice la existencia de un gran número de partículas que estarían dentro del rango de energías accesible para el LHC o la siguiente generación de aceleradores.

A lo largo de la presente tesis se discuten los aspectos fenomenológicos del modelo supersimétrico denominado $\mu\nu$SSM relevantes para el LHC. Además de las propiedades atractivas de los modelos supersimétricos, el $\mu\nu$SSM permite solucionar el denominado problema μ del *Minimal Superymmetric Standard Model* (MSSM) y explicar al mismo tiempo el origen de la masa de los neutrinos. Dentro de este modelo, el gravitino es un buen candidato a materia oscura.

En extensiones supersimétricas del Modelo Estándar, el número bariónico ya no es una simetría accidental y ha de ser obtenida imponiendo algún tipo de simetría discreta. De otro modo los modelos predirían una vida media para el protón inaceptablemente baja. Generalmente este rol lo juega la simetría discreta denominada R-paridad, que fuerza a cada partícula supersimétrica a ser producida a pares. La consecuencia directa de esta simetría es que la partícula supersimétrica más ligera (LSP) será estable. En ese caso existen fuertes límites cosmológicos a las propiedades que ha de tener dicha partícula, que por otro lado la convierten en un candidato a materia oscura ideal. En los aceleradores, la familia de modelos supersimétricos que respetan la R-paridad predice la producción de eventos con una gran cantidad de momento transversal desaparecido (MET).

En su lugar, el $\mu\nu$SSM incluye términos en el lagrangiano que no permiten asignar de forma consistente cargas bajo R-paridad a todas las partículas y por lo tanto esta simetría está explícitamente rota. Dado que las partículas supersimétricas pueden decaer a partículas del Modelo Estándar, la fenomenología del modelo es más rica y debe ser estudiada detalladamente. Aunque existen otros modelos que rompen R-paridad, la estructura del $\mu\nu$SSM es compleja y da lugar a señales únicas.

El objetivo de ésta tesis es llevar a cabo un estudio de las posible señales a las que podría dar lugar el $\mu\nu$SSM en el LHC . En concreto nos enfocamos en el sector electrodébil del modelo, el cual en principio puede ser comprobado con una cierta facilidad en un acelerador de hadrones, de forma que identificamos las señales que pueden aparecer en la producción de los supercompañeros electrodébiles en el LHC. El texto está organizado como se explica a continuación: El capitulo 2 es una breve introducción a la supersimetría, presentando las características mas importantes del marco teórico y presentando los modelos más populares, con sus limitaciones. En el capítulo 3 introducimos el modelo $\mu\nu$SSM, describiendo sus características mas importantes y resumiendo los análisis fenomenológicos previos. El capítulo 4 está dedicado al análisis pormenorizado de las características fenomenológicas más importantes del *left sneutrino*, cuando ésta es la partícula supersimétrica más ligera. Allí mostramos las posibles señales a las que podría dar lugar en el LHC, cuando la desintegración es inmediata. En el capítulo 5 hacemos uso de una serie de puntos representativos del espacio de parámetros del *left-sneutrino*, que pueden producir señales detectables en el LHC. En capítulo 6 se usan las búsquedas de ATLAS de partículas con una vida media larga para poner límites al espacio de parámetros del modelo cuando el *left-sneutrino* es la partícula supersimétrica más ligera y decae a una distancia significativa del punto de interacción primaria, produciendo vértices desplazados. En el capítulo 7 se utilizan las búsquedas de ATLAS de partículas supersimétricas Electrodebiles en espectros comprimidos para poner límites a la masa del *left-sneutrino*, cuando la partícula más ligera es un neutralino tipo bino y el sneutrino es la partícula siguiente. Adicionalmente, en este capítulo explicamos que el proceso descrito es compatible con un exceso local presentado recientemente por la colaboración ATLAS.

El capítulo 8 concluye la tesis resumiendo los principales resultados y perfilando los proyectos futuros que se abren.

Chapter 2

Supersymmetry

In this chapter we introduce supersymmetry and the basics of low energy supersymmetric models. We explain the general features of SUSY models and its phenomenological implications. Finally we present some of the problem of the simplest SUSY extension of the standard mode, the MSSM. The reader could find extensive bibliography reviewing supersymmetry [3, 4, 5, 6].

2.1 Beyond the Standard Model

The Standard Model of particle interactions is a theoretical framework capable to explain most of the experimental evidence related with sub-nuclear physics, with few exceptions like the mass of neutrinos and the origin of Dark matter. During last decades, the predictions form the Standard Model have been confirmed one after the other. Masses of the $W^{\pm}$ and Z bosons predicted by the SM are very close to their experimental vale, and the same happens with their decay patterns. The SM also predicted the existence of new particles, as the charm quark, from the requirement of very suppressed flavor changing neutral currents (FCNC). Finally last necessary piece of the SM was discovered recently at the LHC, with properties which match perfectly the predictions of the SM. It's fair to say that, despite the Dark Matter and neutrino mass, the experimental searches has given no unambiguous hint for new additional structure.[1]

From a theoretical point of view, however, the SM cannot be the end of the story. It will have to be extended to describe physics at very high energy, near the reduced Planck scale $M_p = (8\pi G_{Newton})^{-1/2} = 2.4 \times 10^{18}$, where quantum gravitational effects are expected to be important. From a speculative point of view, is hard to believe that no new physics is present in the vast gap between M_{EW} and M_P. Besides of the personal inclination to expect new physics happening in between, there is one theoretical problem related with the mass of scalar particles in the theory, which requires some form of new physics. Commonly known as the *Hierarchy problem* [16, 17, 18, 19].

The Standard Model requires the existence a neutral complex scalar (H) with the classical potential:

$$V = m_H^2 |H|^2 + \lambda |H|^4. \tag{2.1}$$

[1] There exist significant discrepancies between the experimentally measured value and the predictions of the standard model in the case of some of the decays of B-Mesons [7, 8, 9, 10, 11, 12, 13, 14] and the magnetic anomalous momentum of the muon [15]. Its implications for new physics are however still definitive.

The parameters are such that the minimum of the potential is located at $\langle H \rangle \neq 0$, and the interaction of the scalar with Fermions and Gauge Bosons, together with the H vacuum expectation value (VEV) generates a mass term for each of them. This occurs when $\lambda > 0$ and $m_H^2 < 0$, producing a VEV $\langle H \rangle = \sqrt{-m_H^2/2\lambda}$.

The experimental measured values of the Gauge boson and Higgs masses fix the acceptable values of the parameters on Eq. (2.1). That is $< H >= 174$ GeV, and the quadratic term in the potential, the mass term, must be of order $-(100\text{ GeV})^2$, including the radiative corrections. If the SM was the end of the story, all the radiative contributions to the Higgs mass would be of the Electroweak order or smaller. However, the presence of any form of new physics will translate to huge radiative corrections to the Higgs mass.

The simplest way to illustrate this is to include a new particle, fermion or boson, and calculate the contribution of this diagrams, shown on Fig. 2.1, to the Higgs boson mass. The simplest way of regularizing the UV divergence is to use a cut-off regulator, and then one finds a quadratic dependence on the cut-off scale Λ.

It is possible to translate the divergent behavior when the momentum running in the loop is arbitrary large, to a divergence when the number of dimensions approach 4, in the regularization scheme called dimensional regularization, through this process, one get rid of the quadratic dependence on the cut-off. One however will still get a radiative contribution that depends quadratically on the mass of the particle running inside the loops, and this contributions would be present even when there is not direct coupling between the Higgs boson and the unknown heavy particles, provided they interact with a common intermediate state.

If there exist, for instance, an additional structure unifying the gauge interactions at some High energy scale 10^{15} GeV , with new particles with masses at this scales. An almost exact cancellation between the $\sim 10^{30}\text{GeV}^2$ radiative corrections and the bare value of the Higgs Boson mass should occur leaving a small finite value around the EW scale.

There are different proposals to extend the SM and solve he hierarchy problem. Some invoking the existence of discrete symmetries such as Little Higgs models [20], interpreting the Higgs field as a Non-elementary [21, 22, 23], the existence of extra dimensions [24, 25, 26], and also the existence of supersymmetry.

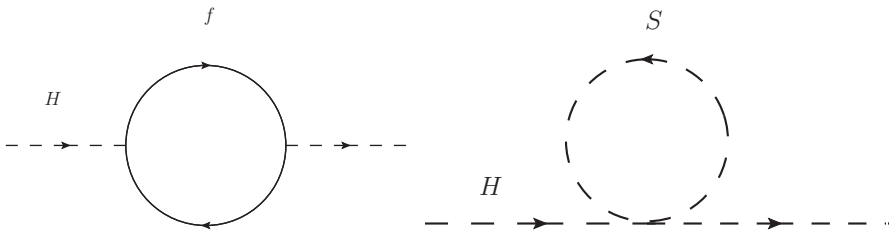

Figure 2.1: One loop diagrams contributing to the Higgs mass parameter m_H^2, by cause of a Dirac fermion and a scalar.

As explained above, the radiative corrections to the mass of the Higgs boson are proportional to the square of the scale of the new physics. Even if one avoids the physical interpretation of a UV cut-off (Λ_{UV}) using dimensional regularization one still gets a correction proportional to the square of the mass of the extended particle content. This correction is only avoided with the unphysical tuning of a counter-term specifically for that purpose.

If the Higgs boson is a fundamental particle, we must assume that there is no new high-mass physics affecting the scalar Higgs or a precise cancellation between all these effects somehow takes place. Supersymmetry, a symmetry that relates bosons and fermions,

constitutes one example of this forbidding radiative corrections to any of the masses when the symmetry is exact.

In the same spirit as for the diagrams in Fig.2.1. Now one ought to include, for each diagram, a new radiative contribution with the exact same quantum numbers and masses, but exchanging fermions for bosons and vice-versa. The result of the calculation has to be exactly the same up to a negative sign, which makes the two contributions cancel each other. This explicit pair cancellation of Feynman diagrams is translated to rules forbidding radiative contributions after writing the Lagrangian in an explicitly supersymmetric language, in the same spirit as Lorentz invariant qualities are visibly invariant when written in a covariant language.

2.2 Introduction to SUSY

Supersymmetric operators acts on Lorentz representations transforming bosonic states into fermionic states and vice-versa:

$$Q|Bosonic\ state\rangle \rightarrow |Fermionic\ state\rangle \qquad Q|Fermionic\ state\rangle \rightarrow |Bosonic\ state\rangle$$

When SUSY is a symmetry of the theory the SUSY generator commute with the rest of operators, therefore the transformation between bosons and fermions do not affect the action of the rest of them.

The Coleman-Mandula theorem [27] establishes the form of the possible symmetries of the *S-matrix* of a non trivial Quantum Field Theory (QFT). It restricts the symmetries, under certain reasonable assumptions, to the direct product of the Poincare Group and internal symmetry groups. The Haag-Lopuszanki-Sohnius extension of Coleman-Mandula theorem [28] allows for extending the symmetry group of a interacting quantum field theory to include this type of transformations, extending the Lie algebra to:

$$\begin{aligned} \left\{Q_\alpha^A, \bar{Q}_{\dot{\beta}}^B\right\} &= 2\sigma_{\alpha\dot{\beta}}^m P_m \delta_B^A, \\ \left\{Q_\alpha^A, Q_\beta^B\right\} &= 0, \\ \left[P_m, Q_\alpha^A\right] &= 0, \\ \left[P_m, P_n\right] &= 0. \end{aligned} \tag{2.2}$$

The single-particle states of a SUSY theory would be irreducible representations of the lie algebra, called *supermultiplets*, which contains fermionic and bosonic states. The particle states inside the same multiplet must share quantum numbers for any symmetry group commuting with the supersymmetry generators, thus they share eigenvalues of $-P^2$, and therefore have equal masses. Similarly for electric charge, weak isospin and color charge. Within a supermultiplet, the number of fermionic degrees of freedom equals the number of bosonic ones.

The basic representations of the supersymmetric algebra are the *chiral* and *vector* superfields, shown in Eq. (2.4) and Eq. (2.6), with chiral derivatives defined on Eq. (2.9) and (2.10). The former includes a two-component Weyl fermion (ψ), a complex scalar field (ϕ) and a spin-2 auxiliary Field eliminated on-shell (F); and the latter includes a massless spin-1 boson (A_μ), a massless spin-1/2 Weyl fermion (λ), a massless spin-1/2 fermion (χ) that can be set $\chi = 0$ by a gauge rotation, and a spin-2 auxiliary field (D). The symbols

θ and $\bar{\theta}$ represent Grassman variables.

$$\bar{D}^{\dot{\alpha}}\Phi = 0 \tag{2.3}$$

$$\Phi = \phi(x) + i\theta\sigma^{\mu}\bar{\theta}\partial_{\mu}\phi + \frac{1}{4}\theta^2\bar{\theta}^2\partial^2\phi + \sqrt{2}\theta\psi - \frac{1}{\sqrt{2}}\theta\theta\partial_{\mu}\psi\sigma^{\mu}\not{\partial} + \theta^2 F \tag{2.4}$$

$$V = V\dagger \tag{2.5}$$

$$V = i\chi - i\chi^{\dagger} - \theta\sigma^{\mu}\theta^{*}A_{\mu} + i\theta^2\bar{\theta}\bar{\lambda} - i\bar{\theta}^2\theta\lambda + \tfrac{1}{2}\theta^2\bar{\theta}^2 D. \tag{2.6}$$

For the action to be invariant under supersymmetric transformations the Lagrangian density should be invariant under action of $Q^A_{\alpha}, \bar{Q}^B_{\dot{\beta}}$, up to a total derivative. This is the case when the Lagrangian density has the structure:

$$\mathcal{L} = \int d^2\theta d^2\bar{\theta}\left[\Phi^{*i}(e^{2g_a T^a V^a})^j_i \Phi_j\right] + \int d^2\theta\left[\left(\frac{1}{4} - i\frac{g_a^2\Theta_a}{32\pi^2}\right)\mathcal{W}^{a\alpha}\mathcal{W}^a_{\alpha} + W(\Phi_i)\right] + h.c. \tag{2.7}$$

Where V^a are vector supermultiplets of a gauge group with a coupling constant g_a and a CP violating angle Θ, and Φ^{*i} are chiral superfields in a representations R of the corresponding gauge group with matrix generators T^{aj}_i. $\mathcal{W}^a_{\alpha}$ is the field strength of the Vector superfield defined as:

$$\mathcal{W}^a_{\alpha} = -\frac{1}{4}\bar{D}\bar{D}D_{\alpha}V^a, \qquad \bar{\mathcal{W}}^a_{\dot{\alpha}} = -\frac{1}{4}DD\bar{D}_{\dot{\alpha}}V^a \tag{2.8}$$

Where D_{α} and $\bar{D}_{\dot{\alpha}}$ are called chiral derivatives and are defined as:

$$D_{\alpha} = \frac{\partial}{\partial\theta^{\alpha}} - i(\sigma^{\mu}\theta^{\dagger})_{\alpha}\partial_{\mu}, \tag{2.9}$$

$$\bar{D}^{\dot{\alpha}} = \frac{\partial}{\partial\theta^{\dagger}_{\dot{\alpha}}} - i(\bar{\sigma}^{\mu}\theta)^{\dot{\alpha}}\partial_{\mu}. \tag{2.10}$$

And $W(\Phi_i)$ is the superpotential (Eq. (2.11)), which is an arbitrary holomorphic function of the chiral superfields invariant under the gauge symmetries of the theory.

$$W = \frac{1}{2}m_{ij}\Phi_i\Phi_j + \frac{1}{3}\Gamma_{ijk}\Phi_i\Phi_j\Phi_k. \tag{2.11}$$

Any radiative contribution to the mass of the components of a chiral supermultiplet, such as the radiative contribution of the Higgs Boson mass, should have the same form as the second term of the second integral on Eq. (2.7). Using the properties of the Grassman integrals is possible to demonstrate that any diagram correcting the superpotential necessarily vanishes under the integral sign (See for example tenth chapter of [3]). Therefore the mass of the Higgs bosons is protected at all orders of perturbation theory in an exact

SUSY theory.

2.3 Soft SUSY breaking

If Supersymmetry was meant to be an exact Symmetry of nature, any known particle would have a superpartner with the same mass and quantum numbers, but different spin. This implies for instance that there should exist a scalar superpartner of the electron (selectron) with same mass and charge. Since the universe is not flooded in selectrons, it is obvious that in a reasonable realization of Supersymmetry in nature it has to be broken somehow, at least at low energy.

To build a realistic model of SUSY we need to include terms in the Lagrangian which break supersymmetry in a way which do not spoil the good features of the theory, i.e. the UV insensitivity of the Higgs potential. This is possible if SUSY is spontaneously broken, that is, if the underlying model is supersymmetric but the vacuum is not. There are several proposals for mechanisms breaking SUSY at very high scales and producing an spectrum of particles with masses on the TeV scale. The general idea of them is that some states break supersymmetry spontaneously at some high energy scale, and this is communicated by some feeble interaction to the rest of the spectrum that conserves SUSY by itself. The communication of the SUSY breaking could be mediated by gravitational interactions [29, 30, 31, 32, 33, 34, 35], heavy gauge mediators [36, 37, 38, 39, 40, 41], extra dimensions [42, 43, 26, 44, 45, 46, 47, 48, 49] anomalies [50, 51] and many more mechanism. Each model predict some differences in how is the effective SUSY breaking at low energy, but we can parametrize our ignorance simply introducing effective terms in the potential that explicitly breaks SUSY.

If broken supersymmetry is still solving the hierarchy problem, the relationship between dimensionless couplings that hold in unbroken symmetry must be maintained. Therefore we could only include *soft* terms, or terms with couplings with mass dimension less than four [52, 53]. This terms would be of the general form:

$$\mathcal{L}_{soft} = -\left(\frac{1}{2}M_a\lambda^a\lambda^a + \frac{1}{6}a^{ijk}\phi_i\phi_j\phi_k + \frac{1}{2}\phi_i\phi_j + t^i\phi_i\right) + h.c - (m^2)^i_j\phi^j * \phi_i, \qquad (2.12)$$

Where λ^a is the fermionic component of a Vector supermultiplet and ϕ_i is the complex scalar component of a chiral supermultiplet. Soft masses for fermions of chiral supermultiplets could have been included as well, however this terms can always be reabsorbed into a redefinition of the superpotential and the rest of the soft terms.

2.4 R-parity

With the structure described in previous sections we should be able to build a model containing the SM. This is the spirit of the minimal supersymmetric extension of the SM, the Minimal Supersymmetric Standard Model (MSSM). On it, each of the known particles lies in a vector or chiral supermultiplet, and thus come with a yet undiscovered superpartner with spin varying in 1/2. Moreover, any supersymmetric model including the SM needs at least an extra Higgs chiral supermultiplet in order to give mass to all the particles with only holomorphic interactions in the superpotential. The extra Higgs supermultiplet is also needed to cancel gauge anomalies.

To fit the SM, the form of the gauge sector in (2.7) is fixed, and the superpotential should include, at least, the Yukawa interactions between the Higgs supermultiplet and the rest of chiral superfields. Notice however that accidental symmetries of the SM Lagrangian, such as Lepton and Baryon number, are no longer necessary symmetries of the Lagrangian. Therefore, the most general superpotential includes terms of the form:

$$\lambda_{ijk}\hat{L}_i\hat{L}_j\hat{e}^c_k + \lambda'_{ijk}\hat{L}_i\hat{Q}_j\hat{d}^c_k + \lambda''_{ijk}\hat{u}_i\hat{d}_j\hat{d}^c_k + \mu'^i\hat{L}_i\hat{H}_u. \tag{2.13}$$

This terms are clearly problematic. In fact, the simultaneous presence of this terms would produce interactions which lead to a unacceptable fast decay of the proton. To avoid this one should impose a discrete symmetry which forbids the presence of this terms. Or at least enough of them to protect the decay of the proton.

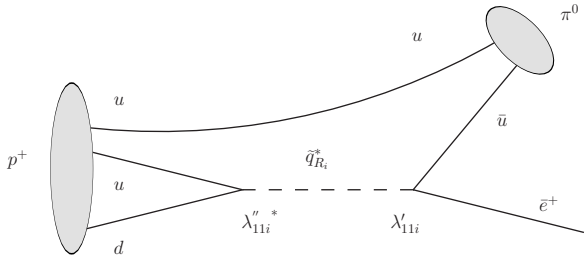

Figure 2.2: In the presence of R-parity violating interactions breaking both lepton and baryon number, squarks would mediate a rapid proton decay. In this example $p \to e^+\pi^0$

One can in principle promote L and B numbers to be *true* discrete symmetries of the Lagrangian, instead of just "accidental symmetries". However, B or L cannot be treated as fundamental Symmetries of Nature, since they are known to be necessarily violated by non-perturbative electroweak effects [54]. We can instead impose a new discrete symmetry, which has the effect of eliminating the L and B violating terms in the renormalizable superpotential. This symmetry is called *R-parity*:

$$P_M = (-1)^{3(B-L)+2s} \tag{2.14}$$

R-parity is a particular case of *R-symmetry*. A continuous *R-symmetry* is a transformation which acts over the anticomuting coordinates as:

$$\theta \to e^{i\alpha}\theta, \quad \bar{\theta} \to e^{-i\alpha}\bar{\theta} \tag{2.15}$$

Is straightforward to see that kinetic part of the Lagrangian is automatically *R-symmetric* including the gauge interactions with chiral superfields. However, The superpotential must carry R charge $+2$ if *R-symmetry* is to be conserved. *R-symmetries* do not commute with supersymmetry, therefore each component of the supermultiplet receives a different charge assignment. Continuous *R-symmetries* could be of course restricted to discrete subgroups,as is the case with *R-parity*. Following the definition of (2.14), each particle of the SM receives a charge assignment of $P_R = +1$ while its superpartner has charge $P_R = -1$.

Imposing *R-parity* has important phenomenological consequences. First, lepton and Barion number are again accidental symmetries of the Lagrangian. Also, any interaction

should have and even number of particles with $P_R = +1$. Therefore, any SUSY particle have to be pair produced. Moreover, all SUSY particles should decay to another SUSY particle plus SM particles, thus the lightest particle with $P_R = -1$ is stable, normally called the *Lightest Supersymmetric Particle* (LSP).

Although *R-parity* forbids all the renormalizable terms of the superpotential violating B and L, is true that allows for non-renormalizable terms that could make the proton decay. For example, *R-parity* doesn't forbid operators such as:

$$\frac{1}{\Lambda_{UV}}\bar{u}\bar{u}\bar{d}\bar{e}, \quad \frac{1}{\Lambda_{UV}}QQQL \tag{2.16}$$

R-parity can be replaced by other discrete symmetries which forbids the proton decay. The Z_2 and Z_3 possibilities has been studied in [55, 56] and the most important cases are *Baryon Triality* (B_3) and *Proton Exality* (P_6), both of them forbid proton decay operators of dimension five or lower, are anomaly-free and free of domain wall problems. The former allow for low energy lepton-number violating terms and the second one forbid both B and L violating terms. Form the point of view of the renormalizable superpotential P_6 is equivalent to *R-parity*, thus we could substitute *R-parity* by P_6 in any further mention without changing the phenomenological implications. In the case of B_3, both the terms λ_{ijk} and λ'_{ijk} are present. Nevertheless stringent experimental constraint exist from the non observation of low energy processes such as $\mu \to e\gamma$ or neutral meson oscillations [57]. For a review on *R-parity* violating models see [58].

2.5 The MSSM

We have already started to describe the characteristics of the MSSM. In this section we will complete the description of the model and mention some of the limitations that it suffers.

The superpotential of the MSSM is:

$$W_{MSSM} = \quad \epsilon_{ab}(Y_{u_{ij}}\hat{H}_u^b\hat{Q}_i^a\hat{u}_j^c + Y_{d_{ij}}\hat{H}_d^b\hat{Q}_i^a\hat{d}_j^c + Y_{e_{ij}}\hat{H}_d^b\hat{L}_i^a\hat{e}_j^c + \mu\hat{H}_d^a\hat{H}_u^b). \tag{2.17}$$

Where the hatted symbols represent chiral supermultiplets, we take $\hat{H}_d^T = (\hat{H}_d^0, \hat{H}_d^-)$, $\hat{H}_u^T = (\hat{H}_u^+, \hat{H}_u^0)$, $\hat{Q}_i^T = (\hat{u}_i, \hat{d}_i)$, $\hat{L}_i^T = (\hat{\nu}_i, \hat{e}_i)$, a, b are $SU(2)$ indices, and $\epsilon_{12} = 1$.

Besides the Yukawa matrices, which are in general 3x3 matrices, there is one dimension-full parameter μ which plays the role of the supersymmetric version of the Higgs boson mass in the Standard Model. Any other mass term involving the Higgs doublets is forbidden in the superpotential because of the holomorphicity of it. Is obvious also why we need two Higgs doublets, since a term of the form $Y_{d_{ij}}\hat{H}_d^{b\dagger}\hat{Q}_i^a\hat{d}_j^c$ is forbidden.

Notice that after expanding the superpotential in term of the component fields, we will not only generate the Yukawa interactions between Higgs bosons and SM fermions, but also between Higgs fermionic partners (Higgsinos) and SM fermion partners (sfermions), see Fig. 2.3. The μ term will also generate a mass term for Higgsinos. In addition, quartic interactions between scalars will also be generated, see Fig. 2.3. .

The kinetic part of the Lagrangian is fixed to include the gauge interactions of the SM. Mind however, that an interaction between the fermion SUSY partner of gauge bosons (gauginos) and the two components of any chiral multiplet charged under the corresponding gauge group will be also generated. For example an interaction bino-electron-selectron will

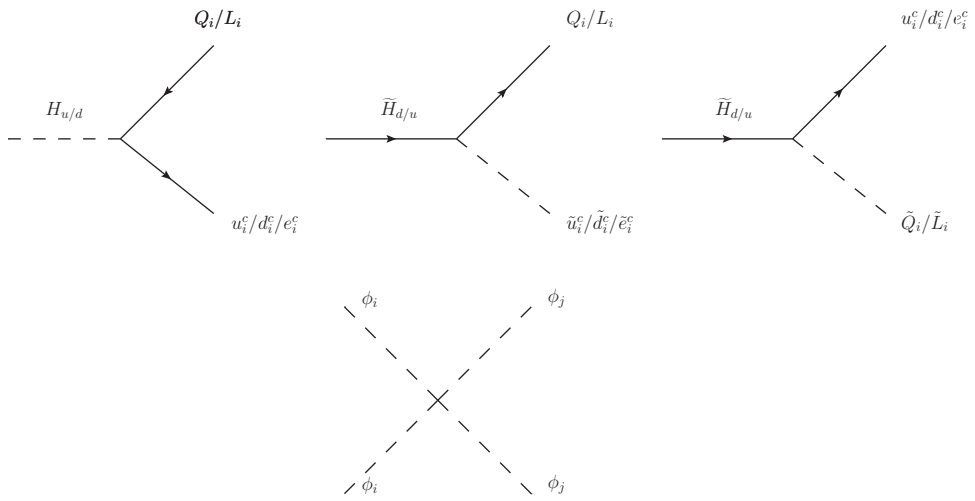

Figure 2.3: Feynman diagrams originated after expanding the terms $\Gamma_{ijk}\Phi_i\Phi_j\Phi_k$ of the superpotential in component fields.

be present proportional to the weak hypercharge, see Fig. 2.4. Finally, the kinetic terms in Eq. (2.7) generate a quartic scalar interaction proportional to the gauge couplings as shown in Fig. 2.4.

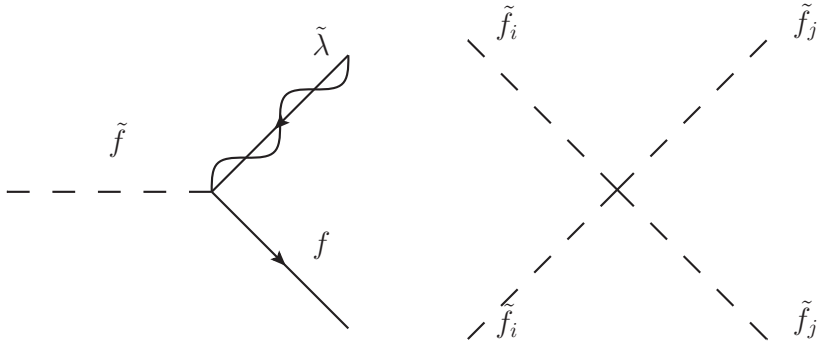

Figure 2.4: Feynman diagrams between gauginos, fermions and sfermions, originated from the gauge interaction between Vector superfields and chiral superfields.

To complete the description of the MSSM, we need to specify the form of the soft supersymmetric breaking terms in the Lagrangian. Applying the general form in Eq. (2.12) to the MSSM content, we get to:

$$\begin{aligned}
\mathcal{L}_{soft}^{MSSM} = & - m^2_{\widetilde{Q}_{ij}}\, \widetilde{Q}_i^{a*}\, \widetilde{Q}_j^a - m^2_{\widetilde{u}^c_{ij}}\, \widetilde{u}_i^{c*}\, \widetilde{u}_j^c - m^2_{\widetilde{d}^c_{ij}}\, \widetilde{d}_i^{c*}\, \widetilde{d}_j^c - m^2_{\widetilde{L}_{ij}}\, \widetilde{L}_i^{a*}\, \widetilde{L}_j^a - m^2_{\widetilde{e}^c_{ij}}\, \widetilde{e}_i^{c*}\, \widetilde{e}_j^c \\
& - m^2_{H_d}\, H_d^{a*}\, H_d^a - m^2_{H_u}\, H_u^{a*} H_u^a - \epsilon_{ab}(b H_u^a H_d^b + c.c.) \\
& - \epsilon_{ab}\left[a_{u_{ij}}\, H_u^b\, \widetilde{Q}_i^a\, \widetilde{u}_j^c - a_{d_{ij}}\, H_d^a\, \widetilde{Q}_i^b\, \widetilde{d}_j^c - a_{e_{ij}}\, H_d^a\, \widetilde{L}_i^b\, \widetilde{e}_j^c + \text{c.c.}\right] \\
& - \frac{1}{2}\left(M_3\, \widetilde{\lambda}_3\, \widetilde{\lambda}_3 + M_2\, \widetilde{\lambda}_2\, \widetilde{\lambda}_2 + M_1\, \widetilde{\lambda}_1\, \widetilde{\lambda}_1 + \text{c.c.}\right) .
\end{aligned} \tag{2.18}$$

In Eq. (2.18), M1, M2 and M3 refer to the soft masses of bino, wino and gluino respectively, $m^2_{\tilde{X}}$ refers to the soft mass of the scalar partners of SM fermions, and the third line we see the trilinear couplings between scalar partners in one to one correspondence with the terms of the superpotential. There is also a coupling between the two Higgs

doublets in correspondence with the μ term. Notice that a linear term as the fourth on Eq. (2.12) is forbidden for all the superfields in the MSSM by gauge invariance. The scalar soft masses $m^2_{\tilde{X}}$ are 3×3 matrices that can in principle have complex entries, but they must be hermitian to ensure the Lagrangian is real.

The parameters in the soft SUSY breaking part of the Lagrangian can have in principle any structure. However, one should think of this terms as the effective remains of some high energy mechanism breaking SUSY, which in each specific realization of high energy SUSY could have a different substructure. They predict generically a common energy scale for the soft parameters ranging from around the TeV scale to tenths of TeV, with some possible hierarchies, for instance between scalar and fermionic SUSY particles, or between colored and color neutral particles.

The reader should have in mind also that, even if there is no a priory theoretical restriction to the structure of the soft parameters, there are important experimental restrictions to the value of them. The inter-generational mixing induced by off diagonal values of soft mass matrices $m^2_{\widetilde{Q}_{ij}}, m^2_{\widetilde{u}^c_{ij}/\widetilde{d}^c_{ij}}, m^2_{\widetilde{L}_i}$ and $m^2_{\widetilde{e}^c_i}$ would mediate rare decays as $B \to X_s\gamma$ or $B \to \mu\mu$ [59], or $\mu^- \to e^-\gamma$ [60], for which exist stringent upper bounds.

2.5.1 Electroweak symmetry breaking in the MSSM.

As already discussed, the MSSM needs two Higgs doublets. This change somewhat how the electroweak symmetry gets broken. Now the classical neutral scalar potential is:

$$\begin{aligned} V_{\text{soft}} = \quad & (|\mu| + m^2_{H_d}) H^{0*}_d H^0_d + (|\mu| + m^2_{H_u}) H^{0*}_u H^0_u \\ & - \left[b H^0_d H^0_u + c.c \right] + \frac{1}{8}\left(g^2 + g'^2\right)\left(H^0_d H^{0*}_d - H^0_u H^{0*}_u\right)^2 . \end{aligned} \tag{2.19}$$

The b term in the scalar potential is the only one that depends on the phase of H^0_u and H^0_d therefore we can make them absorb any phase on b, which thus can be taken real and positive. Moreover, we can use a $U(1)_Y$ gauge rotation to make both fields real and positive. Therefore CP cannot be spontaneously broken by the Higgs scalar potential and can assign the Higgs states to CP-eigenstates:

$$H^0_d = \frac{1}{\sqrt{2}}\left(H^{\mathcal{R}}_d + v_d + i\ H^{\mathcal{I}}_d\right) , \tag{2.20}$$

$$H^0_u = \frac{1}{\sqrt{2}}\left(H^{\mathcal{R}}_u + v_u + i\ H^{\mathcal{I}}_u\right) , \tag{2.21}$$

In the MSSM the quartic term of the scalar potential is fixed. Thus, for electroweak symmetry breaking to happen is necessary that the condition on Eq. (2.22) to be fulfilled. In order for the potential to be bounded from below, is also necessary the condition in Eq. (2.23). The Higgses develop the VEVs determined by the minimization equations of the scalar potential.

$$2b < 2|\mu|^2 + m^2_{H_u} + m^2_{H_d}. \tag{2.22}$$

$$b^2 > (|\mu|^2 + m^2_{H_u})(|\mu|^2 + m^2_{H_d}) \tag{2.23}$$

After electroweak symmetry breaking, the VEVs generate the mass of the Z^0 boson as:

$$v_u^2 + v_d^2 = v^2 = 2\frac{m_Z^2}{g^2 + g'^2} \approx (174)^2. \tag{2.24}$$

The relative size can in principle take any value, and is typically designated as:

$$\tan\beta \equiv \frac{v_u}{v_d}. \tag{2.25}$$

Finally, we can write $\tan\beta$ and m_Z^2 in terms of the parameters of the Lagrangian:

$$\sin(2\beta) = \frac{2b}{m_{H_u}^2 + m_{H_d}^2 + 2|\mu|^2} \tag{2.26}$$

$$m_Z^2 = \frac{|m_{H_u}^2 - m_{H_d}^2|}{\sqrt{1 - \sin^2(2\beta)}} - m_{H_u}^2 - m_{H_d}^2 - 2|\mu|^2. \tag{2.27}$$

Notice here that even if the values of the soft Higgs masses and μ are large, they should cancel each other in order to give the correct mass to the Z^0 boson.

After EWSB we can calculate the eigenstates of the scalar mass matrix and find the expression for the mass of the lightest state, which should be identify with the Higgs Boson discovered with 125 GeV of mass at the LHC:

$$m_{h^0}^2 = \frac{1}{2}\left(m_{A^0}^2 + m_Z^2 - \sqrt{(m_{A^0}^2 - m_Z^2)^2 + 4mZ^2 m_{A^0}^2 \sin^2(2\beta)}\right). \tag{2.28}$$

Where m_{A^0} is the mass of the pseudoscalar Higgs and has the form $m_{A^0}^2 = 2b/\sin(2\beta)$. One can see from Eq. (2.28) that the mass of the lightest Higgs is bounded, at tree level, to be:

$$m_{h^0} < m_Z|\cos(2\beta)| \tag{2.29}$$

If the condition Eq. (2.29) where strong, the mass predicted for the Higgs boson would be wrong and the fate of the MSSM would be doomed. However, one has to remind that below the scale where SUSY is again restored, the h^0 is subject to strong quantum corrections form the Supersymmetric part of the spectrum. The largest of these contributions comes from the top scalar partners and can easily lift the mass of h^0 up to 125 GeV.

2.5.2 The little Hierarchy problem.

We have argue as one of the main justifications to extend the SM to a Supersymmetric theory that the EWSB scale is quadratically sensitive to the existence if new physics. However, the careful reader could have realize that an exact SUSY will predict to low mass for the SM Higgs and needs precisely the strong influence of quantum corrections to provide enough mass. One can argue then at which extent remains the Electroweak Scale non-tuned, since it will be the result of the cancellations between soft masses, the μ term and radiative corrections, all acting above the TeV scale.

A lot of debate has been originated around the so-called "Little Hierarchy Problem", and how to define a quantitative measure of the sensitivity of the EW scale to the specific choice of parameters in the MSSM. This topic is anyhow beyond the scope of this work.

We recall the reader that SUSY still solves the big Hierarchy Problem, meaning that SUSY protects the scalar potential form large quantum corrections from a high energy theory.

2.5.3 Beyond the MSSM

In Eq. (2.17) we have seen that the superpotential includes a dimensionfull parameter μ. To allow the correct $v \approx 174$ GeV to be solution of the minimization equations, μ must be roughly 10^2 or 10^3 GeV, of the same order as $m^2_{H_u}$ and $m^2_{H_u}$. But should the reader recall that while the soft parameters are all of them effectively generated from some mechanisms acting at high energy, the μ parameter is fundamental and there is no reason for it to be at any specific scale. Why should μ be small compared to, for instance, the Planck scale? The scalar potential in the MSSM depends then on dimensionfull parameters that are conceptually very different, yet they should be of the same order and also not far from the electroweak scale to produce the correct EWSB. This riddle is called "the μ problem".

There are multiple proposals to solve this problem, all of them assume that the μ term is absent at tree level in the superpotential and is somehow generated effectively. When the effective μ term is generated by a mechanism associated with the supersymmetry breaking it is no longer fundamentally distinct that the soft terms. And if one can explain why $M_{soft} \ll M_{Planck}$, the same explanation is valid for the scale of the μ term.

One of the most popular solutions is to add a gauge singlet chiral supermultiplet, that develops a VEV after ESWB. The presence of some adimensional coupling between the Higgs doublets and the gauge singlets generates an effective μ term proportional to its VEV, which value is to a great extent fixed by the value of the soft terms. The minimal extension of the MSSM including this idea is the so called Next to Minimal Supersymmetric Standard Model (NMSSM).[2]

The MSSM was built to fit the standard model within. As a result of imposing *R-parity*, required by he stability of the proton, it predicts the existence of a stable particle. Thus provides a viable dark matter candidate in the neutralino. It also changes the running of gauge couplings making them unify. However, it doesn't provide an explanation for the origin of neutrino masses. There are other extensions of the SM that provide a mechanism explaining neutrino physics. In the next chapter we will introduce a model capable of solving the μ problem and explaining neutrino physics at the same time.

[2]For an extensive review of the NMSSM an its phenomenology see [61].

Chapter 3

The $\mu\nu$SSM

In the previous chapter we have introduced the concept of supersymmetry and its minimal viable realization, the MSSM. At the end of the chapter we have listed some of the weaknesses of the MSSM. Now we are going to introduce an extension that solves the enumerated problems while retaining the good features of the MSSM. We are going also to sketch the phenomenology which, as we will see, turns out to be qualitatively different.

The "μ form ν supersymmetric standard model" ($\mu\nu$SSM), introduced and developed in the works of Refs. [62, 63, 64], extends the MSSM including three generations of right-handed neutrino superfields. They can, in principle, couple in the superpotential with the rest of the spectrum in any possible form allowed by gauge invariance, and as we will see, this provides also a solution to the μ problem and generates neutrino masses and mixings.

3.1 The superpotential and soft terms

Given the MSSM particle content with the addition of three generations of right-handed neutrino superfields ($\hat{\nu}^c_i$), the most general renormalizable superpotential respecting the gauge symmetry group of the SM, $SU(3)_C \times SU(2)_L \times U(1)_Y$, with subscripts C, L and Y referring to color, left chirality and weak hypercharge, respectively, can be written as [64]:

$$\begin{aligned} W = \quad & \epsilon_{ab}\left(Y^e_{IJk}\,\hat{L}^a_I\,\hat{L}^b_J\,\hat{e}^c_k + Y^d_{Ijk}\,\delta_{\alpha\beta}\,\hat{L}^a_I\,\hat{Q}^b_{j\alpha}\,\hat{d}^c_{k\beta} + Y^u_{ij}\,\delta_{\alpha\beta}\,\hat{L}^{cb}_4\,\hat{Q}^a_{i\alpha}\,\hat{u}^c_{j\beta}\right) \\ + \quad & \epsilon_{ab}\,Y^\nu_{Ij}\,\hat{L}^{cb}_4\,\hat{L}^a_I\,\hat{\nu}^c_j + \frac{1}{3}\kappa_{ijk}\,\hat{\nu}^c_i\,\hat{\nu}^c_j\,\hat{\nu}^c_k\ , \end{aligned} \tag{3.1}$$

where the summation convention is implied on repeated indexes, with $\alpha, \beta = 1, 2, 3$ $SU(3)_C$ indexes, $a, b = 1, 2$ $SU(2)_L$ indexes with ϵ_{ab} the totally antisymmetric tensor $\epsilon_{12} = 1$, and $I = i, 4$ ($J = j, 4$) with $i, j, k = 1, 2, 3$ the usual family indexes of the SM and with the vector-like Higgs doublet superfields interpreted as a fourth family of vector-like lepton superfields[1] $\hat{L}_4 = (\hat{\nu}_4, \hat{e}_4) = (\hat{H}^0_d, \hat{H}^-_d) = \hat{H}_d$ and $\hat{L}^c_4 = (\hat{e}^c_4, \hat{\nu}^c_4) = (\hat{H}^+_u, \hat{H}^0_u) = \hat{H}_u$. Notice that this interpretation is possible in the $\mu\nu$SSM because R_p is no longer imposed as a symmetry of the Lagrangian. Consequently all fields in the spectrum with the same color, electric charge and spin mix together. In particular, Higgses mix with sleptons and Higgsinos with leptons. From the theoretical viewpoint, this seems to be more satisfactory than the situation in usual SUSY models, where the Higgses are 'disconnected' from the

[1] An extension of the $\mu\nu$SSM by adding to the spectrum of this fourth family a vector-like quark doublet representation has also been discussed, together with its new signals at the LHC, in Refs. [64, 65].

rest of the matter and do not have a three-fold replication[2]. As pointed out in Ref. [64], in this SUSY framework the first scalar particle discovered at the LHC is mainly a sneutrino belonging to a fourth-family vector-like doublet representation.

We can write the superpotential in the usual notation of the $\mu\nu$SSM [62, 63], separating the Higgs and lepton superfields. Thus we can decompose the terms given by the couplings Y^e_{IJk}, Y^d_{Ijk} and Y^ν_{Ij} in two type of terms: Yukawa couplings generating fermion masses, and lepton-number violating couplings. This is possible because, as discussed above, the superfields L_i and H_d have the same gauge quantum numbers, and therefore $\hat{L}_I = \hat{L}_i, \hat{H}_d$. Thus, we can write superpotential (3.1) as follows [62, 63]:

$$\begin{aligned} W = \quad & \epsilon_{ab}\left(Y^e_{ij}\,\hat{H}^a_d\,\hat{L}^b_i\,\hat{e}^c_j + Y^d_{ij}\,\delta_{\alpha\beta}\,\hat{H}^a_d\,\hat{Q}^b_{i\alpha}\,\hat{d}^c_{j\beta} + Y^u_{ij}\,\delta_{\alpha\beta}\,\hat{H}^b_u\,\hat{Q}^a_{i\alpha}\,\hat{u}^c_{j\beta}\right) \\ + \quad & \epsilon_{ab}\left(\lambda_{ijk}\hat{L}^a_i\hat{L}^b_j\hat{e}^c_k + \lambda'_{ijk}\delta_{\alpha\beta}\,\hat{L}^a_i\hat{Q}^b_{j\alpha}\hat{d}^c_{k\beta}\right) \\ + \quad & \epsilon_{ab}\left(Y^\nu_{ij}\,\hat{H}^b_u\,\hat{L}^a_i\,\hat{\nu}^c_j - \lambda_i\,\hat{\nu}^c_i\,\hat{H}^b_u\hat{H}^a_d\right) + \frac{1}{3}\kappa_{ijk}\hat{\nu}^c_i\hat{\nu}^c_j\hat{\nu}^c_k\ , \end{aligned} \tag{3.2}$$

where we have decomposed (in a self-explanatory notation) $Y^e_{IJk} \to \lambda_{ijk}, Y^e_{ij}$; $Y^d_{Ijk} \to \lambda'_{ijk}, Y^d_{ij}$; and $Y^\nu_{Ij} \to Y^\nu_{ij}, -\lambda_i$. The dimensionless complex trilinear couplings form a vector λ_i, the Yukawa matrices Y^ν_{ij}, Y^e_{ij}, Y^d_{ij}, Y^u_{ij}, and the tensors λ_{ijk}, λ'_{ijk}, κ_{ijk} with κ totally symmetric and λ_{ijk} antisymmetric with respect to their first two indexes.

In Eq. (3.2) (and (3.1)), we have defined $\hat{u}_i$, $\hat{d}_i$, $\hat{\nu}_i$, $\hat{e}_i$, and $\hat{u}^c_i$, $\hat{d}^c_i$, $\hat{e}^c_i$, $\hat{\nu}^c_i$, as the left-chiral superfields whose fermionic components are the left-handed fields of the corresponding quarks, leptons, and antiquarks, antileptons, respectively. For example, the superfield $\hat{d}_2$ contains the 2-component complex spinor field s_L (and the complex scalar field $\tilde{s}_L$), whereas $\hat{d}^c_2$ contains the spinor $s^c{}_L = (s_R)^c = i\sigma^2 s^*_R$ (and the scalar $\tilde{s}^*_R = (\tilde{s}_R)^c$), where the superscripts c and $*$ indicate charge conjugate and complex conjugate, respectively, with σ^2 the Pauli matrix. Needless to say, the subscripts L and R on the scalar fields refer to the chirality of the corresponding fermion fields. The superfields $\hat{u}_i$, $\hat{d}_i$, and $\hat{\nu}_i$, $\hat{e}_i$ form the $SU(2)_L$ doublets $\hat{Q}_i = (\hat{u}_i, \hat{d}_i)$ and $\hat{L}_i = (\hat{\nu}_i, \hat{e}_i)$, respectively, and the others are $SU(2)_L$ singlets.

The three terms in the first line of the superpotential in Eq. (3.2) are the usual Dirac Yukawa couplings for quarks and leptons of the MSSM. The two terms in the second line are the conventional trilinear $\not{R}_p$ couplings. As is well known, if the lepton-number violating term, $\lambda'_{ijk}\delta_{\alpha\beta}\epsilon_{ab}\hat{L}^a_i\hat{Q}^b_{j\alpha}\hat{d}^c_{k\beta}$, appears together with the baryon-number violating term, $\lambda''_{ijk}\epsilon^{\alpha\beta\gamma}\hat{d}^c_{i\alpha}\hat{d}^c_{j\beta}\hat{u}^c_{k\gamma}$ where $\epsilon^{\alpha\beta\gamma}$ is the totally antisymmetric tensor $\epsilon^{123} = 1$, they could give rise to experimentally excluded fast proton decay. Nevertheless, as discussed in detail in Ref. [64], λ''_{ijk} can be naturally forbidden, for example through Z_3 Baryon-parity or stringy selection rules. Finally, the three terms in the third line are characteristic of the $\mu\nu$SSM. We will see how they solve the μ problem and generate neutrino masses in Sec. 3.2 and 3.5 respectively. We can also see, from the last line in Eq. (3.2) that is not possible to assign *R-parity* charges to $\hat{\nu}^c_i$ consistently. Nevertheless λ_i and κ_{ijk}, are therefore harmless with respect to proton decay.

Unlike λ_i and κ_{ijk}, the couplings λ_{ijk} and λ'_{ijk} are not useful to solve neither the μ problem nor to generate neutrino masses and mixing[3] (which is the only confirmed source

[2]For alternative constructions with three supersymmetric families of Higgses, see works [66, 67, 68] and references therein.

[3]Notice also that the couplings λ_{ijk} and λ'_{ijk} play no role in the minimization, even if they were present at tree level in the superpotential.

of new physics). In addition, they are constrained by existing bounds on quadratic coupling constant products $\lambda_{ijk}\lambda_{lmn}$, $\lambda_{ijk}\lambda'_{lmn}$ and $\lambda'_{ijk}\lambda'_{lmn}$, coming from bounds on rare processes such as meson oscillations, or flavor violating decays (see Refs. [69, 58, 70] for reviews). Thus, in what follows we will neglect them for simplicity in the superpotential[4], using:

$$\begin{aligned} W = \quad & \epsilon_{ab}\left(Y^e_{ij}\,\hat{H}^a_d\,\hat{L}^b_i\,\hat{e}^c_j + Y^d_{ij}\,\delta_{\alpha\beta}\,\hat{H}^a_d\,\hat{Q}^b_{i\alpha}\,\hat{d}^c_{j\beta} + Y^u_{ij}\,\delta_{\alpha\beta}\,\hat{H}^b_u\,\hat{Q}^a_{i\alpha}\,\hat{u}^c_{j\beta}\right) \\ + \quad & \epsilon_{ab}\left(Y^\nu_{ij}\,\hat{H}^b_u\,\hat{L}^a_i\,\hat{\nu}^c_j - \lambda_i\,\hat{\nu}^c_i\,\hat{H}^b_u\hat{H}^a_d\right) + \frac{1}{3}\kappa_{ijk}\hat{\nu}^c_i\hat{\nu}^c_j\hat{\nu}^c_k\ . \end{aligned} \tag{3.3}$$

By the same token, the soft trilinear parameters in Eq. (3.7) below, will be taken as vanishing in our computations. Nevertheless, the formulas given in the text and Appendix A include for completeness the contributions from λ_{ijk}, λ'_{ijk} and their corresponding soft trilinear parameters.

As mentioned before, the presence of the last terms on Eq. (3.2) break explicitly *R-parity*. Nonetheless, in the limit $Y^\nu_{ij} \to 0$, $\hat{\nu}^c_i$ can be identified in superpotential of Eq. (3.3) as pure singlet superfields without lepton number, similar to the case of the next-to-MSSM, where one extra singlet is added to the spectrum of the MSSM and R_p is not broken. In this limit *R-parity* will be restored. In this spirit Y^ν_{ij} are the parameters which determine the $\not{R}_p$ in the superpotential of Eq. (3.3). As we will see, the smallness of neutrino masses require small values for Y^ν_{ij}, and this violation would be therefore small.

Soft terms

Working in the framework of a typical low-energy SUSY, the Lagrangian containing the soft SUSY-breaking terms related to the superpotential in Eq. (3.2) is given by:

$$\begin{aligned} -\mathcal{L}_{\rm soft} = \quad & \epsilon_{ab}\left(T^e_{ij}\,H^a_d\,\widetilde{L}^a_{iL}\,\widetilde{e}^*_{jR} + T^d_{ij}\,H^a_d\,\widetilde{Q}^b_{iL}\,\widetilde{d}^*_{jR} + T^u_{ij}\,H^b_u\widetilde{Q}^a_{iL}\widetilde{u}^*_{jR} + \text{h.c.}\right) \\ + \quad & \epsilon_{ab}\left(T^\nu_{ij}\,H^b_u\,\widetilde{L}^a_{iL}\widetilde{\nu}^*_{jR} - T^\lambda_i\,\widetilde{\nu}^*_{iR}\,H^a_d H^b_u + \frac{1}{3}T^\kappa_{ijk}\,\widetilde{\nu}^*_{iR}\widetilde{\nu}^*_{jR}\widetilde{\nu}^*_{kR}\ + \text{h.c.}\right) \\ + \quad & \epsilon_{ab}\left(T^\lambda_{ijk}\,\widetilde{L}^a_{iL}\,\widetilde{L}^b_{jL}\,\widetilde{e}^*_{kR} + T^{\lambda'}_{ijk}\,\widetilde{L}^a_{iL}\,\widetilde{Q}^b_{jL}\,\widetilde{d}^*_{kR}\ + \text{h.c.}\right) \\ + \quad & \left(m^2_{\widetilde{Q}_L}\right)_{ij}\widetilde{Q}^{a*}_{iL}\widetilde{Q}^a_{jL} + \left(m^2_{\widetilde{u}_R}\right)_{ij}\widetilde{u}^*_{iR}\widetilde{u}_{jR} + \left(m^2_{\widetilde{d}_R}\right)_{ij}\widetilde{d}^*_{iR}\widetilde{d}_{jR} + \left(m^2_{\widetilde{L}_L}\right)_{ij}\widetilde{L}^{a*}_{iL}\widetilde{L}^a_{jL} \\ + \quad & \left(m^2_{\widetilde{\nu}_R}\right)_{ij}\widetilde{\nu}^*_{iR}\widetilde{\nu}_{jR} + \left(m^2_{\widetilde{e}_R}\right)_{ij}\widetilde{e}^*_{iR}\widetilde{e}_{jR} + m^2_{H_d}H^{a*}_d H^a_d + m^2_{H_u}H^{a*}_u H^a_u \\ + \quad & \frac{1}{2}\left(M_3\,\widetilde{g}\,\widetilde{g} + M_2\,\widetilde{W}\,\widetilde{W} + M_1\,\widetilde{B}^0\,\widetilde{B}^0 + \text{h.c.}\right)\ , \end{aligned} \tag{3.4}$$

where an implicit sum over the (undisplayed) color indexes is assumed in the terms involving squarks and gluinos. The complex trilinear parameters T^λ_i, $T^{d,e,u,\nu}_{ij}$ and $T^{\kappa,\lambda,\lambda'}_{ijk}$ are in correspondence with the trilinear couplings of the superpotential. The squared sfermion masses are required to be 3×3 hermitian matrices in family space, whereas $m_{H_{u,d}}$ are

[4]Altough λ_{ijk} and λ'_{ijk} will appear through loop processes even if they are not present at tree level, as shown in Ref. [63]. Nevertheless their contributions are smaller than order 10^{-9}. Obviously, all existing bounds on quadratic coupling constant products are satisfied, but these contributions are anyway negligible for studying physical processes. Let us remark that λ'_{ijk} are generated at one loop through the equation [63] $\frac{d}{dt}\lambda'_{ijk} = \frac{1}{16\pi^2}\,Y_{d_{jk}}\,\gamma^{H_d}_{L_i}$, with $\gamma^{H_d}_{L_i} = -Y_{\nu_{il}}\lambda_l$. However, for λ_{ijk} higher order contributions are necessary. The antisymmetric character under $i \leftrightarrow j$ of λ_{ijk}, makes the one-loop contribution identically zero, as can be seen from the fact that the one-loop equation $\frac{d}{dt}\lambda_{ijk} = \frac{1}{16\pi^2}\left(Y_{e_{jk}}\,\gamma^{H_d}_{L_i} + Y_{e_{ik}}\,\gamma^{H_d}_{L_j}\right)$ cannot generate antisymmetric contributions.

the real Higgs mass parameters. The parameters $M_{3,2,1}$ are the (generally complex) Majorana masses of the 2-component gluino, Wino and Bino fields, and an implicit sum over the (undisplayed) adjoint representation gauge indexes on the gluino and Wino fields is assumed.

Soft masses of the type $m^2_{H_d\tilde{L}_{iL}} H_d^{a*}\tilde{L}^a_{iL}$+h.c., could have been included in Eq. (3.4). However, they would contribute to the minimization equations of the left sneutrinos with terms $m^2_{H_d\tilde{L}_{iL}}\langle H_d^0\rangle$ (in the right-hand side of Eq. (3.20) below), generating VEVs $\sim$ TeV for them. This would spoil the generalized electroweak-scale seesaw present in the $\mu\nu$SSM, where correct neutrino masses require the VEVs of the left sneutrinos to be small, $\langle\tilde{\nu}_L\rangle \lesssim 10^{-4}$, driven dynamically by the Yukawa couplings. As we will discuss in Eq. (3.26), these small VEVs are necessary because neutrino masses acquire a term of the order of $\langle\tilde{\nu}_L\rangle^2/M$, with $M\sim$ gaugino masses. Thus we will assume in what follows that the above soft masses are not present in our Lagrangian or that they are negligible[5]. Notice that a similar destabilization of the left sneutrino VEVs would arise with trilinear parameters $T^\nu \sim$ TeV. This can be avoided for example if the T^ν are proportional to the small Y^ν, i.e. $T^\nu = A^\nu Y^\nu$ where A_ν can be $\sim$ TeV.

Both assumptions above about the parameters T^ν and $m^2_{H_d\tilde{L}}$ are reliable. Let us recall in this sense that strong upper bounds upon the intergenerational scalar mixing exist (see e.g. Ref. [72]), implying that one can assume that such mixings are negligible, and therefore that the squared sfermion mass matrices in Eq. (3.4) are diagonal in the flavor space. Actually, diagonal squared mass matrices occur in general in supergravity models when the observable matter fields have a diagonal Kähler metric, such as in several string compactifications, or when the dilaton field is the source of SUSY breaking (for a review see Ref. [73]). Also in this case of a diagonal metric, the soft trilinear parameters turn out to be directly proportional to the couplings present in the superpotential. Even with a general Kähler metric, these parameters are already functions of the couplings and their derivatives with respect to the hidden sector fields. Inspired by this structure of supergravity, and also by our interpretation of the Higgs H_d as a fourth-family slepton $\tilde{L}_4$, we will consider that soft masses of the type $m^2_{H_d\tilde{L}_i}$ are not present in the Lagrangian, and assume the following values for soft trilinear parameters:

$$T^e_{ij} = A^e_{ij}Y^e_{ij}\ ,\ \ T^d_{ij} = A^d_{ij}Y^d_{ij}\ ,\ \ T^u_{ij} = A^u_{ij}Y^u_{ij}\ , \tag{3.5}$$

$$T^\nu_{ij} = A^\nu_{ij}Y^\nu_{ij}\ ,\ \ T^\lambda_i = A^\lambda_i\lambda_i\ ,\ \ T^\kappa_{ijk} = A^\kappa_{ijk}\kappa_{ijk}\ , \tag{3.6}$$

$$T^\lambda_{ijk} = A^\lambda_{ijk}\lambda_{ijk}\ ,\ \ T^{\lambda'}_{ijk} = A^{\lambda'}_{ijk}\lambda'_{ijk}\ , \tag{3.7}$$

where the summation convention on repeated indexes does not apply for this case.

So far we have discussed the superpotential and the soft terms of the $\mu\nu$SSM. As we will see in section 3.2, the fifth and sixth terms of the superpotential generate an effective μ term and Majorana masses for the righ-handed neutrinos respectively after EWSB. In this way they provide a solution to the μ problem and generate the neutrino masses and mixings anlges. In the next section we will see the structure of the scalar potential and the characteristic features of the electroweak symmetry breaking in the model.

[5]Although they will appear through loop processes even if they are not present at tree level (see e.g. Ref [71], their contributions are negligible.)

3.2 The scalar potential and the electroweak symmetry breaking

The tree-level neutral scalar potential $V^{(0)}$ receives the F and D term contributions in addition to terms from $\mathcal{L}_{\rm soft}$ in Eq. (3.4), and is therefore given by [62, 63]

$$V^{(0)} = V_{\rm soft} + V_F + V_D \ , \tag{3.8}$$

with

$$\begin{aligned} V_{\rm soft} = & \left(T^{\nu}_{ij} \, H^0_u \, \widetilde{\nu}_{iL} \, \widetilde{\nu}^*_{jR} - T^{\lambda}_i \, \widetilde{\nu}^*_{iR} \, H^0_d H^0_u + \frac{1}{3} T^{\kappa}_{ijk} \, \widetilde{\nu}^*_{iR} \widetilde{\nu}^*_{jR} \widetilde{\nu}^*_{kR} \ + \text{h.c.} \right) \\ + & \left(m^2_{\widetilde{L}_L} \right)_{ij} \widetilde{\nu}^*_{iL} \widetilde{\nu}_{jL} + \left(m^2_{\widetilde{\nu}_R} \right)_{ij} \widetilde{\nu}^*_{iR} \widetilde{\nu}_{jR} + m^2_{H_d} H^{0*}_d H^0_d + m^2_{H_u} H^{0*}_u H^0_u \ , \end{aligned} \tag{3.9}$$

$$\begin{aligned} V_F = & \ \lambda_j \lambda^*_j H^0_d H^{0^*}_d H^0_u H^{0^*}_u + \lambda_i \lambda^*_j \tilde{\nu}^*_{iR} \tilde{\nu}_{jR} H^0_d H^{0*}_d + \lambda_i \lambda^*_j \tilde{\nu}^*_{iR} \tilde{\nu}_{jR} H^0_u H^{0*}_u \\ + & \ \kappa_{ijk} \kappa^*_{ljm} \tilde{\nu}^*_{iR} \tilde{\nu}_{lR} \tilde{\nu}^*_{kR} \tilde{\nu}_{mR} - \big(\kappa_{ijk} \lambda^*_j \tilde{\nu}^*_{iR} \tilde{\nu}^*_{kR} H^{0*}_d H^{0*}_u - Y^{\nu}_{ij} \kappa^*_{ljk} \tilde{\nu}_{iL} \tilde{\nu}_{lR} \tilde{\nu}_{kR} H^0_u \\ + & \ Y^{\nu}_{ij} \lambda^*_j \tilde{\nu}_{iL} H^{0*}_d H^{0*}_u H^0_u + Y^{\nu *}_{ij} \lambda_k \tilde{\nu}^*_{iL} \tilde{\nu}_{jR} \tilde{\nu}^*_{kR} H^0_d + \text{h.c.} \big) \\ + & \ Y^{\nu}_{ij} Y^{\nu *}_{ik} \tilde{\nu}^*_{jR} \tilde{\nu}_{kR} H^0_u H^{0*}_u + Y^{\nu}_{ij} Y^{\nu *}_{lk} \tilde{\nu}_{iL} \tilde{\nu}^*_{lL} \tilde{\nu}^*_{jR} \tilde{\nu}_{kR} + Y^{\nu}_{ji} Y^{\nu *}_{ki} \tilde{\nu}_{jL} \tilde{\nu}^*_{kL} H^0_u H^{0*}_u \ , \end{aligned} \tag{3.10}$$

$$V_D = \frac{1}{8} \left(g^2 + g'^2 \right) \left(\widetilde{\nu}_{iL} \widetilde{\nu}^*_{iL} + H^0_d H^{0*}_d - H^0_u H^{0*}_u \right)^2 \ . \tag{3.11}$$

The electroweak gauge couplings are estimated at the m_Z scale by $e = g \sin\theta_W = g' \cos\theta_W$.

With the choice of CP conservation[6], one can define the neutral scalars as

$$H^0_d = \frac{1}{\sqrt{2}} \left(H^{\mathcal{R}}_d + v_d + i \ H^{\mathcal{I}}_d \right) \ , \tag{3.12}$$

$$H^0_u = \frac{1}{\sqrt{2}} \left(H^{\mathcal{R}}_u + v_u + i \ H^{\mathcal{I}}_u \right) \ , \tag{3.13}$$

$$\widetilde{\nu}_{iR} = \frac{1}{\sqrt{2}} \left(\widetilde{\nu}^{\mathcal{R}}_{iR} + v_{iR} + i \ \widetilde{\nu}^{\mathcal{I}}_{iR} \right) , \tag{3.14}$$

$$\widetilde{\nu}_{iL} = \frac{1}{\sqrt{2}} \left(\widetilde{\nu}^{\mathcal{R}}_{iL} + v_{iL} + i \ \widetilde{\nu}^{\mathcal{I}}_{iL} \right) \ , \tag{3.15}$$

in such a way that after the EWSB they develop the real VEVs

$$\langle H^0_d \rangle = \frac{v_d}{\sqrt{2}} \ , \quad \langle H^0_u \rangle = \frac{v_u}{\sqrt{2}} \ , \quad \langle \widetilde{\nu}_{iR} \rangle = \frac{v_{iR}}{\sqrt{2}} \ , \quad \langle \widetilde{\nu}_{iL} \rangle = \frac{v_{iL}}{\sqrt{2}} \ . \tag{3.16}$$

The eight minimization conditions with respect to v_d, v_u, v_{iR}, v_{iL} can then be written as

$$\begin{aligned} m^2_{H_d} = & -\frac{1}{8} \left(g^2 + g'^2 \right) \left(v_{iL} v_{iL} + v^2_d - v^2_u \right) - \frac{1}{2} \lambda_i \lambda_j v_{iR} v_{jR} - \frac{1}{2} \lambda_i \lambda_i v^2_u \\ & + v_{iR} \tan\beta \left(\frac{1}{\sqrt{2}} T^{\lambda}_i + \frac{1}{2} \lambda_j \kappa_{ijk} v_{kR} \right) + Y^{\nu}_{ij} \frac{v_{iL}}{2 v_d} \left(\lambda_k v_{kR} v_{jR} + \lambda_j v^2_u \right) - \frac{\sqrt{2}}{v_d} V^{(n)}_{v_d} \end{aligned} \tag{3.17}$$

[6]The $\mu\nu$SSM with spontaneous CP violation was studied in Ref. [74].

$$
\begin{aligned}
m^2_{H_u} &= \frac{1}{8}\left(g^2+g'^2\right)\left(v_{iL}v_{iL}+v_d^2-v_u^2\right)-\frac{1}{2}\lambda_i\lambda_j v_{iR}v_{jR}-\frac{1}{2}\lambda_j\lambda_j v_d^2 \\
&+\lambda_j Y^\nu_{ij} v_{iL} v_d-\frac{1}{2}Y^\nu_{ij}Y^\nu_{ik}v_{kR}v_{jR}-\frac{1}{2}Y^\nu_{ij}Y^\nu_{kj}v_{iL}v_{kL} \\
&+\frac{v_{iR}}{\tan\beta}\left(\frac{1}{\sqrt{2}}T^\lambda_i+\frac{1}{2}\lambda_j\kappa_{ijk}v_{kR}\right)-\frac{v_{iL}}{v_u}\left(\frac{1}{\sqrt{2}}T^\nu_{ij}v_{jR}+\frac{1}{2}Y^\nu_{ij}\kappa_{ljk}v_{lR}v_{kR}\right) \\
&-\frac{\sqrt{2}}{v_u}V^{(n)}_{v_u}\,, \qquad (3.18)
\end{aligned}
$$

$$
\begin{aligned}
(m^2_{\tilde{\nu}_R})_{ij}v_{jR} &= \frac{1}{\sqrt{2}}\left(-T^\nu_{ji}v_{jL}v_u+T^\lambda_i v_u v_d-T^\kappa_{ijk}v_{jR}v_{kR}\right)-\frac{1}{2}\lambda_i\lambda_j\left(v_u^2+v_d^2\right)v_{jR}+\lambda_j\kappa_{ijk}v_d v_u v_{kR} \\
&-\kappa_{lim}\kappa_{ljk}v_{mR}v_{jR}v_{kR}+\frac{1}{2}Y^\nu_{ji}\lambda_k v_{jL}v_{kR}v_d+\frac{1}{2}Y^\nu_{kj}\lambda_i v_d v_{kL}v_{jR}-Y^\nu_{jk}\kappa_{ikl}v_u v_{jL}v_{lR} \\
&-\frac{1}{2}Y^\nu_{ji}Y^\nu_{lk}v_{jL}v_{lL}v_{kR}-\frac{1}{2}Y^\nu_{ki}Y^\nu_{kj}v_u^2 v_{jR}\;-\;V^{(n)}_{v_{iR}}\,, \qquad (3.19)
\end{aligned}
$$

$$
\begin{aligned}
(m^2_{\tilde{L}_L})_{ij}v_{jL} &= -\frac{1}{8}\left(g^2+g'^2\right)\left(v_{jL}v_{jL}+v_d^2-v_u^2\right)v_{iL}-\frac{1}{\sqrt{2}}T^\nu_{ij}v_u v_{jR}+\frac{1}{2}Y^\nu_{ij}\lambda_k v_d v_{jR}v_{kR} \\
&+\frac{1}{2}Y^\nu_{ij}\lambda_j v_u^2 v_d-\frac{1}{2}Y^\nu_{il}\kappa_{ljk}v_u v_{jR}v_{kR}-\frac{1}{2}Y^\nu_{ij}Y^\nu_{lk}v_{lL}v_{jR}v_{kR}-\frac{1}{2}Y^\nu_{ik}Y^\nu_{jk}v_u^2 v_{jL} \\
&-V^{(n)}_{v_{iL}}\,, \qquad (3.20)
\end{aligned}
$$

where $\tan\beta \equiv \frac{v_u}{v_d}$, $V^{(n)}_x \equiv \partial V^{(n)}/\partial x$ with $x = v_d,\, v_u,\, v_{iR},\, v_{iL}$, and $V^{(n)}$ represents the n–loop radiative correction to the potential, $V = V^{(0)} + V^{(n)}$.

The scale at which the EWSB conditions are imposed is $M_{EWSB} = \sqrt{m_{\tilde{t}_l} m_{\tilde{t}_h}}$, where $m_{\tilde{t}_l}$ and $m_{\tilde{t}_h}$ correspond to the lightest and heaviest stop mass eigenvalues, respectively, measured at M_{EWSB}.

From Eq. (3.20) we can see that in the limit of $Y^\nu_{ij} \to 0$ the VEVs of the left sneutrinos vanish. However, in the case of Eq. (3.19) the limit of *R-parity* conservation does not imply vanishing of the right sneutrinos VEVs. Then is natural to expect that the value of v_{iR} is of the order of M_{EWSB} while the value of v_{iL} is suppressed.

After the successful EWSB, several effective couplings are generated thanks to the VEVs of the neutral scalars. The 5$^{\text{th}}$ term in the superpotential of Eq. (3.3), together with the VEVs of the right sneutrinos generate an effective coupling between both Higgs superfields:

$$
\frac{v_{iR}}{\sqrt{2}} \;\approx\; 1 \text{ TeV}, \qquad (3.21)
$$

$$
\mu^{\text{eff}} \;=\; \lambda_i \frac{v_{iR}}{\sqrt{2}}. \qquad (3.22)
$$

This solves μ problem of the MSSM [75]. In the $\mu\nu$SSM superpotential, the μ term is absent, as well as Majorana masses for neutrinos. This can be obtained invoking a Z_3 symmetry as in the case of the NMSSM, which implies that only trilinear terms are allowed. Actually, this is what one would expect from a high-energy theory where the low-energy modes should be massless and the massive modes of the order of the high-energy scale. As pointed out in Ref. [64], this is precisely the situation in string constructions, where the massive modes have huge masses of the order of the string scale and the massless ones have only trilinear terms at the renormalizable level. Thus one ends up with an accidental Z_3

symmetry in the low-energy theory.

Besides the usual Dirac masses, the presence of Yukawa interaction between up-type Higgs superfield and neutrinos, generates a Dirac mass for them:

$$\left(m_{\mathcal{D}}^{\text{eff}}\right)_{ij} = Y_{ij}^{\nu}\frac{v_u}{\sqrt{2}} \tag{3.23}$$

In addition, the 6$^{\text{th}}$ term in the superpotential generates effective Majorana masses for the right-handed neutrinos

$$\left(m_{\mathcal{M}}^{\text{eff}}\right)_{ij} = 2\kappa_{ijk}\frac{v_{kR}}{\sqrt{2}} \ . \tag{3.24}$$

As a consequence, we can implement naturally a (generalized) electroweak-scale seesaw in the $\mu\nu$SSM, asking for neutrino Yukawa couplings of the order of the electron Yukawa coupling or smaller (see the first two terms of Eqs. (3.33) and (3.35) below) [62, 63, 76, 77, 74, 78]:

$$Y_{ij}^{\nu} \lesssim 10^{-6} \ . \tag{3.25}$$

This generates Dirac masses for neutrinos of the order of $\left(m_{\mathcal{D}}^{\text{eff}}\right)_{ij} \lesssim 10^{-4}$ GeV, and therefore no 'ad hoc' high-energy scales (larger than a TeV) are necessary to reproduce experimentally consistent neutrino masses.

It is worth reminding that the VEVs of the left sneutrinos are much smaller than the other VEVs in Eq. (3.16), and we can estimate their values as $v_{iL} \lesssim m_{\mathcal{D}}^{\text{eff}}$ [62], thus:

$$\frac{v_{iL}}{\sqrt{2}} \lesssim 10^{-4} \text{ GeV} \ . \tag{3.26}$$

This result allows that the generalized seesaw of the $\mu\nu$SSM, which include the neutralinos, works properly, since the third term $\sim v_L^2/M$ in Eqs. (3.33) and (3.35) below, will be of the same order as the first two.

Finally, the 4$^{\text{th}}$ term in the superpotential of Eq. (3.3) generates effective bilinear $\not{R}_p$ couplings

$$\epsilon_i^{\text{eff}} = Y_{ij}^{\nu}\frac{v_{jR}}{\sqrt{2}} \ , \tag{3.27}$$

as those constituting the bilinear R-parity violating model (BRpV, see Ref. [58] for a review).

Recapitulating, the superpotential of Eq. (3.3) serves both the purposes of solving the μ problem and generating non-zero neutrino masses and mixing solving the ν problem. As a consequence of the new terms introduced in the superpotential to solve these challenges, R_p is explicitly broken with its breaking controlled by the small Yukawa couplings for neutrinos, i.e. R_p is restored for $Y_{ij}^{\nu} \to 0$.

A detailed analysis of the parameter space of the $\mu\nu$SSM was carried out in Ref. [63], finding the regions where a successful spontaneous breaking of the electroweak symmetry happens avoiding the presence of false minima and tachyons, as well as fulfilling the constraints on Landau Poles.

Let us remark that since only dimensionless trilinear couplings are present in the superpotential of Eq. (3.2), the EWSB is determined by the soft SUSY-breaking terms of the scalar potential. Thus all known particle physics phenomenology can be reproduced in the $\mu\nu$SSM with one scale, the about 1 TeV scale of the soft terms, avoiding the introduction of 'ad-hoc' high-energy scales. Upon EWSB, not only Higgses but also left and right sneu-

trinos acquire VEVs as discussed above and, as we will review in Section 3.3, fields with the same color, electric charge and spin mix giving rise to a rich phenomenology.

3.3 The spectrum of the model

Similar to the MSSM, where the couplings and Higgs VEVs determine the mixing of Bino, Wino and Higgsinos, producing the four neutralino states, the new couplings and sneutrino VEVs in the $\mu\nu$SSM induce new mixing of states [62, 63]. Summarizing, in the colorless sector, there are ten neutral fermions (neutralinos-neutrinos), five charged fermions (charginos-leptons), eight neutral scalars and seven neutral pseudoscalars (Higgses-sneutrinos), and seven charged scalars (charged Higgses-sleptons). The associated mass matrices were studied in detail in Ref. [63]. The reader can consult the full form in Appendix A, with the convention of using for the eigenstates the names of the detected particles: neutrinos, leptons, Higgses.

Concerning the neutral scalars, the right and left sneutrino VEVs lead to mixing of the neutral Higgses with the sneutrinos in the scalar potential, giving rise to the 8×8 ('Higgs') mass matrices for scalar and pseudoscalar states. They are written (before and) after replacing the values of the soft masses with the corresponding VEVs obtained through the minimization conditions of Eqs. (3.17)-(3.20), assuming that the sfermion soft mass matrices are diagonal in flavor space, as discussed above Eq. (3.5). Note that after rotating away the pseudoscalar would be Goldstone boson, we are left with seven pseudoscalar states. It is also worth noticing here that the 5×5 Higgs-right sneutrino submatrix is almost decoupled from the 3×3 left sneutrino submatrix, since the mixing occurs through terms proportional to Y^{ν}_{ij} or v_{iL} (see Eqs. (A.9)-(A.11) and (A.25)-(A.27)), and these quantities are very small in order to satisfy neutrino data, as shown in Eqs. (3.25) and (3.26). Besides, the former 5×5 submatrix is of the NMSSM type, apart from the small corrections proportional to Y^{ν}_{ij} (and the fact that in the NMSSM there is only one singlet).

Charged Higgs states mix with right and left sleptons to form the 8×8 ('charged Higgs') mass matrix. Similar to the neutral scalar mass matrices where some sectors are decoupled, the 2×2 charged Higgs submatrix is decoupled from the 6×6 slepton submatrix (see Eqs. (A.38)-(A.41)). In addition, the right sleptons are decoupled from the left ones as can be seen in Eq. (A.42), since the mixing terms are suppressed by the electron-type Yukawa couplings or v_{iL}.

The squark mass matrices, also written in Appendix A. When compared to the MSSM/ NMSSM case, they maintain their structure essentially unaffected, provided that one uses the effective μ term of Eq. (3.22), and neglects the terms proportional to Y^{ν}_{ij}, v_{iL} and λ'_{ijk}.

The neutral fermion ('neutrino') mass matrix includes the neutral gauginos, the Higgsinos, left-handed neutrinos and right-handed neutrinos. It presents a seesaw-like structure with the left-handed neutrinos on the one side and the rest of neutralinos, with masses around the EWSB scale on the other side, and Dirac masses of the order of the Eq. (3.23). This sector will be discussed below in the context of neutrino physics, since it is crucial for determining neutrinos masses and mixing.

Concerning the charged fermions, the MSSM charginos mix with the leptons in the $\mu\nu$SSM giving rise to the 5×5 ('lepton') mass matrix shown in Appendix A. Nevertheless, the 2×2 chargino submatrix is basically decoupled from the 3×3 lepton submatrix (see Eq. (A.71) where the off-diagonal entries are suppressed by Y^{ν}_{ij}, Y^{e}_{ij}, v_{iL}). The former is like the one of the MSSM/NMSSM provided that one uses the effective μ term of Eq. (3.22). Finally, down- and up-quark mass matrices are also given in Appendix A.

3.4 Higgs sector

In the previous section we have sketch the structure of the scalar sector of the $\mu\nu$SSM. There we have mentioned that the left sneutrinos are in practice decoupled from the rest of the mass matrix, leaving a structure for the Higgs sector similar to the NMSSM. Note however that the right sneutrino-Higgs sector in the $\mu\nu$SSM is extended with two additional scalar singlets with respect to the NMSSM. Thus some differences might appear. This has been analyzed in detail in [79].

The mixing between the Higgs states and the right handed neutrinos, Eq. (A.3) and Eq. (A.4), is in general large, but can be suppressed with the condition (see [79]):

$$A_{\lambda_i} = \frac{2\mu}{\sin 2\beta} - \frac{2}{\lambda_i}\sum_{j,k}\kappa_{ijk}\lambda_j\nu_k^c, \tag{3.28}$$

$$A_{\lambda_i} = \frac{2}{\lambda_i}\sum_{j,k}\kappa_{ijk}\lambda_j\nu_k^c, \tag{3.29}$$

for the CP-even and CP-odd sectors, respectively. This conditions can be applied to obtain very light pure singlet scalars, or to make the lightest Higgs-like scalar as heavy as possible. Scenario which produces an upper bound similar to the one of the NMSSM [79], which can reach the 125 GeV even at tree level, for small values of $\tan\beta$ [80] :

$$\left(m_h^{tree}\right) \leq M_Z^2\left(\cos^2 2\beta + \frac{2\lambda\cos^2\theta_W}{g_2^2}\sin^2 2\beta\right). \tag{3.30}$$

The presence of multiple scalar singlets in the spectrum can also affect the Higgs decay phenomenology. As studied in Ref. [79], the coupling Higgs-singlet-singlet could lead to longer decay chains, when kinematically accessible, like

$$h^{SM} \to 2\widetilde{\nu}_{1R}, \quad h^{SM} \to 2\widetilde{\nu}_{2R} \to 4\widetilde{\nu}_{1R}. \tag{3.31}$$

This scalars will eventually decay to fermions, causing multilepton or multijets signals in the decay of the Higgs boson. The presence of light right-handed neutrinos can affect as well the decay chain

$$h^{SM} \to 2\nu_R\nu_R \to 2\nu 2\widetilde{\nu}_{1R}. \tag{3.32}$$

This sequence will now produce a multijet or multilepton signal with the addition of missing energy.

On top of that, some of these decays can be suppressed enough to make the proper decay length of the particles involved comparable to the size of the detector, thus producing displaced vertices in the decay of the Higgs bosons. This possibility, with the light singlets decaying to τ leptons has been studied in Ref. [81].

3.5 Neutrino physics

Concerning the neutral fermions, we have already discussed in Subsection 3.2 that effective Majorana masses for right-handed neutrinos of the order of the EWSB scale are dynamically generated in the $\mu\nu$SSM (see Eq. (3.24)). In addition, the MSSM neutralinos mix with the

left- and right-handed neutrinos giving rise to the 10×10 neutral fermion ('neutrino') mass matrix shown in Eq. (A.65). Notice that the structure of this matrix is that of a generalized electroweak-scale seesaw, since it involves not only the right-handed neutrinos but also the neutralinos. Because of this structure, data on neutrino physics [82, 83, 84] can easily be reproduced at tree level [62, 63, 76, 77, 74, 78], even with diagonal Yukawa couplings [76, 74], i.e. $Y^{\nu}_{ii} = Y^{\nu}_{i}$ and vanishing otherwise.

Qualitatively, we can understand this in the following way. First of all, the three neutrino masses are going to be very small since the entries of the first three rows (and columns) of the matrix of Eq. (A.65) are much smaller than the rest of the entries. Notice in this sense that the latter are of the order of the electroweak scale, whereas the former are of the order of the Dirac masses for neutrinos (see (Eq. (3.23))) [62, 63]. Second, from this matrix one can obtain a simplified formula for the effective mixing mass matrix of the light neutrinos [74]:

$$(m^{\rm eff}_{\nu})_{ij} \simeq \frac{Y^{\nu}_{i} Y^{\nu}_{j} v_u^2}{6\sqrt{2}\kappa v_R}(1-3\delta_{ij}) - \frac{v_{iL} v_{jL}}{4M^{\rm eff}} - \frac{1}{4M^{\rm eff}}\left[\frac{v_d\left(Y^{\nu}_{i} v_{jL} + Y^{\nu}_{j} v_{iL}\right)}{3\lambda} + \frac{Y^{\nu}_{i} Y^{\nu}_{j} v_d^2}{9\lambda^2}\right] , \tag{3.33}$$

with

$$M^{\rm eff} \equiv M - \frac{v^2}{2\sqrt{2}\left(\kappa v_R^2 + \lambda v_u v_d\right)\ 3\lambda v_R}\left(2\kappa v_R^2 \frac{v_u v_d}{v^2} + \frac{\lambda v^2}{2}\right) , \tag{3.34}$$

where $M = \frac{M_1 M_2}{g'^2 M_2 + g^2 M_1}$. Here is assumed $\lambda_i = \lambda$, $v_{iR} = v_R$, and $\kappa_{iii} \equiv \kappa_i = \kappa$ and vanishing otherwise. Also diagonal Yukawa couplings are considered $Y^{\nu}_{ii} \equiv Y^{\nu}_{i}$. Using this approximate formula it is easy to understand how diagonal Yukawas can give rise to off-diagonal entries in the mass matrix. The key point are clearly the extra contributions given by the terms which are not proportional to δ_{ij} (all of them except the second one in Eq. (3.33)) with respect to the ordinary seesaw, where they are absent.

It is worth noticing that the first term (and the second) in Eq. (3.33) is generated through the mixing of left-handed neutrinos ν_L with right-handed neutrinos ν_R-Higgsinos. The rest of the terms also include the gaugino mixing. Let us also remark, that the last two terms in brackets are proportional to v_d, and therefore negligible in the limit of large or even moderate $\tan\beta$ provided that λ is not too small. Concerning Eq. (3.34), the first term is also negligible in this limit, and for typical values of the parameters involved in the seesaw also the second one, i.e. $M^{\rm eff} \sim M$. Under this assumption, the third term in Eq. (3.33) is generated only through the mixing of left-handed neutrinos with gauginos. Therefore, we get a very simple formula that can be used to understand the seesaw mechanism in this model in a qualitative way, that is

$$(m^{\rm eff}_{\nu})_{ij} \simeq \frac{Y^{\nu}_{i} Y^{\nu}_{j} v_u^2}{6\sqrt{2}\kappa v_R}(1-3\delta_{ij}) - \frac{v_{iL} v_{jL}}{4M} . \tag{3.35}$$

As we can understand from the above discussion, neutrino physics in the $\mu\nu$SSM is closely related to the parameters and VEVs of the model, since the values chosen for them must reproduce current data on neutrino masses and mixing angles. For example, for the typical values of the parameters and VEVs in Eqs. (3.21), (3.25) and (3.26), neutrino masses $\lesssim 0.1$ eV as expected, can easily be reproduced.

Let us finally point out that all these arguments explained here give a kind of answer

to the question, why the mixing angles are so different in the quark and lepton sectors? From the $\mu\nu$SSM viewpoint, because no generalized seesaw exists for the quarks.

3.6 Dark Matter in the $\mu\nu$SSM

As explained before, *R-parity* is not a symmetry of the $\mu\nu SSM$ superpotential. Thus the LSP is not stable. Neutralinos or sneutrinos, with very short lifetimes, can no longer be dark matter candidates. Nonetheless, the gravitino can still be a viable DM candidate [85, 86]. If the Gravitino is the LSP, its decay width would be suppressed by the inverse of the Planck mass and by the $\not{R}_p$ parameters. Leading to a Gravitino lifetime larger than the age of the Universe. Searches for $\mu\nu$SSM gravitino dark matter in Fermi-LAT data through gamma-ray lines have been carried out in Refs. [87, 88, 89, 90], obtaining stringent constraints on the gravitino mass and the lifetime.

It is worth noticing that when the gravitino is assumed to be the LSP, the lightest particle of the remaining SUSY spectrum would in fact be the next-to-LSP (NLSP). Nevertheless, the analysis of their phenomenology at the LHC is not altered, since they also decay into ordinary particles using the same channels as if they were the LSP. For instance, as shown in [79], the decay of a neutralino through the channel $\tilde{\chi}^0 \to \Psi_{3/2}\gamma$, can be estimated as:

$$c\tau^{3/2}_{\tilde{\chi}^0} \approx 80 \text{ km } \left(\frac{m_{3/2}}{10 \text{ KeV}}\right)^2 \left(\frac{m_{\tilde{\chi}^0}}{50 \text{ GeV}}\right)^{-5}. \tag{3.36}$$

And one can easily see that the partial width to gravitinos is small provided that the gravitino mass is not much smaller than 10 KeV. One can see for example that for a 100 GeV neutralino, the decay width would be comparable to the ones to SM particles, with decay lengths from mm-m, only if the Gravitino mass is below the KeV scale.

Concerning other cosmological issues in the $\mu\nu$SSM, in Ref. [91] the generation of the baryon asymmetry of the universe was analyzed in the model, with the interesting result that electroweak baryogenesis can be realized.

3.7 The $\mu\nu$SSM with one generation of right-handed neutrinos

The $\mu\nu$SSM as is presented in [62, 63] includes three generations of right-handed neutrino superfields $\hat{\nu}^c$. These superfields, as explained in previous sections, couple with the Higgs doublets to generate an effective μ term after EWSB, and couple in a Yukawa term with left handed neutrino superfields to generate neutrino masses.

For both mechanisms to work is sufficient to include only one generation of $\hat{\nu}^c$. In this case, the generation of the effective μ-term comes from a single right sneutrino. The generated neutrino seesaw is only capable to produce mass for one of the neutrinos, while the two remaining neutrinos receive the mass radiatively. This is obvious if one realizes that the three rows in the neutral fermion mass matrix corresponding to the neutrinos are equal at tree level, thus the mass matrix has two zero eigenvalues. This possibility has been studied in the work [77].

This possibility is equivalent to take the limit in the three generation case where $\lambda_i \equiv \lambda\delta_{i1}$, $Y^\nu_{ij} \equiv Y^\nu_i\delta_{j1}$, $\kappa_{ijk} \equiv \kappa\delta_{1i}\delta_{1j}\delta_{1k}$, $T^\lambda_i \equiv T^\lambda\delta_{i1}$, $T^\nu_{ij} \equiv T^\nu_i\delta_{j1}$ and $T^\kappa_{ijk} \equiv T^\kappa\delta_{1i}\delta_{1j}\delta_{1k}$. Obviously there would be only one relevant right sneutrino VEV, labeled as v_R. The

phenomenology is similar to the three generation case regarding the Higgs physics and the collider signatures, provided one considers a value of v_R large enough to maintain the same μ_{eff}. However, the reduction of the model has bigger consequences regarding neutrino physics. As mentioned, only one family of neutrinos get masses at tree level, which can be calculated [92] as:

$$m_\nu = \frac{1}{4M_{\rm eff}} \sum_i \left[v_i^2 + v_d \left(\frac{2 v_i Y_{\nu_i}}{\lambda} + \frac{v_d Y_{\nu_i}^2}{\lambda^2} \right) \right], \tag{3.37}$$

with

$$M_{\rm eff} \equiv M \left[1 - \frac{v^2}{\sqrt{2} M (\kappa\, v_R^2 + \lambda v_d v_u)\, \lambda v_R} \left(\kappa\, v_R^2 \frac{v_d v_u}{v^2} + \frac{1}{4} \lambda v^2 \right) \right], \tag{3.38}$$

where $v^2 \equiv v_d^2 + v_u^2$, and

$$\frac{1}{M} \equiv \frac{g'^2}{M_1} + \frac{g^2}{M_2}\ . \tag{3.39}$$

Notice that we can simplify Eq. (3.37) taking into account that the second term is proportional to v_d, and therefore considering it negligible in the limit of large or even moderate $\tan\beta \equiv v_u/v_d$ provided that λ is not too small. In Eq. (3.38), the second term is also negligible in this limit, and for typical values of the parameters involved in the seesaw also the third one, i.e. $M_{\rm eff} \approx M$. Under these assumptions, the first term in Eq. (3.37) is generated only through the mixing of left-handed neutrinos with gauginos, and we arrive to the approximate formula:

$$m_\nu \approx \sum_i \frac{v_i^2}{4M}. \tag{3.40}$$

3.8 Previous collider studies

The presence of *R-parity* breaking interactions in the $\mu\nu$SSM produces a rich phenomenology in contrast to the *R-parity* conserving models, generically characterized by signals including a large amount of missing transverse energy. Moreover, the smallness of the $\not{R}_p$ interactions, directly related to the smallness of neutrino mass scale, could produce the unusual scenario of displaced vertices. In addition, the presence of light singlets could complicate the decay chains of the particles, making the collider phenomenology even more diverse.

The collider phenomenology has already started to be studied. The novel Higgs decays in the $\mu\nu$SSM, as mentioned in Sec. 3.4, were studied in [79], as well as the decays of the heavy Higgs. When the lightest neutralinos are lighter than the heavy CP-even Higgs in the $\mu\nu$SSM, the decays $H \to \tilde{\chi}^0 \tilde{\chi}^0$ are kinetically accessible and can produce distinctive signals such as $H \to 2b2\bar{b}2\nu$ or even $H \to 4b4\bar{b}2\nu$. In some cases also produced at displaced vertices. If all neutralinos are heavier, the decays to lighter scalar singlets could produce signals with high multiplicity of b-quarks such as $H \to 2b2\bar{b}$ and $H \to 4b4\bar{b}$. Finally, if the light scalar singlets are light enough, the decay $\widetilde{\nu}_R \to b\bar{b}$ is kinematically forbidden and decays as $H \to 2\tau 2\bar{\tau}$ and $H \to 4\tau 4\bar{\tau}$ are possible. This gives an idea of the characteristic cascades expected in the production of Higgs bosons.

Z decay
4 displaced leptons/τ-jets/jets/photons+$\not{E}_T$
4 leptons/τ-jets/jets/photons

$W^{\pm}$ decay
prompt lepton/τ-jet+
2 displaced leptons/τ-jets/jets/photons+$\not{E}_T$

Table 3.1: Non-standard decays studied in Ref. [93].

Already mentioned before is the work of Ref. [81], where the authors analyze the detection possibilities of the Higgs Boson decaying to a pair of neutralinos that eventually decay to $\nu\tau\bar{\tau}$, with a significant proper decay length. They found that ATLAS and CMS can detect this kind of signature either by looking to multilepton events produced in the SUSY cascade decay chain, when relaxing the requirement for the leptons to come from the primary vertex, or searching for tracks not-pointing back to the primary vertex. In both cases having a moderately high missing transverse energy due to multiple neutrinos.

Finally, the effect of very light scalar singlets or right-handed neutrinos on the decay pattern of electroweak gauge bosons has been studied in [93]. The non-standard decays $W^{\pm} \to \ell\nu_R$, $Z^0 \to \nu_R\nu_R$ and $Z^0 \to \tilde{\nu}_R\tilde{\nu}_R$, lead to the signatures shown in Table 3.1.

These decay channels are constrained by the measured value of the total gauge boson widths, also by the invisible decay width when the right-handed neutrinos decay outside the detector, and constrained by the measured partial width to 4 prompt leptons.

In that work, the authors find regions in the parameter space where the new decays are below the experimental limit. Moreover, they find that the small partial width into these unusual channel makes this signal to be beyond the sensitivity of the LHC, even at High Luminosity phase. They find however, that the future linear colliders could have enough sensitivity to see them.

The work of Ref. [77] makes a thorough study of the phenomenological implications at colliders of the $\mu\nu$SSM focusing on the scenario of a neutralino LSP, studying the possible decay channels and the proper decay length in correlation with neutrino properties. They also study the implication of the presence of multiple singlet superfields in the model. In that work the authors also discuss the possible differences in collider phenomenology of the model with respect to other R-parity breaking schemes.

In this chapter we have presented the structure of the $\mu\nu$SSM and summarize the results of the previous phenomenological analysis of the model. In the next chapters we will analyze new interesting scenarios of the model that had not been studied yet, such as the signals predicted at hadron colliders when the left sneutrino (bino) is the LSP.

Chapter 4

The left sneutrino as LSP

The present chapter, based in the work developed in Ref. [94] analyses the main phenomenological aspects if the left sneutrino as the LSP in the context of the $\mu\nu$SSM.

The left-handed lepton fermion $SU(2)$ doublet (L_i^a), has a supersymmetric counterpart formed by the left slepton and the left sneutrino, constituting the left lepton superfield $\hat{L}_i^a$. Before electroweak symmetry breaking, as both scalars belong to the same doublet, they receive the same contributions to the mass, coming from the soft SUSY breaking lepton mass $m^2_{\widetilde{L}}$. After EWSB the left sleptons receive an extra contribution to the mass as we will see later. Therefore, is a common feature in all supersymmetric models that the left slepton mass is always larger than the left sneutrino mass. Thus, whenever the mechanism generating the soft SUSY breaking masses at low energy causes $m^2_{\widetilde{L}}$ to be small, the left sneutrino will always be the LSP.

In models with *R-parity* conservation there are three neutral stable particles that could be thereupon DM candidates: the lightest sneutrino, the lightest neutralino and the gravitino. The scenario of a left sneutrino reproducing the dark matter density of the universe has been largely ruled out by direct searches [95, 96, 97, 98]. Accordingly, typical collider studies of the left sneutrino assume that it decays involving somehow the neutral fermionic LSP. On the contrary, the collider studies assuming RPV through the trilinear couplings described in Eq. (2.13) typically assume a rather simple phenomenology, mediated by a particular coupling. In comparison, the decays of the sneutrino in the $\mu\nu$SSM can be much richer.

Unlike *R-parity* conserving SUSY models, the scalar sector of the $\mu\nu$SSM mixes every spin-0 neutral particle. Neutral Higgs states, the left sneutrinos and right sneutrinos mix in a single mass matrix. With the assumption of CP-conservation, that means eight scalars on each sector. The large number of scalar states and the amount of parameters controlling the mass matrices could lead us to the misconception that we could choose the parameters to get any desired structure form the mass matrix. On the contrary, as we will see during the present chapter, the influence of the input parameters over a number of phenomenological observables sets tight constraints to the possible structures of the scalar mass matrix.

4.1 Left sneutrino mass

The full form of the scalar mass matrices can be consulted in Appendix A. Here one could notice that all the off-diagonal elements involving the left sneutrino ($m^2_{\widetilde{\nu}_{iLX}}$) are proportional to either v_{iL} or to Y^ν. Given the v_{iL} dependence shown in Sec. 3.2, is straightforward to see that in the limit of $Y^\nu \ll 1$ the left sneutrino decouples from the rest of the scalar

states. On the other hand the right-sneutrino sector mixing with the Higgs sector is not necessarily small. This could be the case when the large value of λ is utilized to contribute to the tree-level mass of the light Higgs Boson.

As explained in Sec. 3.1, the lepton doublet soft SUSY breaking mass should be diagonal, therefore also the off-diagonal elements of the left sneutrino matrix vanish in the limit of *R-parity* conservation. Since the mass sub-matrix for left sneutrinos is effectively decoupled and diagonal, the mass corresponding to the physical left sneutrino state can be well approximated by the value of the diagonal mass entry corresponding to the left sneutrino flavor state ($m^2_{\widetilde{\nu}_{iL}\widetilde{\nu}_{iL}}$):

$$\begin{aligned} m^2_{\widetilde{\nu}^{\mathcal{R}}_{iL}\widetilde{\nu}^{\mathcal{R}}_{jL}} &= \left(m^2_{\widetilde{L}_L}\right)_{ij} + \frac{1}{4}(g^2+g'^2)v_{iL}v_{jL} + \frac{1}{8}(g^2+g'^2)(v_{kL}v_{kL}+v_d^2-v_u^2)\delta_{ij} \\ &\quad + \frac{1}{2}Y^\nu_{ik}Y^\nu_{jk}v_u^2 + \frac{1}{2}Y^\nu_{ik}Y^\nu_{jl}v_{kR}v_{lR} \end{aligned} \tag{4.1}$$

After electroweak symmetry breaking the value of v_{iL} is fixed by the minimization equations of the scalar potential, therefore this VEVs are not independent parameters and its value should be read form the solutions of Eqs. (3.17)-(3.20). However, from a phenomenological perspective results useful to consider the left sneutrino VEV as a input parameter and fix $\left(m^2_{\widetilde{L}_L}\right)_{ij}$ to the value required to make the corresponding v_{iL} a minimum of the scalar potential, roughly:

$$m^2_{\widetilde{L}_{iL}} \approx \frac{1}{8}\left(g^2+g'^2\right)\left(v_u^2-v_d^2\right) + \frac{Y^\nu v_u}{2v_{iL}}v_R\left(-\sqrt{2}A^\nu - \kappa v_R + \frac{\lambda v_R}{\tan\beta}\right), \tag{4.2}$$

With this strategy one can trade the soft mass by its value form the minimization equations on the expression 4.1:

$$\begin{aligned} m^2_{\widetilde{\nu}^{\mathcal{R}}_{iL}\widetilde{\nu}^{\mathcal{R}}_{jL}} &= \frac{1}{4}(g^2+g'^2)v_{iL}v_{jL} + \frac{1}{2}Y^\nu_{ik}Y^\nu_{jk}v_u^2 + \frac{1}{2}Y^\nu_{ik}Y^\nu_{jl}v_{kR}v_{lR} + \frac{\delta_{ij}}{v_{jL}}\left[-\frac{1}{\sqrt{2}}T^\nu_{ik}v_u v_{kR}\right. \\ &\quad \left. + \frac{1}{2}Y^\nu_{ik}\left(\lambda_l v_d v_{kR}v_{lR} + \lambda_k v_d v_u^2 - \kappa_{klm}v_u v_{lR}v_{mR} - Y^\nu_{mk}v_{mL}v_u^2 - Y^\nu_{ml}v_{mL}v_{lR}v_{kR}\right)\right] \end{aligned} \tag{4.3}$$

As can be seen in the appendix, the difference between the scalar and pseudoscalar left sneutrino mass entries are just a term proportional to v_{iL}. This term comes form the D-term contributions to the scalar potential originated by the $U(1)_Y$ and $SU(2)_L$ vector superfields:

$$m^2_{\widetilde{\nu}^{\mathcal{I}}_{iL}\widetilde{\nu}^{\mathcal{I}}_{jL}} = m^2_{\widetilde{\nu}^{\mathcal{R}}_{iL}\widetilde{\nu}^{\mathcal{R}}_{jL}} - \frac{1}{4}\left(g^2+g'^2\right)v_{iL}v_{jL} \tag{4.4}$$

Following the discussion in Sec. 3.2 is straightforward to see that this term is negligible. Therefore we can consider that, when they are sufficiently light, both behave as the LSP. For this reason we are going to refer to them as co-LSP.

From Eq. (4.3) we can retain only the dominant terms, which go with the smaller powers of Y^ν and v_L, to arrive to a simpler expression for the left sneutrino mass:

$$m^2_{\widetilde{\nu}^{\mathcal{I}}_{iL}\widetilde{\nu}^{\mathcal{I}}_{jL}} \approx \frac{Y^\nu v_u}{2v_{iL}} v_R \left(-\sqrt{2}A^\nu - \kappa v_R + \frac{\lambda v_R}{\tan\beta}\right) \tag{4.5}$$

At first glance one can see that unless $\tan\beta \sim 1$ and κ is not larger than λ, the value of the trilinear soft neutrino coupling A^ν is restricted to negative values, otherwise the left sneutrino will have a negative mass. Even if in some cases A^ν could be positive, its value can not be large.

As has been discussed in section ref, the value of v_{iL} has to be roughly $Y^\nu v_u$ to predict the correct neutrino physics in most of the parameter space, this makes obvious that the fraction in front of (4.5) is of order one. Also, v_R is naturally on the order of the TeV, as explained in Sec. 3.2. Evidently, if A^ν is just around a common SUSY scale in the ballpark of the TeV, the mass of the left sneutrino would be dominated by this term and would typically be slightly below the TeV. If A^ν is however of the order of -100 GeV, the cancellation of this term with the second could easily make the left sneutrino relatively light, for a moderated to large value for $\tan\beta$.

From a theoretical point of view this means that the mechanism breaking SUSY at high energy needs to produce a low-energy set of soft parameters on the TeV scale, with the exception of $m_{\widetilde{L}_{iL}}$ and A^ν, which should be of the order of 100 GeV. Once this is true, the minimization equations fix the correct values for the VEV's.

Equation (4.5) is to be understood as a tree-level approximation. Even in the case of universal values for the input parameters of each generation, the mass states would not be exactly degenerate, it will be broken by the effect of the different Yukawa couplings with the H_d doublet through radiative contributions to the mass matrix. In any case this difference is going to be negligible.

When a left sneutrino is the LSP, is natural to have a left slepton as the NLSP. As can be seen in Appendix A the mixing between charged Higgs and sleptons is feeble and vanish in the limit of *R-parity* conservation, analogously to the left sneutrinos. Also the mixing between left and right sleptons, proportional to the lepton Yukawa coupling, is not large. Altogether the left slepton physical mass is going to be very close to the diagonal mass entry:

$$\begin{aligned} m^2_{\widetilde{e}_{iL}\widetilde{e}^*_{jL}} &= m^2_{\widetilde{\nu}^{\mathcal{R}}_{iL}\widetilde{\nu}^{\mathcal{R}}_{jL}} - \frac{1}{4}(g^2+g'^2)v_{iL}v_{jL} + \frac{g^2}{4}(v_u^2 - v_d^2 - v_{kL}v_{kL})\delta_{ij} + \frac{g^2}{4}v_{iL}v_{jL} \\ &\quad -\frac{1}{2}Y^\nu_{ik}Y^\nu_{jk}v_u^2 + \frac{1}{2}Y^e_{il}Y^e_{jl}v_d^2 \end{aligned} \tag{4.6}$$

Therefore, the difference in mass between left sleptons and neutrinos is mainly coming form the D-term contribution $\frac{g^2}{4}(v_u^2 - v_d^2) \approx -m_W^2 \cos 2\beta$. The previous result is natural from a theoretical point of view, since both belong to the same $SU(2)$ doublet. May the reader notice also that this contribution can only be negative for very small values of $\tan\beta$.

Summarizing, we have shown that is viable to obtain in the spectrum of the $\mu\nu$SSM left sneutrinos as LSPs. They can in principle belong to any of the three families of the SM, and if the value of $m_{\widetilde{L}_{iL}}$ and A^ν is universal, the three of them could be co-LSPs. The phenomenological implications of the dominant flavor of the LSP are nevertheless of great importance, since the decay modes of the third family of left-sneutrinos are different with respect of the first two. In addition, the left slepton is slightly heavier and naturally the NLSP.

4.2 Production at colliders

It is usual in phenomenological studies of *R-parity* violating models to consider the single production of the considered SUSY particle through some of the usual *R-parity* violating trilinear couplings described in Sec. 3.1. When the appropriate λ_{ijk} are allowed is possible the direct production of a single sneutrino at lepton colliders. And when the proper λ'_{ijk} couplings are allowed, is possible to produce them also Hadron colliders. In the $\mu\nu$SSM however, this terms ere effectively generated as described in Sec. 3.2 and small, therefore they are ineffective to generate processed at colliders.

The left sneutrino can be generated however in pairs, through the Drell-Yann process mediated by a Z boson. This is possible both in Hadron and electron-positron colliders, and has been studied for *R-parity* conserving models (see for example [99, 100, 101, 102, 103, 104]). Moreover, since the mass gap between the left sneutrinos and sleptons is tight, the production of left sleptons pairs is also a source of sneutrino pairs through the production of Drell-Yann processes mediated by Z and γ with the subsequent decay to sneutrinos and an off-shell $W^{\pm}$. Also the production of sneutrino-slepton, mediated by a $W^{\pm}$ in the s-channel, would be an important source of sneutrino pairs. The first generation of left sneutrinos could in principle also be generated at electron-positron colliders through a diagram with a chargino in the t-channel. However this diagram is irrelevant if the chargino is sufficiently decoupled.

We will elaborate more on the production of the left sneutrino at colliders during the chapters 5 and 6, where we discuss the possible detection of the sneutrino at the LHC.

4.3 Decay of the Left sneutrino

In *R-parity* conserving supersymmetric models the LSP is bounded to be stable. In the $\mu\nu$SSM however, *R-parity* is broken and the LSP decays. In addition, as has been already pointed out, in the $\mu\nu$SSM the rupture of the discreet symmetry is small, thus any decay that would violate an exact *R-parity* is strongly suppressed in comparison with the other available decays. The result is that all the particle spectrum decays through *R-parity* conserving decays whenever kinematically accessible. The decay chain will eventually end up producing the LSP, which would decay through some of the available *R-parity* violating decays. This makes crucial the decay pattern of the LSP, since would dictate the signals expected from the production and decay of any of the heavier SUSY particles.

The relevant interactions of the left sneutrino are given in App. B. Although the number of terms in the expressions is large, only some of them are typically of relevance, and we will discuss some approximations that make possible to express the most relevant contributions in terms of the parameters of the Lagrangian.

In the notation of App. B, Z^H_{il} represents the l-th composition in the flavor basis defined on App. A, for the i-th scalar mass eigenstate. For instance, if the lightest scalar, after the SM higgs, were a pure left electron sneutrino, Z^H_{2l} will be one if $l = 6$ and zero otherwise. Since the left sneutrinos are almost pure, if we want to identify the dominant terms on Eq. (B), we retain only the terms with l equal 4+n (6+n) when using one (three) generation of right handed neutrinos, and i equal 1 (2) if the sneutrino is lighter (heavier) than the Higgs boson, being $n \in 1, 3$ corresponding to the lepton families. However, is straightforward to see that there is no term proportional to this mixing matrix entry, and the dominant values of the mixing matrices corresponding to SM fermions, like for example $U^e_{L,11}$ and $U^e_{R,11}$ for the coupling with electrons.

This is coherent with the fact that there is no term in the Lagrangian coupling the left sneutrino and SM fermions, breaking *R-parity*. There exist however in the scalar potential, after EWSB, terms of the form *left sneutrino-Higgs bosons-Higgs boson*. Which are proportional either to Y^ν or v_L.

The next dominant contributions to the interaction between the left sneutrino and SM particles would involve terms where at most one of the matrix entries does not correspond to the dominant flavor composition. One can understand diagrammatically this interaction as Feynman diagrams with one mass insertion in one of the external legs, as can be seen in Figs. 4.1 and 4.2. Notice that none of the mixings between SM particles and SUSY particles is large, but since all of the decays have to proceed through these small mixings, every channel is a priory relevant.

4.3.1 Decay into quarks

There is no fermions charged under SU(3) in the supersymmetric part of the spectrum, with whom the quarks could mix. Therefore the decay to quarks can only proceed through left sneutrino-Higgs mixing ($Z^H_{2,2/1}$).

In the previous section we have justified the smallness of the left sneutrino flavor composition of the Higgs boson, yet the singlet composition of it is not necessarily small. Notice nevertheless the constraints to a large singlet composition coming from Higgs signal strengths measured at the LHC. Therefore, we will assume in the following a small value of the singlet composition of the Higgs bosons. This is in most regions of parameter space achievable, as explained in Sec. 3.4.

Using the mass insertion approximation on Fig. 4.1 the value of this mixing would be:

$$Z^H_{2,1} \approx \frac{m^2_{H^{\mathcal{R}}_d \widetilde{\nu}^{\mathcal{R}}_i}}{{M_H}^2}; \quad Z^H_{2,2} \approx \frac{m^2_{H^{\mathcal{R}}_u \widetilde{\nu}^{\mathcal{R}}_i}}{{M_h}^2}; \quad Z^A_{2,1} \approx \frac{m^2_{H^{\mathcal{I}}_d \widetilde{\nu}^{\mathcal{I}}_i}}{{M_A}^2} \tag{4.7}$$

However, the mass of the LSP could easily be to close to the mass of the Higgs Boson, making this simplification not valid. Instead we can get to a better approximation through a simple process. Since the submatrices corresponding to the Higgs sector and the left sneutrino are effectively decoupled, we can perform a rotation on the Higgs subsector to diagonalize it, and the terms mixing both sectors are still going to be small. After that, we can approximate the diagonal values by the physical masses, and then apply the mass insertion approximation. Finally, the mixing between the approximate mass eigenstates can be translated to an approximation of the flavor composition writing the mass eigenstates in terms of the flavor basis. The result is:

$$Z^H_{2,1} \approx \frac{\sin\alpha(m^2_{H^{\mathcal{R}}_d \widetilde{\nu}^{\mathcal{R}}_i} \sin\alpha + m^2_{H^{\mathcal{R}}_u \widetilde{\nu}^{\mathcal{R}}_i} \cos\alpha)}{{M_H}^2 - {M_{\widetilde{\nu}^{\mathcal{R}}_i}}^2} - \frac{\cos\alpha(m^2_{H^{\mathcal{R}}_u \widetilde{\nu}^{\mathcal{R}}_i} \sin\alpha - m^2_{H^{\mathcal{R}}_d \widetilde{\nu}^{\mathcal{R}}_i} \cos\alpha)}{{M_h}^2 - {M_{\widetilde{\nu}^{\mathcal{R}}_i}}^2} \tag{4.8}$$

$$Z^H_{2,2} \approx \frac{\cos\alpha(m^2_{H^{\mathcal{R}}_u \widetilde{\nu}^{\mathcal{R}}_i} \sin\alpha - m^2_{H^{\mathcal{R}}_d \widetilde{\nu}^{\mathcal{R}}_i} \cos\alpha)}{{M_h}^2 - {M_{\widetilde{\nu}^{\mathcal{R}}_i}}^2} + \frac{\cos\alpha(m^2_{H^{\mathcal{R}}_d \widetilde{\nu}^{\mathcal{R}}_i} \sin\alpha + m^2_{H^{\mathcal{R}}_u \widetilde{\nu}^{\mathcal{R}}_i} \cos\alpha)}{{M_H}^2 - {M_{\widetilde{\nu}^{\mathcal{R}}_i}}^2} \tag{4.9}$$

$$Z^A_{2,1} \approx \frac{\sin\beta(m^2_{H^{\mathcal{I}}_d \widetilde{\nu}^{\mathcal{I}}_i} \sin\beta + m^2_{H^{\mathcal{I}}_u \widetilde{\nu}^{\mathcal{I}}_i} \cos\beta)}{{M_A}^2 - {M_{\widetilde{\nu}^{\mathcal{I}}_i}}^2} + \frac{\cos\beta(m^2_{H^{\mathcal{I}}_u \widetilde{\nu}^{\mathcal{I}}_i} \sin\beta - m^2_{H^{\mathcal{I}}_d \widetilde{\nu}^{\mathcal{I}}_i} \cos\beta)}{{M_{\widetilde{\nu}^{\mathcal{I}}_i}}^2} \tag{4.10}$$

$$Z^A_{2,2} \approx \frac{\cos\beta(m^2_{H_d^{\mathcal{I}}\widetilde{\nu}_i^{\mathcal{I}}}\sin\beta + m^2_{H_u^{\mathcal{I}}\widetilde{\nu}_i^{\mathcal{I}}}\cos\beta)}{{M_A}^2 - {M_{\widetilde{\nu}_i^{\mathcal{I}}}}^2} - \frac{\sin\beta(m^2_{H_u^{\mathcal{I}}\widetilde{\nu}_i^{\mathcal{I}}}\sin\beta - m^2_{H_d^{\mathcal{I}}\widetilde{\nu}_i^{\mathcal{I}}}\cos\beta)}{{M_{\widetilde{\nu}_i^{\mathcal{I}}}}^2} \tag{4.11}$$

Where the angle α diagonalizes the H_u, H_d submatrix:

$$\cos\alpha = \frac{m^2_{H_d^{\mathcal{R}}\widetilde{H}_u^{\mathcal{R}}}}{m^2_{H_d^{\mathcal{R}}\widetilde{H}_d^{\mathcal{R}}} - m^2_{H_u^{\mathcal{R}}\widetilde{H}_u^{\mathcal{R}}}}$$
$$\sin\alpha = \sqrt{1 - \frac{m^2_{H_d^{\mathcal{R}}\widetilde{H}_u^{\mathcal{R}}}}{m^2_{H_d^{\mathcal{R}}\widetilde{H}_d^{\mathcal{R}}} - m^2_{H_u^{\mathcal{R}}\widetilde{H}_u^{\mathcal{R}}}}} \tag{4.12}$$

And the mass of the Heavy scalar/pseudoscalar can be roughly estimated as:

$$v_{iR}\tan\beta\left(\frac{1}{\sqrt{2}}T_i^{\lambda} + \frac{1}{2}\lambda_j\kappa_{ijk}v_{kR}\right) \tag{4.13}$$

This approximation rely on several rough assumptions and depends on masses and angles that can't be calculated with exactitude a priory, just estimated. It's quantitative results has to be used with caution, but they allow us to have a qualitative idea on how would this mixings behave in terms of the different parameters, and the physical masses.

First, in the decoupling limit and if the mass of the left sneutrino is small, we recover the mass insertion approximation. But we can also see that when ${M_h}^2 \sim M_{\widetilde{\nu}_i^{\mathcal{R}}}$ the mixing can be large, both for up and down Higgs flavors. Finally, the sign of the mixing depends also on whether the left sneutrino is heavier or lighter than the Higgs boson. This is irrelevant for the coupling with quarks, since there is only one dominant term, but it will be important in other cases.

In the case of the pseudoscalar left sneutrino, one can still use the mass insertion approximation to calculate the mixing with H_d. Since the dominant value of the coupling is given by $\frac{1}{2}Y^{\nu}_{il}\lambda_m v_{lR}v_{mR}$, and this is suppressed by the mass of the pseudoscalar Higgs approximated by its diagonal mass entry. One can straightforwardly obtain the following expression for the largest effective interaction of the pseudoscalar sneutrino decay into down-type quarks:

$$\frac{Y^b Y^{\nu}}{\lambda}\frac{\lambda}{(2A^{\lambda} + \sqrt{2}\kappa v_R)\tan\beta} \tag{4.14}$$

One can obtain the same result, for a moderate to large value of $\tan\beta$, retaining the first term of Eq. (4.10), keeping the leading terms on Eq. (A.9) and approximating M_A^2 as in Eq. (4.13).

In the general case, the partial width to up and down quarks, corresponding to the diagrams of Fig. 4.1 a) and b) are:

$$\Gamma_{\widetilde{\nu}_i \to d_j d_j} \approx \frac{M_{\widetilde{\nu}}}{16\pi}|Y_{d_j}Z^{H/A}_{i,1}|^2 \tag{4.15}$$

$$\Gamma_{\widetilde{\nu}_i \to u_j u_j} \approx \frac{M_{\widetilde{\nu}}}{16\pi}|Y_{u_j}Z^{H/A}_{i,2}|^2 \tag{4.16}$$

Summarizing, the decay of the left sneutrino to a couple of quarks is mediated by the off-diagonal mass terms mixing left sneutrino and Higgs states, and therefore suppressed. However, if the mass of the left sneutrino is close to the mass of the physical Higgs states

(light, heavy or pseudoscalar), the mixing can be enhanced and consequently the decays.

4.3.2 Decay into charged leptons

The mixing between left sneutrino and down-type Higgs can be used also to describe the decay of the sneutrino to leptons through the diagram 4.1 c). In this case the contribution to the partial width would have the same form as in Eq. (4.14), but replacing the down-type quark Yukawa coupling by the leptonic corresponding one:

$$\frac{Y^e Y^\nu}{\lambda} \frac{\lambda}{(2A^\lambda + \sqrt{2}\kappa v_R)\tan\beta}, \tag{4.17}$$

keeping in mind that if the mass separation between any of the Higgs states and the sneutrino is small, this expression wouldn't capture the strong mixing between both states.

Since in the SM leptons mix with with supersymmetric charged fermions, there are other possible diagrams mediating the decay of the sneutrino to leptons. On Fig. 4.1 d) we can see the Feynman diagram mediated by the mixing lepton-higgsino. This diagram is proportional to the lepton Yukawa coupling in the vertex, and to the mixing $U^{e,*}_{R,j5}$ in the external leg, where $j \in 1,3$. This mixing can be estimated using the mass insertion approximation to be $\frac{Y^\nu_{jj} v_{Rj}}{\sum \lambda_i v_{Ri}}$. Thus the contribution of this diagram would be:

$$\frac{Y^e_{jj} Y^\nu_{jj} v_{Rj}}{\sum \lambda_i v_{Ri}}, \tag{4.18}$$

Notice that this diagram can give rise to lepton flavor violating decays of the sneutrino. Finally, combining the two possible diagrams we have the approximate decay widths:

$$\Gamma_{\widetilde{\nu}_i \to e_j e_j} \approx \frac{M_{\widetilde{\nu}}}{16\pi} |Y_{e_j} Z^{H/A}_{i,1} - \frac{Y_{e_j} Y_{\nu_j} v_{R_j}}{\sum \lambda_l v_{R_l}}|^2 \tag{4.19}$$

$$\Gamma_{\widetilde{\nu}_i \to e_i e_j} \approx \frac{M_{\widetilde{\nu}}}{16\pi} |\frac{Y_{e_i} Y_{\nu_j} v_{R_j}}{\sum \lambda_l v_{R_l}}|^2 \tag{4.20}$$

In Eq. (4.19) the contribution of both diagrams can cancel each other depending on the sign of the mixing sneutrino-Higgs. Notice also that the contribution form the diagram 4.1 d) would only be relevant for tau left-sneutrinos, since the corresponding diagrams for the first two families will be strongly suppressed by the small value of the corresponding Yukawa coupling.

When the mixing sneutrino-Higgs is enhanced by a small mass separation, the first term of Eq. (4.19) dominates the leptonic decays.

4.3.3 Decay into neutrinos

The Feynman diagrams shown in Fig. 4.1 e) and f) describe the decay of the scalar and pseudoscalar sneutrino into neutrinos, here the vertex is mediated by the gauge interaction sneutrino-neutrino-gaugino, and the mixing gaugino-neutrino. This mixing, labeled as $U^v_{j,4/5}$ where $j \in 1,3$, and 4 (5) stands for bino (wino). This mixings can be approximated using again the mass insertion approximation to be:

$$U^v_{j,4} \approx g'^2 \frac{v_L}{4M_1}, \quad U^v_{j,5} \approx g^2 \frac{v_L}{4M_2}. \tag{4.21}$$

There can be in principle a diagram mediating this decay also through the mixing Higgs-sneutrino as in previous sections. This decay will be nevertheless strongly suppressed both by the small neutrino Yukawa coupling, and the small mixing between left and right handed neutrinos. The complete interactions and given in Appendix B. The above terms are rough approximations of the first and second terms , respectively, multiplying the projectors $P_{L,R}$ in Eqs. B.7. Summing over the three generations of neutrinos, the partial width is:

$$\Gamma_{\widetilde{\nu}_i \to \nu\nu} \approx \frac{M_{\widetilde{\nu}}}{16\pi} \left| \frac{g_1^2 \sqrt{\sum v_{L_l}^2}}{\sqrt{2} M_1} + \frac{g_2^2 \sqrt{\sum v_{L_l}^2}}{\sqrt{2} M_2} \right|^2 \tag{4.22}$$

Note that the decay now looks independent of the mixing sneutrino-Higgs. Actually there is one diagram similar to Fig. 4.1 c) for neutrinos, but the smallness of Y^ν and the mixing $\nu - \nu^c$ make the diagram irrelevant. From Eq. (4.22) is evident also that the partial width is independent of the generation of the left sneutrino.

4.3.4 Decay into gauge bosons

Whenever kinematically accessible, the Feynman diagrams shown in Fig. 4.2 a) - g) will make the left sneutrino decay to a couple of gauge bosons. In this case, besides the diagrams mediated by the mixing sneutrino-Higgs, the left sneutrino couples directly to gauge bosons. Like on Fig. 4.2 a) and d), where we can see the direct coupling of the left sneutrinos to $W^\pm$ and Z, suppressed by the value of the corresponding VEV. The coupling mediated by the mixing of the left sneutrino with up and down type Higgses, as depicted in Fig.4.2 b), c), e) and f) would be proportional to the mixings described in section 4.3.1. Notice that the contribution from the different diagrams won't always add up and can indeed cancel each other, depending on the signs of the mixings.

As a consequence of the mixing of the scalar sneutrino with $H_{u,d}^{\mathcal{R}}$ discussed above, a sizable decay channel into photons could also be generated. This decay, schematically described in Fig. 4.3.1 g) is generated radiatively with the most important contributions generated with $W^\pm$ and top-quarks running in the loop.

$$\widetilde{\nu}_{iL}^{\mathcal{R}} \to \gamma\gamma \tag{4.23}$$

4.3.5 Decay into Higgs Bosons

The left sneutrino couples directly to the Higgs bosons, after electroweak symmetry breaking, through F-Terms generated by the neutrino Yukawa coupling and D-terms. Assuming the light Higgs to be H_u dominated, the relevant couplings are the terms on Sec. C proportional to $Z_{i,3+1}^H Z_{j,2}^H Z_{k,2}^H$.

Assuming that the decay of the left sneutrino to a couple of higgses is kinematically accessible, the left sneutrino could decay to a couple of light Higgs bosons. The corresponding Feynman diagram is shown on Fig. 4.3. Is manifest that the third term could be neglected in front of the other two, because of the presence of extra factor of Y^ν and/or v_L. The corresponding partial width is calculated on Eq. (4.24).

$$\Gamma_{\widetilde{\nu}_L \to hh} \approx \frac{\sqrt{1 - \frac{M_h^2}{M_{\widetilde{\nu}_i}^2}}}{4\pi M_{\widetilde{\nu}_i}} \left| \lambda Y_{ii}^\nu v_d + \frac{g_1^2 + g_2^2}{4} v_{Li} \right|^2 \tag{4.24}$$

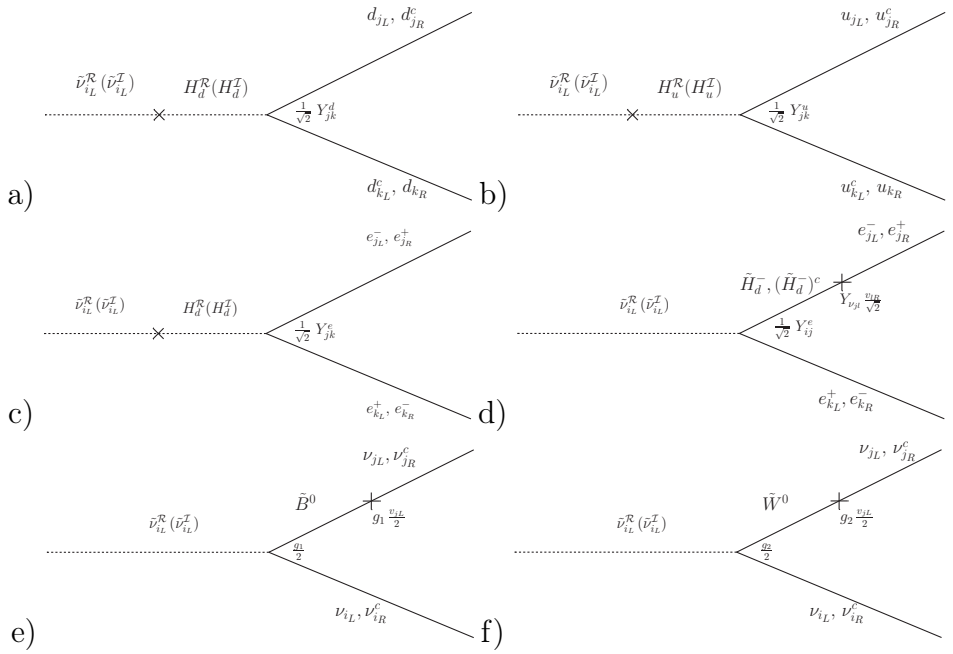

Figure 4.1: Dominant diagrams in the decay of the sneutrino to fermions.

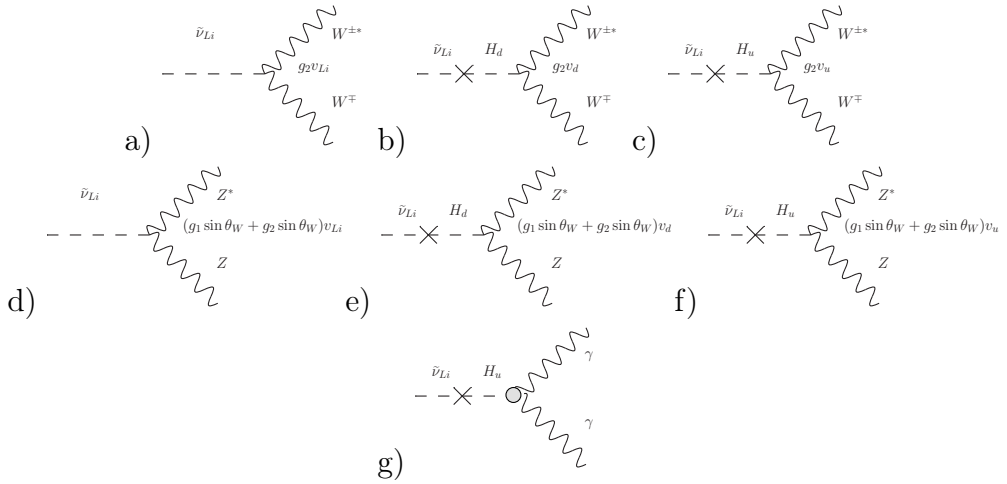

Figure 4.2: Dominant diagrams in the decay of the sneutrino to gauge bosons.

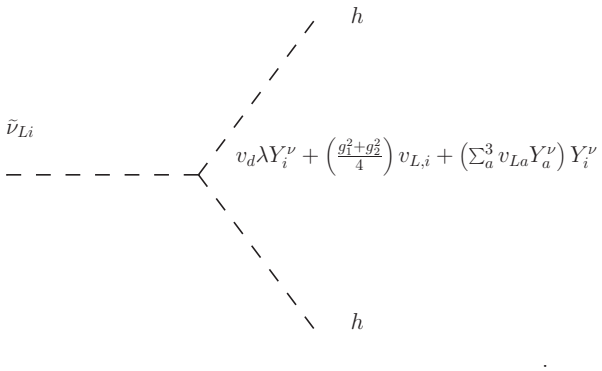

Figure 4.3: Dominant diagrams in the decay of the sneutrino to Higgs bosons.

4.4 Branching fractions and proper life-time

The interactions of the left sneutrino with SM particles open many possible channels for the decay of the left sneutrino to non supersymmetric particles. All of this channels are suppressed by the limit of very small *R-parity* violation. However, with no reason to consider none of them to be a priory dominant, besides kinematics.

We should expect for the behavior of the left sneutrino a wide variation depending of the different values of the parameters, but we can expect some general features common in most cases. We can see in Fig. 4.4 to 4.9 the branching fractions of scalar and pseudoscalar left sneutrinos for different choices of parameters, generations and masses, calculated using the approximated analytical expressions described in the previous sections.

We are focusing first on the real left sneutrino and in the case where the left sneutrino belong to the first two generations. It differs with the third generation since for them the Yukawa interaction Y^e_{ij} is negligible. The branching fractions for different decay channels is shown in Fig. 4.4.

For low masses, below 100 GeV, the decay is completely dominated by the $\nu\nu$ channel (red line on Fig. 4.4). The decays mediated by Fig.4.1 d) are irrelevant, and the decays mediated by the mixing with the Higgs are sub dominant, but present. While decays to gauge bosons and Higgs pairs are kinematically forbidden. Note that the decays described in Eq. (4.22) depend on the soft gaugino masses and the sneutrino VEV, thus in principle the decays to $b\bar{b}$ and $\tau\bar{\tau}$ could be of more relevance in points of the parameter space where the gauginos are very heavy or the left sneutrino VEVs specially small. One should remind however the influence of this parameters on Eq (3.33), thus such a point could be in conflict with neutrino physics.

When the mass of the left sneutrino is close to the mass of the Higgs bosons the contribution from the channels mediated by the mixing with the Higgs are enhanced, to the point that the decay to $b\bar{b}$ (green doted line) and $\tau\bar{\tau}$ (pink dotted line) are dominant. Of special interest is the decay to a couple of photons (yellow line), because of its detection possibilities at colliders.

When the kinematic threshold of the decay $W^{\pm}W^{\mp *}$ is reached by the mass of the left sneutrino, the decays depicted on Fig. 4.2 take over the decays of the left sneutrino. This is a generic behavior, but again the decays to neutrinos can be more important in the high mass region if gaugino soft masses are smaller or the VEV bigger, within the values admissible by Eq (3.33).

If the real left sneutrino belong to the third generation, its behavior is slightly different, due to the influence of Y^{τ}. The branching fractions are illustrated, for values of $\lambda = 1$ and $M_1 = M_2 = 1500$ in Fig. 4.5 and for $\lambda = 0.2$ and $M_1 = M2 = 500$ on Fig. 4.6.

At low masses, the decay to $\nu\nu$ is still dominant, but now the decays to $\tau\bar{\tau}$ and $\tau\bar{l}$ are important. For the parameters chosen, the neutrino channel is always dominant, but if for λ small and big gaugino masses, the leptonic channels could overcome the $\nu\nu$ channel.

In the vicinity to the Higgs boson mass, we see an enhancement of the channels mediated by the mixing Higgs-sneutrino similar to the one shown on Fig. 4.4. Mind however that there exist a cancellation of the leptonic channel happening in the vicinity of the maximum mixing point. This cancellation correspond to the destructive interplay between the two terms in Eq. (4.19).

For larger masses the decays to gauge bosons dominate the decay of the left sneutrino. We can see however on Fig. 4.5, that the decay to $W^{\pm}W^{\mp}$ could be suppressed at a specific mass. This cancellation is the result of the interplay between the diagrams 4.2 a)-c), and is not specific of the left sneutrinos of the third generation, but depends on the point of

the parameter space.

The behavior of the imaginary left sneutrino is quite different, tough considerably simpler. The pseudoscalar left sneutrino do not couple with gauge bosons, if CP is not violated, also there is no light pseudoscalar to whom have an enhanced mixing similar to the real left sneutrino. The relevant diagram for its decay are Fig. 4.1 d), e) and f). Therefore the only relevant decays are $\widetilde{\nu}^{\mathcal{I}}_{Li} \to \nu\nu$ and $\widetilde{\nu}^{\mathcal{I}}_{Li} \to \tau\bar{l}$.

When the pseudoscalar belongs to the first or second generation, the branching fractions are determined by the first term of Eq. (4.19) and Eq. (4.22), the ratio between the decays value does not depend much of the mass of the sneutrino. The dominant decay will be $\widetilde{\nu}^{\mathcal{I}}_{Li} \to \nu\nu$. Similarly as for the real sneutrino, the decay to leptons could be more important if soft gaugino masses are large and/or v_L is small, with the restrictions aforementioned.

For a tauonic pseudoscalar left sneutrino, the diagram 4.1 d) is again important. Depending on the value of λ, soft gauginos masses and v_L, the decay $\widetilde{\nu}^{\mathcal{I}}_{Li} \to \tau\bar{l}$ can even be dominant over $\widetilde{\nu}^{\mathcal{I}}_{Li} \to \nu\nu$.

May the reader notice that the branching fractions shown in Fig.4.4-4.9 are not comprehensive of all the phenomenology of the left sneutrino. They pretend to be illustrative examples of the general behavior in the mass range most interesting for collider searches. There are regions of the parameter space where some specific channel could be enhanced or suppressed in comparison with the behavior shown of this plots.

We have discussed so far about which of the decay widths is bigger, but we have not address the question of how big could be the total width. This could be of the greatest importance if, as we will see, the proper life time is long enough to have consequences for collider experiments.

Following the formulas (4.19) and (4.22), which could serve as good examples of the order of magnitude of the total width, we can make a rough estimation of the numbers involved. It is reasonable to estimate the fraction in front to be $\frac{M_{\tilde{\nu}}}{16\pi} \sim \mathcal{O}(\text{GeV})$, also to say that $\frac{Y^\tau}{\lambda} \sim g_1 \sim g_2 \sim \mathcal{O}(0.1)$. Finally, is reasonable that $\frac{v_L}{M_{1,2}} \sim Y^\nu \sim \mathcal{O}(10^{-6})$, to have a viable neutrino sector. Altogether we can estimate:

$$\Gamma \sim \mathcal{O}(\text{GeV}) \times (\mathcal{O}(0.1))^2 \times (\mathcal{O}(10^{-6}))^2 \sim 10^{-14}\ \text{GeV} \tag{4.25}$$

Which can be converted into a proper decay length of: $\frac{\hbar \cdot c}{\Gamma} \sim \mathcal{O}(\text{cm})$. Of the same order of magnitude as, for instance, the inner detector of ATLAS. Notice that the hierarchy between the typical widths of the heavier SUSY particles and the LSP width is similar to the hierarchy that exist between the electroweak scale and the neutrino mass scale, since both have a common origin.

We show in Figs. 4.10 to 4.12 the proper decay length for the same scenarios as for the branching fractions. We can see that the proper decay length is larger when the left sneutrinos belong to the two first generations. A behavior expected since there are additional decay diagrams with a significant contribution to the tauonic left sneutrino.

We can also observe that around the mass of the Higgs boson, the proper decay length drops dramatically as a result of the enhanced mixing sneutrino-Higgs. For large masses we can also observe how the decays channels to $W^\pm W^\mp$ and ZZ have a strong impact reducing the value of $c\tau$.

The value of the proper decay length of the imaginary left sneutrinos is similar to the real counterpart for low masses, but is always larger for masses above 110 GeV, due to the contributions of the diagrams mediated by the mixing sneutrino-Higgs and the diboson decays for the real sneutrino.

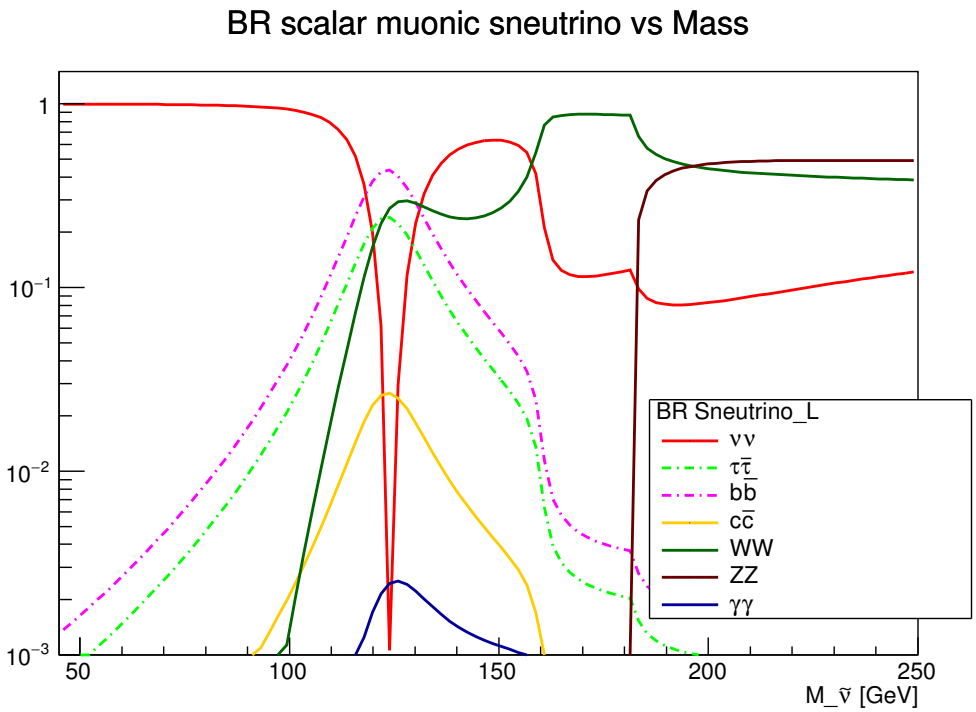

Figure 4.4: Partial widths as a function of mass for a muonic real left sneutrino LSP.

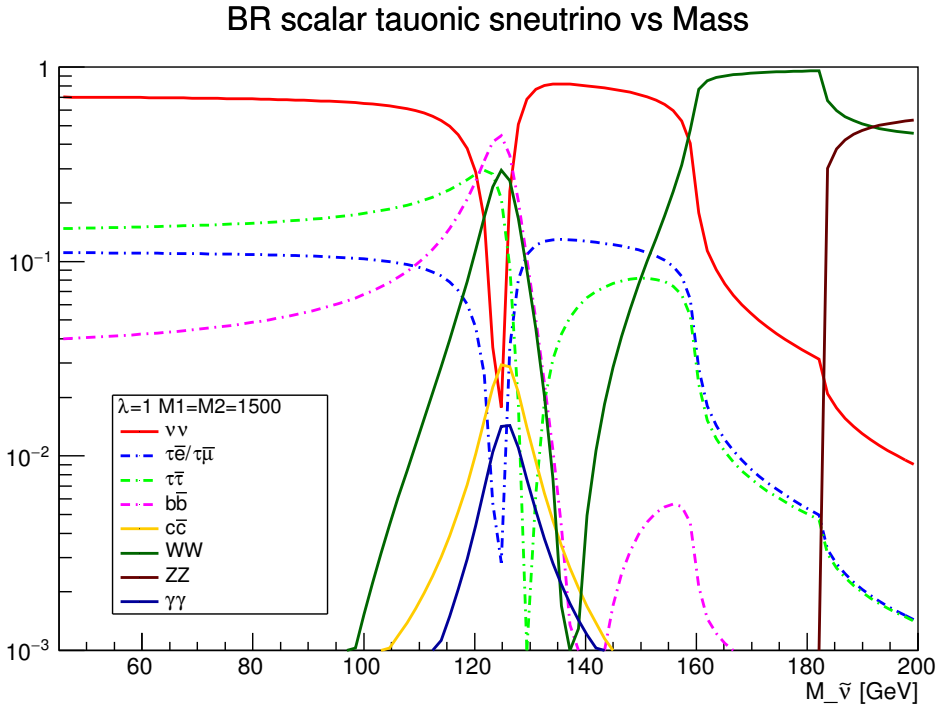

Figure 4.5: Partial widths as a function of mass for a tauonic real left sneutrino LSP.

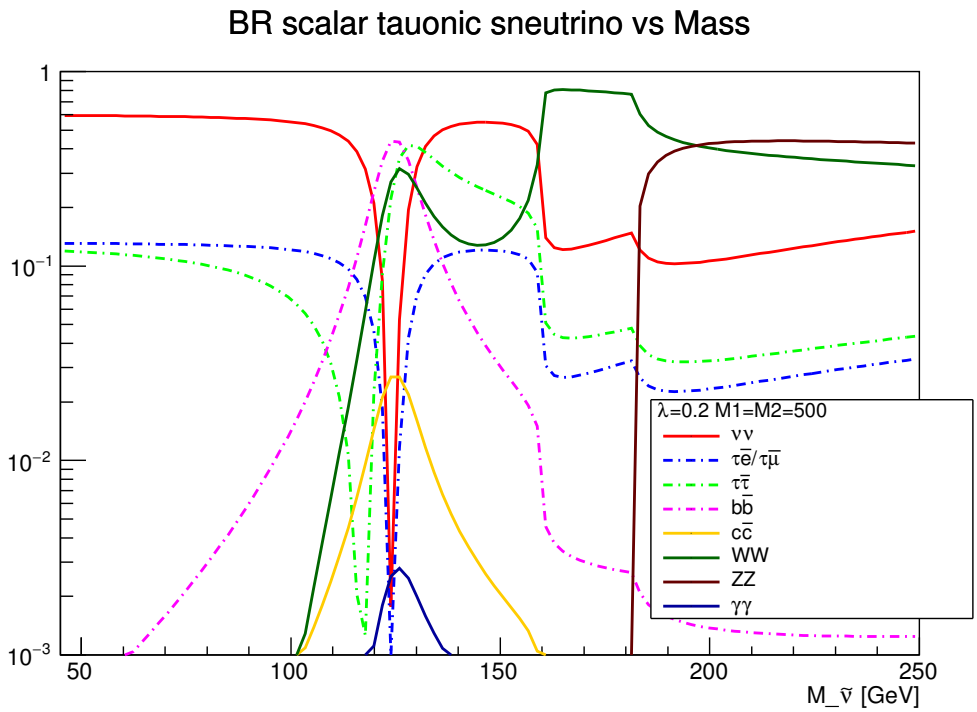

Figure 4.6: Partial widths as a function of mass for a tauonic real left sneutrino LSP.

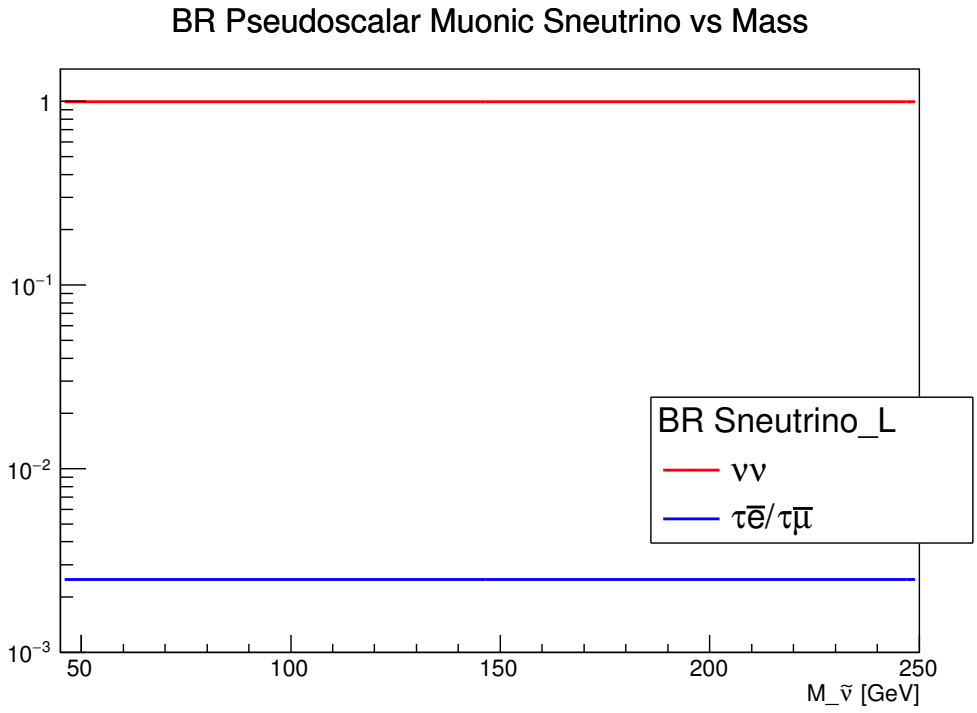

Figure 4.7: Partial widths as a function of mass for a imaginary left sneutrino LSP.

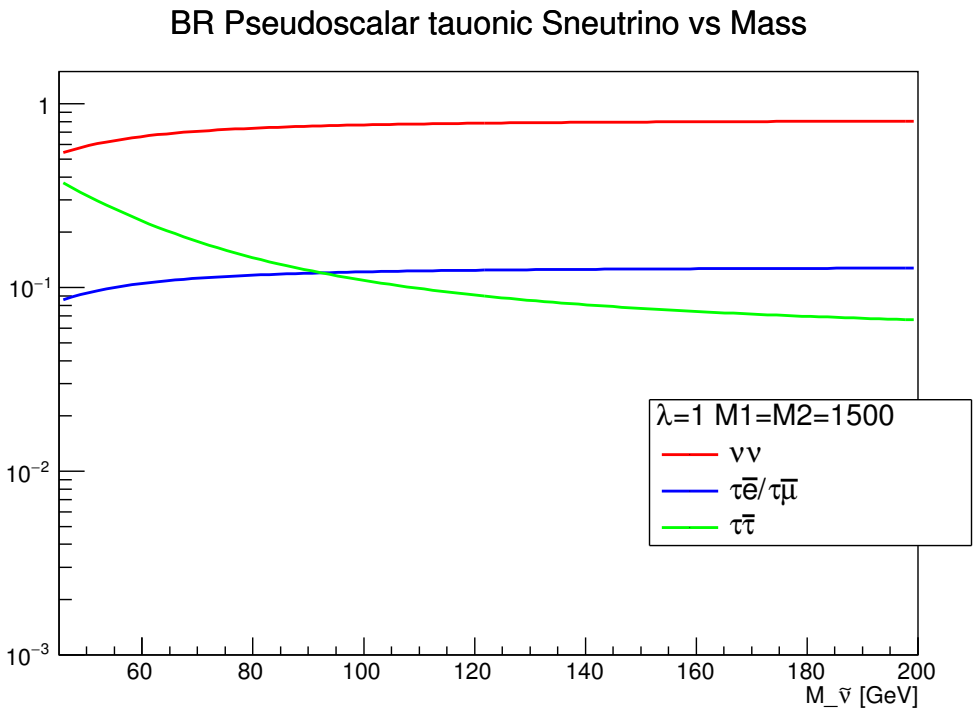

Figure 4.8: Partial widths as a function of mass for a imaginary left sneutrino LSP.

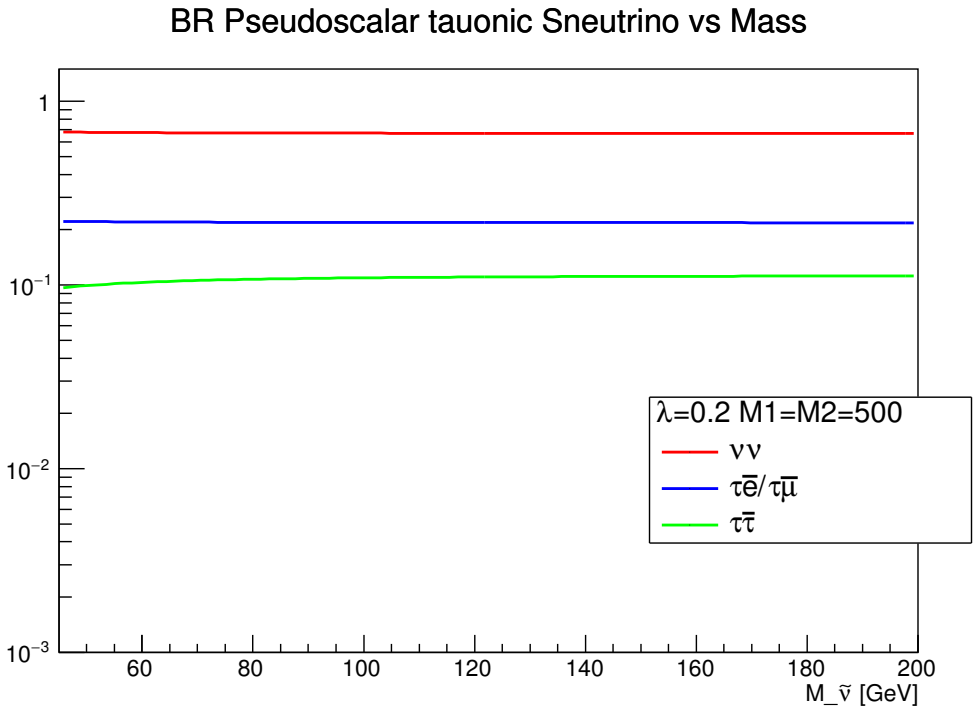

Figure 4.9: Partial widths as a function of mass for a imaginary left sneutrino LSP.

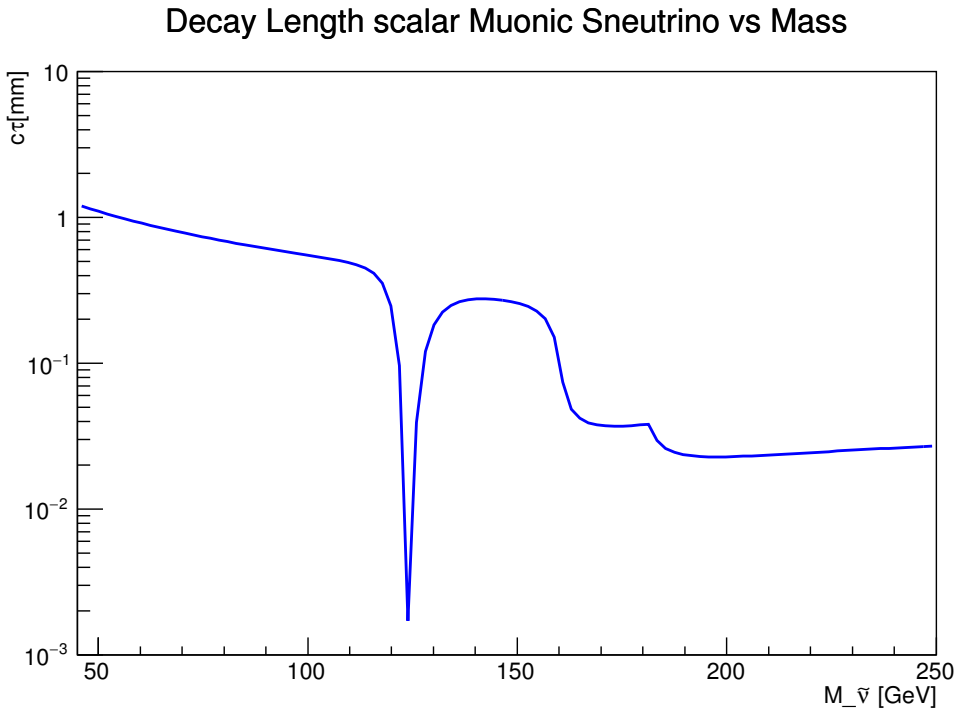

Figure 4.10: Decay length as a function of mass for a left sneutrino LSP.

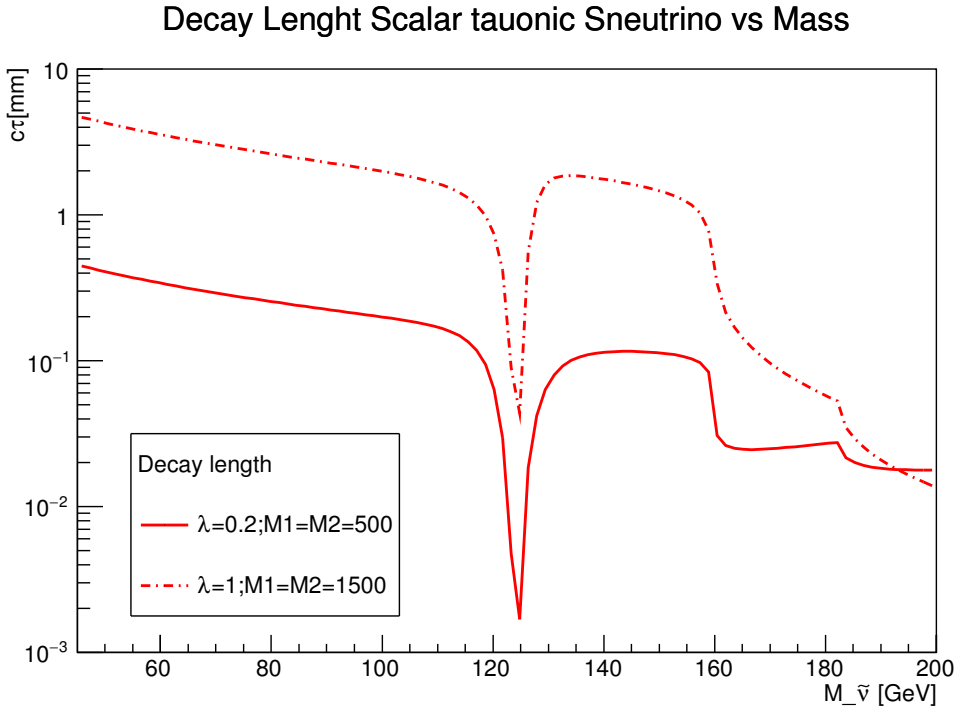

Figure 4.11: Decay length as a function of mass for a left sneutrino LSP.

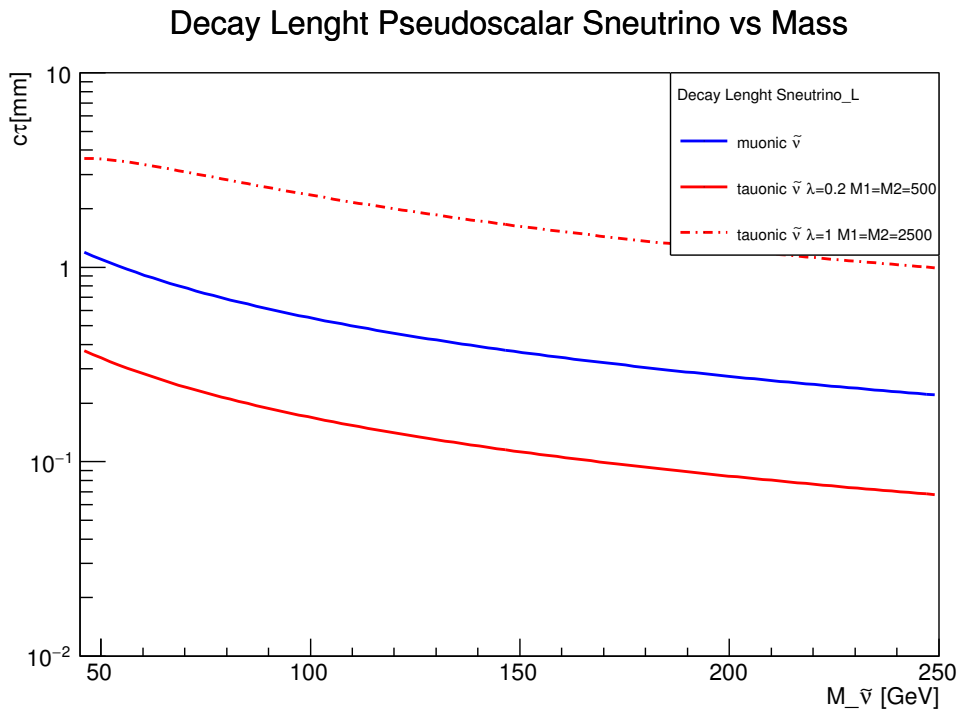

Figure 4.12: Decay length as a function of mass for a left sneutrino LSP.

4.5 Experimental searches for sneutrinos

There exist multiple analysis looking for the production and decay of the left sneutrino at colliders, both at LEP and at the LHC. This searches can be generically classified in searches for RPC decays of the sneutrino and RPV decays. In the former case, the pair production of sneutrinos and sleptons can be detected through the RPC conserving decays $\tilde{\nu} \to \nu\chi^0/ \to \ell\chi^\pm$ and $\tilde{\ell} \to \ell\chi^0/ \to \nu\chi^\pm$. These searches can constrain the mass of the slepton to be above 580 GeV for ATLAS [105] and 450 GeV for CMS [106]. Notice however that this searches use the energetic leptons and large MET resulting form the decays described above. In this sense these searches are ineffective for the sneutrino discussed in this chapter, since the slepton can only decay with a similar topology through the chain $\tilde{\ell} \to W^*\tilde{\nu} \to \ell 3\nu$ where the lepton coming from the off-shell W is going to be too soft.

Searches for RPV decays of sleptons, as for example [107], can however cover many of the decays described in Sec. 4.3. For instance the decay to quarks, mimicking the decays mediated by λ'_{ikk} coupling, or the decays to leptons corresponding to the decays mediated by λ_{ijk}. Nevertheless the limits obtained in these searches cannot be directly quoted, since the simplified models used to obtain lower limits on the mass allow only one single decay channel, something generically not true for the $\mu\nu$SSM sneutrino.

Whenever the mass of the sneutrino is within the kinematic reach for pair production at LEP, its searches are also relevant. Moreover a lepton collider can be sensitive to the soft mesons produced in the decay of the slepton. One more time, lower limits on the mass of the sneutrino or slepton cannot be directly applied because of the varied number of channels accessible for the $\mu\nu$SSM sneutrino.

Other searches searches not directly designed to look for sneutrinos can be pertinent

when they look for a signal similar to the ones possible combining the decay channels described in Sec. 4.3. That is the case of the mono-jet and mono-photon searches when the sneutrino decays to neutrino pairs. Also the searches for lepton pairs in association with missing transverse momentum, or jets plus MET are topologies possible for the left sneutrino LSP. In general this searches suffer from the reduced branching fraction since the decays of the left sneutrino are distributed among the multiple possibilities. Moreover, light sneutrinos tend to produce softer leptons/jets and smaller amount of MET than the particles for which the analysis were originally designed. And when the mass of the sneutrino is high enough to produce clearly discernible events, the production crossection is typically too low.

Summarizing, is not possible to establish robust exclusion limit on the mass of the left sneutrino LSP given the number of possible decay channels of it. This does not tell however that limits doesn't exist, but rather that each scenario is constrained from different signals and should be checked individually. One can put a generic lower bound nonetheless on $M_Z/2$, since the contribution of the left sneutrino to the total width of the Z boson would be well above the experimental uncertainties on its measured value.

Chapter 5

Searching for left sneutrino LSP at the LHC

In this chapter, based on the work [94], we analyze the relevant signals expected at the LHC for a left sneutrino LSP. Here we will study separately BPs with left sneutrinos co-LSP of the first two families, and left sneutrinos LSP of the third family, since their phenomenology is very different. Based on this BPs we propose search strategies that could lead to a discovery of the left sneutrino at the end of RUN 2.

In the previous chapter, we have seen the general features of the left sneutrino as the LSP. Based on approximated analytical formulas,we select the most interesting scenarios and we picked a selection of representative BPS for which we calculated the mass spectrum and decay modes using a suitable modified version of `SARAH` code [108, 109, 110] as well as the `SPheno` v3.3.6 code [111, 112]. These results were linked to `MadGraph5_aMC@NLO` v2.3.2.2 [113] and `PYTHIA` 6.428 [114] tools, in order to make the full analysis of detection of signals at the LHC.

In section 3.5 is explained how the data on neutrino physics can be reproduced at tree level in the $\mu\nu$SSM, even with diagonal Yukawa couplings Y^{ν}_{ii}. Nevertheless, for this first analysis focused on the detection at the LHC, it will be operationally simpler to work with only one family of right-handed neutrinos and its sneutrino partner. Thus we leave the three-family case for a future work [115], since our LHC analysis is not going to be essentially modified by this simplification. As a consequence, we will work with the following non-vanishing parameters: $\tan\beta$, $v_{1R} \equiv, \lambda \equiv \lambda, A^{\lambda}_{1} \equiv A^{\lambda}, \kappa_{111} \equiv \kappa, A^{\kappa}_{111} \equiv A^{\kappa}, and Y^{\nu}_{i1}, A^{\nu}_{i1}$. For the last two parameters we will assume universality, $Y^{\nu}_{i1} \equiv Y^{\nu}$ and $A^{\nu}_{i1} \equiv A^{\nu}$, since in this way we will have three large enough diagonal left sneutrino masses, mimicking the case of three families of right sneutrinos. We will also have v_{iL}, not necessarily universal. Summarizing, the free parameters in the neutral scalar sector at the low scale M_{EWSB}, are in our analysis:

$$\lambda, \kappa, Y^{\nu}, \tan\beta, v_{iL}, v_R, A^{\lambda}, A^{\kappa}, A^{\nu}. \tag{5.1}$$

Concerning the soft parameters of Eq. (3.4), for simplicity in the computation we will consider that the trilinear ones, as well as the scalar masses, are universal, i.e, $A^{u,d,e}_{ij} = A^{u,d,e}$ and $m_{\tilde{Q}_{iL},\tilde{u}_{iR},\tilde{d}_{iR},\tilde{e}_{iR}} = m_{\tilde{Q}_L,\tilde{u}_R,\tilde{d}_R,\tilde{e}_R}$, respectively. Altogether, we have the following free parameters:

$$M_1, M_2, M_3, m_{\tilde{Q}_L}, m_{\tilde{u}_R}, m_{\tilde{d}_L}, m_{\tilde{e}_R}, A^u, A^d, A^e. \tag{5.2}$$

We have discussed in Sec. 4.1 the neutral scalar and pseudoscalar matrices, and we

have seen how a left sneutrino can become the LSP. We have seen also the relation between the masses of left scalar and pseudoscalar sneutrinos, and sleptons. The final necessary condition we found is that A^ν ∼-100 GeV to obtain the pseudoscalar left sneutrino as the LSP with mass ∼ 100 GeV. The LSP can in principle belong to any of the three families of the SM, but as we have seen in Sec. 4.4 this can have crucial implications for the signals produced at the LHC.

We can assign different values for the input parameters associated to each family. This is the case for example of the left sneutrino VEVs, v_{iL}. Thus if we choose $v_{1L} = v_{2L} > v_{3L}$, we obtain from the approximate expression Eq. (4.5) that the electron sneutrino $\tilde{\nu}^{\mathcal{I}_{eL}}$ and the muon sneutrino $\tilde{\nu}^{\mathcal{I}_{\mu L}}$ have masses degenerate and behave as co-LSP. Although this degeneracy is broken by the mixing of the mass matrices and by loop corrections, the mass difference is going to be negligible. For example, for the BP in Table 5.1 to be analyzed afterwards, $\tilde{\nu}^{\mathcal{I}_{eL}}$ is 0.0002 GeV heavier than $\tilde{\nu}^{\mathcal{I}_{\mu L}}$. We have discussed in Sec. 4.1 that scalar and pseudoscalar sneutrinos are co-LSPs, we conclude then that in this case there are four co-LSP: $\tilde{\nu}^{\mathcal{I}_{eL}}$, $\tilde{\nu}^{\mathcal{I}_{\mu L}}$, $\tilde{\nu}^{\mathcal{R}_{eL}}$ and $\tilde{\nu}^{\mathcal{R}_{\mu L}}$. Alternatively, if we choose $v_{1L} = v_{2L} < v_{3L}$, then we obtain that tau sneutrinos $\tilde{\nu}^{\mathcal{I}_{\tau L}}$ and $\tilde{\nu}^{\mathcal{R}_{\tau L}}$ are co-LSP. Obviously, in the case of universal VEVs one obtains that the left sneutrinos of the three families , scalar and pseudoscalar, become co-LSP.

Let me finally remark that another equivalent strategy to find non-degenerated families of sneutrinos, is to allow for non-universality of the parameters A^ν_{ij} or Y^ν_{ij}, while keeping v_{iL} universal.

5.1 Electron and muon left sneutrinos co-LSPs

Following the discussion in the previous subsection,we show in Table 5.1 a benchmark point (BP) with the right properties to produce $\widetilde{\nu}^{\mathcal{I}}_{\mu L}$, $\widetilde{\nu}^{\mathcal{R}}_{\mu L}$, $\widetilde{\nu}^{\mathcal{I}}_{eL}$ and $\widetilde{\nu}^{\mathcal{R}}_{eL}$ co-LSPs, with masses of about 125.4 GeV. The input parameters at the low scale M_{EWSB} can be found in the first box of the table. Concerning the input soft parameters, as discussed below Eq. (4.5), the most relevant one for our computation is A^ν and we have used the value $-A^\nu = 386$ GeV $\sim \kappa v_R/\sqrt{2}$. Other relevant soft parameters are the gaugino masses M_1 and M_2, since Bino and Wino mediate the decay channels of the left sneutrino (see Fig. 4.1). We take them as 600 and 900 GeV, respectively, and for M_3 we choose 1600 GeV. For the rest of trilinear parameters, for simplicity in the computation we assume $A_{u_{ij},d_{ij},e_{ij}} = A_{u,d,e}$, and $A^d = A^e = A^\lambda = -A^\kappa = 1$ TeV with the exception of $A^u \sim -3.1$ TeV in order to reproduce the mass of the Higgs. As we will discuss below, the negative value of A^κ is necessary to avoid tachyonic pseudoscalar right sneutrinos. The one of A^u it to avoid tachyonic left sneutrinos due to the loop corrections. In the same spirit of simplicity, we use $m_{\tilde{Q}_L,\tilde{u}_R,\tilde{d}_R} =$ 1.3 TeV[1] and $m_{\tilde{e}_R} = 1$ TeV. Finally, we have $\tan\beta = 10$, corresponding to the following Higgs VEVs: $v_u/\sqrt{2} = 170.84$ GeV, $v_d/\sqrt{2} = 17.08$ GeV.

[1]As analyzed in Refs. [116, 117, 118, 119, 120, 121, 122]using a numerical minimization of the potential, large values of A^t may give rise to an unstable electroweak ground state decaying rapidly to a charge and color breaking (CCB) minima (see e.g. Ref. [123]). Using the results of Refs. [117, 118], we have been able to check that our point around the maximal mixing corresponds to a metastable vacuum. The dangerous additional possibility of rapid thermal tunneling [118] is dependent on the thermal evolution of the Universe, and to analyze it is beyond the scope of this work. Nevertheless, it is worth noticing that CCB minima are not a crucial subject in our study of the sneutrino LSP. We can easily modify A^t and/or stop soft masses obtaining the same kind of signals discussed here. For example, keeping $A^t \sim -3.1$ TeV but increasing $m_{\tilde{t}}$ in a few hundred GeV we can enter in a safe stable region [116, 117, 118, 119, 120, 121, 122]. Also the same situation can be obtained reducing $|A^t|$ and properly changing $m_{\tilde{t}}$.

Table 5.1: Benchmark point producing $\widetilde{\nu}^{\mathcal{I}}_{\mu L}$,$\widetilde{\nu}^{\mathcal{R}}_{\mu L}$, $\widetilde{\nu}^{\mathcal{I}}_{eL}$ and $\widetilde{\nu}^{\mathcal{R}}_{eL}$ co-LSPs, with masses of 125.4 GeV. Input parameters, and soft masses obtained from the minimization conditions, are given in the first and second boxes at the low scale M_{EWSB}. Sparticle physical masses are shown in the third box (with their dominant compositions written in brackets). Sneutrino branching ratios (larger than 10^{-4}) and decay widths are shown in the fourth and fifth boxes, respectively. VEVs, soft parameters, sparticle masses and decay widths are given in GeV.

λ	0.2	κ	0.3	Y^ν	5×10^{-7}
$v_{1,2L}/\sqrt{2}$	3×10^{-4}	$v_{3L}/\sqrt{2}$	5×10^{-6}	$v_R/\sqrt{2}$	1350
$\tan\beta$	10	A^u	-3177	$A^{d,e}$	1000
A^λ	1000	A^κ	-1000	A^ν	-386
M_1	600	M_2	900	M_3	1600
$m^2_{\tilde{Q}_L,\tilde{u}_R,\tilde{d}_R}$	1.69×10^6	$m^2_{\tilde{e}_R}$	10^6	–	–
m^2_{Hd}	3.62×10^6	m^2_{Hu}	-1.09×10^5	$m^2_{\tilde{\nu}_R}$	0.750×10^5
$m^2_{\tilde{L}_{eL}}$	0.968×10^4	$m^2_{\tilde{L}_{\mu L}}$	0.968×10^4	$m^2_{\tilde{L}_{\tau L}}$	0.935×10^6
$m_{h_1(H^{\mathcal{R}}_u)}$	124.2	$m_{h_2(\tilde{\nu}^{\mathcal{R}}_{\mu L})}$	125.4	$m_{h_3(\tilde{\nu}^{\mathcal{R}}_{eL})}$	125.4
$m_{h_4(\tilde{\nu}^{\mathcal{R}}_R)}$	501.2	$m_{h_5(\tilde{\nu}^{\mathcal{R}}_{\tau L})}$	972.4	$m_{h_6(H^{\mathcal{R}}_d)}$	1934.4
–	–	$m_{A^0_2(\tilde{\nu}^{\mathcal{I}}_{\mu L})}$	125.4	$m_{A^0_3(\tilde{\nu}^{\mathcal{I}}_{eL})}$	125.4
$m_{A^0_4(\tilde{\nu}^{\mathcal{I}}_{\tau L})}$	972.4	$m_{A^0_5(\tilde{\nu}^{\mathcal{I}}_R)}$	1100	$m_{A^0_6(H^{\mathcal{I}}_d)}$	1933.9
–	–	$m_{H^-_2(\tilde{\mu}_L)}$	145.4	$m_{H^-_3(\tilde{e}_L)}$	145.4
$m_{H^-_4(\tilde{\tau}_L)}$	946.9	$m_{H^-_5(\tilde{e}_R)}$	1000.9	$m_{H^-_6(\tilde{\mu}_R)}$	1000.9
$m_{H^-_7(\tilde{\tau}_R)}$	1000.9	$m_{H^-_8(H^-_d)}$	1936.2	–	–
$m_{\lambda^0_4(\tilde{H}^0_u/\tilde{H}^0_d)}$	264.8	$m_{\lambda^0_5(\tilde{H}^0_u/\tilde{H}^0_d)}$	279.6	$m_{\lambda^0_6(\tilde{B}^0)}$	600.3
$m_{\lambda^0_7(\nu_R)}$	809.6	$m_{\lambda^0_8(\tilde{W}^0)}$	919.8	–	–
$m_{\lambda^-_4(\tilde{H}^-_d/(\tilde{H}^+_u)^c)}$	272.1	$m_{\lambda^-_5(\tilde{W}^-)}$	920	–	–
$m_{\tilde{u}_1(\tilde{t}_L/\tilde{t}_R)}$	1112	$m_{\tilde{u}_2(\tilde{c}_R)}$	1340	$m_{\tilde{u}_3(\tilde{u}_R)}$	1340
$m_{\tilde{u}_4(\tilde{u}_L)}$	1343	$m_{\tilde{u}_5(\tilde{c}_L)}$	1343	$m_{\tilde{u}_6(\tilde{t}_L/\tilde{t}_R)}$	1465
$m_{\tilde{d}_1(\tilde{b}_L)}$	1310.6	$m_{\tilde{d}_2(\tilde{b}_R)}$	1338.8	$m_{\tilde{d}_3(\tilde{s}_R)}$	1338.8
$m_{\tilde{d}_4(\tilde{d}_R)}$	1338.8	$m_{\tilde{d}_5(\tilde{s}_L)}$	1344.9	$m_{\tilde{d}_6(\tilde{d}_L)}$	1344.9
$m_{\tilde{g}}$	1619.5	–	–	–	–
BR($A^0_2 \to \nu\nu$)		0.9744	BR($A^0_3 \to \nu\nu$)		0.9908
BR($A^0_2 \to \mu^\pm e^\mp$)		0.0058	BR($A^0_2 \to \mu^+\mu^-$)		0.0055
BR($A^0_2 \to \mu^\pm \tau^\mp$)		0.0054	BR($A^0_{2,3} \to \tau^+\tau^-$)		0.0003
BR($A^0_{2,3} \to \bar{b}b$)		0.0017	BR($A^0_{2,3} \to \bar{c}c$)		0.0007
BR($A^0_{2,3} \to gg$)		0.0061	–		–
BR($h_{2,3} \to \nu\nu$)		0.0015	–		–
BR($h_2 \to \tau^+\tau^-$)		0.0863	BR($h_3 \to \tau^+\tau^-$)		0.0828
BR($h_{2,3} \to \bar{b}b$)		0.468	BR($h_{2,3} \to \bar{c}c$)		0.033
BR($h_{2,3} \to gg$)		0.122	BR($h_{2,3} \to \gamma\gamma$)		0.003
BR($h_{2,3} \to W^\pm W^{\mp *}$)		0.256	BR($h_{2,3} \to ZZ^*$)		0.028
$\Gamma(h_{2,3})$		6.7×10^{-11}	$\Gamma(A^0_{2,3})$		1.0×10^{-13}

The soft masses obtained from the minimization conditions of Eqs. (3.17)-(3.20) are shown in the second box of the table. In particular, from Eq. (4.2) it is easy to check that one can obtain $m^2_{\tilde{L}_{\tau L}} \sim (1\text{ TeV})^2$ corresponding to the VEV $v_{3L}/\sqrt{2} = 5 \times 10^{-6}$ GeV, and two smaller soft masses $m^2_{\tilde{L}_{e,\mu L}} \sim (100\text{ GeV})^2$ corresponding to larger VEVs, $v_{1,2L}/\sqrt{2} = 3 \times 10^{-4}$ GeV.

The sparticle physical masses are shown in the third box of the table, with their dominant compositions written in brackets. The masses of the neutral 'Higgses' can be found

in $1^{st} - 4^{th}$ rows of that box. There we have followed the notation of Appendices A and A for the dominant compositions. The scalar mass eigenstates are denoted by $h_{1,...,6}$, since we are considering only one family of right-handed neutrinos and the scalar partner. The pseudoscalars are denoted by $A^0_{2,...,6}$, because we associate A^0_1 to the Goldstone boson eaten by the Z. The composition of the latter is dominated by the $H^{\mathcal{I}}_u$ (98.9%), with the second most important composition $H^{\mathcal{I}}_d$ ($\sim 1\%$). By convention, the masses are labelled in ascending order, so that for example $m_{A^0_1} < m_{A^0_2} < ...$

As evident from Eq. (4.2) (or Eq. (4.5)), because of the small low-energy soft masses of the first two families of lepton doublets ~ 100 GeV (since we assume $v_{1L} = v_{2L} > v_{3L}$), we are able to get as LSP with a mass of 125.4 GeV a pseudoscalar state dominated by the muon left sneutrino $A^0_2(\widetilde{\nu}^{\mathcal{I}}_{\mu L})$, with co-LSPs essentially degenerate in mass $A^0_3(\widetilde{\nu}^{\mathcal{I}}_{eL})$ and the scalar partners $h_2(\widetilde{\nu}^{\mathcal{R}}_{\mu L})$, $h_3(\widetilde{\nu}^{\mathcal{R}}_{eL})$. On the other hand, because of the large soft mass of the third family of lepton doublets ~ 1 TeV, we obtain $A^0_4(\widetilde{\nu}^{\mathcal{I}}_{\tau L})$ and $h_5(\widetilde{\nu}^{\mathcal{R}}_{\tau L})$ with masses of 972.4 GeV. All these states are very pure left sneutrinos (>99.99%), confirming our statement above that the left sneutrino submatrix is almost decoupled from the Higgs-right sneutrino submatrix. Actually, for this BP, because of the not very large value of λ, the Higgses and right sneutrinos are also almost decoupled. They are quite pure right sneutrino states (>99.96%) or Higgs states (>98.86%). In particular, we obtain $h_1(H^{\mathcal{R}}_u)$ as the SM-like Higgs with a mass of 124.2 GeV, and $h_6(H^{\mathcal{R}}_d)$ and $A^0_6(H^{\mathcal{I}}_d)$ as the heavy scalar and pseudoscalar Higgses with masses of about 1934 GeV (see Eq. (A.4) vs. Eqs. (A.3) and (A.19), where the factor $\frac{1}{\tan\beta}$ vs. $\tan\beta$ is crucial). The second most important composition for these states is ($\sim 1\%$) $H^{\mathcal{R}}_d$, $H^{\mathcal{R}}_u$ and $H^{\mathcal{I}}_u$, respectively. For the right sneutrino states we obtain $h_4(\widetilde{\nu}^{\mathcal{R}}_R)$ and $A^0_5(\widetilde{\nu}^{\mathcal{I}}_R)$ with masses of 501.2 GeV and 1100 GeV, respectively. These values can be reproduced using the following approximate formulas from Eqs. (A.8) and (A.24):

$$m^2_{\widetilde{\nu}^{\mathcal{R}}_R} \approx 2\kappa^2 v^2_R + \frac{1}{\sqrt{2}}\kappa A^k v_R \ , \quad m^2_{\widetilde{\nu}^{\mathcal{I}}_R} \approx -\frac{3}{\sqrt{2}}\kappa A^k v_R \ . \tag{5.3}$$

The masses for 'charged Higgses' are written in $5^{th} - 7^{th}$ rows of the third box of Table 5.1. Following the notation of Appendix A, they are labeled as $H^-_{2,...,8}$, since we associate the first state to the Goldstone bosons eaten by the $W^\pm$. The composition of this first state is dominated by the H^+_u (98.9%), with the second most important composition H^{-*}_d ($\sim 1\%$). As a consequence of the result in Eq. (4.6), there are two light (one heavy) left sleptons associated to the light (heavy) left sneutrinos, $H^-_2(\tilde{\mu}_L)$, $H^-_3(\tilde{e}_L)$ ($H^-_4(\tilde{\tau}_L)$), with masses of 145.4 (946.9) GeV. Thus $H^-_2(\tilde{\mu}_L)$ and $H^-_3(\tilde{e}_L)$ are the co-NLSPs with masses almost degenerate. Concerning the right sleptons, they are decoupled from the left ones as already discussed in Subsection 3.3. We can also see in Eq. (A.43) that their masses are basically determined by the soft masses. As a consequence, they have negligible off-diagonal entries, and there are three states $H^-_5(\tilde{\mu}_R)$, $H^-_6(\tilde{e}_R)$ and $H^-_7(\tilde{\tau}_R)$ with masses of about 1 TeV. Since the slepton and Higgs submatrices are decoupled, all these states are very pure sleptons (>99.97%). Finally, there is a charged Higgs (>98.9%), $H^-_8(H^-_d)$, whose second most important composition is ($\sim 1\%$) H^{+*}_u. As expected, this state is heavy with a mass of about 1.9 TeV, as those of the heavy neutral scalar $h_6(H^{\mathcal{R}}_d)$ and pseudoscalar $A^0_6(H^{\mathcal{I}}_d)$ (compare Eq. (A.35) with Eqs. (A.3) and (A.19)).

The masses for 'neutrinos' are shown in $8^{th} - 9^{th}$ rows of the third box of Table 5.1. The mass eigenstates are denoted as $\lambda^0_{4,...,8}$, since we associate the first three states to the SM left-handed neutrinos. The other five eigenstates arise from the mixing of MSSM-like neutralinos and the right-handed neutrino. As can be deduced from the matrix in

Eq. (A.65), we obtain almost pure Wino, Bino, Higgsinos and right-handed neutrino states. The $\lambda_8^0(\tilde{W}^0)$ and $\lambda_6^0(\tilde{B}^0)$ states with 99.1% and 99.3% of Wino and Bino composition, respectively, have masses of 919.8 and 600.3 TeV, respectively, and these are determined approximately by the soft masses M_2 and M_1:

$$m_{\tilde{W}^0} \approx M_2 \ , \ \ m_{\tilde{B}^0} \approx M_1 \ . \tag{5.4}$$

The Higgsinos have a mixing of order 50%, and the two states, $\lambda_4^0(\tilde{H}_u^0/\tilde{H}_d^0)$ and $\lambda_5^0(\tilde{H}_u^0/\tilde{H}_d^0)$, have similar masses of 264.8 and 279.6 GeV, respectively, which are determined approximately by the effective μ term in Eq. (3.22):

$$m_{\tilde{H}_{u,d}^0} \approx \lambda \frac{v_R}{\sqrt{2}} \ . \tag{5.5}$$

Finally, the $\lambda_7^0(\nu_R)$ state has a 99.8% of right-handed neutrino composition. Its mass is 809.6 GeV and can be approximated by the effective Majorana mass of Eq. (3.24)

$$m_{\nu_R} \approx 2\kappa \frac{v_R}{\sqrt{2}} \ . \tag{5.6}$$

Notice that from Eqs. (5.3) and (5.6) we obtain

$$m^2_{\tilde{\nu}_R^7} \approx -\frac{3}{2} A^k m_{\nu_R} \ , \tag{5.7}$$

and therefore A^k and m_{ν_R} (i.e. the product κv_R) must have opposite signs in order to avoid tachyonic pseudoscalar right sneutrinos. In particular, in our BP we choose a negative value for A^k.

The masses for 'leptons' are shown in 10^{th} row of the third box. The mass eigenstates are denoted as $\lambda_{4,5}^{\pm}$, since we associate the first three states to the SM leptons. As discussed in Subsection 3.3,the 2×2 MSSM-like chargino submatrix is basically decoupled from the 3×3 lepton submatrix. Thus we obtain almost pure charged Wino, Higgsino. The $\lambda_5^-(\tilde{W}^-)$ mass of 920 GeV can be approximated by the soft mass M_2:

$$m_{\tilde{W}^{\pm}} \approx M_2 \ . \tag{5.8}$$

The charged Higgsinos have a mixing of order 50%, and the state $\lambda_4^-(\tilde{H}_d^-/(\tilde{H}_u^+)^c)$ have a mass of 272.1 GeV, which can be approximated by the value of the effective μ term, as for the neutral Higgsinos in Eq. (5.5):

$$m_{\tilde{H}^{\pm}} \approx \lambda \frac{v_R}{\sqrt{2}} \ . \tag{5.9}$$

The squarks masses are shown in $11^{th} - 14^{th}$ rows of the same box. They were discussed in Subsection 3.3. As a consequence of their structure, all squark masses are of the order of the corresponding soft masses ~ 1.3 TeV, except the lightest and the heaviest ones which because of the large top Yukawa coupling driven mixing between the left and right stops, obtain masses of the order of 1.1 and 1.4 TeV, respectively.

The gluinos masses are shown in 15^{th} row. They are of the order of 1.6 TeV, determined by the value of M_3:

$$m_{\tilde{g}} \approx M_3 \ . \tag{5.10}$$

Let us finally remark that it is easy to obtain other masses for the electron and muon sneutrinos co-LSPs, as can be deduced from the discussion below Eq. (4.5). A simple way to decrease (increase) the mass of the LSP is to increase (decrease) the left sneutrino VEVs. However, in this work we focus in the narrow range of masses $118 - 132$ GeV where the decays of the LSP can be treated as prompt, as seen in section 4.4. On the other hand, for a tau sneutrino LSP the range is broader and a richer collider phenomenology could be obtained.

5.2 Tau left sneutrino LSP

In Table 5.2, we have adopted the strategy discussed below Eq. (4.5) in order to produce a tau left sneutrino LSP, $\widetilde{\nu}^{\mathcal{I}}_{\tau L}$, namely to use similar input parameters as in Table 5.1 but with $v_{1L} = v_{2L} < v_{3L}$. In this case, the masses obtained from Eq. (4.5) are different from the ones in Table 5.1, with the mass of the pseudoscalar state essentially degenerate with the mass of its scalar partner $\widetilde{\nu}^{\mathcal{R}}_{\tau L}$, but not with the other families of sneutrinos. In the third box of Table 5.2, we see that the $A^0_2(\widetilde{\nu}^{\mathcal{I}}_{\tau L})$ is the LSP with a mass of 126.4 GeV basically degenerate with the one of the state $h_2(\widetilde{\nu}^{\mathcal{R}}_{\tau L})$, which is the co-LSP. The next heavier state is now the $h_3(\widetilde{\nu}^{\mathcal{R}}_{R})$ with a mass of 501.2 GeV, since the other two families of left sneutrinos have masses of 776.4 GeV. The spectrum for the charged scalars is modified accordingly with respect to Table 5.1, e.g. $H^-_2(\tilde{\tau}_L)$ is the NLSP with a mass of 146.9 GeV, and no other state has mass degeneracy with this one.

Notice that we have modified in this table the values of the soft masses M_1 and M_2, with respect to Table 5.1, lowering them to 300 and 500 GeV, respectively. This is because the gaugino masses affect the seesaw mechanism generating neutrinos masses, as discussed in Subsection 3.3. Therefore, we have to choose the values of M_1 and M_2 in such a way that the mass of the heavier neutrino is maintained below the upper bound on the sum of neutrino masses ~ 0.23 eV [124], and above the square root of the mass-squared difference $\Delta m^2_{atm} \sim 2.42 \times 10^{-3}\text{eV}^2$ [125].

From the discussion below Eq. (4.5), one deduces that a simple way to decrease the mass of the LSP is to increase the left sneutrino VEVs. In particular, we show in Table 5.3 a point similar to the one of Table 5.2 but with $v_{3L}/\sqrt{2} = 5 \times 10^{-4}$ GeV. In this way, we obtain $\widetilde{\nu}^{\mathcal{I}}_{\tau L}$ and $\widetilde{\nu}^{\mathcal{R}}_{\tau L}$ co-LSPs with masses of about 97.8 GeV. The mass of the $\tilde{\tau}_L$ NLSP also decreases and becomes 122 GeV. For this point, the SM-like Higgs is heavier than the LSP and therefore, following our convention, is labeled as $h_2(H^{\mathcal{R}}_u)$ in the table.

Following the same strategy, in order to increase the mass of the LSP we can simply decrease the value of the concerned VEV. We show in Table 5.4 the case with $v_{3L}/\sqrt{2} = 3 \times 10^{-4}$ GeV giving rise to $\widetilde{\nu}^{\mathcal{I}}_{\tau L}$ and $\widetilde{\nu}^{\mathcal{R}}_{\tau L}$ co-LSPs with masses of about 146 GeV, and a $\tilde{\tau}_L$ NLSP with a mass of 163.6 GeV. In Table 5.5 we show another case with a larger sneutrino mass. For that we take $v_{3L}/\sqrt{2} = 9.48 \times 10^{-5}$ GeV obtaining now a $\widetilde{\nu}^{\mathcal{I}}_{\tau L}$ and $\widetilde{\nu}^{\mathcal{R}}_{\tau L}$ co-LSPs with masses of about 311 GeV. We have also changed the value of M_1 and λ to keep the Bino more massive than the LSP and to avoid too light mass scale for neutrinos, while having enough multileptonic decays. The value of A_λ is chosen in order to minimize the singlet composition of h_1 avoiding a decrease in its mass.

As we will discuss in Section 5.4, this range of sneutrino masses of about 95–310 GeV is the appropriate one for our analysis of signal detection.

Table 5.2: Benchmark point producing $\widetilde{\nu}^{\mathcal{I}}_{\tau L}$ and $\widetilde{\nu}^{\mathcal{R}}_{\tau L}$ co-LSPs, with masses of 126.4 GeV. Input parameters, and soft masses obtained from the minimization conditions, are given in the first and second boxes at the low scale M_{EWSB}. Sparticle masses are shown in the third box (with their dominant compositions written in brackets). Squark and gluino masses are the same as in Table 5.1 and not shown. Sneutrino branching ratios (larger than 10^{-4}) and decay widths are shown in the fourth and fifth boxes, respectively. VEVs, soft parameters, sparticle masses and decay widths are given in GeV.

λ	0.2	κ	0.3	Y^{ν}	5×10^{-7}
$v_{1,2L}/\sqrt{2}$	1×10^{-5}	$v_{3L}/\sqrt{2}$	4×10^{-4}	$v_R/\sqrt{2}$	1350
$\tan\beta$	10	A^u	-3177	$A^{d,e}$	1000
A^{λ}	1000	A^{κ}	-1000	A^{ν}	-400
M_1	300	M_2	500	M_3	1600
$m^2_{\tilde{Q}_L,\tilde{u}_R,\tilde{d}_R}$	1.69×10^6	$m^2_{\tilde{e}_R}$	10^6	–	–
m^2_{Hd}	3.62×10^6	m^2_{Hu}	-1.06×10^5	$m^2_{\tilde{\nu}_R}$	0.750×10^5
$m^2_{\tilde{L}_{eL}}$	0.598×10^6	$m^2_{\tilde{L}_{\mu L}}$	0.598×10^6	$m^2_{\tilde{L}_{\tau L}}$	1.35×10^4
$m_{h_1(H^{\mathcal{R}}_u)}$	124.2	$m_{h_2(\tilde{\nu}^{\mathcal{R}}_{\tau L})}$	126.4	$m_{h_3(\tilde{\nu}^{\mathcal{R}}_R)}$	501.2
$m_{h_4(\tilde{\nu}^{\mathcal{R}}_{eL})}$	776.4	$m_{h_5(\tilde{\nu}^{\mathcal{R}}_{\mu L})}$	776.4	$m_{h_6(H^{\mathcal{R}}_d)}$	1934.4
–	–	$m_{A^0_2(\tilde{\nu}^{\mathcal{I}}_{\tau L})}$	126.4	$m_{A^0_3(\tilde{\nu}^{\mathcal{I}}_{eL})}$	776.4
$m_{A^0_4(\tilde{\nu}^{\mathcal{I}}_{\mu L})}$	776.4	$m_{A^0_5(\tilde{\nu}^{\mathcal{I}}_R)}$	1099.9	$m_{A^0_6(H^{\mathcal{I}}_d)}$	1933.9
–	–	$m_{H^-_2(\tilde{\tau}_L)}$	146.9	$m_{H^-_3(\tilde{\mu}_L)}$	786.8
$m_{H^-_4(\tilde{e}_L)}$	786.8	$m_{H^-_5(\tilde{e}_R)}$	1000.4	$m_{H^-_6(\tilde{\mu}_R)}$	1000.5
$m_{H^-_7(\tilde{\tau}_R)}$	1000.5	$m_{H^-_8(H^-_d)}$	1936.2	–	–
$m_{\lambda^0_4(\tilde{H}^0_u/\tilde{H}^0_d)}$	241.2	$m_{\lambda^0_5(\tilde{H}^0_u/\tilde{H}^0_d)}$	280.8	$m_{\lambda^0_6(\tilde{B}^0)}$	317.2
$m_{\lambda^0_7(\tilde{W}^0)}$	531.4	$m_{\lambda^0_8(\nu_R)}$	809.6	–	–
$m_{\lambda^-_4(\tilde{H}^-_d/(\tilde{H}^+_u)^c)}$	264	$m_{\lambda^-_5(\tilde{W}^-)}$	531.5	–	–
$\mathrm{BR}(A^0_2\to\nu\nu)$		0.4430	$\sum_{l=e,\mu,\tau}\mathrm{BR}(A^0_2\to\tau^{\pm}l^{\mp})$		0.5548
$\mathrm{BR}(A^0_2\to\bar{b}b)$		0.0008	$\mathrm{BR}(A^0_2\to gg)$		0.0015
$\mathrm{BR}(h_2\to\nu\nu)$		0.0059	$\sum_{l'=e,\mu}\mathrm{BR}(h_2\to\tau^{\pm}l'^{\mp})$		0.0048
$\mathrm{BR}(h_2\to\tau^+\tau^-)$		0.1168	$\mathrm{BR}(h_2\to\mu^+\mu^-)$		0.0003
$\mathrm{BR}(h_2\to\bar{b}b)$		0.4315	$\mathrm{BR}(h_2\to\bar{c}c)$		0.0306
$\mathrm{BR}(h_2\to gg)$		0.1143	$\mathrm{BR}(h_2\to\gamma\gamma)$		0.003
$\mathrm{BR}(h_2\to W^{\pm}W^{\mp*})$		0.2624	$\mathrm{BR}(h_2\to ZZ^*)$		0.0301
$\Gamma(h_2)$		6.75×10^{-11}	$\Gamma(A^0_2)$		9.14×10^{-13}

Similarly, we could have worked with a fix value for v_{3L} but varying the value of A^{ν}. For example, for $v_{3L}/\sqrt{2}=5\times10^{-4}$ GeV as in Table 5.3, with A^{ν} in the range between -385 and -435 GeV one can obtain the $\widetilde{\nu}^{\mathcal{I}}_{\tau L}$ LSP with a mass in the range of about 95 and 145 GeV. Needless to say, we could also play around with the other relevant input parameters for our computation, i.e. λ, κ, Y^{ν}, $\tan\beta$, v_R, still obtaining this range of masses for the LSP.

5.3 Decay Modes.

In section 4.3 we have described the decay pattern of the left sneutrino LSP through some approximate formulas, based on the mass insertion approximation. We can illustrate now this formulas with the values the BPs presented in previous sections.

In the discussion of Sec. 4.3 is shown that the $H^{u/d}$ of the left scalar sneutrino is

Table 5.3: The same as in Table 5.2 but for $\widetilde{\nu}^{\mathcal{I}}_{\tau L}$ and $\widetilde{\nu}^{\mathcal{R}}_{\tau L}$ co-LSPs with masses of 97.8 GeV considering $v_{3L}/\sqrt{2} = 5 \times 10^{-4}$ GeV and $A^{\nu} = -385$ GeV. In the first and second boxes we show only the parameters whose values have changed.

$m^2_{\widetilde{L}_{eL}}$	0.454×10^6	$m^2_{\widetilde{L}_{\mu L}}$	0.454×10^6	$m^2_{\widetilde{L}_{\tau L}}$	0.692×10^4
$m_{h_1(\tilde{\nu}^{\mathcal{R}}_{\tau L})}$	97.8	$m_{h_2(H^{\mathcal{R}}_u)}$	124.7	$m_{h_3(\tilde{\nu}^{\mathcal{R}}_R)}$	501.2
$m_{h_4(\tilde{\nu}^{\mathcal{R}}_{\mu L})}$	676.8	$m_{h_5(\tilde{\nu}^{\mathcal{R}}_{eL})}$	676.8	–	–
–	–	$m_{A^0_2(\tilde{\nu}^{\mathcal{I}}_{\tau L})}$	97.8	$m_{A^0_3(\tilde{\nu}^{\mathcal{I}}_{\mu L})}$	676.8
$m_{A^0_4(\tilde{\nu}^{\mathcal{I}}_{eL})}$	676.8	$m_{A^0_5(\tilde{\nu}^{\mathcal{I}}_R)}$	1099.9	–	–
–	–	$m_{H^-_2(\tilde{\tau}_L)}$	122	$m_{H^-_3(\tilde{\mu}_L)}$	666.8
$m_{H^-_4(\tilde{e}_L)}$	666.8	$m_{H^-_5(\tilde{e}_R)}$	1000.2	$m_{H^-_6(\tilde{\mu}_R)}$	1000.2
$m_{H^-_7(\tilde{\tau}_R)}$	1000.2	–	–	–	–
$\mathrm{BR}(A^0_2 \to \nu\nu)$		0.5515	$\sum_{l=e,\mu,\tau} \mathrm{BR}(A^0_2 \to \tau^{\pm} l^{\mp})$		0.4483
$\mathrm{BR}(h_1 \to \nu\nu)$		0.507	$\sum_{l=e,\mu,\tau} \mathrm{BR}(h_1 \to \tau^{\pm} l^{\mp})$		0.3889
$\mathrm{BR}(h_1 \to \bar{b}b)$		0.0854	$\mathrm{BR}(h_1 \to \bar{c}c)$		0.0053
$\mathrm{BR}(h_1 \to gg)$		0.00112	$\mathrm{BR}(h_1 \to \gamma\gamma)$		0.0005
$\mathrm{BR}(h_1 \to W^{\pm}W^{\pm *})$		0.0013	–		–
$\Gamma(h_1)$		9.3×10^{-13}	$\Gamma(A^0_2)$		8.5×10^{-13}

Table 5.4: The same as in Table 5.2 but for $\widetilde{\nu}^{\mathcal{I}}_{\tau L}$ and $\widetilde{\nu}^{\mathcal{R}}_{\tau L}$ co-LSPs with masses of 146 GeV, choosing $v_{3L}/\sqrt{2} = 3\times10^{-4}$ GeV. In the first and second boxes we show only the parameters whose values have been changed.

$m^2_{\widetilde{L}_{eL}}$	0.590×10^6	$m^2_{\widetilde{L}_{\mu L}}$	0.590×10^6	$m^2_{\widetilde{L}_{\tau L}}$	1.87×10^4
$m_{h_1(H^{\mathcal{R}}_u)}$	124.8	$m_{h_2(\tilde{\nu}^{\mathcal{R}}_{\tau L})}$	146	$m_{h_3(\tilde{\nu}^{\mathcal{R}}_R)}$	501.2
$m_{h_4(\tilde{\nu}^{\mathcal{R}}_{eL})}$	771.3	$m_{h_5(\tilde{\nu}^{\mathcal{R}}_{\mu L})}$	771.13	–	–
$m_{A^0_2(\tilde{\nu}^{\mathcal{I}}_{\tau L})}$	146	$m_{A^0_3(\tilde{\nu}^{\mathcal{I}}_{eL})}$	771.3	$m_{A^0_4(\tilde{\nu}^{\mathcal{I}}_{\mu L})}$	771.3
$m_{A^0_5(\tilde{\nu}^{\mathcal{I}}_R)}$	1100	–	–	–	–
$m_{H^-_2(\tilde{\tau}_L)}$	163.6	$m_{H^-_3(\tilde{\mu}_L)}$	786.8	$m_{H^-_4(\tilde{e}_L)}$	786.8
$m_{H^-_5(\tilde{e}_R)}$	1000.5	$m_{H^-_6(\tilde{\mu}_R)}$	1000.5	$m_{H^-_7(\tilde{\tau}_R)}$	1000.5
$\mathrm{BR}(A^0_2 \to \nu\nu)$		0.3250	$\sum_{l=e,\mu,\tau} \mathrm{BR}(A^0_2 \to \tau^{\pm} l^{\mp})$		0.6719
$\mathrm{BR}(A^0_2 \to \bar{b}b)$		0.0007	$\mathrm{BR}(A^0_2 \to gg)$		0.0021
$\mathrm{BR}(h_2 \to \nu\nu)$		0.1668	–		–
$\mathrm{BR}(h_2 \to \tau^+\tau^-)$		0.2492	$\sum_{l'=e,\mu} \mathrm{BR}(h_2 \to \tau^{\pm} l'^{\mp})$		0.2284
$\mathrm{BR}(h_2 \to \bar{b}b)$		0.0716	$\mathrm{BR}(h_2 \to \bar{c}c)$		0.0056
$\mathrm{BR}(h_2 \to gg)$		0.0293	$\mathrm{BR}(h_2 \to \gamma\gamma)$		0.0007
$\mathrm{BR}(h_2 \to W^{\pm}W^{\mp *})$		0.2198	$\mathrm{BR}(h_2 \to ZZ^*)$		0.028
$\Gamma(h_2)$		1.69×10^{-12}	$\Gamma(A^0_2)$		8.7×10^{-13}

enhanced when its mass is in the vicinity of the Higgs boson. And that such a behavior is not observed for the pseudoscalar state. We can see an example of this taking a look for example in (the fourth box of) Table 5.1 that, for the BP analyzed there, the result of the numerical computation for the decays of the light left sneutrinos into charm quarks, using the interaction in Appendix B, is $\mathrm{BR}(A^0_{2,3} \to \bar{c}c) = 0.0007$. Of course, decays into top quarks are kinematically forbidden, given the sneutrino mass considered there of 125.4 GeV. Nevertheless,for the scalar sneutrino the numerical computation using the interaction in Appendix B gives $\mathrm{BR}(h_{2,3} \to \bar{c}c) = 0.033$ for the BP of Table 5.1. A much bigger result than for the pseudoscalar sneutrino. The enhanced mixing is the reason also why

Table 5.5: The same as in Table 5.2 but for $\widetilde{\nu}^{\mathcal{I}}_{\tau L}$ and $\widetilde{\nu}^{\mathcal{R}}_{\tau L}$ co-LSPs with masses of 310.9 GeV. In the first, second and third boxes we show only the parameters whose values have been changed.

λ	0.35	A^{λ}	3714	$v_{3L}/\sqrt{2}$	9.48×10^{-5}
M_1	500	–	–	–	–
m^2_{Hd}	1.90×10^7	m^2_{Hu}	-1.42×10^5	$m^2_{\widetilde{\nu}_R}$	-4.345×10^4
$m^2_{\widetilde{L}_{eL}}$	0.590×10^6	$m^2_{\widetilde{L}_{\mu L}}$	0.590×10^6	$m^2_{\widetilde{L}_{\tau L}}$	7.55×10^4
$m_{h_1(H^{\mathcal{R}}_u)}$	125.3	$m_{h_2(\widetilde{\nu}^{\mathcal{R}}_{\tau L})}$	310.9	$m_{h_3(\widetilde{\nu}^{\mathcal{R}}_R)}$	523.3
$m_{h_4(\widetilde{\nu}^{\mathcal{R}}_{eL})}$	778.1	$m_{h_5(\widetilde{\nu}^{\mathcal{R}}_{\mu L})}$	778.1	$m_{h_6(H^{\mathcal{R}}_d)}$	4423
$m_{A^0_2(\widetilde{\nu}^{\mathcal{I}}_{\tau L})}$	310.9	$m_{A^0_3(\widetilde{\nu}^{\mathcal{I}}_{eL})}$	778.1	$m_{A^0_4(\widetilde{\nu}^{\mathcal{I}}_{\mu L})}$	778.1
$m_{A^0_5(\widetilde{\nu}^{\mathcal{I}}_R)}$	1079.4	$m_{A^0_6(H^{\mathcal{I}}_d)}$	4420.7	–	–
$m_{H^-_2(\widetilde{\tau}_L)}$	311	$m_{H^-_3(\widetilde{\mu}_L)}$	780.4	$m_{H^-_4(\widetilde{e}_L)}$	780.4
$m_{H^-_5(\widetilde{e}_R)}$	985.2	$m_{H^-_6(\widetilde{\mu}_R)}$	985.2	$m_{H^-_7(\widetilde{\tau}_R)}$	988.3
$m_{H^-_8(H^-_d)}$	4421.4	–	–	–	–
$m_{\lambda^0_4(\tilde{H}^0_u/\tilde{H}^0_d)}$	421.6	$m_{\lambda^0_5(\tilde{H}^0_u/\tilde{H}^0_d)}$	484.8	$m_{\lambda^0_6(\tilde{B}^0)}$	501.4
$m_{\lambda^0_7(\tilde{W}^0)}$	567.1	$m_{\lambda^0_8(\nu_R)}$	814.5	–	–
$m_{\lambda^-_4(\tilde{H}^-_d/(\tilde{H}^+_u)^c)}$	436.7	$m_{\lambda^-_5(\tilde{W}^-)}$	563.4	–	–
$\mathrm{BR}(A^0_2 \to \nu\nu)$		0.0569	$\sum_{l=e,\mu,\tau} \mathrm{BR}(A^0_2 \to \tau^{\pm} l^{\mp})$		0.7565
$\mathrm{BR}(A^0_2 \to \bar{b}b)$		0.0002	$\mathrm{BR}(A^0_2 \to gg)$		0.0070
$\mathrm{BR}(h_2 \to \nu\nu)$		0.0374	$\mathrm{BR}(h_2 \to h_1 h_1)$		0.2877
$\mathrm{BR}(h_2 \to \tau^+\tau^-)$		0.1846	$\sum_{l'=e,\mu} \mathrm{BR}(h_2 \to \tau^{\pm} l'^{\mp})$		0.3308
$\mathrm{BR}(h_2 \to \bar{b}b)$		0.0005	$\mathrm{BR}(h_2 \to gg)$		0.005
$\mathrm{BR}(h_2 \to W^{\pm}W^{\mp *})$		0.1017	$\mathrm{BR}(h_2 \to ZZ^*)$		0.0475
$\Gamma(h_2)$		8.13×10^{-13}	$\Gamma(A^0_2)$		5.3×10^{-13}

the numerical result of Table 5.1 using the interaction in Appendix B, shows that the BR into bottom quarks is the largest one with a value $\mathrm{BR}(h_{2,3} \to \bar{b}b) = 0.468$, while for the pseudoscalar is only $\mathrm{BR}(A_{2,3} \to \bar{b}b) = 0.0017$.

As a consequence of the mixing of the scalar sneutrino with $H^{\mathcal{R}}_{u,d}$ discussed above, a sizable decay channel into photons is generated:

$$\widetilde{\nu}^{\mathcal{R}}_{iL} \to \gamma\gamma \ , \tag{5.11}$$

, with $\mathrm{BR}(h_{2,3} \to \gamma\gamma) = 0.003$ as shown in Tables 5.1 and 5.2. For an early work analyzing $\tilde{\nu}_L \to \gamma\gamma$ in the context of trilinear $\not{R}_p$, see Ref. [126], where a negligible BR$\sim 10^{-6}$ was obtained. This decay of the scalar sneutrino into two photons in a way not very different from the Higgs, can be very interesting for our purposes. Let us recall in this sense that the Higgs was discovered thanks to this kind of decay. Although the associated BR is far from being the dominant one, the diphoton signal is very clear and easy to disentangle from the SM backgrounds.

Notice however, that for other masses of the sneutrino as in Tables 5.3–5.5, the BR to photons is decreased. For example, in Table 5.3 one obtains $\mathrm{BR}(h_{2,3} \to \gamma\gamma) = 0.0005$. This is because the mixing of the scalar left sneutrino with the SM Higgs is reduced when the separation between their masses is increased. In addition, the BR of the $H^{\mathcal{R}}_u$ to diphoton is maximal in the vicinity of the mass of the SM Higgs.

For the leptonic decays, the approximation obtained through the mass insertion is better and the equations give a good approximation of the full numerical value. We can see for example that for an electron sneutrino LSP the contribution in Eq. (4.18) is proportional

to Y^e, and therefore suppressed with respect to the one in Eq. (4.17), where typically $\frac{\lambda v_R}{(2A^\lambda+\sqrt{2}\kappa v_R)\tan\beta} \approx 10^{-2}$. For a muon sneutrino LSP, however, Y^μ is larger than Y^e and we obtain for the BP in Table 5.1 that the contribution in Eq. (4.18) is a factor of order 3 larger than that of Eq. (4.17). See e.g. in Table 5.1 that $\mathrm{BR}(A_2^0 \to \mu^\pm\mu^\mp) = 0.0055$ whereas $\mathrm{BR}(A_2^0 \to \tau^\pm\tau^\mp) = 0.0003$. Notice also that $\mathrm{BR}(A_2^0 \to \bar{b}b) = 0.0017$ is larger than the later mainly because of the factor 3 of color that has to be included in the computation.

On the other hand, for a tau sneutrino LSP, the contribution in Eq. (4.18) is larger than Eqs. (4.17) and Eqs. (4.14). As a consequence, in this case one dominant decay channel for the pseudoscalar (and scalar) left sneutrino is into leptons:

$$\widetilde{\nu}_{\tau L}^{\mathcal{I},\mathcal{R}} \to \tau_L^+ l_L^- \ , \tau_R^- l_R^+ \ , \tag{5.12}$$

where $l = e, \mu, \tau$. In Table 5.2, we see for example that $\sum_{l=e,\mu,\tau} BR(A_2^0 \to \tau^\pm l^\mp) = 0.55$. Similar results, 0.44, 0.67, and 0.75, are obtained in Tables 5.3–5.5, respectively, where other tau sneutrino masses are analyzed.

Finally, the sneutrino can decay to neutrinos. For an electron or muon pseudoscalar sneutrino LSP, the contributions in Eq. (4.22) are of the order of 10 larger than the largest one in Eq. (4.17) which is proportional to Y^μ. This is the reason why in Table 5.1 we obtain $\mathrm{BR}(A_2^0 \to \nu\nu) = 0.97$ and $\mathrm{BR}(A_3^0 \to \nu\nu) = 0.99$. As a consequence, the dominant decay channel is the one shown in Fig. 4.1 e) and f) into neutrinos

$$\widetilde{\nu}_{i_L}^{\mathcal{I}} \to \nu_{i_L}\nu_{j_L} \ , \nu_{i_R}^c \nu_{j_R}^c \ . \tag{5.13}$$

For a tau sneutrino LSP, the contributions in Eq. (4.22) are of the same order as that in Eq. (4.19)-(4.19), and therefore there are two dominant decay channels, those in Eqs. (5.13) and (5.12). The relative size between them depends on the values of the gaugino masses M_1 and M_2 necessary to reproduce the correct neutrino physics as discussed in Section 3.5, and the left sneutrino VEVs v_{iL}. In Table 5.2, we see for example that $\sum_{l=e,\mu,\tau} BR(A_2^0 \to \tau^\pm l^\mp) = 0.55$ vs $\mathrm{BR}(A_2^0 \to \nu\nu) = 0.44$.

As we will discuss in detail in the next section,scalar and pseudoscalar sneutrinos can be produced in pairs at the LHC, and as a consequence, some of the above decay modes can give rise to detectable signals. In particular, this is the case of diphoton plus missing transverse energy (MET) from sneutrinos of any family combining the channel in Eq. (5.11) with that of Eq. (5.13), and diphoton plus leptons from tau sneutrinos combining the channels in Eqs. (5.11) and (5.12). An interesting multilepton signal can also be produced combining the decay channels for scalar and pseudoscalar tau sneutrinos in Eq. (5.12).

5.4 Detection at the LHC.

The dominant pair production channels of sleptons at Hadron colliders were studied in Refs. [99, 100, 101, 102, 103, 104]. In Figs. 7.1–5.3, we show the detectable signals discussed above from a pair production at the LHC of sneutrinos LSP.The sparticles are denoted in the figures by their dominant composition.

Concerning the sneutrino production,the direct one of e.g. Fig. 7.1a occurs via a Z channel giving rise to a pair of scalar and pseudoscalar left sneutrinos. As discussed in Section 4.1, these states have essentially degenerate masses and therefore are co-LSPs. On the other hand, since the left slepton in the same $SU(2)$ doublet as the left sneutrino, it becomes the NLSP, and its direct production and decay is another important source

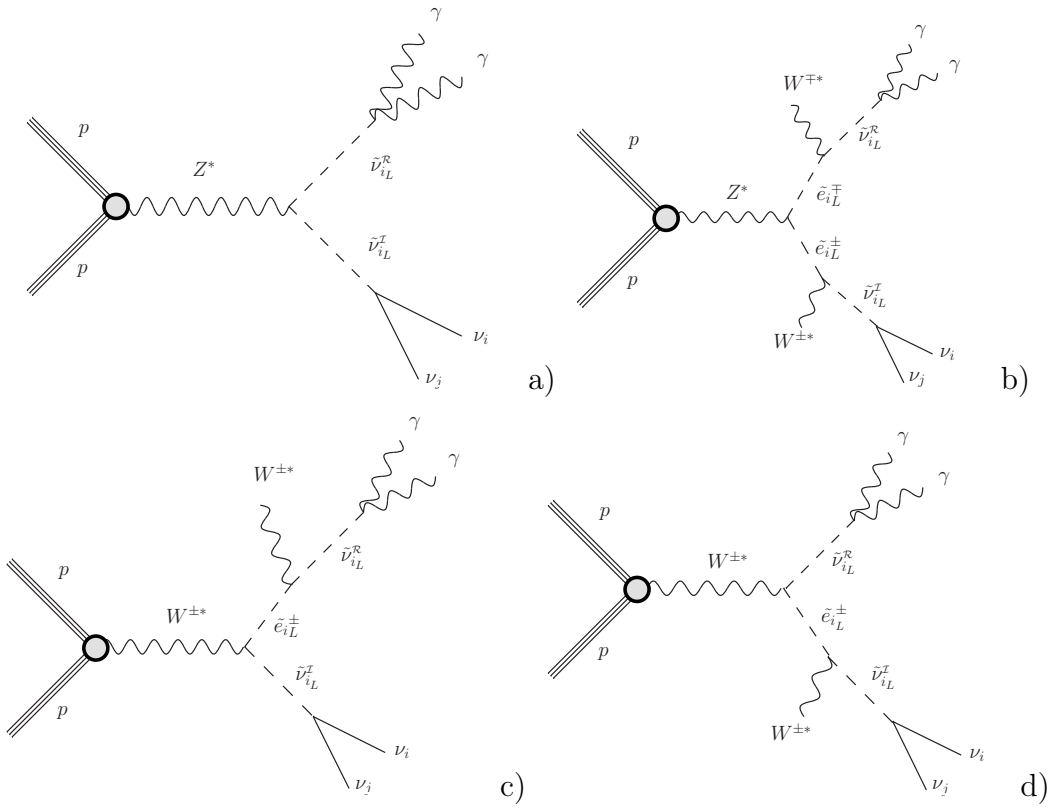

Figure 5.1: Dominant decay channels into diphoton plus neutrinos from a pair production at the LHC of scalar and pseudoscalar sneutrinos LSP of any of the three families, $\widetilde{\nu}^{\mathcal{I}}_{iL}$, with $i = e, \mu, \tau$. Filled circles indicate effective interactions.

of the sneutrino LSP. In particular, pair production can be obtained through a γ or a Z decaying into $\tilde{e}^{+}_{iL}\tilde{e}^{-}_{iL}$ (Fig. 7.1b), with the sleptons dominantly decaying into a (scalar or pseudoscalar) sneutrino plus an off-shell $W^{\pm}$ producing a soft meson or a pair of a lepton and a neutrino ($\tilde{e}^{\pm}_{iL} \to e^{\pm}_{j}\ \nu_k\ \widetilde{\nu}^{\mathcal{R},\mathcal{I}}_{lL}$), which are usually undetectable. Besides, sneutrinos can be pair produced through a $W^{\pm}$ decaying into $\tilde{e}^{\pm}_{iL}\widetilde{\nu}_{jL}$ (Figs. 7.1c-d), with the slepton decaying as before.

Concerning the signals, we will study first diphoton plus MET arising from the production and decay of a pair of sneutrinos $\widetilde{\nu}^{\mathcal{I}}_{i_L}\ \widetilde{\nu}^{\mathcal{R}}_{i_L}$ of any family, $i = e, \mu, \tau$, as shown in Fig. 7.1. Second, we will focus on other channels that can be produced via the $\widetilde{\nu}_{\tau_L}$ LSP, given the large value of the tau Yukawa coupling. This is the case of diphoton plus leptons, and multileptons, as shown in Figs. 5.2 and 5.3, respectively.

These signatures for a sneutrino LSP are similar to the final states presented in several analysis of ATLAS and CMS. In particular, those including photons plus MET/leptons (see for example Refs. [127, 128, 129, 130, 131, 132]). However, these searches are designed typically towards the production of colored sparticles in the context of R_p conservation. Therefore, the analysis normally requires a large amount of MET, several energetic jets or a large effective mass. Thus, these searches are inefficient looking for events of direct pair production of the sneutrino in our scenario.

We have also confronted all our BPs with LHC searches [128, 133, 134, 135, 136, 137, 138, 139, 140, 141, 142, 132] using `CheckMATE` 2 [143, 144, 145, 146, 147, 148], and LEP searches using `HiggsBounds-4.3.1` [149, 150, 151, 152, 153]. In the case of the multilepton signal, there exist generic searches for production of three or more leptons, which include also signal regions with a low missing transverse momentum and total transverse energy

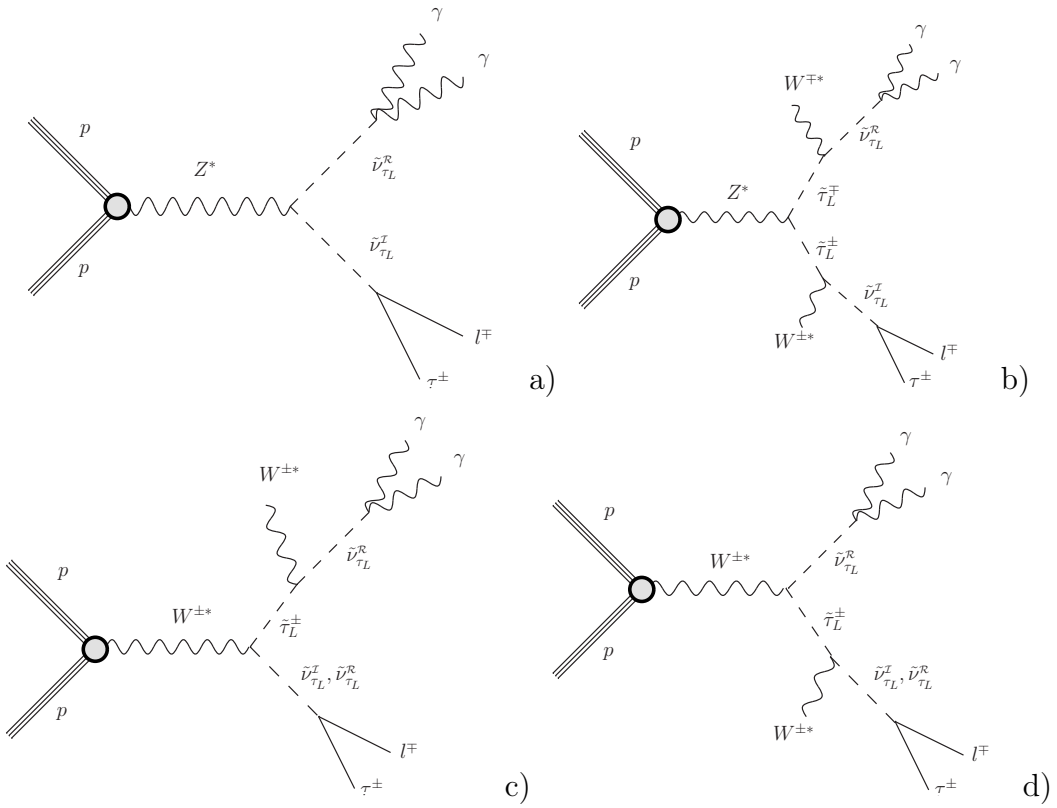

Figure 5.2: Dominant decay channels into diphoton plus leptons ($l = e, \mu, \tau$) from a pair production at the LHC of scalar and pseudoscalar sneutrinos LSP of the third family $\widetilde{\nu}_{\tau L}$. Filled circles indicate effective interactions.

Table 5.6: Madgraph cuts. P_T is given in GeV.

P_T for *jets*	$\lvert\eta\rvert$ for *jets*	P_T for e, μ	$\lvert\eta\rvert$ for e, μ	P_T for γ	$\lvert\eta\rvert$ for γ
> 20	< 5	> 10	< 2.5	> 10	< 2.5

(see Refs. [154, 155]). In these works, by lepton is meant e, μ or hadronically decaying τ ($\tau_{\rm h}$) candidate. These searches are close to be sensitive to our signal, and an updated analysis with current data could put constraints on the sneutrino LSP scenario. Let us finally remark that past collider searches in the context of trilinear $\not{R}_p$ couplings [156, 157, 158, 159, 160, 161, 162, 163, 164, 165, 166, 167, 168] are ineffectual for our scenario.

The strategy that we will follow for the analyses of the sneutrino signals in the $\mu\nu$SSM is the following. Ten thousand events are generated for each case with `MadGraph5_aMC@NLO` [113] at leading order (LO) of perturbative QCD simulating the production of the described process. We include the next-to-leading order (NLO) [103] and next-to-leading logarithmic accuracy (NLL) [169] results using a K-factor of about 1.2. The hard process simulation is then passed for decay and hadronization to `PYTHIA` [114]. The output is passed through a naive and fast detector simulation (`PGS`) [170]. The standard card for `MadGraph5_aMC@NLO` is used, which includes the cuts presented in Table 5.6. `PYTHIA` is executed with initial state radiation (ISR), final state radiation (FSR) and multiple interactions switched on. Besides, `PYTHIA` will consider the τ lepton as stable to make it decay with the `TAUOLA` [171, 172] routine within `PGS`. The package `PGS` is finally executed using a card designed for ATLAS, as shown in Table 5.7. The output of `PGS` is passed through some selection criteria to avoid overlapping and to discard the events outside the detector coverage according to

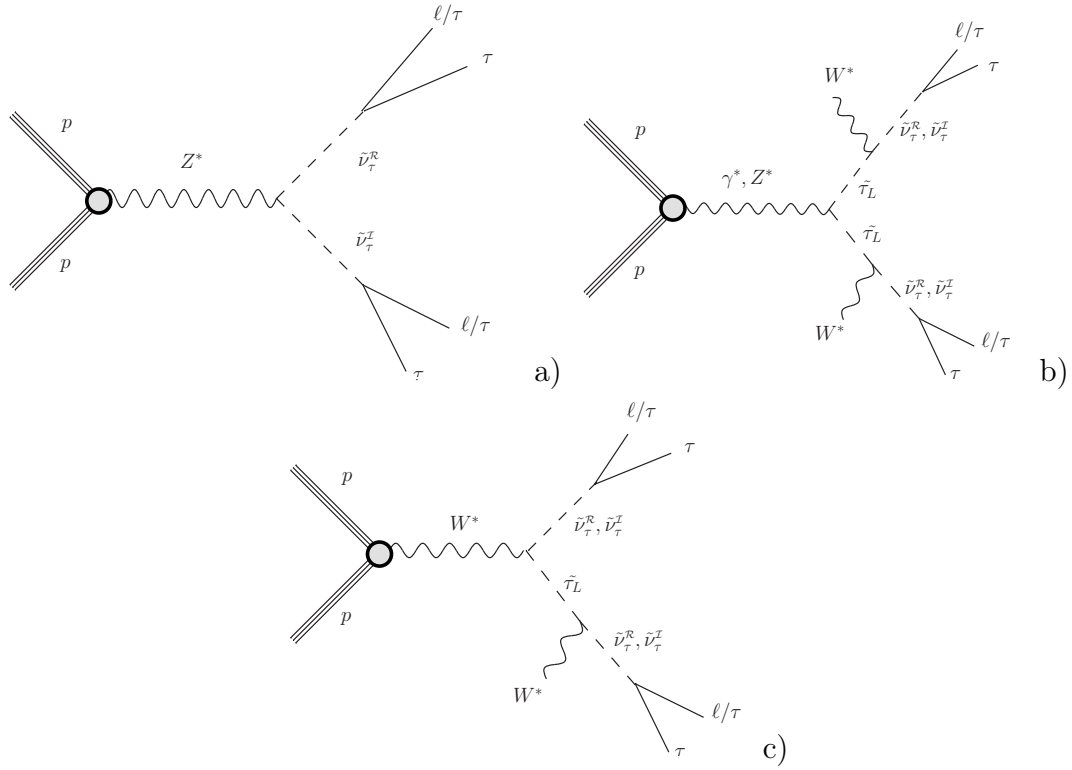

Figure 5.3: Decay channels into multileptons ($l = e, \mu, \tau$) from a pair production at the LHC of scalar and pseudoscalar sneutrinos LSP of the third family $\widetilde{\nu}_{\tau L}$. Filled circles indicate effective interactions.

Table 5.7: `PGS` configuration. ECAL and HCAL stand for Electromagnetic Calorimeter and Hadronic Calorimeter, respectively.

η cells in calorimeter	81	ϕ cells in calorimeter	63
η width of calorimeter cells	0.1	ϕ width of calorimeter cells	0.09973
ECAL resolution	0.01	ECAL resolution $\times\sqrt{E}$ (GeV$^{1/2}$)	0.1
HCAL resolution $\times\sqrt{E}$ (GeV$^{1/2}$)	0.8	MET resolution	0.2
Calorimeter cell edge crack fraction	0.00	Jet finding algorithm	anti-k_t [147]
Calorimeter trigger cluster finding seed threshold	3.0	Calorimeter trigger cluster finding shoulder threshold	0.5
Calorimeter k_t cluster finder one size (ΔR)	0.7	Outer radius of tracker (m)	1.0
Magnetic field (T)	2.0	Sagitta resolution (m)	5×10^{-6}
Track finding efficiency	0.98	Minimum track P_T (GeV/c)	0.30
Tracking η coverage	2.5	e/gamma η coverage	3.0
Muon η coverage	2.4	Tau η coverage	2.0

Ref. [173]. That is, first candidate events should pass the requirements of Table 5.8. After the previous process, overlapping objects are removed applying the following requirements in this precise order: First, if two electrons as candidates are identified within $\Delta R = 0.05$ of each other, the one with lower transverse momentum (P_T) is discarded. Here ΔR is defined as $\sqrt{(\Delta\Phi)^2 + (\Delta\eta)^2}$, where $\Delta\Phi$ is the difference in involved azimuthal angles while $\Delta\eta$ is the difference of concerned pseudo-rapidities. Then if an electron and a jet candidates are within $\Delta R = 0.2$ of each other, the jet is discarded. All remaining leptons are required to be separated by more than $\Delta R = 0.4$ from the closest remaining jet. Whenever an electron and a muon candidates overlap within $\Delta R = 0.01$, both are discarded. Also, if two muons

Table 5.8: Event filtering. P_T is given in GeV.

P_T for *jets*	$\|\eta\|$ for *jets*	P_T for e	$\|\eta\|$ for e	P_T for μ	$\|\eta\|$ for μ	P_T for $\tau_{\rm h}$	$\|\eta\|$ for $\tau_{\rm h}$	P_T for γ	$\|\eta\|$ for γ
> 30	< 4.5	> 15	< 2.47 & outside $1.37 - 1.52$	> 10	< 2.5	> 10	< 2.5	> 25	2.37 & outside $1.37 - 1.52$

Table 5.9: Analysis of the signal with diphoton plus MET from production and decay of a pair of sneutrino co-LSPs of the type $\widetilde{\nu}_{eL}$ or $\widetilde{\nu}_{\mu L}$, corresponding to the BP in Table 5.1. Production cross sections are shown in fb in the first box for a $\widetilde{\nu}_{eL}/\widetilde{\nu}_{\mu L}$ mass of 125.4 GeV. The number of events of the signal and background is shown in the second box, together with the effect of a set of cuts, assuming 13 TeV centre-of-mass energy with $\mathcal{L} = 300$ fb^{-1}. Energies, momenta and invariant mass are given in GeV.

$\sigma(pp \to Z^* \to h_2 A_2^0)$	107.08
$\sigma(pp \to \gamma^*, Z^* \to H_2^+ H_2^- \to h_2 A_2^0 + W^+_{\rm soft} W^-_{\rm soft})$	21.89
$\sigma(pp \to W^{\pm *} \to H_2^\pm\ h_2/A_2^0 \to h_2 A_2^0 + W^\pm_{\rm soft})$	142.8
$\sigma(pp \to Z^* \to h_3 A_3^0)$	106.536
$\sigma(pp \to \gamma^*, Z^* \to H_3^+ H_3^- \to h_3 A_3^0 + W^+_{\rm soft} W^-_{\rm soft})$	20.12
$\sigma(pp \to W^{\pm *} \to H_3^\pm\ h_3/A_3^0 \to h_3 A_3^0 + W^\pm_{\rm soft})$	142.4

Dataset	$N_{\rm ev}$	$E_T^{\rm miss}$ > 200	$P_{T1}^{\gamma 1}$ > 100	$P_{T2}^{\gamma 2}$ > 50	N_γ=2	$N_l = 0$	ΔR < 1.5	$M_{\gamma\gamma} \in$ [115, 135]
Signal	449.45±0.02	103.6±0.8	80.3±0.7	41.0±0.5	41.0±0.5	36.4±0.5	35.9±0.5	34.1±0.5
$2jets$ +I/FSR	10^7	0	0	0	0	0	0	0
jet +I/FSR	10^7	0	0	0	0	0	0	0
H (ggF)	5424	0	0	0	0	0	0	0
Z+H	120.8±0.4	6.9±0.3	5.9±0.3	3.3±0.2	3.3±0.2	3.2±0.2	3.1±0.2	2.9±0.2
Z+ISR	11310±40	104±11	97±10	33±6	33±6	33±6	8±3	1±1
W+FSR	2.14×10^5 ±76	60±9	57±9	13±4	13±4	6±3	1.4±1.4	0
$\frac{S}{\sqrt{B}}$	—	7.9±0.5	6.3±0.4	5.9±0.7	5.9±0.7	5.6±0.7	10±2	17±3

are separated by less than $\Delta R = 0.05$, both are removed. τ's as candidates are required to be separated by more than $\Delta R = 0.2$ from the closest e or μ; otherwise they are discarded. Finally, photons are required to be separated by $\Delta R = 0.4$ from any reconstructed jet and $\Delta R = 0.01$ from any e [174]. A similar process, with a higher number of events when required by precision, is implemented to generate background samples at NLO.

Diphoton plus MET

The pair production of left sneutrinos can generate one scalar and one pseudoscalar, as shown in Fig. 7.1. This opens the possibility of the pseudoscalar sneutrino decaying into neutrinos, i.e., producing MET, and the scalar sneutrino decaying into two photons in a way not very different from the Higgs.

In what follows, we will discuss first the case of sneutrinos co-LSPs of the first two families ($\widetilde{\nu}_{eL}$, $\widetilde{\nu}_{\mu L}$) with masses of about 125 GeV as representative in order to search for a signal. This is because the sensible range of masses turns out to be

$$118 \lesssim m_{\widetilde{\nu}_{iL}} \lesssim 132 \ \text{GeV} \ , \tag{5.14}$$

in order to treat the sneutrinos as promptly decaying particles with a decay length $\lesssim$

Table 5.10: The same as in Table 5.9 but showing the production cross sections and the event sample generated with 14 TeV centre-of-mass energy.

$\sigma(pp \to Z^* \to h_2 A_2^0)$	119.95
$\sigma(pp \to \gamma^*, Z^* \to H_2^+ H_2^- \to h_2 A_2^0 + W^+_{\rm soft} W^-_{\rm soft})$	25.43
$\sigma(pp \to W^{\pm *} \to H_2^\pm\ h_2/A_2^0 \to h_2 A_2^0 + W^\pm_{\rm soft})$	160.7
$\sigma(pp \to Z^* \to h_3 A_3^0)$	119.83
$\sigma(pp \to \gamma^*, Z^* \to H_3^+ H_3^- \to h_3 A_3^0 + W^+_{\rm soft} W^-_{\rm soft})$	23.35
$\sigma(pp \to W^{\pm *} \to H_3^\pm\ h_3/A_3^0 \to h_3 A_3^0 + W^\pm_{\rm soft})$	158.9

Dataset	N_{ev}	$E_T^{\rm miss}$ > 200	$P_{T1}^{\gamma 1}$ > 100	$P_{T2}^{\gamma 2}$ > 50	N_γ=2	$N_l = 0$	ΔR < 1.5	$M_{\gamma\gamma} \in$ $[115, 135]$
Signal	503.40±0.02	116.3±0.9	95.0±0.8	50.8±0.6	50.5±0.6	43.8±0.6	43.3±0.6	38.8±0.6
$2jets$ +I/FSR	10^7	0	0	0	0	0	0	0
jet +I/FSR	10^7	0	0	0	0	0	0	0
H (ggF)	6104	0	0	0	0	0	0	0
Z+H	133.76 ±0.01	7.9±0.3	6.7±0.3	3.5±0.2	3.5±0.2	3.4±0.2	3.3±0.2	3.0±0.2
Z+ISR	9284.91 ±0.09	90±3	82±3	26±2	26±2	25±2	8±1	1.2±0.3
W+FSR	23708±2	57±9	54±9	5±3	5±3	1.6±1.61	0	0
$\frac{S}{\sqrt{B}}$	—	9.3±0.5	8.0±0.4	8.7±0.7	8.7±0.7	8.1±0.6	13.0±0.8	19±1

0.1 mm. For the case of the tau sneutrino, $\widetilde{\nu}_{\tau_L}$, where decay lengths of this order can be obtained for masses $\gtrsim$ 95 GeV, the above mass range is still valid because outside it the number of events turns out to be too small, as we will discuss below.

The case of $\widetilde{\nu}_{e_L}$ and $\widetilde{\nu}_{\mu_L}$ co-LSPs is shown in Table 5.9. The cross sections for the pair production of sneutrinos calculated by `MadGraph5_aMC@NLO` 2.3.2.2 at LO for 13 TeV centre-of-mass energy, including a K-factor of 1.2 for the NLO results, are shown in the first box of that Table. The first, second and third rows of that box correspond to the diagrams in Figs. 7.1a, 7.1b and 7.1c-d, respectively. Taking into account these values for the cross sections, the BRs of the corresponding Table 5.1, and using an integrated luminosity of $\mathcal{L} = 300$ fb^{-1}, we obtain a signal with about 449 events. Although this BP suffers from a significant SM background mainly due to the Z+H channel which decays in a similar way, we found that the number of expected events for the signal is still sufficient to give a significant evidence. The effect of a set of cuts on missing transverse energy $E_T^{\rm miss}$, P_T for the leading and sub-leading photons, a lepton veto, a maximum angular separation of photons, and a selection cut on the invariant mass of the diphoton system, is summarized in the second box of Table 5.9. As a final result of the analysis, we obtain 34.1 ±0.5 events with a significant evidence of $\frac{S}{\sqrt{B}} = 17 \pm 3$. For $\mathcal{L} = 100$ fb^{-1} to be reached in Run 2 we just have to rescale the number of events by a factor 1/3 and correspondingly the significance by $1/\sqrt{3}$. For completeness, we show in Table 5.10 the results for this BP with 14 TeV centre-of-mass energy.

Concerning the case of the $\widetilde{\nu}_{\tau_L}$ LSP of a similar mass, we can see in the fourth box of Table 5.2 that it has a significant BR to neutrinos. After a straightforward computation, we obtain a number of events of 7.5 ± 0.2. The background is the same as in Table 5.9, and therefore we obtain $\frac{S}{\sqrt{B}} \sim 3.8 \pm 0.6$. This BP can also give rise to a signal with diphoton plus leptons, to be analyzed subsequently, implying that a tau left sneutrino LSP could be distinguished from electron and muon left sneutrinos co-LSPs. For the other $\widetilde{\nu}_{\tau L}$ masses studied in Tables 5.3 and 5.4, although the BRs to neutrinos are still significant, the number

Table 5.11: Analysis of the signal with two photons plus leptons from production and decay of a pair of $\widetilde{\nu}_{\tau L}$ LSPs, corresponding to the BP in Table 5.2. Production cross sections are shown in fb in the first box for a $\widetilde{\nu}_{\tau L}$ mass of 126.4 GeV. The number of events of the signal and background is shown in the second box, together with the effect of a set of cuts, assuming 13 TeV of energy with $\mathcal{L} = 300$ fb^{-1}. Momenta and invariant mass are given in GeV.

$\sigma(pp \to Z^* \to h_2 A_2^0)$	103.58
$\sigma(pp \to \gamma^*, Z^* \to H_2^+ H_2^- \to h_2 A_2^0 \ + W^+_{\rm soft} W^-_{\rm soft})$	21.91
$\sigma(pp \to W^{\pm *} \to H_2^\pm h_2 / A_2^0 \to h_2 A_2^0 \ + W^\pm_{\rm soft})$	138.36
$\sigma(pp \to W^{\pm *} \to H_2^\pm h_2 \to h_2 h_2 \ + W^\pm_{\rm soft})$	69.18

Dataset	N_{ev}	$P_{T1}^{\gamma 1} > 100$	$P_{T2}^{\gamma 2} > 50$	N_γ=2	$N_{\tau_{had}} = 1$ & $N_{e,\mu,\tau_{had}} > 1$	$\Delta R < 1.5$	$M_{\gamma\gamma} \in [115, 135]$
Signal	128.136±0.007	67.8±0.4	25.4±0.3	25.4±0.3	5.9±0.2	4.9±0.1	4.7±0.1
Z+H	73.26±0.06	35.4±0.3	10.0±0.3	10.0±0.3	0.54±0.06	0.21±0.04	0.21±0.04
W+H	151.2±0.5	71.3±0.3	19.9±0.1	19.9±0.1	0.28±0.03	0.14±0.01	0.13±0.01
Z+ISR	53949±40	1394±42	210±17	210±17	7±3	0	0
W+FSR	71414±204	8776±116	1922±58	1922±58	17±5	0±0	0±0
$\frac{S}{\sqrt{B}}$	—	0.67±0.01	0.55 ± 0.02	0.55±0.02	1.2±0.2	8.4±0.9	8.1±0.9

of events of the signal diphoton plus MET turns out to be too small to be detected.

The case with all sneutrinos degenerate in mass would give rise to a superposition of the signals discussed so far. For instance, if the three families of sneutrinos have a mass of 126 GeV, the number of events expected for the signal diphoton plus MET will be the sum of both contributions discussed above, that is 41.6 ± 0.5 events with a significance of $\frac{S}{\sqrt{B}} = 21 \pm 1$. In addition, the signal with diphoton plus leptons, specific for the $\widetilde{\nu}_{\tau L}$, would also be present.

Diphoton plus leptons

For the case of the left sneutrino LSP dominated by the tau composition, $\widetilde{\nu}_{\tau L}$, another expected signal is diphoton plus leptons, as shown in Fig 5.2. For this signal the adequate range of masses turns out be

$$95 \lesssim m_{\widetilde{\nu}_{\tau_L}} \lesssim 145 \ \text{GeV} \ . \tag{5.15}$$

For the lower bound, notice that the selection cuts used to discriminate the decay of the sneutrino from the background require energetic photons and a large amount of missing energy. Therefore, a sneutrino with a small mass would lead to a small boost of the final photons and neutrinos. Thus reducing the mass of the sneutrino reduces the number of events in the signal region, although the cross section increases. Moreover, when the separation between the masses of the scalar left sneutrino and the SM Higgs is increased, the BR to diphoton is decreased. Altogether, the number of events drops fast when the mass of the left sneutrino is below 95 GeV. Actually, we already mentioned that about this mass is also the limit where the LSP cannot be treated as a promptly decaying particle. On the other hand, the decrease of the cross section for large sneutrino masses, and therefore of the number of events, gives rise to the upper bound of 145 GeV.

The results for a sneutrino mass of about 126 GeV, similar to the one studied above, are shown in Table 5.11. The discussion is similar to that above, although in this case we do not have two families of sneutrinos with degenerate masses, and therefore the different production mechanisms will only give rise to $\widetilde{\nu}_\tau \widetilde{\nu}_\tau$, thus reducing the number of events. These are further suppressed by the BR($A_2^0 \to \tau^\pm l^\mp$) compared to BR($A_2^0 \to \nu\nu$) in the

Table 5.12: The same as in Table 11 but for the BP in Table 5.3 corresponding to a $\widetilde{\nu}_{\tau L}$ LSP with a mass of 97.8 GeV.

$\sigma(pp \to Z^* \to h_1 A_2^0)$	265.92
$\sigma(pp \to \gamma^*, Z^* \to H_2^+ H_2^- \to h_1 A_2^0 \ + W^+_{\rm soft} W^-_{\rm soft})$	42.67
$\sigma(pp \to W^{\pm^*} \to h_1^\pm h_1 / A_2^0 \to h_1 A_2^0 \ + W^\pm_{\rm soft})$	325.2
$\sigma(pp \to W^{\pm^*} \to h_1^\pm h_1 \to h_1 h_1 \ + W^\pm_{\rm soft})$	162.6

Dataset	N_{ev}	$P_{T1}^{\gamma_1} > 100$	$P_{T2}^{\gamma_2} > 50$	N_γ=2	$N_{\tau_{had}} = 1$ & $N_{e,\mu,\tau_{had}} > 1$	$\Delta R < 1.5$	$M_{\gamma\gamma} \in [85, 105]$
Signal	44.438±0.002	14.4±0.1	3.96±0.06	3.96±0.06	0.82±0.03	0.81±0.03	0.78±0.03
Z+H	73.26±0.06	35.4±0.3	10.0±0.3	10.0±0.3	0.54±0.06	0.21±0.04	0.03±0.01
W+H	151.2±0.5	71.28±0.3	19.9±0.1	19.9±0.1	0.28±0.03	0.14±0.01	0±0
Z+ISR	53949±40	1394±42	210±17	210±17	7±3	0	0
W+FSR	71415±204	8776±116	1922±58	1922±58	17±5	0±0	0±0
$S/\sqrt{B}$	—	0.14 ±0.002	0.085 ±0.003	0.0085 ±0.003	0.17±0.03	1.4±0.2	5±1

Table 5.13: The same as in Table 5.11 but for the BP in Table 5.4 corresponding to a $\widetilde{\nu}_{\tau L}$ LSP with a mass of 146 GeV.

$\sigma(pp \to Z^* \to h_2 A_2^0)$	60.48
$\sigma(pp \to \gamma^*, Z^* \to H_2^+ H_2^- \to h_2 A_2^0 \ + W^+_{\rm soft} W^-_{\rm soft})$	14.69
$\sigma(pp \to W^{\pm^*} \to H_2^\pm h_2 / A_2^0 \to h_2 A_2^0 \ + W^\pm_{\rm soft})$	87.24
$\sigma(pp \to W^{\pm^*} \to H_2^\pm h_2 \to h_2 h_2 \ + W^\pm_{\rm soft})$	43.62

Dataset	N_{ev}	$P_{T1}^{\gamma_1} > 100$	$P_{T2}^{\gamma_2} > 50$	N_γ=2	$N_{\tau_{had}} = 1$ & $N_{e,\mu,\tau_{had}} > 1$	$\Delta R < 1.5$	$M_{\gamma\gamma} \in [135, 155]$
Signal	24.47±0.01	15.51±0.06	6.72±0.06	6.72±0.06	1.68±0.03	1.09±0.03	1.01±0.03
Z+H	73.26±0.06	35.4±0.3	10.0±0.3	10.0±0.3	0.54±0.06	0.21±0.04	0.03±0.01
W+H	151.2±0.5	71.3±0.3	19.9±0.1	19.9±0.1	0.28±0.03	0.14±0.01	0±0
Z+ISR	53949±40	1394±42	210±17	210±17	7±3	0	0
W+FSR	71414±204	8776±116	1922±58	1922±58	17±5	0±0	0±0
$S/\sqrt{B}$	—	0.153 ±0.002	0.145 ±0.004	0.145 ±0.004	0.34±0.06	1.8±0.2	6±2

case of $\widetilde{\nu}_{e,\mu}$ LSP. Nevertheless, this signal with photons plus leptons is very attractive and worth to be searched at the LHC.

Now, a different set of cuts is taken into account for convenience, as shown in the second box of Table 5.11. To distinguish the signal from the background in this case, instead of using the missing energy coming from neutrinos, we require two leptons in the final state of which one of them must be an hadronically decaying tau. Since every leptonic decay of the tau sneutrino includes at least one tau, we expect to reduce significantly more the background than the signal itself. Using an integrated luminosity of $\mathcal{L} = 300$ fb^{-1}, we obtain 4.7 ± 0.1 events with a significant evidence of $\frac{S}{\sqrt{B}} = 8.1 \pm 0.9$.

In order to confirm the range of sneutrino masses of about 95–145 GeV adequate to observe this kind of signal, we have also analyzed in Tables 5.12 and 5.13 the two extreme cases of about 98 and 146 GeV, respectively. Note that for both cases the BR of the scalar sneutrino decaying into photons is suppressed with respect to the previous case of 126 GeV. Although for the case of 98 GeV, the cross sections are increased with respect to the case of 126 GeV in Table 5.11, the final products would have less P_T, and E_T, thus the efficiency of the selection cuts would be smaller. We apply the same set of selection cuts to the signal calculated with this new point as in the previous case, but selecting now a new invariant mass window for the diphoton system of ±10 around 98 GeV. The rest

Table 5.14: Analysis of the signal with multileptons from production and decay of a pair of $\widetilde{\nu}_{\tau L}$ LSPs. The number of events of the signal and background is shown, together with the effect of a set of cuts, assuming 13 TeV centre-of-mass energy with $\mathcal{L} = 20$ fb^{-1}. The subindex l in the dataset denotes leptonically decaying tops and gauge bosons. Three possible masses of $\widetilde{\nu}_{\tau L}$, 132, 146 and 311 GeV are analyzed, with the last two obtained using the BPs of Tables 5.4 and 5.5.

Dataset	$N_l \geq 4$ & $N_{\tau_h} \geq 2$	$N_b = 0$	THT$\leq$ 20 GeV	W-veto	Z-veto	$\frac{S}{\sqrt{B}}$
$\bar{t}t_l$	306 ± 66	174 ± 50	14±14	0 ± 0	0 ± 0	–
$\bar{t}th$	3 ± 2	0±0	0 ± 0	0 ± 0	0 ± 0	–
$\bar{t}t\bar{t}t$	0.8 ± 0.5	0 ± 0	0 ± 0	0 ± 0	0 ± 0	–
$\bar{t}tV_l$	1.2 ± 0.3	0.6 ± 0.2	0.12 ± 0.09	0.12 ± 0.09	0.12 ± 0.09	–
VV_l	6 ± 4	6 ± 4	3 ± 3	3 ± 3	3 ± 3	–
VVV	2 ± 1	0.8 ± 0.8	0 ± 0	0 ± 0	0 ± 0	–
tV_l	15 ± 5	14 ± 5	8 ± 4	8 ± 4	8 ± 4	–
tVV_l	1.0 ± 0.3	0.6 ± 0.2	0.10 ± 0.08	0.10 ± 0.08	0.10 ± 0.08	–
Total	334 ± 66	196 ± 64	25 ± 15	11 ± 5	11 ± 5	–
Signal 132 GeV	36 ± 2	36 ± 2	20 ± 2	17 ± 1	16 ± 1	4.8 ± 2.2
Signal 146 GeV	68 ± 3	66 ± 3	37 ± 2	31 ± 2	29 ± 2	8.8 ± 4.0
Signal 311 GeV	18.2 ± 0.5	17.9 ± 0.5	8.9 ± 0.4	7.6 ± 0.4	7.5 ± 0.2	2.2 ± 1.0

of the analysis is completely analogous, and the results are presented in the second box of Table 5.12. For this extreme case we still obtain 0.78 ± 0.03 events with a significant evidence of $\frac{S}{\sqrt{B}} = 5 \pm 1$.

Finally, to explore the largest possible value of the sneutrino mass, we have considered the case of 146 GeV. We show the final results in Table 5.13. As can be seen, the production cross sections are reduced with the increase of the mass. We are not considering points with sneutrino masses larger than 146 GeV because the possible signal gets likely lost behind the SM backgrounds. The results of the different selection cuts for this extreme case are presented in the second box of Table 5.13. As a final result, 1.01 ± 0.03 events with a significant evidence of $\frac{S}{\sqrt{B}} = 6 \pm 2$ are obtained.

Multileptons

For the tau left sneutrino, we can see in Tables 5.4 and 5.5 that the BRs for the decay of the scalar state $\widetilde{\nu}^{\mathcal{R}}_{\tau_L}$ into leptons are significant. This gives rise to a non negligible number of events with both sneutrinos decaying into leptons, as shown in Fig 5.3. With the appropriate analysis, these events could constitute a possible signal to be detected at the LHC. Moreover, these decay channels of the LSP include always at least one τ, a feature that can be exploited to unravel the signal.

The main backgrounds for this type of signature would be the production of top quarks through the channels $\bar{t}t$ and $\bar{t}t\bar{t}t$; the production of gauge bosons ZZ, WW and ZW; the associated production of both $\bar{t}tV$, tV and tVV; and the top associated Higgs production $\bar{t}th$. Since the proposed hard process would not produce quarks, we expect a hadronic activity in the events significantly smaller than the one associated with background events including a leptonically decaying top t_l. We will show that it is possible to separate the multilepton signal from the SM backgrounds. This is particularly true for sneutrinos with large masses, since the produced leptons are then expected to be more energetic than the ones produced in the decay of gauge bosons.

The Monte Carlo events generated and processed as in the previous signals, but in this case with an integrated luminosity of $\mathcal{L} = 20$ fb^{-1}, are analyzed and summarized in

Table 5.14 for three different sneutrino masses of 132, 146 and 311 GeV. Production cross sections for the case of 146 GeV are already shown in Table 5.13. For 310 GeV these are much lower. At first we select events with at least 4 leptons with $P_T \geq 100$, 80, 40 and 40 GeV, respectively, requiring also at least two of them to be $\tau_{\rm h}$'s. The second selection rejects events with b-tagged jets in order to reduce backgrounds coming from top decays. In the next step we reject events with a total transverse hadronic energy (THT) greater than 20 GeV. Finally we apply a veto to the transverse mass and invariant mass of the light leptons, compatible with the mass of the W and Z respectively. Summarizing the results shown in Table 5.14, it is possible to detect $\widetilde{\nu}_{\tau_L}$ in the mass range

$$130 \lesssim m_{\widetilde{\nu}_{\tau L}} \lesssim 310 \ \text{GeV} \ , \tag{5.16}$$

decaying leptonically with a significance $\frac{S}{\sqrt{B}}$ greater than 3.

Equations (5.14), (5.15) and (5.16) establish the adequate range of left sneutrino masses for our analysis of the BPs introduced in Section 5.2, and Tables 5.1–5.5. As we can see, the masses overlap in some ranges, and in these cases the corresponding BP can give rise to different detectable signals.

5.5 Conclusions and outlook

We have carried out an analysis of the LHC phenomenology associated to the left sneutrino LSP in the $\mu\nu$SSM. We have studied the dominant pair production channels, prompt decays, and the detection of the new signals.

As a result of the different behaviors of scalar and pseudoscalar sneutrino states, a diphoton signal in combination with neutrinos (producing missing transverse energy), or a diphoton with leptons, can appear at the LHC.

The former can be detected with a centre-of-mass energy of 13 TeV and the integrated luminosity of 100 fb^{-1}, for a sneutrino LSP of any family in the mass range 118–132 GeV. The diphoton plus leptons signal can be probed for the case of a tau sneutrino LSP with a mass in the range 95–145 GeV.

We have discussed several benchmark points producing these signals, which undoubtedly deserve proper experimental attention. We have also shown that the number of expected events are capable of giving a significant evidence.

A multilepton signal from a tau sneutrino LSP can also appear detectable at the LHC with a centre-of-mass energy of 13 TeV, even with the integrated luminosity of 20 fb^{-1}. It is possible to detect it in the mass range of 130–310 GeV. We have discussed that existing generic searches at the LHC are close to be sensitive to this lepton signal, suggesting that they deserve experimental attention. An updated analysis with current data could constrain the sneutrino LSP scenario.

Displaced vertices of the order of the millimeter can appear for sneutrino masses $\lesssim 100$ GeV. Imposing in addition that the sneutrino mass is larger than 45 GeV, not to disturb the experimentally well measured decay width of the Z, we have found that the number of events can be large.

For example, more than 1000 multilepton events at the parton level from the production and decay of a tau sneutrino pair can emerge for an integrated luminosity of 20 fb^{-1} and 13 TeV centre-of-mass energy. These events have the clear advantage that the SM backgrounds are negligible and hence the signal significance is high. However, the analysis

of displaced vertices turns out to be quite complicated, and dedicated studies are necessary. The efficiency identifying events characterized by the presence of a displaced vertex has a non-trivial dependence on the position of the vertex, as well as the number of tracks and the mass associated to them, among others. Therefore, a reliable analysis requires a precise simulation of the decay length, the boost of the long-lived particle, and the particles produced in the secondary vertex. This analysis, in our model, is expected to depend on the parameters correlated with neutrino physics and is clearly beyond the scope of the present work, although this is cover in the next chapter.

Chapter 6

Looking for the left sneutrino LSP with displaced-vertex searches

In the present chapter, based on the work [92], we analyze a displaced dilepton signal expected at the LHC for a tau left sneutrino as the lightest supersymmetric particle with a mass in the range 45–100 GeV. The sneutrinos are pair produced via a virtual W, Z or γ in the s channel and, given the large value of the tau Yukawa coupling, their decays into two dileptons or a dilepton plus missing transverse energy from neutrinos can be significant. To probe the tau left sneutrinos we compare the predictions of the $\mu\nu$SSM with the ATLAS search for long-lived particles using displaced lepton pairs in pp collisions at $\sqrt{s} = 8$ TeV, allowing us to constrain the parameter space of the model. We also consider an optimization of the trigger requirements used in existing displaced-vertex searches by means of a High Level Trigger that exploits tracker information. This optimization is generically useful for a light metastable particle decaying into soft charged leptons. The constraints on the sneutrino turn out to be more stringent. We finally discuss the prospects for the 13 TeV LHC searches as well as further potential optimizations.

6.1 Introduction

As analyzed in section 4.4, a tau left sneutrino LSP with masses below 100 GeV decays mainly to $\nu\nu$ and[1] $\tau\ell$. Moreover, the decay length is in general above 0.1 mm. Making the signal potentially detectable in searches for long lived particles.

A promptly decaying sneutrino as the LSP was analyzed in the previous chapter, based on Ref. [94], with a decay length $\lesssim$ 0.1 mm. In this chapter we will analyze the interesting case of displaced vertices of the order of the millimeter, generated by a sneutrino in the range of masses $45 - 100$ GeV. The lower bound is imposed not to disturb the decay width of the Z. We will focus on the simplest case of the $\mu\nu$SSM with one right-handed neutrino superfield discussed in Sec. 3.7, and leave the case of three families where all the neutrinos get contributions to their masses at tree level for a forthcoming publication [175].

To probe the $\widetilde{\nu}_\tau$ LSP, the dilepton displaced-vertex searches are found to be most promising. We compare the $\mu\nu$SSM predictions with the ATLAS search [176] for long-lived particles using displaced lepton pairs $\ell\ell$ in pp collisions at $\sqrt{s} = 8$ TeV, which allows us to constrain the parameter space of the model. Nevertheless, the existing searches [176, 177] are designed for a generic purpose and thus not optimized for light metastable particles such

[1] In what follows, the symbol ℓ will be used for an electron or a muon, $\ell = e, \mu$, and charge conjugation of fermions is to be understood where appropriate.

as the $\widetilde{\nu}_\tau$.We therefore consider also a possibility of improving these searches by lowering trigger thresholds, relying on a High Level Trigger that utilizes tracker information. As it turns out, this optimization is quite feasible and considerably improves the sensitivity of the displaced-vertex searches. We also consider an optimization of the 13 TeV LHC searches and show the prospects for investigating the $\mu\nu$SSM parameter space by searching for the $\widetilde{\nu}_\tau$ at the 13 TeV LHC run. Possibilities of further improvements for these searches will also be discussed.

The chaper is organized as follows. In Section 6.2, we will introduce the phenomenology of the $\widetilde{\nu}_\tau$ LSP, studying its pair production channels at the LHC, as well as the signals. These consist of two dileptons or a dilepton plus missing transverse energy (MET) from the sneutrino decays. On the way, we will analyze the decay widths, BRs and decay lengths. In Section 6.3, we consider first the existing dilepton displaced-vertex searches, and discuss its feasibility and significance on $\widetilde{\nu}_\tau$ searches. Then, we study an optimization by using a High Level Trigger with tracker information. We also show our prescription for recasting the ATLAS 8-TeV result [176] to the case of the $\widetilde{\nu}_\tau$. We then show the current reach of this search on the $\mu\nu$SSM parameter space based on the ATLAS 8-TeV result [176], and the prospects for the 13-TeV searches in Section 6.4. Our conclusions and prospects for future work are presented in Section 6.5.

6.2 Tau left sneutrino LSP phenomenology

The dominant pair production channels of sleptons at large hadron colliders were studied in Refs. [99, 100, 101, 102, 103, 104]. In Fig. 6.1, we can see the production channels at the LHC for the case of the $\widetilde{\nu}_\tau$ LSP which is the one interesting for our analysis. The direct production of Fig. 6.1a occurs via a Z channel giving rise to a pair of scalar and pseudoscalar left sneutrinos. As discussed in previous chapters, these states have essentially degenerate masses and are therefore co-LSPs. On the other hand, since the left stau is in the same $SU(2)$ doublet as the tau left sneutrino, it becomes the next-to-LSP (NLSP). The mass splitting is mainly due to the usual D-term contribution. As explained in section 4.1 taking into account the particular values of $\tan\beta$ and the sneutrino mass (as well as the loop corrections to sneutrino and stau masses), the typical mass difference is about 20-30 GeV.Thus the direct production and decay is another important source of the $\widetilde{\nu}_\tau$ LSP. In particular, pair production can be obtained through a γ or Z decaying into two staus, as shown in Fig. 6.1b, with the latter dominantly decaying into a (scalar or pseudoscalar) sneutrino plus an off-shell W producing a soft meson or a pair of a charged lepton and a neutrino. Besides, sneutrinos can be pair produced through a W decaying into a stau and a (scalar or pseudoscalar) sneutrino as shown in Fig. 6.1c, with the stau decaying as before. The number of sneutrino pairs produced through these channels at 8 and 13 TeV for integrated luminosities of 20.3 and 300 fb^{-1}, respectively, are shown in Table 6.1.

In Fig. 6.1, we also show the detectable decay of the pair-produced $\widetilde{\nu}_\tau$ into $\tau\,\ell/\tau$. As a result of the mixing between left sneutrinos and Higgses, the sizable decay of $\widetilde{\nu}_\tau$ into $\tau\tau$ is possible because of the large value of the tau Yukawa coupling. Other sizable decays into $\tau\,\ell/\tau$ can occur through the Yukawa interaction of $\widetilde{\nu}_\tau$ with τ and charged Higgsinos, via the mixing between the latter and ℓ or τ. To analyze these processes we can recall the approximate formulas for the partial decay widths of the scalar/pseudoscalar tau left sneutrino of Sec. 4.3.2, and adapt them for the one generation case. The one into $\tau\tau$ is

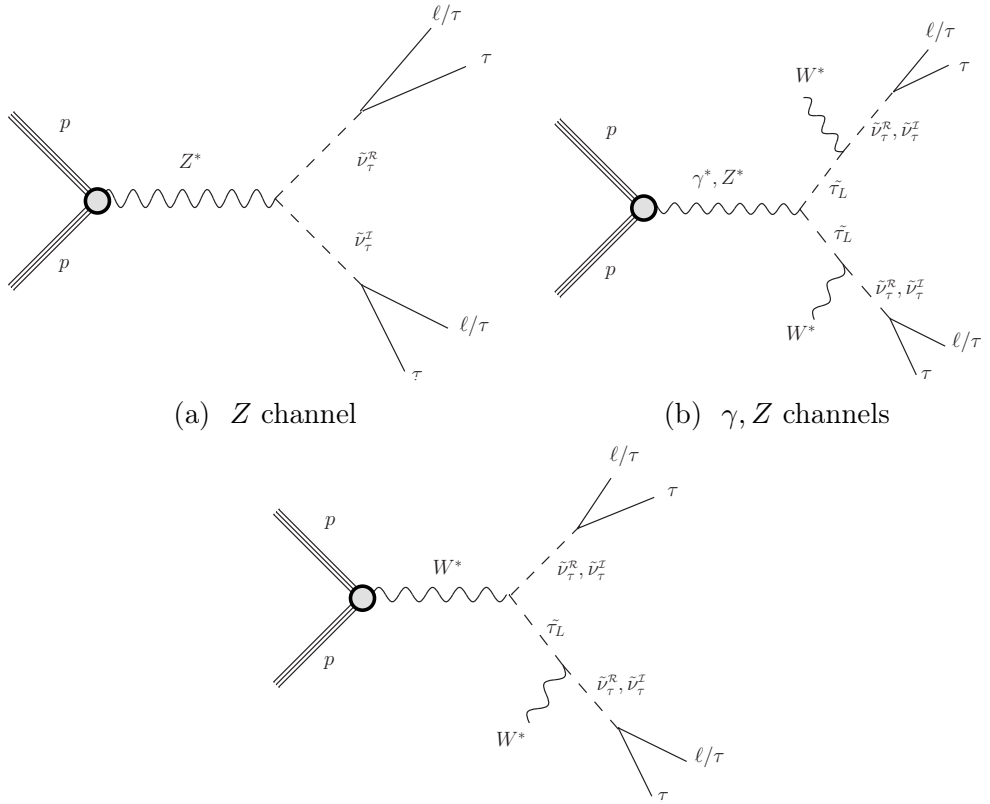

(a) Z channel (b) γ, Z channels

(c) W channel

Figure 6.1: Decay channels into two $\tau\,\ell/\tau$, from a pair production at the LHC of scalar and pseudoscalar tau left sneutrinos co-LSPs. Decay channels into one $\tau\,\ell/\tau$ plus neutrinos are the same but substituting in (a), (b) and (c) one of the two vertices by a two-neutrino vertex.

given by:

$$\Gamma\left(\widetilde{\nu}_\tau \to \tau\tau\right) \approx \frac{m_{\widetilde{\nu}_\tau}}{16\pi}\left(Y_\tau Z^{H/A}_{\widetilde{\nu}_\tau H_d} - Y_{\nu_\tau}\frac{Y_\tau}{\lambda}\right)^2, \tag{6.1}$$

where $Y_\tau \equiv Y_{e_{33}}$, and $Z^{H/A}$ is the matrix which diagonalizes the mass matrix for the scalar/pseudoscalar Higgses $(H_d, H_u, \widetilde{\nu}_R, \widetilde{\nu}_i)$ [63]. The latter is determined by the neutrino Yukawas, which are the order parameters of the $\not{R}_p$. The contribution of λ in the second term of Eq. (6.1) is due to the charged Higgsino mass that can be approximated by the value of μ. The partial decay width into $\tau\ell$ can then be approximated for both sneutrino states by the second term of Eq. (6.1) with the substitution $Y_{\nu_\tau} \to Y_{\nu_\ell}$:

$$\Gamma\left(\widetilde{\nu}_\tau \to \tau\ell\right) \approx \frac{m_{\widetilde{\nu}_\tau}}{16\pi}\left(Y_{\nu_\ell}\frac{Y_\tau}{\lambda}\right)^2. \tag{6.2}$$

On the other hand, the gauge interactions of $\widetilde{\nu}_\tau$ with neutrinos and Binos (Winos) can produce also a large decay width into neutrinos, via the gauge mixing between these gauginos and neutrinos. This partial decay width can be approximated for scalar and pseudoscalar sneutrinos as

$$\sum_i \Gamma\left(\widetilde{\nu}_\tau \to \nu_\tau\nu_i\right) \approx \frac{m_{\widetilde{\nu}_\tau}}{16\pi}\frac{1}{2M^2}\sum_i v_i^2, \tag{6.3}$$

Table 6.1: Number of sneutrino pairs produced through each of the channels shown on Fig. 6.1a-6.1b, at 8 TeV and 13 TeV with integrated luminosity of 20.3fb^{-1} and 300 fb^{-1} respectively.

	8-TeV				13-TeV			
$m_{\widetilde{\nu}_\tau}$ (GeV)	50	60	80	100	50	60	80	100
Through Z boson	66,357	22,370	6,095	2,448	1,794,242	622,800	179,750	75,567
Through W boson	66,600	34,869	12,838	5,915	1,860,483	997,200	385,558	184,750
Through γ, Z bosons	6,585	3,954	1,703	851	226,283	139,367	62,550	32,683

with M a kind of average of Bino and Wino masses defined in Eq. (3.34). The relevant diagrams for $\widetilde{\nu}_\tau$ searches that include this decay mode are the same as in Fig. 6.1, but substituting one of the $\tau\,\ell/\tau$ vertices by a two-neutrino vertex.

Let us remark that other decay channels of the $\widetilde{\nu}_\tau$ can be present and have been taken into account in our numerical computation, but they turn out to be negligible for the sneutrino masses that we are interested in this work. For example, decay to bottoms can occur through a term similar to the first one of Eq. (6.1)with the substitution of Y_τ by Y_b. As we will comment below and was discussed in Chapter 4, this term is very small. In particular, it is negligible with respect to the second one in Eq. (6.1) which is present for decays into leptons.

It is also worth noticing here that because the $\tilde{\nu}_\tau$ in the $\mu\nu$SSM has several relevant decay modes, the LEP lower bound on the sneutrino mass of about 90 GeV [178, 179, 180, 181, 161, 162] obtained under the assumption of BR one to leptons, via trilinear $\not{R}_p$ couplings, is not directly applicable in this case. We have checked that no constraint on the $\tilde{\nu}_\tau$ mass is obtained from these searches in the cases studied in this work. We have obtained similar conclusions from LEP mono-photon search (gamma + MET) [182], and LHC mono-photon and mono-jet (jet+MET) searches [133, 134]. Concerning LEP searches for staus [178, 179, 180, 181, 161, 162], in the $\mu\nu$SSM the left stau does not decay directly but through an off-shell W and a $\tilde{\nu}_\tau$. Thus, searches for its direct decay are not relevant in this model. On the other hand, the sneutrino mass can in principle be constrained using searches for final states as those produced in the $\mu\nu$SSM. However, we have checked that this is not the case. For example, for the final state $\tau\mu\mu\nu\tau\mu\mu\nu$ (see table 6.2), taking into account the value of the production cross section at LEP for a pair of left staus, and the BRs of W into $\mu\nu$ and $\tilde{\nu}_\tau$ into $\tau\nu$, no effective constraint is obtained in our scenario. For the other possible topologies, with W into quarks or $\tilde{\nu}_\tau$ into $\nu\nu$, the results of the analyses turn out to be the same, as shown in table 6.2. It is straightforward to see there that our scenario is unconstrained, even considering the most disfavored (and unrealistic) values for the branching ratios, BR($\tilde{\nu} \to \ell\tau$) = 1 or BR($\tilde{\nu} \to \nu\nu$) = 1. In addition, we are not taking into account the possible effect of the different geometry of the decays when comparing with the final states considered in the searches, which are not originated in the same manner.

To analyze now the BRs into leptons, we have to focus on the decay channels where the τ's in the final state decay leptonically. Let us study e.g. the BR to $\mu\mu$, since the ee channel can be discussed in a similar way, and the BR to $e\mu$ fulfills BR($\widetilde{\nu}_\tau \to e\mu$) $\approx$ BR($\widetilde{\nu}_\tau \to \mu\mu$) + BR($\widetilde{\nu}_\tau \to ee$) given that the BRs of the τ decays into electrons or muons (plus neutrinos) are similar ≈ 0.17. To quantify roughly the value BR($\widetilde{\nu}_\tau \to \mu\mu$), we can

Table 6.2: Possible topologies emerging from the production of a pair of tau left sneutrinos from staus.In the last two columns the production cross section of the most constrained signal, considering the worst-case scenario, is compared with the experimental upper limit. The values $\mathrm{BR}(W \to \mu\nu) = 0.1063$, $\mathrm{BR}(W \to qq') = 0.6741$, and $\mathrm{BR}(\tau \to \mu\nu) = 0.1739$ are used for the computation, as well as $1/4$ as the maximum value of $\mathrm{BR}(\tilde{\nu} \to \ell\tau) \times BR(\tilde{\nu} \to 2\nu)$. In order to simplify the notation, $\mathrm{BR}(\tilde{\nu} \to \ell\tau)$ means the sum of the three BRs to $e\tau$, $\mu\tau$ and $\tau\tau$, and the factor $1/3$ are coming from considering the different channels.

Process	Topology	Signal upper crossection	Exclusion
$\tilde{\tau}^{\pm}\tilde{\tau}^{\mp} \to 2(W^{\pm} \to \ell^{\pm}\nu)$ $+2(\tilde{\nu} \to \ell\tau)$	$4\ell + 2\tau + \not{E}_T$	(0.13 pb) $\times$ $(0.1063)^2$ $\times \mathrm{BR}(\tilde{\nu} \to \ell\tau)^2 \times \left(\frac{1}{3}\right)^2$ $\leq 1.6 \times 10^{-4}$ pb	[hep-ex/0310054] Fig.14 1.5×10^{-2} pb
$\tilde{\tau}^{\pm}\tilde{\tau}^{\mp} \to 2(W^{\pm} \to \ell^{\pm}\nu)$ $+(\tilde{\nu} \to \ell\tau) + (\tilde{\nu} \to 2\nu)$	$3\ell + \tau + \not{E}_T$	(0.13 pb) $\times$ $(0.1063)^2 \times 2$ $\times \mathrm{BR}(\tilde{\nu} \to \ell\tau) \times \frac{1}{3} \times (0.1739)$ $\times \mathrm{BR}(\tilde{\nu} \to 2\nu) \leq 4.3 \times 10^{-5}$ pb	[hep-ex/0310054] Fig.18 2×10^{-2} pb
$\tilde{\tau}^{\pm}\tilde{\tau}^{\mp} \to 2(W^{\pm} \to \ell^{\pm}\nu)$ $+2(\tilde{\nu} \to 2\nu)$	$2\ell + \not{E}_T$	(0.13 pb) $\times$ $(0.1063)^2$ $\times \mathrm{BR}(\tilde{\nu} \to 2\nu)^2 \leq 1.5 \times 10^{-3}$ pb	[hep-ex/0310054] Fig.6 6×10^{-2} pb
$\tilde{\tau}^{\pm}\tilde{\tau}^{\mp} \to (W^{\pm} \to \ell^{\pm}\nu)$ $+(W^{\pm} \to qq') + 2(\tilde{\nu} \to \ell\tau)$	$3\ell + 2\tau + jets + \not{E}_T$	(0.13 pb) $\times$ 2 $\times$ (0.1063) $\times$(0.6741) $\times$ $\mathrm{BR}(\tilde{\nu} \to \ell\tau)^2$ pb $\times \left(\frac{1}{3}\right)^2 \leq 2.1 \times 10^{-3}$	[hep-ex/0310054] Fig.18 2×10^{-2} pb
$\tilde{\tau}^{\pm}\tilde{\tau}^{\mp} \to (W^{\pm} \to \ell^{\pm}\nu)$ $+(W^{\pm} \to qq') + (\tilde{\nu} \to \ell\tau)$ $+(\tilde{\nu} \to 2\nu)$	$2\ell + 1\tau + jets + \not{E}_T$	(0.13 pb) $\times$ 2 $\times$ (0.1063) $\times$(0.6741) $\times$ 2 $\times$ $\mathrm{BR}(\tilde{\nu} \to \ell\tau)$ $\times \mathrm{BR}(\tilde{\nu} \to 2\nu) \times \left(\frac{1}{3}\right)$ $\leq 3.1 \times 10^{-3}$ pb	[hep-ex/0310054] Fig.12 5×10^{-2} pb
$\tilde{\tau}^{\pm}\tilde{\tau}^{\mp} \to (W^{\pm} \to \ell^{\pm}\nu)$ $+(W^{\pm} \to qq') + 2(\tilde{\nu} \to 2\nu)$	$\ell + jets + \not{E}_T$	(0.13 pb) $\times$ 2 $\times$ (0.1063) $\times$(0.6741) $\times$ $\mathrm{BR}(\tilde{\nu} \to 2\nu)^2$ $\leq 1.9 \times 10^{-2}$ pb	[hep-ex/0401026] Fig.6 5×10^{-2} pb
$\tilde{\tau}^{\pm}\tilde{\tau}^{\mp} \to 2(W^{\pm} \to qq')$ $+2(\tilde{\nu} \to \ell\tau)$	$2\ell + 2\tau + jets$	(0.13 pb) $\times$ $(0.6741)^2$ $\times \mathrm{BR}(\tilde{\nu} \to \ell\tau)^2 \times \left(\frac{1}{3}\right)^2$ $\leq 6.6 \times 10^{-3}$ pb	[hep-ex/0310054] Fig.12 5×10^{-2} pb
$\tilde{\tau}^{\pm}\tilde{\tau}^{\mp} \to 2(W^{\pm} \to qq')$ $+(\tilde{\nu} \to \ell\tau) + (\tilde{\nu} \to 2\nu)$	$\ell + \tau + jets + \not{E}_T$	(0.13 pb) $\times$ $(0.6741)^2$ $\times$2 $\times$ $\mathrm{BR}(\tilde{\nu} \to \ell\tau) \times \left(\frac{1}{3}\right)$ $\times$(0.1739) $\times$ $\mathrm{BR}(\tilde{\nu} \to 2\nu)$ pb $\leq 1.7 \times 10^{-3}$	[hep-ex/0310054] Fig.12 5×10^{-2} pb
$\tilde{\tau}^{\pm}\tilde{\tau}^{\mp} \to 2(W^{\pm} \to qq')$ $+2(\tilde{\nu} \to 2\nu)$	$jets + \not{E}_T$	(0.13 pb) $\times$ $(0.6741)^2$ $\times \mathrm{BR}(\tilde{\nu} \to 2\nu) \leq 6 \times 10^{-2}$ pb	[hep-ex/0310054] Fig.20 5×10^{-1} pb

use the following formula:

$$\mathrm{BR}\left(\widetilde{\nu}_{\tau} \to \mu\mu\right) \approx 0.068 \times \left(1 + \frac{r}{3}\right)^{-1}, \tag{6.4}$$

with

$$r \approx \left(\frac{\lambda}{Y_{\tau}}\right)^2 \frac{2m_{\nu}}{Y_{\nu}^2 M}, \tag{6.5}$$

where we have neglected the first term in Eq. (6.1), which is a sensible approximation for small sneutrino masses around 50 GeV provided that λ is not large, and we have used the neutrino mass formula discussed below Eq. (3.39), $m_{\nu} \approx \sum_i v_i^2/4M$, implying that the decay width in Eq. (6.3) can be written as $(m_{\widetilde{\nu}_{\tau}}/16\pi)2m_{\nu}/M$. In addition, we have set all neutrino Yukawas with a common value Y_{ν} in order to simplify the analysis. In what follows we will continue with this strategy, which does not essentially modify the results. Now, in the above equations and for typical values of the parameters such as e.g. $Y_{\nu} = 5 \times 10^{-7}$,

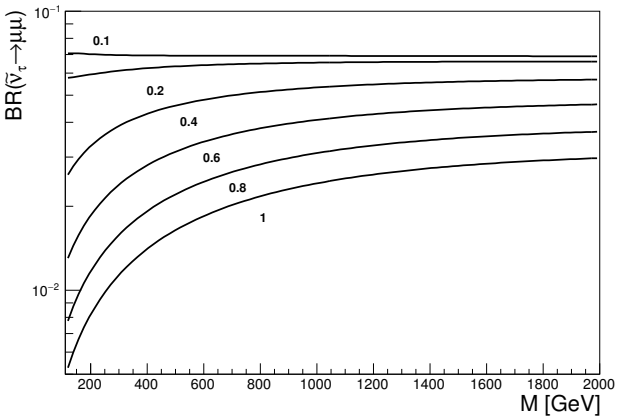

(a) Branching ratio

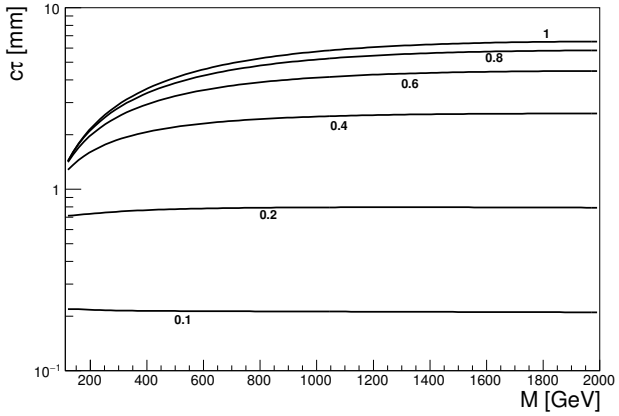

(b) Decay length

Figure 6.2: (a) BR versus M for the decay of a $\widetilde{\nu}_\tau$ with $m_{\widetilde{\nu}_\tau} = 60$ GeV into $\mu\mu$; (b) Proper decay distance $c\tau$ of the $\widetilde{\nu}_\tau$ versus M. In both plots (a) and (b), the neutrino Yukawas are set to $Y_\nu = 5 \times 10^{-7}$, and several values of the coupling λ are used such as $\lambda = 0.1$, 0.2, 0.4, 0.6, 0.8, 1.

$m_\nu = 0.05$ eV and $M = 1$ TeV, one obtains $r = 0.4$ and therefore a BR($\widetilde{\nu}_\tau \to \mu\mu$) $\lesssim 0.06$ for $\lambda \gtrsim Y_\tau$.

In this approximation, we can also write the proper decay distance as

$$c\tau \approx 0.22 \times \left(\frac{Y_\nu}{5 \times 10^{-7}}\right)^{-2} \left(\frac{\lambda}{Y_\tau}\right)^{2} \left(1 + \frac{r}{3}\right)^{-1} \left(\frac{m_{\widetilde{\nu}_\tau}}{60 \text{ GeV}}\right)^{-1} \text{mm}, \tag{6.6}$$

obtaining $c\tau \gtrsim 0.2$ mm for $\lambda \gtrsim Y_\tau$. Thus the latter is a necessary condition on λ in order to obtain suitable displaced vertices. In fact, as we will see in the next sections, we will need decay lengths larger than about a millimeter in order to be constrained by the current experimental results.

To compute numerically the mass spectrum and decay modes, we used a suitable modified version of the `SARAH` code [108] as well as the `SPheno` 3.3.6 code [111, 112]. As an example, we show in Fig. 6.2a the BR for the decay of a scalar sneutrino $\widetilde{\nu}_\tau^{\mathcal{R}}$ with a mass of 60 GeV into $\mu\mu$, for $Y_\nu = 5 \times 10^{-7}$ (a similar figure is obtained in the case of the pseudoscalar $\widetilde{\nu}_\tau^{\mathcal{I}}$). This is plotted as a function of M for several values of the coupling λ. Values of M smaller than 111.3 GeV are not considered since the $\widetilde{\nu}_\tau$ would no longer be the LSP

in favor of the gauginos. Other parameters, whose effect on the sneutrino decay properties is less significant, as can be understood from previous formulas, are set to be $\kappa = 0.3$, $\tan\beta = 10$, and $\frac{v_R}{\sqrt{2}} = 1350$ GeV, throughout this work. Concerning the quantity $\sum_i v_i^2$ in Eq. (6.3), this is determined using Eq. (3.37) with the heavier neutrino mass fixed by the experimental constraints in the range $m_\nu \sim [0.05, 0.23]$ eV, i.e. below the upper bound on the sum of neutrino masses ~ 0.23 eV [124], and above the square root of the mass-squared difference $\Delta m^2_{\rm atm} \sim 2.42 \times 10^{-3}{\rm eV}^2$ [125]. In Fig. 6.2a we chose as an example $m_\nu = 0.05$ eV. Finally, given the sneutrino mass formula in Eq. (4.5), there is enough freedom to tune A_{ν_i} in order to get the $\widetilde{\nu}_\tau$ as the LSP with a mass of 60 GeV as in the case of Fig. 6.2a. We can see in the figure that small values of λ and large values of M favor larger BRs to dileptons. These results can be easily deduced from Eqs. (6.4) and (6.5).

In Fig. 6.2b, we show the proper decay distance $c\tau$ of the $\widetilde{\nu}^{\mathcal{R}}_\tau$ for the same values of the parameters as in Fig. 6.2a. Large values of λ and M favor larger decay lengths, as can be understood from Eqs. (6.6) and (6.5). As mentioned before, we need decay lengths larger than about a millimeter, and therefore for these values of the parameters the coupling is constrained to be $\lambda \gtrsim 0.2$. For example, for $\lambda = 1$ we can see that the upper bound on the decay length is $c\tau = 7$ mm. However, large values of λ also favor smaller BRs into leptons, and therefore less stringent constraints on the parameter space. The interplay between these effects will be analyzed in the next sections. In addition, the values of Y_ν and $m_{\widetilde{\nu}_\tau}$ also play an important role in the analysis. We can see in Eq. (6.6) that smaller values favor larger decay lengths. For example, for $m_{\widetilde{\nu}_\tau} = 60$ GeV as in Fig. 6.2 but $Y_\nu = 10^{-7}$, we have checked that the upper bound on the decay length is $c\tau = 20$ mm for the case of $\lambda = 1$. For $Y_\nu = 5 \times 10^{-7}$ as in Fig. 6.2 but $m_{\widetilde{\nu}_\tau} = 80$ GeV, the upper bound for $\lambda = 1$ turns out to be smaller as expected, $c\tau = 4$ mm. Let us finally remark that Y^ν cannot be made arbitrarily small. because of the relation $\nu_i \sim Y^\nu v_u$ discussed in chapter 3, this would imply that v_i has to be also small coming into conflict with Eq. (3.37) and the constraint discussed above, $m_\nu \sim [0.05, 0.23]$ eV. Thus a reasonable range for Y_ν is between 10^{-6} and 10^{-7}.

6.3 Long-lived particle searches at the LHC

As discussed in the previous section, a tau left sneutrino $\widetilde{\nu}_\tau$ can decay into a pair of leptons with a proper lifetime of $\gtrsim 100$ μm (see Fig. 6.2b), long enough to have a visible separation from the production point. This signal can be compared with the searches for long-lived particles at the LHC.

There are various long-lived particle searches at the LHC, and each of them aims at a signature specific to a particular kind of particles. We thus first need to discuss which search strategy is most sensitive to $\widetilde{\nu}_\tau$. Since they are electrically neutral, we are unable to use disappearing track searches or metastable charged particle searches to probe them. On the other hand, as we have seen above, the decay products of the sneutrinos include charged particles, and therefore we may detect the longevity of the sneutrinos by reconstructing their decay vertices, using the charged tracks associated with the daughter particles. This type of search strategies is dubbed as the displaced-vertex searches.

Both the ATLAS and CMS experiments have been searching for displaced vertices. The ATLAS 8-TeV analysis [176] searches for events containing at least one long-lived particle decaying at a significant distance from the production point ($\gtrsim 1$ mm), looking for decays into two leptons or into five or more charged particles. The latter search channel focuses on processes that produce a higher amount of charged particles and/or missing energy,

compared with the decay of the $\widetilde{\nu}_\tau$. We will however see below that the dilepton search channel in the ATLAS 8-TeV analysis is general enough as to be sensitive to the decay of the $\widetilde{\nu}_\tau$. On the other hand, the current 13-TeV displaced-vertex search performed by the ATLAS collaboration [183] is optimized for long-lived gluinos, so it is not possible to use it for our purpose. As for the CMS, the 8-TeV analysis presented in Ref. [177] gives a limit comparable to the ATLAS 8 TeV bound if the decay distance of sneutrinos is $\gtrsim 3$ cm—although this CMS search is in principle sensitive to shorter decay distances as the selection cut requires $|d_0| < 12\sigma_d \sim 180$ μm (d_0 is the transverse impact parameter of tracks and σ_d is its uncertainty), their limits are terminated at a much larger value of $c\tau$ especially for soft displaced vertices (see, *e.g.*, Fig. 6 in Ref. [177]). Given that the ATLAS 8-TeV analysis provides bounds for smaller $c\tau$ compared with those from the CMS study, to make the discussions concrete, we focus on displaced-vertex searches with the ATLAS detector in what follows.

The ATLAS displaced-vertex search in Ref. [176] is based on the 8-TeV data with an integrated luminosity of 20.3 fb^{-1}. Among the various search channels studied in the analysis, the dilepton displaced-vertex selection channel, where each displaced vertex is formed from at least two oppositely-charged leptons, may be used for the long-lived $\widetilde{\nu}_\tau$ search. As we mentioned above, we focus on the decay processes of $\widetilde{\nu}_\tau$ in which τ leptons in the final state decay into leptons, in order to utilize this selection channel.

In the dilepton displaced-vertex search, each event must satisfy the muon or electron trigger requirement.[2] For the muon trigger, a muon candidate is identified only in the muon spectrometer, without utilizing the tracking information, and required to have a transverse momentum of $p_{\rm T} > 50$ GeV and the pseudorapidity of $|\eta| < 1.07$. For the electron trigger, only a high-energy deposit in the electromagnetic calorimeter is required, again without tracker requirements. This has a less effective background rejection performance compared with the muon trigger, and thus a relatively strong criterion is imposed on the transverse momentum of electrons: either a single electron with $p_{\rm T} > 120$ GeV or two electrons with $p_{\rm T} > 40$ GeV. The events which have passed these triggers are then required to be subject to the object reconstruction and filtering criteria. Finally, with the help of the retracking procedure, a dilepton displaced vertex is reconstructed from two oppositely-charged lepton tracks: $\mu^+\mu^-$, e^+e^-, or $e^\pm\mu^\mp$. Here, the lepton tracks are required to satisfy $p_{\rm T} > 10$ GeV, $0.02 \leq |\eta| < 2.5$, and $d_0 > 2$ mm (2.5 mm) for muons (electrons). In addition, the invariant mass of the tracks, $m_{\rm DV}$, should be larger than 10 GeV. The position of the reconstructed displaced vertices must satisfy $r_{\rm DV} < 300$ mm, $|z_{\rm DV}| < 300$ mm, and $\sqrt{(x_{\rm DV} - x_{\rm PV})^2 + (y_{\rm DV} - y_{\rm PV})^2} \geq 4$ mm, where the subscripts DV and PV indicate that the corresponding coordinates are those of the displaced vertex and the primary vertex, respectively. The effect of the first two conditions is almost negligible in our analysis since the decay distance of sneutrinos is $\lesssim 10$ mm as shown in Fig. 6.2b, while the third condition does affect our analysis, as we shall see below.

With these requirements, the ATLAS collaboration searched for dilepton displaced vertices and found no event, while the numbers of background events are expected to be $1.0 \pm 0.2^{+0.3}_{-0.6} \times 10^{-3}$, $2.4 \pm 0.9^{+0.8}_{-1.5} \times 10^{-3}$, and $2.0 \pm 0.5^{+0.3}_{-1.4} \times 10^{-3}$ for the e^+e^-, $e^\pm\mu^\mp$, and $\mu^+\mu^-$ channels, respectively. The dominant source of the background is accidental crossings of independent lepton tracks. As we see, this search is basically background free. With this result, strong limits were imposed on long-lived particles which decay into leptons.

We however cannot directly apply the limits provided by the ATLAS collaboration

[2] In the ATLAS search, the missing-energy and jets triggers are also used. These triggers are ineffective in our setup.

(Fig. 13 of Ref. [176]) to the left sneutrino case, since the ATLAS analysis simulates the decay of a heavy gluino into a light and a heavy neutralino. The former case represents a highly boosted light particle decaying into a pair of muons, while the latter represents a heavy non-boosted particle decaying in the same way. Yet, the sneutrino features a light non-boosted particle. This analysis can be extended, nevertheless, combining information from both situations by considering the fact that the difference in the strength of the upper limits basically comes from the efficiency in passing the event selection requirements (the decay products from a sufficiently heavy neutralino are so energetic that almost all the events pass the selection criteria),[3] while the position of the minimum of the limits is determined by the boost factors of the neutralinos. Thus, what we can do is shifting upwards the limit corresponding to the non-boosted neutralino to make its minimum to coincide with the one of the line corresponding to the light boosted neutralino.[4] The resultant limit for the dimuon channel is displayed as a function of the decay distance $c\tau$ in the purple-shaded solid line in Fig. 6.3. We also show the limits corresponding to the light boosted and heavy non-boosted cases in the green-hatched dotted and yellow-hatched dash-dotted lines, respectively, which are taken from Fig. 13 (c) of Ref. [176]. We analyzed the limits for the ee and $e\mu$ channels in a similar manner using Figs. 13 (a) and (b) in Ref. [176], respectively, obtaining very similar plots. As seen from Fig. 6.3, the ATLAS displaced-vertex search is sensitive to a decay distance larger than about a few mm. This stems from the requirements that the impact parameter d_0 of the muon tracks be larger than 2 mm and the transverse distance between the displaced vertices and the primary vertices be larger than 4 mm, as we mentioned above. We will discuss a possibility of relaxing these requirements later.

Another obstacle for the left sneutrino case is the trigger requirement. Since left sneutrinos we consider in this paper have a mass of $\lesssim 100$ GeV and are less boosted, their decay products have relatively small momenta. On the other hand, the ATLAS 8-TeV analysis requires rather high thresholds for lepton momenta, especially for electrons, since it aims at generic long-lived particles such as metastable neutrinos produced by the decays of colored particles. In particular, the events must satisfy the following requirements [176]:

- One muon with $p_{\rm T} > 50$ GeV and $|\eta| < 1.07$, one electron with $p_{\rm T} > 120$ GeV or two electrons with $p_{\rm T} > 40$ GeV.
- One pair e^+e^-, $\mu^+\mu^-$ or $e^\pm\mu^\mp$ with $p_{\rm T} > 10$ GeV and $0.02 < |\eta| < 2.5$ for each one.

To estimate the sensitivity of this search strategy, samples of simulated Monte Carlo (MC) events are used to study the efficiency of the triggering and off-line selection processes for signal events. In each event two sneutrinos are created in the pp collision as described in Section 6.2. All simulated samples are generated using `MadGraph5_aMC@NLO` 2.6.0 [113] and `PYTHIA` 8.230 [184]. In particular, ten thousand events are generated for each case with `MadGraph5_aMC@NLO` 2.6.0 at leading order (LO) of perturbative QCD simulating the

[3] In the ATLAS search [176], the light neutralino events can pass the trigger requirement since the missing-energy and jets triggers are also used, but the vertex-level efficiency deteriorates for such events. With keeping this in mind, we here assume that all of the neutralino events satisfy the trigger requirements—the dilepton trigger for the heavy case and the missing-energy/jets trigger for the light case—and the difference in the sensitivities originates from that in the vertex-level efficiencies. This assumption is fairly reasonable since the leptons (jets) in the final state are very active in the heavy (light) neutralino case.

[4] We however note that there is also an efficiency loss for a boosted system as the final state muons tend to be collinear with each other, whose effect is not taken into account in this prescription. The neglect of this effect thus results in a rather conservative limit.

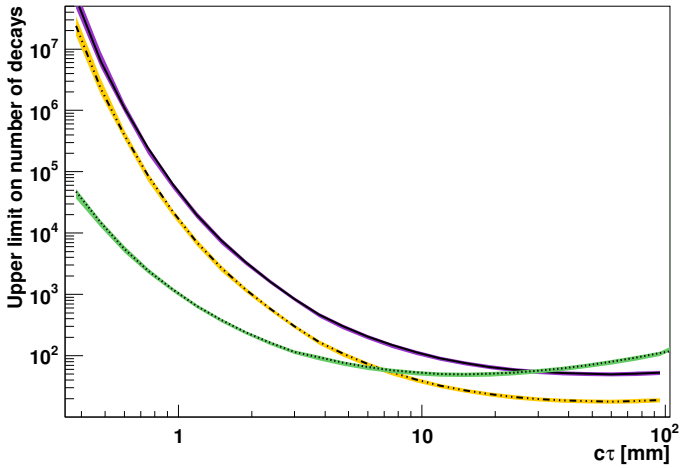

Figure 6.3: Upper limit at 95% confident level on the number of tau left sneutrinos decaying into dimuons at $\sqrt{s} = 8$ TeV for an integrated luminosity of 20.3 fb^{-1}, shown in the purple-shaded solid line. We also show the limits given in Fig. 13 (c) of Ref. [176], which we use to obtain our limit: green-hatched dotted (yellow-hatched dash-dotted) line corresponding to a light boosted neutralino of 50 GeV (heavy non-boosted neutralino of 1000 GeV) from the decay of a heavy gluino of 1300 GeV.

Table 6.3: Cutflow of the selection requirements for $\widetilde{\nu}_\tau \to \mu\mu$, for the 8-TeV analysis with integrated luminosity of 20.3 fb^{-1}, where $\epsilon_{\rm sel}$ is the selection efficiency.

	Through Z boson				Through W boson				Through γ, Z bosons			
$m_{\widetilde{\nu}_\tau}$ (GeV)	50	60	80	100	50	60	80	100	50	60	80	100
$p_{\rm T_{trigger}}$	2,280	4,241	6,828	8,063	2,335	3,703	3,840	7,515	1,616	2,233	3,396	4,374
dilepton sel.	1,069	2,096	3,517	4,333	1,135	1,881	3,740	3,968	1,550	2,150	3,273	4,208
$\epsilon_{\rm sel}$	0.1069	0.2096	0.3517	0.4333	0.1135	0.1881	0.374	0.3968	0.1550	0.2150	0.3273	0.4208

production of the described process. We include the next-to-leading order (NLO) [103] and next-to-leading logarithmic accuracy (NLL) [169] results using a K-factor of about 1.2. We also use `DELPHES v3` [144] for the detector simulation. The effect of these selections for different masses and for the three production processes at $\sqrt{s} = 8$ TeV with an integrated luminosity of 20.3 fb^{-1}, is shown in Tables 6.3 and 6.4 for the $\mu\mu$ and μe channels, respectively. The trigger requirement for electrons is too restrictive and makes the selection efficiency for the dielectron channel to be a few percent level, and thus ineffective for light sneutrino searches. In these tables, $\epsilon_{\rm sel}$ is the selection efficiency for each case. Using these results and the BRs discussed in Sec. 6.2, we can compute the prediction for the number of decays $\widetilde{\nu}_\tau \to \mu\mu/\mu e$ passing the trigger and event selection requirements. Notice however that $\epsilon_{\rm sel}$ is not large.

The ATLAS 8-TeV search strategy discussed above is, of course, not optimized for the present setup. Nevertheless, in principle it is possible to optimize the trigger requirements for left sneutrino searches by relaxing the thresholds, as there are a variety of different lepton triggers with lower momentum thresholds used in the ATLAS experiment. For instance, for the muon trigger, the ATLAS 8-TeV analysis uses only the muon spectrometer and requires $p_{\rm T} > 50$ GeV, as discussed above. On the other hand, the `mu24i` trigger [185], which is an isolated single muon trigger at the event-filter, also uses the information from the inner

Table 6.4: The same as in Table 6.3 but for $\widetilde{\nu}_\tau \to \mu e$.

	Through Z boson				Through W boson				Through γ, Z bosons			
$m_{\widetilde{\nu}_\tau}$ (GeV)	50	60	80	100	50	60	80	100	50	60	80	100
$p_{\mathrm{T}_{\mathrm{trigger}}}$	659	1,347	2,526	3,612	678	1,138	2,134	3,067	878	1,249	2,329	3,287
dilepton sel.	618	1,253	2,315	3,278	628	1,061	1,972	2,803	827	1,160	2,109	2,978
ϵ_{sel}	0.0618	0.1253	0.2315	0.3278	0.0628	0.1061	0.1972	0.2803	0.0827	0.116	0.2109	0.2978

Table 6.5: Cutflow of the selection requirements for $\widetilde{\nu}_\tau \to \mu\mu$, for the optimized 8-TeV analysis with integrated luminosity of 20.3 fb^{-1}, where ϵ_{sel} is the selection efficiency.

	Through Z boson				Through W boson				Through γ, Z bosons			
$m_{\widetilde{\nu}_\tau}$ (GeV)	50	60	80	100	50	60	80	100	50	60	80	100
$p_{\mathrm{T}_{\mathrm{trigger}}}$	6,687	7,775	8,682	9,144	6,520	7,343	7,359	8,846	6,961	7,471	8,387	8,916
dilepton sel.	6,637	7,707	8,589	9,027	6,409	7,198	7,229	8,594	6,701	7,288	8,151	8,647
ϵ_{sel}	0.6637	0.7707	0.8589	0.9027	0.6409	0.7198	0.7229	0.8594	0.6701	0.7288	0.8151	0.8647

detector and requires the transverse momentum threshold of $p_{\mathrm{T}} > 24$ GeV.[5] With the help of the inner detector information, this `mu24i` trigger has a good performance in a wider range of the pseudorapidity of tracks, and thus we can also relax the requirement on η; from $|\eta| < 1.07$ to $|\eta| < 2.5$ [185]. To exploit this trigger instead of that used in Ref. [176] can significantly enhance the sensitivity to light sneutrinos, since the typical momentum of muons from the sneutrino decays is a few tens of GeV. A side effect of the reduction of the momentum threshold is, of course, an increase of the number of background events. According to Ref. [185], the enhancement in the number of events due to the relaxation of the trigger requirement is expected to be ~ 10. Since the main background in the displaced-vertex search is accidental crossings of uncorrelated lepton tracks [176], we can estimate the increase in the number of background events by scaling this according to the number of events passing the trigger. Given that the number of background muon vertices in the ATLAS 8-TeV search is as low as $\sim 2 \times 10^{-3}$ [176], we can safely conclude that the number of background events can still be regarded as zero even if we relax the trigger requirement for muons. Another restriction we need to take into account is the requirement on the impact parameter d_0 of muon tracks adopted by `mu24i`; $|d_0| < 1$ cm is required [186, 187] for the `mu24i` trigger, which indicates that the efficiency should be reduced for sneutrinos with $c\tau \gtrsim 1$ cm. Nevertheless, this again causes a negligible effect on left sneutrino searches in the present setup since the sneutrinos have a proper decay distance smaller than 1 cm,[6] as shown in Fig. 6.2b. We therefore conclude that the use of the `mu24i` trigger instead of the present one in Ref. [176] is very powerful and promising for the left sneutrino searches.

We may also use a lower p_{T} threshold for the electron trigger. However, we are unable to estimate the increase in the number of background events in this case from, say, Ref. [188], since the plot does not show the corresponding trigger rate for $p_{\mathrm{T}} > 120$ GeV. Considering this, in the following 8-TeV analysis, we only use the muon trigger with $p_{\mathrm{T}} > 24$ GeV and consider the $\mu^+\mu^-$ and $\mu^\pm e^\mp$ channels to be conservative. We however note that we can certainly optimize the electron trigger as well, which indeed improves the sensitivity

[5] This trigger should also satisfy a loose isolation selection, the sum of the p_{T} of tracks in a cone of $\Delta R < 0.2$ centered around the muon candidate after eliminating the muon transverse momentum $(p_{\mathrm{T}})_\mu$ should be smaller than $0.12 \times (p_{\mathrm{T}})_\mu$; this requirement is so loose that almost all isolated muons from the Z-boson decays pass the criterion. Since the muons coming from the sneutrino decays are also expected to be isolated, we can expect that this requirement scarcely affects the sneutrino event selection. For this reason, we do not take account this effect in the following analysis.

[6] This is the reason why we show only a small $c\tau$ region in Fig. 6.3.

Table 6.6: The same as in Table 6.5 but for $\widetilde{\nu}_\tau \to \mu e$.

	Through Z boson				Through W boson				Through γ, Z bosons			
$m_{\widetilde{\nu}_\tau}$ (GeV)	50	60	80	100	50	60	80	100	50	60	80	100
$p_{\mathrm{T}_{\mathrm{trigger}}}$	4,014	5,255	6,508	7,420	3,853	4,754	6,054	6,974	6,118	6,748	7,116	8,293
dilepton sel.	3,943	5,094	6,267	7,067	3,763	4,624	5,830	6,637	4,917	5,515	6,360	6,961
ϵ_{sel}	0.3943	0.5094	0.6267	0.7067	0.3763	0.4624	0.5830	0.6637	0.4917	0.5515	0.6360	0.6916

considerably and thus is worth a further dedicated study.

After all, we use the following criteria for the optimized 8-TeV analysis:

- At least one muon with $p_{\mathrm{T}} > 24$ GeV.
- One pair $\mu^+\mu^-$ or $e^\pm\mu^\mp$ with $p_{\mathrm{T}} > 10$ GeV and $0.02 < |\eta| < 2.5$ for each one.

The effect of these selections for different masses and for the three production processes, is shown in Tables 6.5 and 6.6 for the $\mu\mu$ and μe channels, respectively. We see that a sizable number of signal events is expected to pass the selection criteria. We can compare these results with those of Table 6.3. For instance, there $\epsilon_{\mathrm{sel}} \simeq 0.11$ is obtained for a 50-GeV sneutrino produced via a Z-boson, whereas $\epsilon_{\mathrm{sel}} \simeq 0.66$ is obtained in Table 6.5, with a significant improvement in the event selection.

Table 6.7: Cutflow of the selection requirements for $\widetilde{\nu}_\tau \to \mu\mu$, for the optimized 13-TeV analysis with integrated luminosity of 300 fb^{-1}, where ϵ_{sel} is the selection efficiency.

	Through Z boson				Through W boson				Through γ, Z bosons			
$m_{\widetilde{\nu}_\tau}$ (GeV)	50	60	80	100	50	60	80	100	50	60	80	100
$p_{\mathrm{T}_{\mathrm{trigger}}}$	5,797	7,011	8,077	8,581	5,643	6,539	7,587	8,281	5,885	6,634	7,716	8,316
dilepton sel.	5,739	6,941	7,995	8,469	5,587	6,411	7,384	8,020	5,705	6,459	7,485	8,000
ϵ_{sel}	0.5739	0.6941	0.7995	0.8469	0.5587	0.6411	0.7384	0.8020	0.5705	0.6459	0.7485	0.8

Table 6.8: The same as in Table 6.7 but for $\widetilde{\nu}_\tau \to \mu e$.

	Through Z boson				Through W boson				Through γ, Z bosons			
$m_{\widetilde{\nu}_\tau}$ (GeV)	50	60	80	100	50	60	80	100	50	60	80	100
$p_{\mathrm{T}_{\mathrm{trigger}}}$	5,344	6,386	7,458	8,149	4,929	5,751	6,961	7,698	6,836	5,971	6,912	7,698
dilepton sel.	4,312	5,203	6,138	6,718	3,901	4,652	5,647	6,226	3,089	4,883	5,629	6,257
ϵ_{sel}	0.4312	0.5203	0.6138	0.6718	0.3901	0.4652	0.5647	0.6226	0.3089	0.4883	0.5629	0.6257

We also study the prospects for the 13-TeV LHC run. Since we do not have any dedicated searches for dilepton displaced vertices with the 13-TeV data so far, we just assume background-free in our estimation. Again, we consider an optimization of the trigger requirements in the 13-TeV analysis using the existing result for the performance of the ATLAS trigger system [189], taking account of the trigger rate for the 8-TeV analysis. Since the trigger rate for `mu24i` is $\lesssim 100$ Hz [185], we expect a sufficiently low background as long as the trigger rate in the 13-TeV searches does not exceed about 100 Hz. According to Ref. [189], a p_{T} threshold of 26 GeV [190, 191] for both muon and electron ensures the trigger rate to be $\lesssim 100$ Hz.[7] These triggers again rely on the use of the inner tracker,[8] and

[7] Given a higher instantaneous luminosity ($\sim 2 \times 10^{34}$ cm^{-2}s^{-1}) compared with those considered in Ref. [189], the momentum threshold is raised from the ones in Ref. [189] so that the trigger rates are kept at a similar level.

[8] For the tracking performance in the 13 TeV run, see Ref. [192].

Table 6.9: The same as in Table 6.7 but for $\widetilde{\nu}_\tau \to ee$.

	Through Z boson				Through W boson				Through γ, Z bosons			
$m_{\widetilde{\nu}_\tau}$ (GeV)	50	60	80	100	50	60	80	100	50	60	80	100
$p_{\mathrm{T}_{\mathrm{trigger}}}$	4,724	5,766	6,892	7,633	4,177	4,943	6,046	6,750	4,414	5,132	6,078	6,836
dilepton sel.	1,886	2,413	3,011	3,428	1,627	1,996	2,476	2,797	1,868	2,200	2,739	3,089
ϵ_{sel}	0.1886	0.2413	0.3011	0.3428	0.1627	0.1996	0.2476	0.2797	0.1868	0.2200	0.2739	0.3089

thus are effective in the region of $|\eta| < 2.5$. With this observation, we use the following criteria for the 13-TeV analysis:

- At least one electron or muon with $p_{\mathrm{T}} > 26$ GeV.
- One pair $\mu^+\mu^-$, e^+e^-, or $e^\pm\mu^\mp$ with $p_{\mathrm{T}} > 10$ GeV and $0.02 < |\eta| < 2.5$ for each one.

The effect of these selections for different masses and for the three production processes at $\sqrt{s} = 13$ TeV with integrated luminosity of 300 fb^{-1}, is shown in Tables 6.7, 6.8, and 6.9 for the $\mu\mu$, μe, and ee channels, respectively.[9] We however note that a more elaborate optimization may be considered; for example, we may also use the dilepton triggers, which may be more effective since we can lower the momentum threshold for these triggers [189]. In any case, to use a High Level Trigger with inner-detector information is technically quite feasible and expected to result in a considerable improvement in displaced-vertex searches. We also note in passing that this possible improvement is not only for the ATLAS analysis but also for the CMS one [177], where again tracker information is not used in the trigger requirement.

Now we discuss how to obtain the limits for light sneutrinos. The limits from the ATLAS search [176] can be translated into a vertex-level efficiency, taking into account the lack of observation of events for any value of the decay length. Therefore, $\epsilon_{\mathrm{vert}}(c\tau)$ can be obtained as the ratio of the number of signal events compatible with zero observed events (which in this case is 3) and that corresponding to the upper limits given in Ref. [176] (with an appropriate modification described above); for example, we can use the purple-shaded solid line of Fig. 6.3 to obtain the vertex-level efficiency $\epsilon^{\mu\mu}_{\mathrm{vert}}(c\tau)$ for the dimuon channel. By multiplying the number of the events passing the trigger and event selection criteria, which is computed above, with this vertex-level efficiency, we can estimate the total number of signal events; for the 8-TeV case, this is given for the $\mu\mu$ channel by

$$\begin{aligned} \#\mathrm{Dimuons} &= \left[\sigma(pp \to Z \to \widetilde{\nu}_\tau\widetilde{\nu}_\tau)\epsilon^Z_{\mathrm{sel}} + \sigma(pp \to W \to \widetilde{\nu}_\tau\widetilde{\tau})\epsilon^W_{\mathrm{sel}} + \sigma(pp \to \gamma, Z \to \widetilde{\tau}\widetilde{\tau})\epsilon^{\gamma,Z}_{\mathrm{sel}}\right] \\ &\times \mathcal{L} \times \left[\mathrm{BR}(\widetilde{\nu}^{\mathcal{R}}_\tau \to \mu\mu)\ \epsilon^{\mu\mu}_{\mathrm{vert}}(c\tau^{\mathcal{R}}) + \mathrm{BR}(\widetilde{\nu}^{\mathcal{I}}_\tau \to \mu\mu)\ \epsilon^{\mu\mu}_{\mathrm{vert}}(c\tau^{\mathcal{I}})\right], \end{aligned} \tag{6.7}$$

where the selection efficiencies $\epsilon^Z_{\mathrm{sel}}$, $\epsilon^W_{\mathrm{sel}}$ and $\epsilon^{\gamma,Z}_{\mathrm{sel}}$ are given in Tables 6.3 and 6.5. The same formula can be applied for the $e\mu$ channel shown in Tables 6.4 and 6.6, using the corresponding BRs, selection efficiencies, and vertex-level efficiencies (which turn out to be similar). For the 13-TeV prospects the selection efficiencies for the three channels can be found in Tables 6.7–6.9, and we use the same vertex-level efficiency as in the 8-TeV case and assume zero background.[10] As a result, if this predicted number of signal events is above

[9] The efficiency of the ee channel is worse than the other channels due to the isolation requirement for electrons implemented in the detector simulation with `DELPHES v3` [144].

[10] Notice that in the 13-TeV long-lived gluino search [183] the estimated number of background events is still much smaller than zero, $\sim 10^{-2}$, which is similar in size to that in the 8-TeV search [176]. We therefore expect that the background in the 13-TeV dilepton displaced-vertex search is also as low as the 8-TeV one.

3 the corresponding parameter point of the model is excluded so that this is compatible with zero number of events.

We note in passing that the optimization strategy we have discussed in this section is generically useful for the searches of other metastable particles which have a relatively short lifetime and a small mass and whose decay products contain soft leptons. We thus hope this kind of search strategies to be considered seriously in the LHC experiments.

Another possibility to improve the sensitivity is to search for shorter displaced vertices. As can be seen from Fig. 6.2b, in some regions of parameter space, the decay distance of a sneutrino is predicted to be $\lesssim 1$ mm, to which the current ATLAS search is less sensitive. However, we may even probe such sub-millimeter region by relaxing the impact-parameter requirements for lepton tracks as well as the condition on the reconstructed position of displaced vertices, given the extremely low background in this search [176]. In fact, it is shown in Refs. [193, 194] for metastable gluinos that sub-millimeter displaced vertices can be probed using the existing vertex-reconstruction technique, though this is not directly applicable to the present case. Moreover, there are several existing searches which are sensitive to sub-millimeter region [177, 195, 196, 197]. In any case, to assess the possibility of searching for shorter dilepton displaced vertices, a dedicated study with a full consideration of the detector performance is required; we thus do not discuss this possibility in this paper and hand this over to experimentalists.

6.4 Results

By using the method described in the previous section, we now evaluate the current and potential limits on the $\mu\nu$SSM parameter space from the displaced-vertex searches with the 8-TeV ATLAS result [176], and discuss the prospects for the 13-TeV searches.

The 8-TeV current limits are given in Figs. 6.4 and 6.5, with the neutrino mass scale fixed to be 0.05 and 0.23 eV, respectively, and all of the neutrino Yukawa couplings set to be a common value Y_ν: 10^{-7}, 5×10^{-7}, and 10^{-6} GeV in the top, middle, and bottom panels, respectively. The yellow, red, blue, and green lines correspond to the sneutrino mass of 50, 60, 80, and 100 GeV, respectively, with the bands representing the uncertainties that come from those in Ref. [176]. Notice that for these sneutrino masses, values of M smaller than 92.7, 111.3, 148.4, and 185.5 GeV, respectively, are not interesting for our analysis since the tau left sneutrino would no longer be the LSP in favor of the gauginos. To obtain the reaches, we have combined the results from the $\mu\mu$ and $e\mu$ channels. The region of the parameter space inside each line is excluded from the displaced-vertex searches.

We can see in the top panel of Fig. 6.4, where $Y_\nu = 10^{-7}$, that for $m_{\widetilde{\nu}_\tau} = 50$ GeV the upper bound on the average gaugino mass M (see Eq. (3.39)) is of about 500 (900) GeV for $\lambda = 0.1$ (1). As discussed in Section 6.2, small values of λ favor larger BRs, and as a consequence the gaugino mass is more constrained. If λ is too small, however, the limit on M disappears since the lifetime of the left sneutrino goes into the sub-millimeter regime, as can be seen from Eq. (6.6). On the other hand, small sneutrino masses produce larger decay lengths, and gaugino masses turn out to be also more constrained. For example, for $m_{\widetilde{\nu}_\tau} = 50$ and 60 GeV the upper bound on M for $\lambda = 1$ is of about 700 and 1100 GeV, respectively. In the middle panel, the larger value of the neutrino Yukawa $Y_\nu = 5\times10^{-7}$ gives rise to smaller decay lengths, and therefore the figures are shifted to the right with a lower limit for λ of about 0.3. The case of $Y_\nu = 10^{-6}$ in the bottom panel is more extreme, and the lower limit on λ is now of about 0.7. Finally, in Fig. 6.5 we show the same cases as in Fig. 6.4 but for the neutrino mass scale 0.23 eV. To increase the neutrino mass produces an increase in the left sneutrino VEVs, and therefore the $\widetilde{\nu}_\tau$ decay width into neutrinos

is larger. As a consequence, its BR into leptons as well as its decay length are smaller giving rise to less stringent constraints on the parameter space, as shown in the figure. In particular, there is almost no constraint on the parameter space shown in the bottom panel in Fig. 6.5.

The potential limits using the optimization of the trigger requirements explained in the previous section, are shown in Figs. 6.6 and 6.7. They turn out to be more stringent than the previous ones without optimization. For example, we can see in the top panel of Fig. 6.6 that for $m_{\widetilde{\nu}_\tau} = 50$ GeV the upper bound on M is of about 200 (500) GeV for $\lambda = 0.1$ (1), to be compared with the ones of Fig. 6.4. Moreover, in the case of $Y_\nu = 10^{-6}$ and $m_\nu \sim 0.23$ eV shown in the bottom panel in Fig. 6.7, now some limits are imposed on light sneutrino masses, which can be compared to the bottom panel in Fig. 6.5. This result indicates that the trigger optimization discussed above can significantly improve the sensitivity of left sneutrino searches.

The 13 TeV prospects are illustrated in Figs. 6.8 and 6.9. Here, we combine the $\mu\mu$, $e\mu$ and ee channels. As we can see, the constraints on the parameter space of the $\mu\nu$SSM turn out to be very strong. For example, in the top panel of Fig. 6.8 and for $\lambda = 0.1$, the upper bound on M is as small as about 100, 200, and 350 GeV for $m_{\widetilde{\nu}_\tau} \approx 50, 80$, and 100 GeV. Such small M region would be probed in other strategies like ordinary electroweak gaugino searches, which makes it possible to cover a considerable range of the parameter space for the left sneutrino LSP with a mass in the range 45–100 GeV. Furthermore, now it is possible to probe a wide range of the parameter space even for the heavier neutrino mass case, $m_\nu \sim 0.23$ eV, as shown in Fig 6.9. All in all, we conclude that the dilepton displaced-vertex searches can be a powerful probe of the $\mu\nu$SSM parameter space, especially if we optimize them by making the most of the performance of the inner detectors of the ATLAS and CMS experiments.

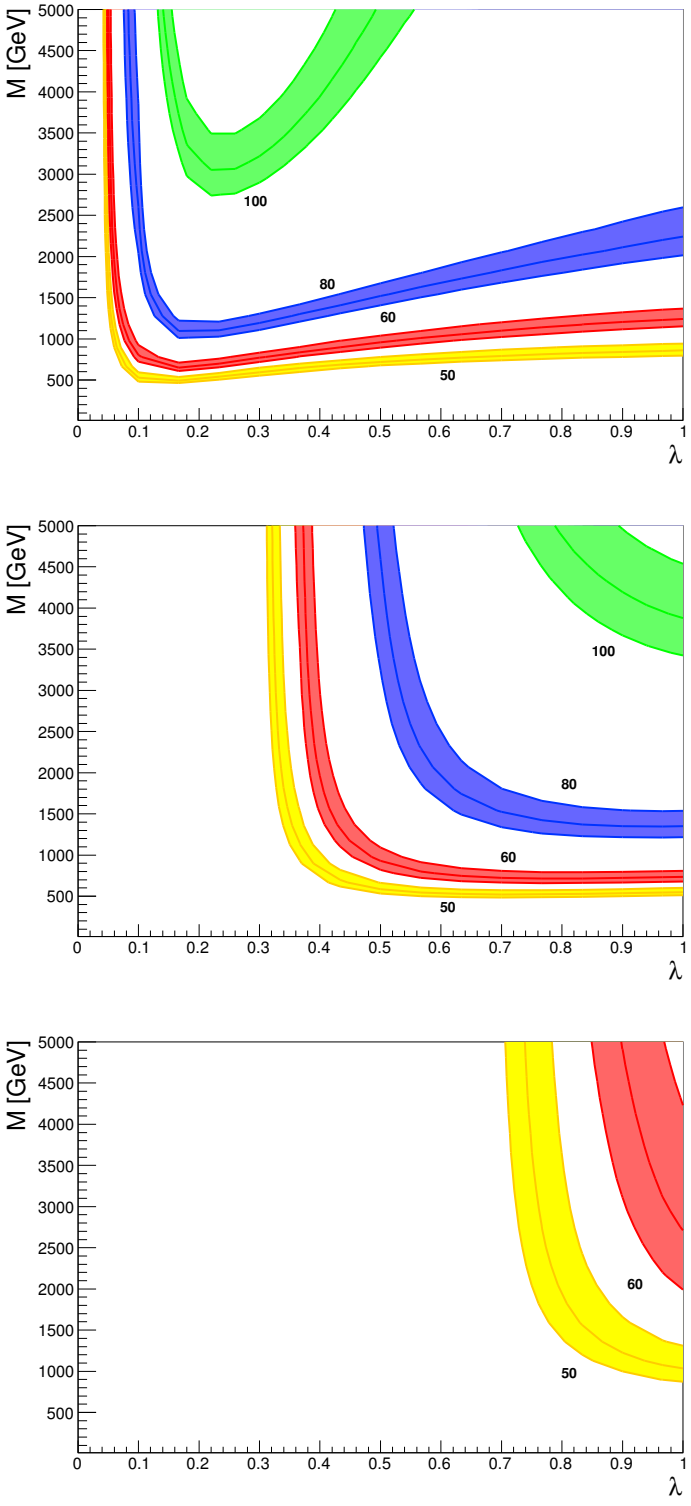

Figure 6.4: Limits on the $\mu\nu$SSM parameter space from the ATLAS 8-TeV displaced-vertex search with an integrated luminosity of 20.3 fb^{-1} [176], combining the $\mu\mu$ and $e\mu$ channels. The region inside each colored line is excluded. The neutrino mass scale is fixed to be $m_\nu \sim 0.05$ eV, and the neutrino Yukawa couplings are set to $Y_\nu = 10^{-7}$, 5×10^{-7}, and 10^{-6} in the top, middle, and bottom panels, respectively. The yellow, red, blue, and green lines correspond to the sneutrino mass of 50, 60, 80 and 100 GeV, respectively.

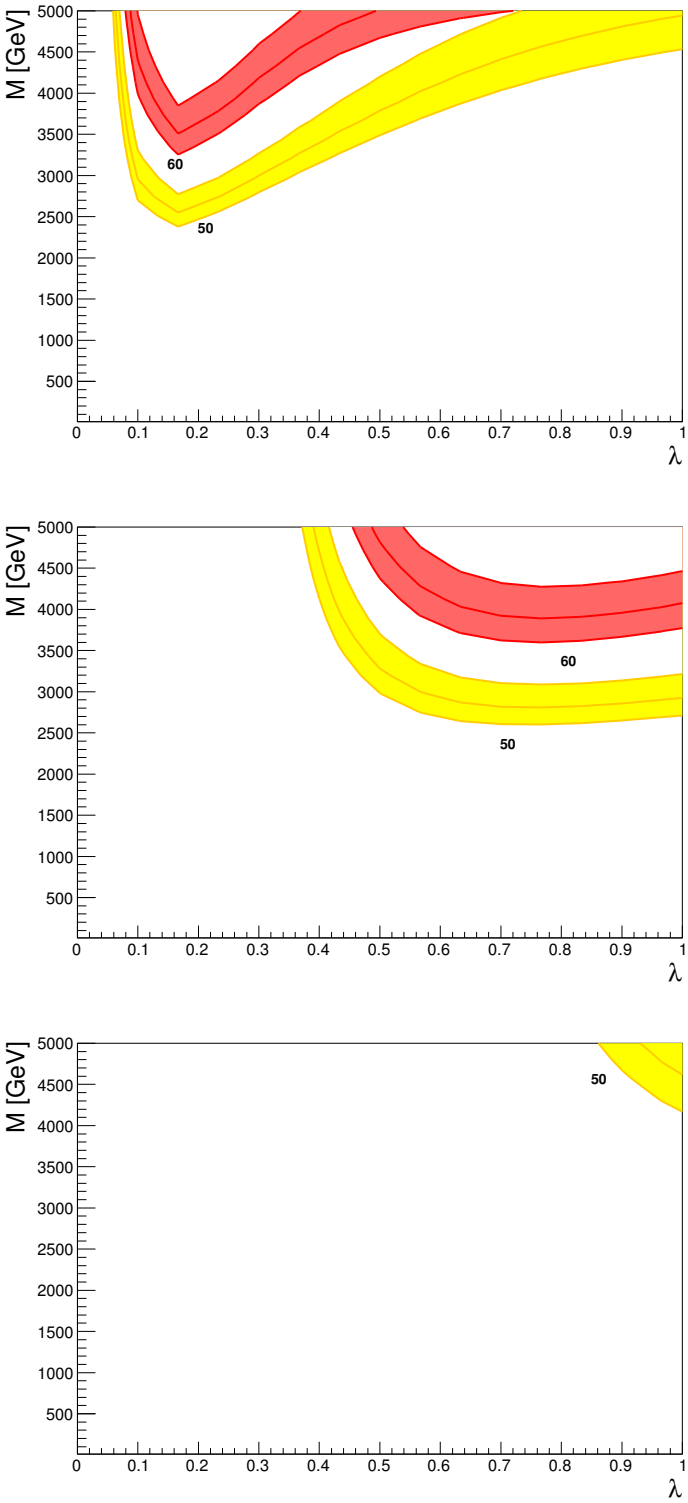

Figure 6.5: The same as in Fig. 6.4 but with the neutrino mass scale fixed to $m_\nu \sim 0.23$ eV.

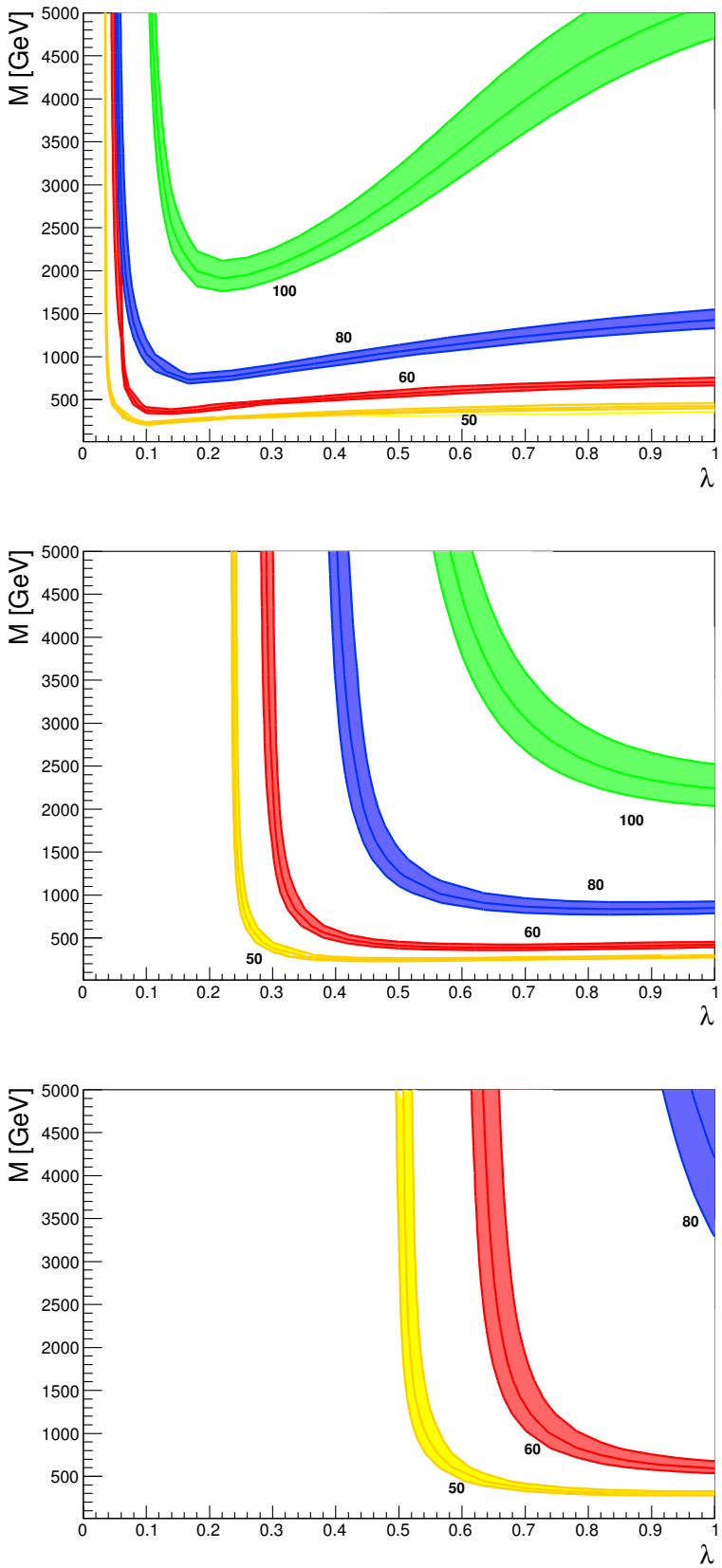

Figure 6.6: The same as in Fig. 6.4 where $m_\nu \sim 0.05$ eV, but considering the optimization of the trigger requirements discussed in the text.

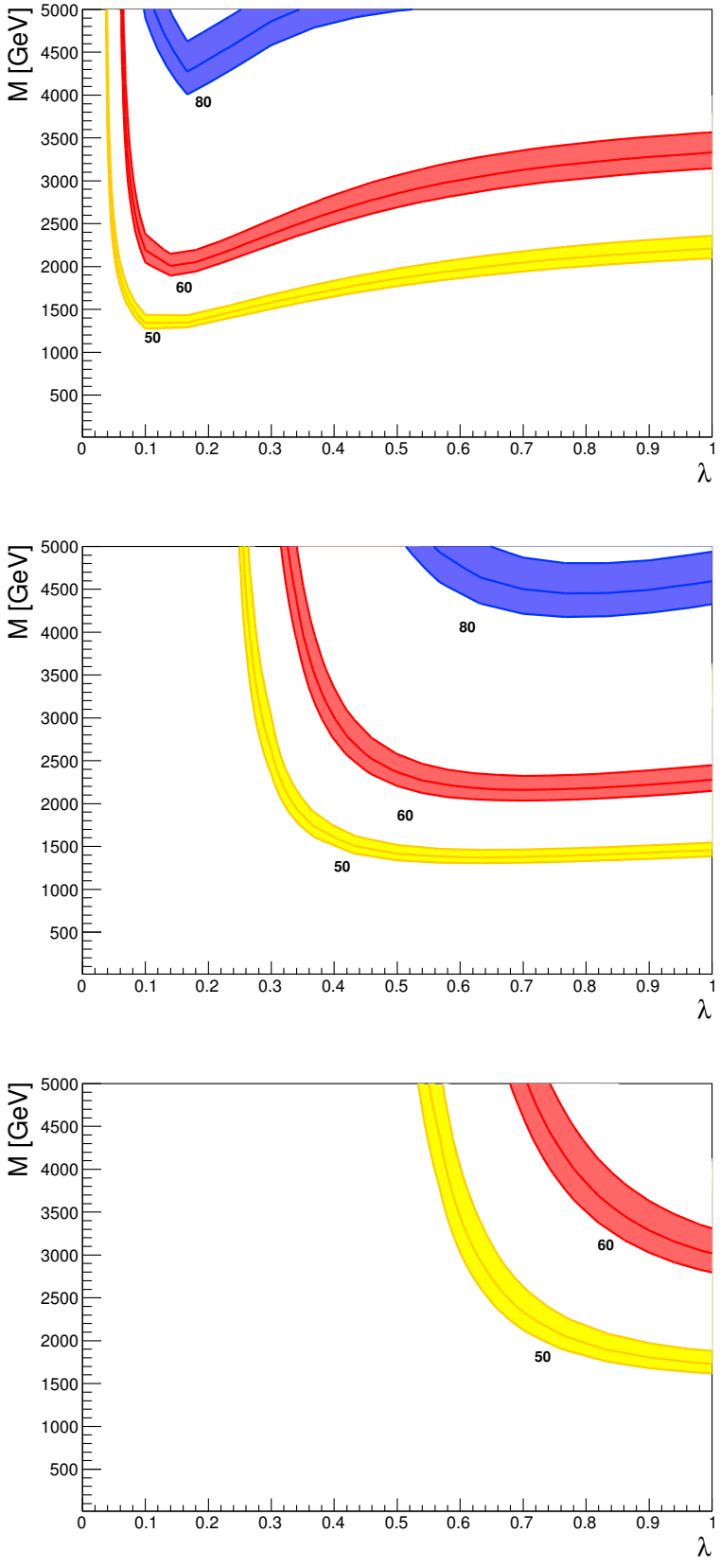

Figure 6.7: The same as in Fig. 6.6 but with the neutrino mass scale fixed to $m_\nu \sim 0.23$ eV.

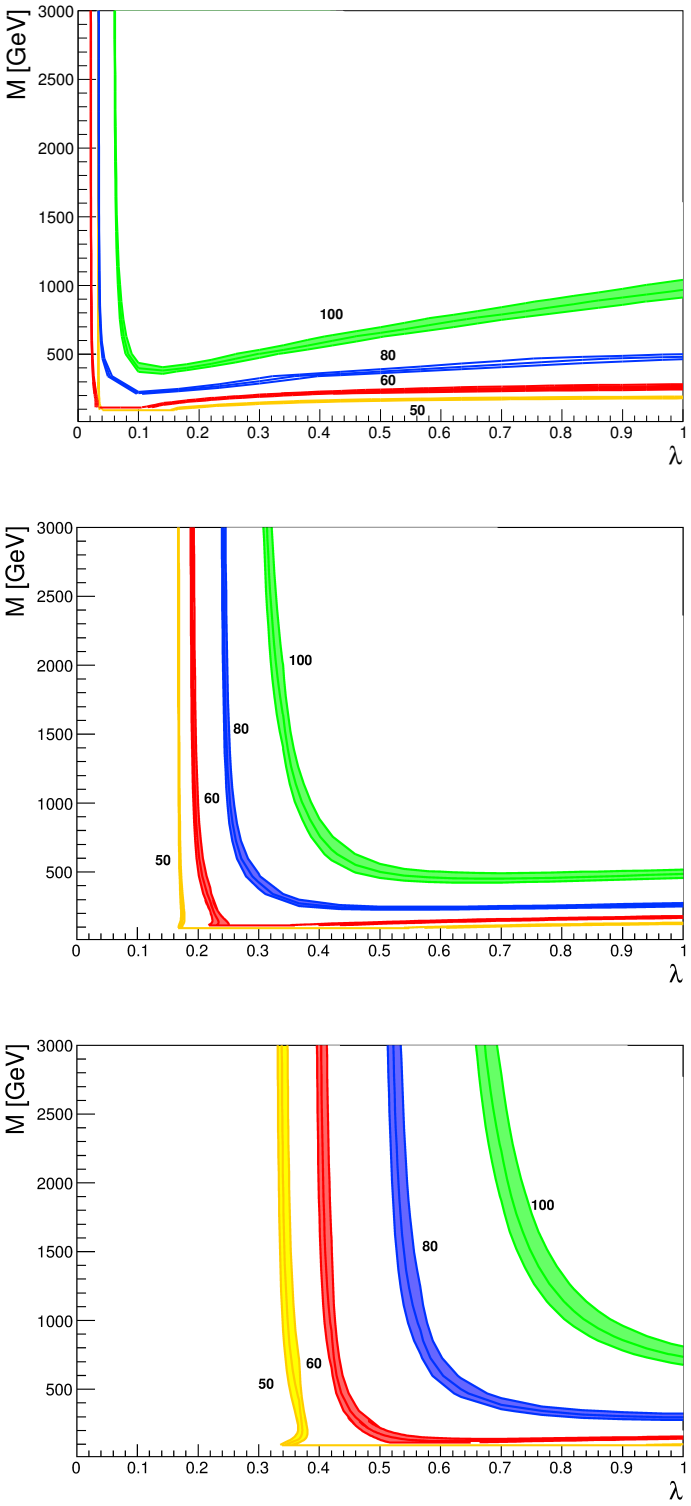

Figure 6.8: The same as in Fig. 6.4 where $m_\nu \sim 0.05$ eV, but analyzing the prospects for the 13-TeV search with an integrated luminosity of 300 fb^{-1}, combining the $\mu\mu$, $e\mu$ and ee channels, and considering also the optimization of the trigger requirements discussed in the text.

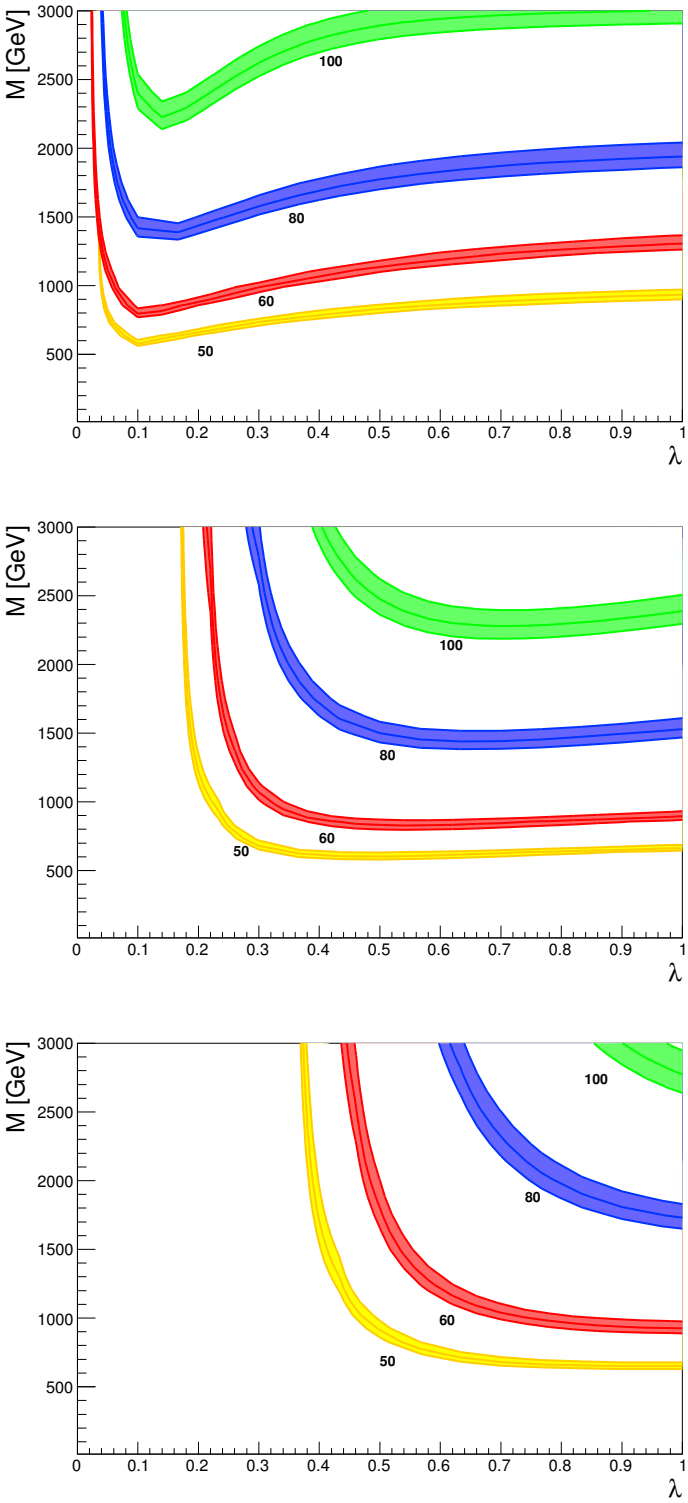

Figure 6.9: The same as in Fig. 6.8 but with the neutrino mass scale fixed to $m_\nu \sim 0.23$ eV.

6.5 Conclusions and outlook

We have analyzed the sensitivity of the displaced dilepton searches at the LHC to a tau left sneutrino LSP with a mass in the range 45–100 GeV in the framework of the $\mu\nu$SSM. The sneutrino LSP is produced via the Z-boson mediated Drell-Yan process or through the W- and γ/Z-mediated process accompanied with the production and decay of the left stau NLSP. Due to the R_p violating term present in the $\mu\nu$SSM, the left sneutrino LSP becomes metastable and eventually decays into the standard model leptons. Because of the large value of the tau Yukawa coupling, a large fraction of the sneutrino LSP decays into a pair of tau leptons or a tau lepton and a light charged lepton, while the rest decays into a pair of neutrinos. It is found that the decay distance of the left sneutrino tends to be as large as $\gtrsim 1$ mm, which thus can be a good target of displaced vertex searches. We have found that the displaced dilepton search channel is most sensitive to the sneutrino LSP, where at least one of the pair-produced left sneutrinos is required to decay into $\tau\tau$ or $\tau\ell$ with the final-state tau leptons decaying leptonically. To evaluate the prospects of this search strategy, we recast the result of the ATLAS 8-TeV dilepton search to obtain the potential limit on the $\mu\nu$SSM parameter space from the 8-TeV LHC data. It is found that even the present data set potentially gives a constraint on the left sneutrino LSP, especially when the Yukawa couplings and mass scale of neutrinos are rather small. We have also discussed an optimization of the trigger requirements exploited in the ATLAS search based on a High Level Trigger that utilizes the tracker information. It turns out that this optimization can considerably improve the sensitivity of the displaced dilepton search. Moreover, we have estimated the potential limits obtained at the 13-TeV LHC run and found that wide range of the $\mu\nu$SSM parameter space can be probed at the LHC Run 3.

As mentioned above, we may consider further optimization for the sneutrino LSP search. Given the low background in the dilepton displaced-vertex search, we may relax the condition on the impact parameter of lepton tracks used for the reconstruction of displaced vertices, as well as that on the reconstructed position of displaced vertices. With such a relaxation, it may be possible to detect sub-millimeter dilepton displaced vertices, which allows us to probe sneutrinos with a shorter lifetime. A further optimization for the trigger requirements is another interesting option to improve the potential of this search. For instance, we may also use the dilepton triggers, which accommodate a lower momentum threshold. Such optimizations highly rely on the detector performance and thus a more dedicated study is required to assess their prospects.

Displaced sneutrino decay signature is useful not only for its discovery but also for the determination of parameters relevant to the sneutrino decay properties. For example, measurement of the lifetime of the sneutrino LSP through the reconstruction of displaced vertices allows us to constrain the parameters in Eq. (6.6), such as Y_ν, M, and λ. In addition, it is in principle possible to measure the mass of the sneutrino LSP since it can decay into visible particles such as $\tau\tau$ and $\tau\ell$; by using hadronically decaying tau leptons, we may fully reconstruct the momenta of the final-state leptons. Although this may be rather challenging, it is worth investigating this possibility in the future.

In this work, we focus on the simplest case of the $\mu\nu$SSM with one right-handed neutrino superfield. Of course, the metastable left sneutrino can also appear if we introduce three right-handed neutrinos so that they give masses to light neutrinos at tree level. In this case, the sneutrino couplings should be chosen so that the neutrino oscillation data is reproduced, which may have some implications for the sneutrino decay properties. Another interesting possibility is to consider a different LSP, which can be again long-lived due to the small R_p violation. In particular, a colored LSP such as the stop LSP may be interesting as its

production cross section is quite large at the LHC. Even in this case, we may still probe it by searching for, e.g., multi-track displaced vertices. These subjects will be discussed in another occasion [175].

Chapter 7

Electroweak superpartners scrutinized at the LHC in events with multi-leptons

The present chapter is based on the work [198] were we analyze a multi-lepton signal plus missing transverse energy from neutrinos expected at the LHC for a bino-like neutralino as the lightest supersymmetric particle (LSP), when the left sneutrino is the next-to-LSP and hence a suitable source of binos. Left sneutrinos/sleptons are pair produced at pp collisions decaying to binos, with the latter decaying via RPV to $W\ell$ or $Z\nu$.

This signal can be compared with LHC searches for electroweak superpartners through chargino-neutralino production. The reduced cross section of the sneutrino/slepton production in comparison with the one of the latter process, limits the sensitivity of the searches to small sneutrino/slepton masses. Although the resulting compressed spectrum typically evades the aforementioned searches, we show that analyses using recursive jigsaw reconstruction are sensitive to these scenarios. As a by-product, we find that the region of bino masses $110 - 120$ GeV and sneutrino masses $120 - 140$ GeV can give rise to a tri-lepton signal compatible with the local excess recently reported by ATLAS.

7.1 Introduction

The phenomenology of the left sneutrino as the LSP in the $\mu\nu$SSM has been analyzed in Ref. [94]. In particular, the pair production and prompt decays of sneutrinos/sleptons producing signals with diphoton plus missing transverse energy (MET) from neutrinos, di-lepton plus MET, and multi-leptons, in the range of 100 GeV to 300 GeV, was studied. Displaced-vertex decays of the sneutrino LSP have also been recently studied in Ref. [92] through signals with di-lepton pairs, covering senutrino masses between 45 and 100 GeV. The phenomenology of a neutralino LSP was analyzed in the past in Refs. [76, 77, 81, 80].

In this chapter, we analyze the interesting case when the bino-like neutralino is the LSP, with the sneutrino the next-to-LSP (NLSP). Thus the decays $\tilde{\nu} \to \nu\tilde{\chi}^0$ and $\tilde{\ell} \to \ell\tilde{\chi}^0$ dominate over the RPV ones, which are suppressed by the smallness of Y_ν. Thereby pair production of sneutrinos/sleptons at the LHC will be a source of bino pairs. Subsequently, binos will decay via RPV couplings to $W\ell$ or $Z\nu$, giving rise to signals with multi-leptons plus MET from neutrinos. We will compare these $\mu\nu$SSM signals with recent searches for electroweak superpartners at the LCH using an integrated luminosity of 36.1 fb^{-1}, through chargino-neutralino pair production in R-parity conserving (RPC) models [105, 107]. We will obtain that the reduced cross section of sneutrino/slepton pair production in comparison with the latter, makes these searches insensitive if the mass of the sneutrinos is

large. However, for a small sneutrino mass, the small difference with the masses of the gauge bosons and binos makes these searches also ineffective. We will show nevertheless, that there exist optimized ATLAS analyses [199] to detect chargino-neutralino pair production in the MSSM when the mass spectrum is compressed, that have a promising sensitivity to our scenario. In fact, we will also obtain regions of bino and sneutrino masses in the $\mu\nu$SSM producing a tri-lepton signal compatible with the local excess reported by ATLAS [199], where it was studied in the context of simplified RPC models, assuming wino-like chargino-neutralino production with a bino-like LSP. This scenario was further elaborated in Ref. [200] including dark matter constraints and the measured anomalous magnetic moment of the muon.

The chapter is organized as follows. In Section 7.2 we will introduce the phenomenology of the bino-like LSP with the sneutrino as the NLSP, studying their relevant pair production at the LHC, as well as the signals. On the way, we will analyze the decay widths, BRs and decay lengths of the bino. In Section 7.3, we will consider the recent ATLAS searches for multi-leptons plus MET, and discuss their feasibility and significance on bino searches in the $\mu\nu$SSM. We will also show our prescription for recasting the ATLAS result [199] to the case of the sneutrino-bino scenario. We then will show the prospects for the 100 and 300 fb^{-1} searches in Section 7.4. Our conclusions are presented in Section 7.5.

7.2 Bino-like LSP phenomenology

The pair production cross section of bino-like neutralinos at large hadron colliders is very small, since there is no direct coupling between the bino flavor state and the gauge bosons, and we are assuming that the rest of the spectrum remains decoupled. Binos are produced mainly through virtual Z bosons in the s channel exploiting their small Higgsino flavor composition, or through the t channel interchange of virtual first generation squarks, strongly suppressed by their large masses. Nevertheless, the bino-like LSP can be produced in the decay of other SUSY particles, which although heavier, have a higher production cross section at the LHC. That is the case when the left sneutrino is the NLSP. After production, the left sneutrinos decay to the bino LSP.

The dominant pair production channels of sleptons at hadron colliders were studied in Refs. [99, 100, 101, 102, 103, 104]. The main production channels at the LHC are through a virtual Z boson on the s channel for the pair production of scalar and pseudoscalar left sneutrinos $\tilde{\nu}\tilde{\nu}$, a virtual W boson for the production of a left slepton and a (scalar or pseudoscalar) sneutrino $\tilde{\ell}\tilde{\nu}$, and both virtual Z and γ for the pair production of left sleptons $\tilde{\ell}\tilde{\ell}$. Note that although the left sneutrino is lighter than its corresponding left slepton as discussed in the Introduction, since the mass separation is always smaller than m_W, the phase space suppression makes the decay $\tilde{\ell} \to \tilde{\chi}^0 + \ell$ dominant.

In Fig. 7.1, we show the production channels as well as the decay of the sneutrino and slepton to produce the bino LSP. The right sleptons can be also a source of bino LSP at the LHC. If their masses are similar to the ones of the left sleptons, an additional diagram as the third one of Fig. 7.1 will be present. However, the production cross section corresponding to this extra diagram is significantly smaller than for those shown in Fig. 7.1. Altogether, the number of binos produced after the decay of right sleptons is around a tenth of the number produced through left sneutrinos/sleptons.

If the mass of the bino-like neutralino lies between the Higgs and Z masses, the possible two body decays are to $W\ell$ and $Z\nu$, as shown also in Fig. 7.1. There we only depicted the decay of each neutralino pair to W and Z, and the leptonic decays of the latter. Note

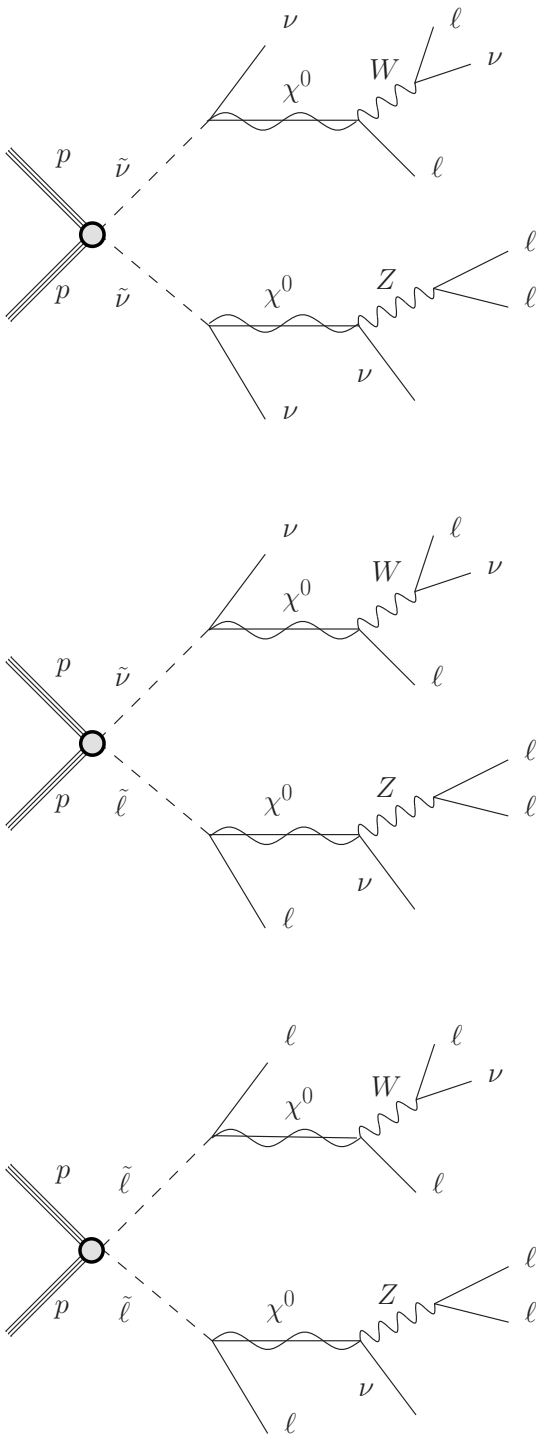

Figure 7.1: Relevant diagrams of the benchmark $\mu\nu$SSM scenario of RPC left sneutrino/slepton pair production, followed by the RPV decay of the bino-like LSP, $\tilde{\chi}^0$.

that both neutralinos can also decay to Z or W indistinctly, and that the hadronic decay of the W boson, as well as the invisible decay of one of the Z's, contribute to the signal of leptonic searches, in addition to the diagrams displayed. The bino decays are mediated through the RPV mixing between the bino and neutrinos. Although three body decays involving virtual Higgs boson or other virtual heavier scalars are possible, all of them suffer from kinematic suppression. Thus the relevant diagrams will be the two body decays, and approximate formulas for the partial decay widths are as follows:

$$\Gamma_{\tilde{\chi}^0 \to W\ell} \approx \frac{g_2^2 m_{\tilde{\chi}^0}}{16\pi} \left(1 - \frac{m_W^2}{m_{\tilde{\chi}^0}^2}\right)^2 \left(1 + \frac{m_{\tilde{\chi}^0}^2}{2m_W^2}\right) \left|U^V_{\tilde{B}\nu_i}\right|^2 , \tag{7.1}$$

$$\Gamma_{\tilde{\chi}^0 \to Z\nu} \approx \frac{g_2^2 m_{\tilde{\chi}^0}}{16\pi \cos^2\theta_W} \left(1 - \frac{m_Z^2}{m_{\tilde{\chi}^0}^2}\right)^2 \left(1 + \frac{m_{\tilde{\chi}^0}^2}{2m_Z^2}\right) \left|U^V_{\tilde{B}\nu_i}\right|^2 , \tag{7.2}$$

where U^V is the matrix that diagonalizes the mass matrix for the neutral fermions [63, 94].

If we neglect the kinematic factors, and sum over the two light families of leptons, $\Gamma_{\tilde{\chi}^0 \to W\ell}/\Gamma_{\tilde{\chi}^0 \to Z\nu} \approx 2\cos^2\theta_W$. Thus the decay to $W\ell$ will always be at least about a factor of 1.5 larger than the decay to $Z\nu$. On the other hand, when the mass of the LSP is close to the masses of the gauge bosons, the difference in mass can have a significant impact on the relative size of the partial widths through those kinematic factors. All in all, for values of the left sneutrino VEVs that produce an acceptable mass scale for neutrinos, and given the small value of M_1, Eqs. (7.1) and (7.2) predict widths $\gtrsim 5 \times 10^{-13}$ GeV corresponding to $c\tau \lesssim 0.3$ mm. This is short enough to expect most of the decays to happen inside the fiducial region defined by the values of the transverse impact parameter (d_0^{PV}) and the longitudinal impact parameter (z_0^{PV}) relative to the primary vertex, considered in prompt ATLAS and CMS searches. Subsequently, the W and Z bosons will decay promptly producing leptons, neutrinos or jets. Thus the neutralino could be detectable in events including leptons, jets and/or MET.

Note that if the mass of the LSP drops below the mass of the W boson, its decay is still possible and will proceed through three-body decays mediated by off-shell gauge bosons and scalars. The total width will be in this case smaller, due to the reduced phase space, and will lead to leptons and/or quarks originated at displaced vertices. This signal cannot be tested with the usual sparticles searches, but rather with dedicated analysis. The study of this possibility, although interesting, is beyond the scope of this work.

If the mass of the bino-like neutralino is larger than the one of the Higgs boson, the decay $\tilde{\chi}^0 \to h\nu$ is also possible, with the dominant diagram mediated by the sneutrino-Higgs mixing. The approximate formula for the corresponding partial decay width is given by:

$$\Gamma_{\tilde{\chi}^0 \to h\nu} \approx \frac{g_1^2 m_{\tilde{\chi}^0}}{64\pi} \sqrt{1 - \left(\frac{m_h}{m_{\tilde{\chi}^0}}\right)^2} \left|Z^H_{\tilde{\nu}h}\right|^2 , \tag{7.3}$$

where Z^H is the matrix that diagonalizes the mass matrix for the neutral scalars [63, 94]. On the one hand, the relative size of the decay of neutralino to Higgs compared to the decay to gauge bosons, is suppressed by the kinematic factors when $m_{\tilde{\chi}^0} \gtrsim m_h$. On the other hand, the contribution of the sneutrino-Higgs mixing is not necessarily small compared with the bino-neutrino mixing. As discussed in detail in Ref. [94], this mixing can be enhanced when the mass separation between $m_{\tilde{\nu}}$ and m_{h^0} is small, and as a result, in this case the decays of neutralinos to gauge bosons is smaller. Although we take into account

the channel $\tilde{\chi}^0 \to h\nu$ in our numerical computation, from the perspective of the searches for the neutralino at the LHC using events with leptons, it is not useful since the BR of the Higgs boson to light leptons is small.

7.3 Electroweak searches at the LHC

As shown in the previous section, the production and decay of the sneutrino (and slepton) NLSP when the neutralino is the LSP can produce signals including up to six leptons plus MET. These $\mu\nu$SSM signals can be compared with searches for electroweak SUSY partners at the LHC.

The ATLAS analyses [105] and [107] use an integrated luminosity of 36.1 fb^{-1} of proton-proton (pp) collision data delivered by the LHC at a center-of-mass energy of $\sqrt{s} = 13$ TeV, to search for events with two or three leptons and four or more leptons, respectively. The former analysis targets direct chargino/neutralino and slepton production in R-parity conserving (RPC) models, whereas the latter includes the study of simplified R-parity violating (RPV) scenarios with a lepton-number violating term [58], targeting direct production of chargino/neutralino, slepton/sneutrino, and gluinos.

In the case of sleptons/sneutrinos analyzed in Ref. [107], the result puts a lower bound of 1.06 TeV on their masses assuming a single RPV channel available for the decay of the neutralino LSP. Although this assumption is allowed in simplified trilinear RPV scenarios, it is not in fact possible in the $\mu\nu$SSM where the small BRs of the leptonic decays of the gauge bosons contribute to the computation. We have checked that no constraint on the sneutrino/slepton mass is obtained from these searches in the cases studied in this work.

The ATLAS analyses also use a moderate to large amount of MET to discriminate against backgrounds, thus they are not sensitive to a compressed spectrum where this amount is not large. Production cross sections for chargino/neutralino pairs at the LHC [201, 202] are much larger than the production cross sections for slepton pairs [169]. Thus the kinematic requirement for a mass separation between sleptons and neutralinos to have enough MET, forces the sleptons in the $\mu\nu$SSM to have masses where the expected number of pairs produced at the LCH is not enough to obtain bounds.

A novel approach for the identification of events coming from the production of sparticles in compressed spectra, where the decay products carry low momenta, is the recursive jigsaw reconstruction (RJR) technique [203, 204]. This has made possible to design competitive searches for chargino-neutralino pairs even in scenarios where the mass splitting is close to the mass of the gauge bosons [199]. As we will analyze below, the same analysis can be used to put constraints on the slepton/sneutrino NLSP pair production when the neutralino is the LSP in the $\mu\nu$SSM.

The ATLAS chargino-neutralino search using RJR in Ref. [199] is based on the 13-TeV data with 36.1 fb^{-1}. All the search channels analyzed require two or three leptons originated from the decay of the gauge bosons plus MET. The different signal regions are optimized to target specific mass splittings between the produced chargino-neutralino and the neutralino LSP, for which the initial state radiation (ISR) signal regions are designed to maximize the sensitive to the case where $\Delta m = m_{\tilde{\chi}_1^\pm/\tilde{\chi}_2^0} - m_{\tilde{\chi}_1^0}$ is in the range between 100 and 160 GeV. Since the production cross section of the left sneutrino/slepton is much smaller than the chargino-neutralino one, the ISR signal regions have the largest sensitivity to the mass range where the production cross section is not negligible, and $m_{\tilde{\chi}^0} \gtrsim m_Z$.

In the ISR signal regions, the events have to fit in the "compressed decay tree" described in Ref. [199]. A signal sparticle system S decays to a set of visible momenta V and invisi-

Region	$m_{\ell\ell}$ [GeV]	m_T^W [GeV]	$\Delta\phi^{CM}_{ISR,I}$	R_{ISR}	$p_T^{CM}{}_{ISR}$ [GeV]	$p_T^{CM}{}_{I}$ [GeV]	p_T^{CM} [GeV]
SR3ℓ_ISR	$\in (75, 105)$	$>$100	$>$2.0	$\in (0.55, 1.0)$	$>$100	$>$80	$<$25
Region	m_Z [GeV]	m_J [GeV]	$\Delta\phi^{CM}_{ISR,I}$	R_{ISR}	$p_T^{CM}{}_{ISR}$ [GeV]	$p_T^{CM}{}_{I}$ [GeV]	p_T^{CM} [GeV]
SR2ℓ_ISR	$\in (80, 100)$	$\in (50, 110)$	$>$2.8	$\in (0.4, 0.75)$	$>$180	$>$100	$<$20

Table 7.1: Selection criteria for the 3ℓ_ISR and 2ℓ_ISR signal regions. The variables are defined in Refs. [199] and [203].

ble momentum I recoils from a jet-radiation system ISR. The preselection criteria require exactly three light leptons (electron or muon), and between one and three non b-tagged jets. The transverse momentum of the leptons must fulfill $p_T^{\ell_{1/2}} > 25$ and $p_T^{\ell_3} > 20$ GeV. The selection criteria applied to the events after preselection are given in Table 7.1.

At first at least one same-flavor opposite sign (SFOS) pair is required, and from the formed SFOS pairs the one with invariant mass closest to M_Z should be in the range $(75, 105)$. The remaining lepton is used to construct the W-boson transverse mass, m_T^W, as follows:

$$m_T^W = \sqrt{2p_T^\ell E_T^{miss}(1 - \cos\Delta\phi)}\,, \tag{7.4}$$

where $\Delta\phi$ is the azimuthal opening angle between the lepton associated with the W boson and the missing transverse momentum. After that, the following variables are used as discriminant:

- $p_T^{CM}{}_{ISR}$: The magnitude of the vector-summed transverse momenta of the jets assigned to the ISR system.
- $p_T^{CM}{}_{I}$: The magnitude of the vector-summed transverse momenta of the invisible system.
- p_T^{CM}: The magnitude of the vector-summed transverse momenta of the CM system.
- $R_{ISR} \equiv \vec{p}_I^{CM} \cdot \hat{p}_T^{CM}{}_S / p_T^{CM}{}_S$: Serves as an estimate of $m_{\tilde{\chi}_1^0}/m_{\tilde{\chi}_2^0/\tilde{\chi}_1^\pm}$. This corresponds to the fraction of the momentum of the system that is carried by its invisible system I, with momentum $\vec{p}_I^{CM}$ in the CM frame. As $p_T^{CM}{}_S$ grows, it becomes increasingly hard for backgrounds to possess a large value in this ratio, unlike compressed signals where this feature is exhibited [203].
- $\Delta\phi^{CM}_{ISR,I}$: The azimuthal opening angle between the ISR system and the invisible system in the CM frame.

Our analysis is implemented using the `Madanalysis v5.17` [205, 206, 207] package, and validated with simulated Monte Carlo (MC) events corresponding to the production of neutralino-chargino pairs in the context of the MSSM decaying to a neutralino LSP and leptonically decaying gauge bosons, with selected masses of $m_{\tilde{\chi}_1^\pm/\tilde{\chi}_2^0} = 200$ and $m_{\tilde{\chi}_1^0} = 100$ GeV. Ten thousand events are generated using `MadGraph5_aMC@NLO v2.6.3.2` [113] at leading order (LO) of perturbative QCD simulating the production of the described process with the standard model files for the MSSM. Events are then passed for showering and hadronization to `PYTHIA v8.201` [114] using the A14 tune [208], and then to `DELPHES v3.3.3` [144] for detector simulation. The results of the events selection are compared with the cutflow table provided by the ATLAS collaboration, as shown in Table 7.2. The first column reproduces the unweighted yields from the ATLAS analysis, the second one

Cut applied	ATLAS yield	Implemented yield	Normalized yield
Trigger matching & Preselection	1829	1398	1829
$m_{\ell\ell} \in (75, 105)$ GeV & $m_T^W > 100$ GeV	533	406	531
$\Delta\phi_{ISR,I}^{CM} > 2.0$	408	308	403
$R_{ISR} \in (0.55, 1.0)$	157	179	234
$p_T^{CM}{}_{ISR} > 100$ GeV	115	132	173
$p_T^{CM}{}_{I} > 80$ GeV	114	115	150
$p_T^{CM} < 25$ GeV	73	68	89

Table 7.2: Comparison between the ATLAS cutflow shown in the auxiliary figures of Ref. [199] and our implementation.

presents the unweighted yields from our implementation, and the last one the same yields but normalized to the number of events in the first column. As can be seen from the table, the numbers agree within a 20% error, thus we use this implementation to obtain the efficiency map of the ATLAS search for different masses of sneutrinos/sleptons and neutralinos.

The sneutrino/slepton pair production is simulated in a similar way, but with model files generated using a suitable modified version of `SARAH` code [108, 109, 110], and the spectrum is generated using `SPheno` v3.3.6 code [111, 112]. Cross sections are calculated at NLO+NLL using `Resummino v2.01` [209, 210, 211, 212, 202]. For each selected point, ten thousand MC events are generated as explained and passed through the described selection criteria. The results are then compared with the expected (S_{exp}^{95}) and observed (S_{obs}^{95}) upper limits obtained in the ATLAS search.

The processes described in Fig. 7.1 show the highest yield of the possible combinations of neutralino decays, when the mass separation between slepton/sneutrino and neutralino is not large enough to make the first produced leptons to contribute, which would be excluded from the ATLAS searches. Other possibilities, like W decaying hadronically or both neutralinos decaying to Z bosons, with only one of them decaying leptonically, contribute also to the signal, but with smaller yields. The possibility of both neutralinos decaying to Z bosons, with the latter decaying to leptons, produce a negligible contribution caused both by the small corresponding BR and the excess of predicted signal leptons.

The points analyzed in the $\mu\nu$SSM parameter space show all a worse efficiency passing the selection requirements of SR2ℓ_ISR in comparison with SR3ℓ_ISR. Thus the results discussed in the next section are derived from the limits corresponding to SR3ℓ_ISR.

7.4 Results

By using the method described in the previous section, we now calculate the current and potential limits on the two-dimensional parameter space $m_{\tilde{\nu}} - m_{\tilde{\chi}^0}$ of the $\mu\nu$SSM from the searches with the 36.1 fb^{-1} ATLAS result [199], and discuss the prospects for the 100 and 300 fb^{-1} searches.

We have assumed that the three families of left sneutrinos and sleptons are degenerated and therefore all of them contribute to the signal. Our result in the mass regions considered is that no points can be excluded from current data. It is also worth noting that the observed limit in the 3ℓ_ISR signal region (S_{obs}^{95}= 15.3) is significantly larger than the expected limit (S_{exp}^{95}= $6.9^{+3.1}_{-2.2}$), due to a 3.02 sigma excess [199]. Points of our parameter space in the region

$m_{\tilde{\chi}^0}$	120 GeV	$m_{\tilde{\nu}}$	125 GeV	$m_{\tilde{\ell}}$	145 GeV
BR($\tilde{\ell}_i \to \ell_i \tilde{\chi}^0$)	1	BR($\tilde{\nu}_i \to \nu \tilde{\chi}^0$)	1	BR($\tilde{\chi}^0 \to We/\mu$)	3.5×10^{-1}
BR($\tilde{\chi}^0 \to W\tau$)	2.9×10^{-2}	BR($\tilde{\chi}^0 \to Z\nu$)	2.4×10^{-1}	$\Gamma_{\tilde{\chi}^0}$	1.28×10^{-12} GeV
$\epsilon_{W_\ell Z_\ell}$	0.0092	$\epsilon_{W_h Z_\ell}$	0.0021	$\epsilon_{Z_\ell Z_\nu}$	0.0215
$\sigma(pp \to \tilde{\nu}\tilde{\nu})$	143.75 fb	$\sigma(pp \to \tilde{\nu}\tilde{\ell})$	276.32 fb	$\sigma(pp \to \tilde{\ell}\tilde{\ell})$	80.94 fb
Events above background in Sℓ3_ISR: 5.1					

Table 7.3: Benchmark point of the $\mu\nu$SSM in Sℓ3_ISR. In the third row the efficiency ϵ passing the selection requirements is shown.

$m_{\tilde{\chi}^0} \in (110, 120)$ and $m_{\tilde{\nu}} \in (120, 140)$ predict a number of events similar to the observed excess. As an example, Table 7.3 shows a benchmark point which predicts 5.1 events above background in Sℓ3_ISR.

If the observed local excess were due to a statistical fluctuation, and the observed upper limit converged to the expected limit, we can easily infer the potential bounds on the parameter space of the sneutrino-neutralino mass in the $\mu\nu$SSM. For 100 and 300 fb^{-1} to be reached at the end of Run 2, we just have to rescale the limits by $\sqrt{100/36.1}$ and $\sqrt{300/36.1}$, respectively. The result is shown in Fig. 7.2.

In this figure, the solid black line shows the points where the sneutrino and neutralino are degenerated in mass. The green area enclose the excluded region for 100 fb^{-1} if no excess is observed, and the yellow area shows the same for 300 fb^{-1}. The prospects show a potential exclusion of sneutrino masses up to 160 and 185 GeV for 100 and 300 fb^{-1}, respectively. We can see that this region extends up to the solid line, reflecting the fact that the search will be fully sensitive to the degenerated scenario. For a given sneutrino mass, smaller value of the neutralino mass does not give rise to a worse sensitivity until the kinematic functions in Eq. (7.2) make the product $BR(\tilde{\chi}^0 \to Z\nu) \times BR(\tilde{\chi}^0 \to W\ell)$ too small and the search becomes ineffective. On the other hand, for a given neutralino mass the larger the value of the sneutrino mass the smaller the production cross section becomes, limiting the exclusion scope. Notice also that in the lower-right corner the limits are weaker due to the mass separation between sneutrino and neutralino, as a consequence of the increased energy of the produced leptons in the decay of sleptons.

7.5 Conclusions and outlook

We have analyze a multi-lepton signal plus missing transverse energy from neutrinos expected at the LHC for a bino-like neutralino LSP, in the framework of the $\mu\nu$SSM. Assuming that the left sneutrino is the NLSP, together with left sleptons which are close in mass they decay to binos after pair production at pp collisions. Subsequently, the binos decay promptly to $W\ell$ or $Z\nu$ via RPV couplings. All in all, these signals include up to six leptons plus MET. To evaluate the prospects of this search strategy, we have recast the result of the ATLAS chargino-neutralino search using RJR, based on the 13-TeV data with 36.1 fb^{-1} [199]. This analysis is sensitive to three charged leptons of the two light families produced by a compressed spectrum of electroweak superpartners. This is also our situation, because the reduced cross section of the sneutrino/slepton production in comparison with the chargino-neutralino one, limits the sensitivity of the searches to small sneutrino/slepton masses. Although in these mass regions, no points of the parameter space of the $\mu\nu$SSM can be excluded, the prospects show a potential exclusion of sneutrino masses up to 160

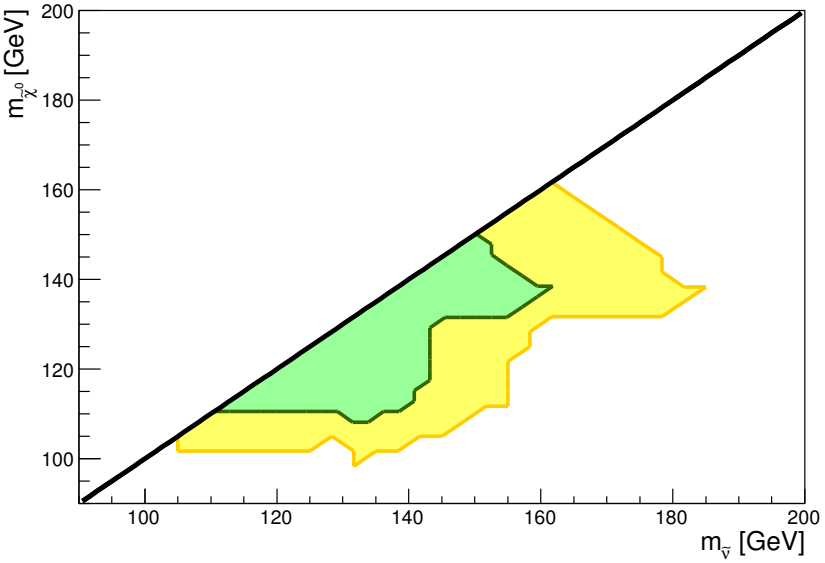

Figure 7.2: Regions of the $\mu\nu$SSM that will be probed by the signal with three leptons plus MET from neutrinos discussed in the text in the two-dimensional parameter space $m_{\tilde{\nu}} - m_{\tilde{\chi}^0}$, for the 13-TeV search with an integrated luminosity of 100 fb^{-1} (green) and 300 fb^{-1} (yellow).

and 185 GeV for 100 and 300 fb^{-1}, respectively.

These limits can be complemented in the future by searches for displaced decays of the neutralino when its mass is below the threshold of the W mass. In this case, three-body decays mediated by off-shell gauge bosons and scalars will produced a small total width due to the reduced phase space, leading to signals with lepton and/or quarks originated at displaced vertices. Dedicated studies will also be necessary to search for events with high multiplicities of leptons, when the mass separation between sneutrino and neutralino is not small. On the other hand, in this work, we have focused on the bino-like LSP. Another interesting possibility would be to study the case of a wino-like LSP. The different couplings involved as well as new RPV decays could modify the sensitivity of the searches to the new compressed spectrum. We plan to cover this possibility in a forthcoming publication [213].

Let us finally mention a by-product of our analysis in the region of bino (sneutrino) mass $110 - 120$ $(120 - 140)$ GeV, where we find that a tri-lepton signal is compatible with the local excess reported by ATLAS.

Chapter 8

Conclusiones

El último capítulo está dedicado a resumir los principales resultados de la tesis. En la que hemos analizado la fenomenología del sector electrodébil del $\mu\nu$SSM relevante para las búsquedas en aceleradores.

En primer lugar hemos estudiado la fenomenología del left sneutrino cuando este es la partícula supersimétrica más ligera. Hemos analizado las regiones del espacio de parámetros donde puede ser la LSP, con la conclusión de que un valor absoluto pequeño para el acoplo *soft* trilineal del neutrino es suficiente para que la masa física del sneurtrino left sea del orden d 100 GeV, y que además ha de ser negativa para evitar que el sneutrino sea taquiónico. Hemos visto también que que la diferencia de masas entre los sneutrinos reales e imaginarios es despreciable, por lo tanto podemos considerarlos co-LSP. Hemos observado también que la masa de los sleptones es ligeramente mayor que la de los sneutrinos correspondientes, siendo esta diferencia originada por la contribución de un término D. Hemos estudiado los canales de producción en el LHC, encontrando que el más importante para la producción en pares es mediado por un bosón Z en en canal-s. Mientras que la producción de pares slepton-sneutrino y slepton-slepton es también una buena fuente de La producción de pares slepton-sneutrino y de sleptones está mediada por un W o un Z/*gamma* en el canal-s respectivamente. Hemos estudiado a su vez los posibles canales de desintegración del left sneutrino y la diferencia entre las partículas escalares y pseudoescalares, así como la diferencia entre partículas de la primera y segundo familia con respecto de la tercera. Hemos encontrado que la mezcla realzada debido a la cercanía en masas del sneutrino y el bosón de Higgs provoca que el left sneutrino escalar decaiga imitando el patrón de desintegración del bosón de Higgs. Hemos observado que cuando la masa del left sneutrino es más pequeña, la desintegración está dominada por los canales a neutrinos en el caso de las dos primeras familias con el añadido del canal a dos leptones en el caso de la tercera familia. En el caso de los sneutrinos pseudoescalares hemos encontrado que la desintegración está, a todas las masas, dominada por el canal a neutrinos para las dos primeras familias con el añadido del canal a leptones para la tercera. Hemos obtenido el resultado de que la longitud propia de desintegración es del orden del milímetro cuando la masa del sneutrino no es muy próxima a la masa del bosón de Higgs, pero que está por debajo de la escala de los milímetros para la tercera familia si la masa está por encima de los 95 GeV.

Estos resultados nos permiten identificar los escenarios más prometedores desde el punto de vista de las búsquedas de señales puntuales en el LHC. Dados los distintos comportamientos de las partículas escalares y pseudoescalares, es posible producir un señal que incluya dos fotones más momento transverso perdido, o una señal con dos fotones y dos leptones. La primera puede ser detectada con una energía en el centro de masas de 13 TeV y una luminosidad integrada de 100fb$^-$1, para un sneutrino de cualquier familia en el rango

118-132 GeV. Y la señal de dos fotones y dos leptones puede ser estudiada para el caso del tau sneutrino en un rango de masas de 95-145 GeV. Adicionalmente, es posible producir una señal con cuatro leptones originada del tau sneutrino, detectable en el LHC con una energía en el centro de masas de 13 TeV, incluso con una luminosidad de 20 fb^{-1}. Dicha señal podría ser detectada en el rango de masas de 130-310 GeV. Existen búsquedas en el LHC que buscan genéricamente por multi-leptones que están cerca de ser sensibles a este escenario, y que con más luminosidad podrían poner límites a la masa del sneurtrino.

La predicción de vértices desplazados del orden de milímetros hace posible aplicar las búsquedas del LHC de leptones producidos en vértices secundarios al sneutrino en el $\mu\nu$SSM. Hemos analizado la sensibilidad de estas búsquedas a un left sneutrino de la tercera familia en el rango de masas de 45-100 GeV en el contexto del $\mu\nu$SSM.Hemos observado que el canal de búsqueda usando pares de leptones es el más sensible al sneutrino LSP, que puede ser observado cuando éste es producido en pares y decae en $\tau\tau$ o $\tau\ell$. hemos adaptado las búsquedas de ATLAS a nuestro escenario y hemos obtenido limites al espacio de parámetros. También hemos discutido una optimización de los *triggers* de la búsqueda que podría mejorar en gran medida los límites, aumentando el área del espacio de parámetros que podría ser explorada.

Finalmente hemos analizado una señal de multi-leptones con momento transverso perdido proveniente de neutrinos esperada en el LHC para un neutralino tipo bino cuando es el LSP, en el contexto del $\mu\nu$SSM. Asumiendo que el sneutrino left es el NLSP, además de los sleptones con una pequeña separación en masa, donde ambos decaen a un par de binos tras ser producidos en colisiones de protones. Hemos adaptado las búsquedas de ATLAS de pares chargino-neutralino en espectros comprimidos usando *Recursive jigsaw reconstruction*, para encontrar límites a este escenario. Con el resultado de que no es posible excluir ningún punto del espacio de parámetros con los datos actuales. Sin embargo, calculamos el potencial de exclusión re-escalando los límites, obteniendo una cota de 160 GeV y de 185 GeV para 100fb^{-1} y 300fb^{-1} de luminosidad integrada respectivamente. Como resultado adicional del análisis, encontramos en la región de masas del neutralino (sneutrino) 1120-120 (120-140) GeV una señal incluyendo 3 leptones compatible con el exceso local reportado por ATLAS.

Los análisis llevados a cabo en al presente tesis abren al puerta a otros trabajos en el futuro. Una extensión del estudio presentado en la tesis sobre el left sneutrino como LSP, incluyendo tres generaciones de neutrinos right-handed, y correlacionando las señales con los valores de los ángulos de mezcla de los neutrinos merece la pena ser realizado.

La adaptación de los análisis de ATLAS y CMS de partículas con vidas medias largas ha demostrado ser muy útil para explorar el espacio de parámetros del $\mu\nu$SSM. Por lo tanto búsquedas similares de otras partículas supersimétricas como LSP, que esperamos que tengan vidas medias largas, constituyen un siguiente paso interesante en el análisis de la fenomenología. Ejemplos de ello son los stops, los gluinos o los sleptones right. Es importante resaltar que el tamaño de la longitud media de desintegración del LSP en el $\mu\nu$SSM está directamente relacionado con el tamaño de la masa de los neutrinos. Por lo tanto la predicción de vértices desplazados de la escala del milímetro es una predicción natural del modelo, si necesidad de incluir escalas ad-hoc o parámetros anormalemente pequeños.

Los planes para construir un colisionadores de electrones-positrones con energías de 500 GeV motiva también le diseño de estrategias de búsqueda para partículas cuya masa no haya sido ya limitada por el LHC a estar por encima del alcance energético de dichos aceleradores. Este es el caso de las partículas electrodebiles e el $\mu\nu$SSM. En este sentido merece la pena llevar a cabo estudios específicos de la fenomenología del $\mu\nu$SSM con más

posibilidad de ser vista dichos aceleradores.

Conclusions

This last chapter is devoted to summarize the main results of the thesis, where we have analyzed the phenomenology of the electroweak sector of the $\mu\nu$SSM, relevant for collider searches.

As explained in the text, the $\mu\nu$SSM is a well-motivated model of supersymmetry (SUSY) which addresses the solution to the μ problem of SUSY models simultaneously with one of the most intriguing questions yet to solve in particle physics, the origin of neutrino masses. In particular, the origin of the smallness of neutrino masses in the $\mu\nu$SSM is directly related with the decay amplitude of the lightest particle of the SUSY spectrum. Thus, where most of beyond standard models propose ad-hoc scales for the energy and lifetime of the particles, in the $\mu\nu$SSM these values are directly related with neutrino physics. The predictions of the model are in this sense robust and point to a coherent search strategy.

At first we have focused on the study of the left sneutrino phenomenology when it is the lightest supersymmetric particle (LSP). We have analyzed if there are natural regions of the parameter space where it can become the LSP, finding in our framework that it is sufficient to tune the neutrino trilinear soft coupling A_ν. We have also obtained that scalar and pseudoscalar left sneutrinos are basically degenerated in mass, and therefore both can be considered co-LSPs. In addition, the mass of the left slepton, which is in the same $SU(2)$ doublet as the left sneutrino, is only slightly larger than the one of the latter due to the small D-term contribution. As a consequence, the sleptons are also relevant for our analysis of production and decay of electroweak superpartners. In this sense, we have analyzed in detail the production channels at the LHC. The most important diagram for sneutrino pair production is mediated by an off-shell Z boson in the s-channel, while the production of sneutrino-slepton and sleptons pairs is as well a good source of sneutrino pairs, given the small mass gap between them. These two last possibilities are mediated by off-shell W and Z,γ bosons in the s-channel, respectively.

Then, we have studied the possible decay channels of the left sneutrinos and the differences for scalar and pseudoscalar states, as well as the differences between the first two families and the third one. We have found that the enhanced mixing between the scalar sneutrino and the SM Higgs boson makes the sneutrino decay mimicking the decays of the latter. We have also found that for smaller masses the sneutrino decays dominantly to neutrinos in the case of the first two families, and also to lepton pairs in the case of the third one. For the pseudoscalar sneutrinos we have found that for all masses it decays dominantly to neutrinos for the first two families and also to lepton pairs for the third one. We have found also that the proper decay length of the left sneutrino is in the mm scale for for masses not close to the Higgs boson mass for the two first families, but is below the mm scale for the third family if the mass is above 95 GeV.

This results allow us to identify the most promising prompt signals expected from the production of sneutrino pairs at the LHC. Given the different behaviors of scalar and

pseudoscalar sneutrino states, a diphoton signal in combination with neutrinos (producing missing transverse energy), or a diphoton with leptons, can appear at the LHC. The former can be detected with a centre-of-mass energy of 13 TeV and the integrated luminosity of 100 fb^{-1}, for a sneutrino LSP of any family in the mass range 118–132 GeV. The diphoton plus leptons signal can be probed for the case of a tau sneutrino LSP with a mass in the range 95–145 GeV. In addition a multilepton signal from a tau sneutrino LSP can also appear detectable at the LHC with a centre-of-mass energy of 13 TeV, even with the integrated luminosity of 20 fb^{-1}. It is possible to detect it in the mass range of 130–310 GeV. We have discussed that existing generic searches at the LHC are close to be sensitive to this lepton signal, suggesting that they deserve experimental attention. An updated analysis with current data could constrain the sneutrino LSP scenario.

The prediction of displaced vertices of the order of the millimeter makes possible to apply LHC searches for lepton pairs produced at secondary vertices. We have analyzed the sensitivity of these searches to a tau left sneutrino LSP with a mass in the range 45–100 GeV in the framework of the $\mu\nu$SSM. We have found that the displaced dilepton search channel is most sensitive to the sneutrino LSP, where at least one of the pair-produced left sneutrinos is required to decay into $\tau\tau$ or $\tau\ell$ with the final-state tau leptons decaying leptonically. We recast the ATLAS 8-TeV dilepton search to obtain potential limit on the parameter space finding constraints to on the left sneutrino LSP. We have also discussed an optimization of the trigger requirements exploited in the ATLAS search that can considerably improve the sensitivity of the displaced dilepton search, finding that with this optimizations a wide range of of the $\mu\nu$SSM parameter space can be probed at the LHC Run 3.

Finally, we have analyzed a multi-lepton signal plus missing transverse energy from neutrinos expected at the LHC for a bino-like neutralino LSP, in the framework of the $\mu\nu$SSM. Assuming that the left sneutrino is the NLSP, together with left sleptons which are close in mass they decay to binos after pair production at pp collisions. We have recasted the ATLAS search for chargino-neutralino pairs in compressed scenarios using *Recursive jigsaw reconstruction*, to evaluate the limits on this scenario. We have found that in the mass region relevant for the search no points of the parameters space of the $\mu\nu$SSM can be excluded, however we show a potential exclusion of sneutrino masses up to 160 and 185 GeV for 100 and 300 fb^{-1}, respectively.As a by-product of our analysis in the region of bino (sneutrino) mass $110 - 120$ $(120 - 140)$ GeV, we find that a tri-lepton signal is compatible with the local excess reported by ATLAS.

The analysis made in the present thesis open the door for many other interesting works in the future. An extension of the study presented in the thesis on left sneutrino LSP, including three generations of right handed neutrino superfields and correlating the signals with the values of neutrino mixing angles deserves to be studied.

The recasting of ATLAS and CMS searches for long-lived particles has proven to be a very useful tool to probe the $\mu\nu$SSM. Thus similar searches for other SUSY particles as LSPs, that are potentially long lived, constitute a interesting next step on the analysis of the $\mu\nu$SSM phenomenology. Such as the stops, gluinos or right sleptons. Notice that the size of the decay length of the LSP i the $\mu\nu$SSM is directly related to the size of neutrino masses. Thus the prediction of displaced vertices on the mm scale is a natural prediction of the model without the inclusion of ad-hoc scales or abnormally small parameters.

The plans to build a electron-positron collider with energies of 500 GeV motivate also the design of search strategies for particles which mass bounds are not pushed by the LHC above the energy limit. That will be the case of the electroweak particles of the $\mu\nu$SSM. In this sense worth making specific studies of the sensitivity prospects of electron-positron colliders for the $\mu\nu$SSM.

Acknowledgments

This work was supported by a FPI MINECO – Severo Ochoa predoctoral grant. The author also thanks the Spanish Agencia Estatal de Investigación by partial support through the grants FPA2012-34694 and FPA2015-65929-P (MINECO/FEDER, UE), IFT Centro de Excelencia Severo Ochoa SEV-2012-0249 and SEV-2016-0597, Consolider-Ingenio 2010 Programme MultiDark CSD2009-00064 and Red Consolider MultiDark FPA2017-90566-REDC.

Appendix A

Mass Matrices

We write below the tree-level mass matrices generated in the $\mu\nu$SSM. Upon EWSB, fields with the same color, electric charge and spin mix. To name them we follow the convention of using for the eigenstates the names of detected particles: Higgs, neutrinos, leptons. In what follows we use i, j, k, l, m, n as family indexes, and a, b as the indices for the physical states (mass eigenstates), not to be confused with $a, b = 1, 2$ used in Appendix **??** as $SU(2)_L$ index. We include in the formulas for completeness the contribution due to lepton-number violating couplings λ_{ijk} and λ'_{ijk} in the superpotential of Eq. (3.2) and soft Lagrangian of Eq. (3.4).

A.1 Scalar Mass Matrices

The scalar mass matrices generated in the $\mu\nu$SSM were computed in Appendix A.1 of Ref. [63] with the assumption of CP conservation for simplicity. In this Appendix, we write those equations and replace the values of the soft masses obtained through the minimization conditions in Eqs. (3.17)-(3.20), assuming that slepton soft mass matrices are diagonal in flavor space.

Mass Matrix for Higgses

Higgses mix with left and right sneutrinos. In the basis $S^T = (H_d^{\mathcal{R}}, H_u^{\mathcal{R}}, \tilde{\nu}_{iR}^{\mathcal{R}}, \tilde{\nu}_{jL}^{\mathcal{R}})$, one obtains the following mass terms for scalar Higgses in the Lagrangian:

$$-\frac{1}{2} S^T m_h^2 S\,, \tag{A.1}$$

where m_h^2 is the 8×8 (symmetric) matrix obtained computing the second derivative of the scalar potential of Eq. (3.8) with respect to the fields

$$m_h^2 = \begin{pmatrix} m^2_{H_d^{\mathcal{R}} H_d^{\mathcal{R}}} & m^2_{H_d^{\mathcal{R}} H_u^{\mathcal{R}}} & m^2_{H_d^{\mathcal{R}} \tilde{\nu}_{jR}^{\mathcal{R}}} & m^2_{H_d^{\mathcal{R}} \tilde{\nu}_{jL}^{\mathcal{R}}} \\ m^2_{H_u^{\mathcal{R}} H_d^{\mathcal{R}}} & m^2_{H_u^{\mathcal{R}} H_u^{\mathcal{R}}} & m^2_{H_u^{\mathcal{R}} \tilde{\nu}_{jR}^{\mathcal{R}}} & m^2_{H_u^{\mathcal{R}} \tilde{\nu}_{jL}^{\mathcal{R}}} \\ m_{\tilde{\nu}_{iR}^{\mathcal{R}} H_d^{\mathcal{R}}} & m_{\tilde{\nu}_{iR}^{\mathcal{R}} H_u^{\mathcal{R}}} & m^2_{\tilde{\nu}_{iR}^{\mathcal{R}} \tilde{\nu}_{jR}^{\mathcal{R}}} & m^2_{\tilde{\nu}_{iR}^{\mathcal{R}} \tilde{\nu}_{jL}^{\mathcal{R}}} \\ m^2_{\tilde{\nu}_{iL}^{\mathcal{R}} H_d^{\mathcal{R}}} & m^2_{\tilde{\nu}_{iL}^{\mathcal{R}} H_u^{\mathcal{R}}} & m^2_{\tilde{\nu}_{iL}^{\mathcal{R}} \tilde{\nu}_{jR}^{\mathcal{R}}} & m^2_{\tilde{\nu}_{iL}^{\mathcal{R}} \tilde{\nu}_{jL}^{\mathcal{R}}} \end{pmatrix}\,, \tag{A.2}$$

$$\begin{aligned} m^2_{H_d^{\mathcal{R}} H_d^{\mathcal{R}}} &= m^2_{H_d} + \frac{1}{8}(g^2+g'^2)(3v_d^2 - v_u^2 + v_{iL}v_{iL}) + \frac{1}{2}\lambda_i\lambda_j v_{iR}v_{jR} + \frac{1}{2}\lambda_i\lambda_i v_u^2 \\ &= \frac{1}{4}(g^2+g'^2)v_d^2 + v_{iR}\tan\beta\left(\frac{1}{\sqrt{2}}T_i^{\lambda} + \frac{1}{2}\lambda_j\kappa_{ijk}v_{kR}\right) + Y^{\nu}_{ij}\frac{v_{iL}}{2v_d}\left(\lambda_k v_{jR}v_{kR} + \lambda_j v_u^2\right)\,, \end{aligned} \tag{A.3}$$

$$
\begin{aligned}
m^2_{H_u^{\mathcal{R}} H_u^{\mathcal{R}}} &= m^2_{H_u} + \frac{1}{8}(g^2+g'^2)(-v_d^2+3v_u^2-v_{iL}v_{iL}) + \frac{1}{2}\lambda_i\lambda_j v_{iR}v_{jR} + \frac{1}{2}\lambda_i\lambda_i v_d^2 \\
&\quad -Y^\nu_{ij}\lambda_j v_d v_{iL} + \frac{1}{2}Y^\nu_{ik}Y^\nu_{ij}v_{jR}v_{kR} + \frac{1}{2}Y^\nu_{ik}Y^\nu_{jk}v_{iL}v_{jL} \\
&= \frac{1}{4}(g^2+g'^2)v_u^2 + v_{iR}\frac{1}{\tan\beta}\left(\frac{1}{\sqrt{2}}T^\lambda_i + \frac{1}{2}\lambda_j\kappa_{ijk}v_{kR}\right) \\
&\quad -\frac{v_{iL}}{v_u}\left(\frac{1}{\sqrt{2}}T^\nu_{ij}v_{jR} + \frac{1}{2}Y^\nu_{ij}\kappa_{ljk}v_{lR}v_{kR}\right) \,, \qquad \text{(A.4)}
\end{aligned}
$$

$$
m^2_{H_u^{\mathcal{R}} H_d^{\mathcal{R}}} = -\frac{1}{4}(g^2+g'^2)v_d v_u - \frac{1}{\sqrt{2}}T^\lambda_i v_{iR} - \frac{1}{2}\lambda_k\kappa_{ijk}v_{iR}v_{jR} + v_d v_u\lambda_i\lambda_i - Y^\nu_{ij}\lambda_j v_u v_{iL} \,, \qquad \text{(A.5)}
$$

$$
m^2_{\widetilde{\nu}_{iR}^{\mathcal{R}} H_d^{\mathcal{R}}} = -\frac{1}{\sqrt{2}}T^\lambda_i v_u - \lambda_k\kappa_{ijk}v_u v_{jR} + \lambda_i\lambda_j v_d v_{jR} - \frac{1}{2}Y^\nu_{ji}\lambda_k v_{jL}v_{kR} - \frac{1}{2}Y^\nu_{jk}\lambda_i v_{jL}v_{kR} \,, \qquad \text{(A.6)}
$$

$$
m^2_{\widetilde{\nu}_{iR}^{\mathcal{R}} H_u^{\mathcal{R}}} = -\frac{1}{\sqrt{2}}T^\lambda_i v_d + \frac{1}{\sqrt{2}}T^\nu_{ji}v_{jL} - \lambda_k\kappa_{ilk}v_d v_{lR} + \lambda_i\lambda_j v_u v_{jR} + Y^\nu_{jk}\kappa_{ilk}v_{jL}v_{lR} + Y^\nu_{jk}Y^\nu_{ji}v_u v_{kR} \,, \qquad \text{(A.7)}
$$

$$
\begin{aligned}
m^2_{\widetilde{\nu}_{iR}^{\mathcal{R}}\widetilde{\nu}_{jR}^{\mathcal{R}}} &= \left(m^2_{\widetilde{\nu}_R}\right)_{ij} + \sqrt{2}T^\kappa_{ijk}v_{kR} - \lambda_k\kappa_{ijk}v_d v_u + \kappa_{ijk}\kappa_{lmk}v_{lR}v_{mR} + 2\kappa_{ilk}\kappa_{jmk}v_{lR}v_{mR} \\
&\quad +\frac{1}{2}\lambda_i\lambda_j(v_d^2+v_u^2) + Y^\nu_{lk}\kappa_{ijk}v_u v_{lL} - \frac{1}{2}(Y^\nu_{kj}\lambda_i + Y^\nu_{ki}\lambda_j)v_d v_{kL} + \frac{1}{2}Y^\nu_{ki}Y^\nu_{kj}v_u^2 + \frac{1}{2}Y^\nu_{ki}Y^\nu_{lj}v_{kL}v_{lL} \\
&= \sqrt{2}T^\kappa_{ijk}v_{kR} - \lambda_k\kappa_{ijk}v_d v_u + \kappa_{ijk}\kappa_{lmk}v_{lR}v_{mR} + 2\kappa_{ilk}\kappa_{jmk}v_{lR}v_{mR} + \frac{1}{2}\lambda_i\lambda_j(v_d^2+v_u^2) \\
&\quad -Y^\nu_{lk}\kappa_{ijk}v_u v_{lL} - \frac{1}{2}\left(Y^\nu_{kj}\lambda_i + Y^\nu_{ki}\lambda_j\right)v_d v_{kL} + \frac{1}{2}Y^\nu_{ki}Y^\nu_{kj}v_u^2 + \frac{1}{2}Y^\nu_{li}Y^\nu_{kj}v_{kL}v_{lL} \\
&\quad +\frac{\delta_{ij}}{v_{jR}}\left[-\frac{1}{\sqrt{2}}T^\nu_{ki}v_{kL}v_u + \frac{1}{\sqrt{2}}T^\lambda_i v_u v_d - \frac{1}{\sqrt{2}}T^\kappa_{ilk}v_{lR}v_{kR} + \lambda_l\kappa_{ilk}v_d v_u v_{kR}\right. \\
&\quad -\kappa_{lim}\kappa_{lnk}v_{mR}v_{nR}v_{kR} - \frac{1}{2}\lambda_i\lambda_l(v_d^2+v_u^2)v_{lR} - Y^\nu_{lk}\kappa_{ikm}v_u v_{lL}v_{mR} \\
&\quad \left.+\frac{1}{2}\left(Y^\nu_{kl}\lambda_i + Y^\nu_{ki}\lambda_l\right)v_d v_{kL}v_{lR} - \frac{1}{2}Y^\nu_{ki}Y^\nu_{kl}v_u^2 v_{lR} - \frac{1}{2}Y^\nu_{ki}Y^\nu_{lm}v_{kL}v_{lL}v_{mR}\right] \,, \qquad \text{(A.8)}
\end{aligned}
$$

$$
m^2_{\widetilde{\nu}_{iL}^{\mathcal{R}} H_d^{\mathcal{R}}} = \frac{1}{4}(g^2+g'^2)v_d v_{iL} - \frac{1}{2}Y^\nu_{ij}\lambda_j v_u^2 - \frac{1}{2}Y^\nu_{ij}\lambda_k v_{kR}v_{jR} \,, \qquad \text{(A.9)}
$$

$$
m^2_{\widetilde{\nu}_{iL}^{\mathcal{R}} H_u^{\mathcal{R}}} = -\frac{1}{4}(g^2+g'^2)v_u v_{iL} + \frac{1}{\sqrt{2}}T^\nu_{ij}v_{jR} + \frac{1}{2}Y^\nu_{ik}\kappa_{ljk}v_{lR}v_{jR} - Y^\nu_{ij}\lambda_j v_d v_u + Y^\nu_{ij}Y^\nu_{kj}v_u v_{kL} \,, \qquad \text{(A.10)}
$$

$$
\begin{aligned}
m^2_{\widetilde{\nu}_{iL}^{\mathcal{R}}\widetilde{\nu}_{jR}^{\mathcal{R}}} &= \frac{1}{\sqrt{2}}T^\nu_{ij}v_u - \frac{1}{2}Y^\nu_{ij}\lambda_k v_d v_{kR} - \frac{1}{2}Y^\nu_{ik}\lambda_j v_d v_{kR} + Y^\nu_{ik}\kappa_{jlk}v_u v_{lR} + \frac{1}{2}Y^\nu_{ij}Y_{\nu_{kl}}v_{kL}v_{lR} \\
&\quad +\frac{1}{2}Y^\nu_{il}Y^\nu_{kj}v_{kL}v_{lR} \,, \qquad \text{(A.11)}
\end{aligned}
$$

$$
\begin{aligned}
m^2_{\widetilde{\nu}_{iL}^{\mathcal{R}}\widetilde{\nu}_{jL}^{\mathcal{R}}} &= \left(m^2_{\widetilde{L}_L}\right)_{ij} + \frac{1}{4}(g^2+g'^2)v_{iL}v_{jL} + \frac{1}{8}(g^2+g'^2)(v_{kL}v_{kL} + v_d^2 - v_u^2)\delta_{ij} \\
&\quad +\frac{1}{2}Y^\nu_{ik}Y^\nu_{jk}v_u^2 + \frac{1}{2}Y^\nu_{ik}Y^\nu_{jl}v_{kR}v_{lR} \\
&= \frac{1}{4}(g^2+g'^2)v_{iL}v_{jL} + \frac{1}{2}Y^\nu_{ik}Y^\nu_{jk}v_u^2 + \frac{1}{2}Y^\nu_{ik}Y^\nu_{jl}v_{kR}v_{lR} + \frac{\delta_{ij}}{v_{jL}}\left[-\frac{1}{\sqrt{2}}T^\nu_{ik}v_u v_{kR}\right. \\
&\quad \left.+\frac{1}{2}Y^\nu_{ik}\left(\lambda_l v_d v_{kR}v_{lR} + \lambda_k v_d v_u^2 - \kappa_{klm}v_u v_{lR}v_{mR} - Y^\nu_{mk}v_{mL}v_u^2 - Y^\nu_{ml}v_{mL}v_{lR}v_{kR}\right)\right] \,. \qquad \text{(A.12)}
\end{aligned}
$$

This matrix is diagonalized by an orthogonal matrix Z^H:

$$
Z^H m_h^2 \; {Z^H}^T = \left(m_h^2\right)^{\text{dia}} \,, \qquad \text{(A.13)}
$$

with

$$
S = {Z^H}^T h \,, \qquad \text{(A.14)}
$$

where the 8 entries of the matrix h are the 'Higgs' mass eigenstate fields. In particular,

$$H_d^{\mathcal{R}} = Z_{b1}^H h_b\,, \quad H_u^{\mathcal{R}} = Z_{b2}^H h_b\,, \quad \tilde{\nu}_{iR}^{\mathcal{R}} = Z_{bi}^H h_b\,, \quad \tilde{\nu}_{jL}^{\mathcal{R}} = Z_{bj}^H h_b\,. \tag{A.15}$$

In the case of considering only one family of right-handed neutrinos as we do in Appendix B, the last two equalities can be written as

$$\tilde{\nu}_R^{\mathcal{R}} = Z_{b3}^H h_b\,, \quad \tilde{\nu}_{3+iL}^{\mathcal{R}} = Z_{b3+i}^H h_b\,. \tag{A.16}$$

Mass Matrix for Pseudoscalar Higgses

Following similar arguments as above, in the basis $P^T = (H_d^{\mathcal{I}}, H_u^{\mathcal{I}}, \tilde{\nu}_{iR}^{\mathcal{I}}, \tilde{\nu}_{jL}^{\mathcal{I}})$, one obtains the following mass terms for pseudoscalar Higgses in the Lagrangian:

$$-\frac{1}{2} P^T m_{A^0}^2 P\,, \tag{A.17}$$

where $m_{A^0}^2$ is the 8×8 (symmetric) matrix

$$m_{A^0}^2 = \begin{pmatrix} m^2_{H_d^{\mathcal{I}} H_d^{\mathcal{I}}} & m^2_{H_d^{\mathcal{I}} H_u^{\mathcal{I}}} & m^2_{H_d^{\mathcal{I}} \tilde{\nu}_{jR}^{\mathcal{I}}} & m^2_{H_d^{\mathcal{I}} \tilde{\nu}_{jL}^{\mathcal{I}}} \\ m^2_{H_u^{\mathcal{I}} H_d^{\mathcal{I}}} & m^2_{H_u^{\mathcal{I}} H_u^{\mathcal{I}}} & m^2_{H_u^{\mathcal{I}} \tilde{\nu}_{jR}^{\mathcal{I}}} & m^2_{H_u^{\mathcal{I}} \tilde{\nu}_{jL}^{\mathcal{I}}} \\ m_{\tilde{\nu}_{iR}^{\mathcal{I}} H_d^{\mathcal{I}}} & m_{\tilde{\nu}_{iR}^{\mathcal{I}} H_u^{\mathcal{I}}} & m^2_{\tilde{\nu}_{iR}^{\mathcal{I}} \tilde{\nu}_{jR}^{\mathcal{I}}} & m^2_{\tilde{\nu}_{iR}^{\mathcal{I}} \tilde{\nu}_{jL}^{\mathcal{I}}} \\ m^2_{\tilde{\nu}_{iL}^{\mathcal{I}} H_d^{\mathcal{I}}} & m^2_{\tilde{\nu}_{iL}^{\mathcal{I}} H_u^{\mathcal{I}}} & m^2_{\tilde{\nu}_{iL}^{\mathcal{I}} \tilde{\nu}_{jR}^{\mathcal{I}}} & m^2_{\tilde{\nu}_{iL}^{\mathcal{I}} \tilde{\nu}_{jL}^{\mathcal{I}}} \end{pmatrix}\,, \tag{A.18}$$

$$m^2_{H_d^{\mathcal{I}} H_d^{\mathcal{I}}} = m^2_{H_d^{\mathcal{R}} H_d^{\mathcal{R}}} - \frac{1}{4}(g^2+g'^2)v_d^2 \tag{A.19}$$

$$m^2_{H_u^{\mathcal{I}} H_u^{\mathcal{I}}} = m^2_{H_u^{\mathcal{R}} H_u^{\mathcal{R}}} - \frac{1}{4}(g^2+g'^2)v_u^2\,, \tag{A.20}$$

$$m^2_{H_u^{\mathcal{I}} H_d^{\mathcal{I}}} = \frac{1}{\sqrt{2}} T_i^{\lambda} v_{iR} + \frac{1}{2}\lambda_k \kappa_{ijk} v_{iR} v_{jR}\,, \tag{A.21}$$

$$m^2_{\tilde{\nu}_{iR}^{\mathcal{I}} H_d^{\mathcal{I}}} = \frac{1}{\sqrt{2}} T_i^{\lambda} v_u - \lambda_k \kappa_{ijk} v_u v_{jR} - \frac{1}{2} Y^{\nu}_{ji} \lambda_k v_{jL} v_{kR} + \frac{1}{2} Y^{\nu}_{jk} \lambda_i v_{jL} v_{kR}\,, \tag{A.22}$$

$$m^2_{\tilde{\nu}_{iR}^{\mathcal{I}} H_u^{\mathcal{I}}} = \frac{1}{\sqrt{2}} T_i^{\lambda} v_d - \frac{1}{\sqrt{2}} T^{\nu}_{ji} v_{jR} - \lambda_k \kappa_{ilk} v_d v_{lR} + Y^{\nu}_{jk} \kappa_{ilk} v_{jL} v_{lR}\,, \tag{A.23}$$

$$m^2_{\tilde{\nu}_{iR}^{\mathcal{I}} \tilde{\nu}_{jR}^{\mathcal{I}}} = m^2_{\tilde{\nu}_{iR}^{\mathcal{R}} \tilde{\nu}_{jR}^{\mathcal{R}}} - 2\left(\sqrt{2} T^{\kappa}_{ijk} v_{kR} - \lambda_k \kappa_{ijk} v_d v_u + \kappa_{ijk}\kappa_{lmk} v_{lR} v_{mR}\right)\,, \tag{A.24}$$

$$m^2_{\tilde{\nu}_{iL}^{\mathcal{I}} H_d^{\mathcal{I}}} = -\frac{1}{2} Y^{\nu}_{ij} \lambda_j v_u^2 - \frac{1}{2} Y^{\nu}_{ij} \lambda_k v_{kR} v_{jR}\,, \tag{A.25}$$

$$m^2_{\tilde{\nu}_{iL}^{\mathcal{I}} H_u^{\mathcal{I}}} = -\frac{1}{\sqrt{2}} T^{\nu}_{ij} v_{jR} - \frac{1}{2} Y^{\nu}_{ik} \kappa_{ljk} v_{lR} v_{jR}\,, \tag{A.26}$$

$$\begin{aligned} m^2_{\tilde{\nu}_{iL}^{\mathcal{I}} \tilde{\nu}_{jR}^{\mathcal{I}}} = & -\frac{1}{\sqrt{2}} T^{\nu}_{ij} v_u + \frac{1}{2} Y^{\nu}_{ij} \lambda_k v_d v_{kR} - \frac{1}{2} Y^{\nu}_{ik} \lambda_j v_d v_{kR} + Y^{\nu}_{il} \kappa_{jlk} v_u v_{kR} \\ & - \frac{1}{2} Y^{\nu}_{ij} Y^{\nu}_{lk} v_{lL} v_{kR} + \frac{1}{2} Y^{\nu}_{ik} Y^{\nu}_{lj} v_{lL} v_{kR}\,, \end{aligned} \tag{A.27}$$

$$m^2_{\tilde{\nu}_{iL}^{\mathcal{I}} \tilde{\nu}_{jL}^{\mathcal{I}}} = m^2_{\tilde{\nu}_{iL}^{\mathcal{R}} \tilde{\nu}_{jL}^{\mathcal{R}}} - \frac{1}{4}(g^2+g'^2) v_{iL} v_{jL}\,, \tag{A.28}$$

and, in order to simplify some of these formulas, the entries of the mass matrix for Higgses

are used when appropriate. The matrix of Eq. (A.18) is diagonalized by an orthogonal matrix Z^A:

$$Z^A m^2_{A^0} \; {Z^A}^T = \left(m^2_{A^0}\right)^{\rm dia} \;\; , \tag{A.29}$$

with

$$P = {Z^A}^T A^0 \, , \tag{A.30}$$

where the 8 entries of the matrix A^0 are the 'pseudoscalar Higgs' mass eigenstate fields. In particular,

$$H_d^{\mathcal{I}} = Z^A_{b1} h_b \, , \quad H_u^{\mathcal{I}} = Z^A_{b2} h_b \, , \quad \tilde{\nu}^{\mathcal{I}}_{iR} = Z^A_{bi} h_b \, , \quad \tilde{\nu}^{\mathcal{I}}_{jL} = Z^A_{bj} h_b \, . \tag{A.31}$$

In the case of considering only one family of right-handed neutrinos as we do in Appendix B, the last two equalities can be written as

$$\tilde{\nu}^{\mathcal{I}}_{R} = Z^A_{b3} h_b \, , \quad \tilde{\nu}^{\mathcal{I}}_{3+iL} = Z^A_{b3+i} h_b \, . \tag{A.32}$$

Mass Matrix for Charged Higgses

Charged Higgses mix with left and right sleptons. In the basis $C^T = (H_d^{-\,*}, H_u^+, \widetilde{e}^*_{iL}, \widetilde{e}^*_{jR})$, one obtains the following mass terms in the Lagrangian:

$$- C^{*T} m^2_{H^+} C \, , \tag{A.33}$$

where $m^2_{H^+}$ is the 8×8 (symmetric) matrix

$$m^2_{H^+} = \begin{pmatrix} m^2_{H_d^- H_d^{-\,*}} & m^2_{H_d^- H_u^+} & m^2_{H_d^- \widetilde{e}^*_{jL}} & m^2_{H_d^- \widetilde{e}^*_{jR}} \\ m^2_{H_u^{+\,*} H_d^{-\,*}} & m^2_{H_u^{+\,*} H_u^+} & m^2_{H_u^{+\,*} \widetilde{e}^*_{jL}} & m^2_{H_u^{+\,*} \widetilde{e}^*_{jR}} \\ m^2_{\widetilde{e}_{iL} H_d^{-\,*}} & m^2_{\widetilde{e}_{iL} H_u^+} & m^2_{\widetilde{e}_{iL} \widetilde{e}^*_{jL}} & m^2_{\widetilde{e}_{iL} \widetilde{e}^*_{jR}} \\ m^2_{\widetilde{e}_{iR} H_d^{-\,*}} & m^2_{\widetilde{e}_{iR} H_u^+} & m^2_{\widetilde{e}_{iR} \widetilde{e}^*_{jL}} & m^2_{\widetilde{e}_{iR} \widetilde{e}^*_{jR}} \end{pmatrix} \, , \tag{A.34}$$

$$m^2_{H_d^- H_d^{-\,*}} = m^2_{H_d^{\mathcal{R}} H_d^{\mathcal{R}}} - \frac{1}{4}(g^2+g'^2)v_d^2 + \frac{g^2}{4}(v_u^2 - v_{iL}v_{iL}) - \frac{1}{2}\lambda_i\lambda_j v_u^2 + \frac{1}{2}Y^e_{ik}Y^e_{jk}v_{iL}v_{jL} \, , \tag{A.35}$$

$$\begin{aligned} m^2_{H_u^{+\,*} H_u^+} &= m^2_{H_u^{\mathcal{R}} H_u^{\mathcal{R}}} - \frac{1}{4}(g^2+g'^2)v_u^2 + \frac{g^2}{4}(v_d^2 + v_{iL}v_{iL}) - \frac{1}{2}\lambda_i\lambda_i v_d^2 + Y^\nu_{ij}\lambda_j v_d v_{iL} \\ &\quad - \frac{1}{2}Y^\nu_{ik}Y^\nu_{jk}v_{iL}v_{jL} \, , \end{aligned} \tag{A.36}$$

$$m^2_{H_u^{+\,*} H_d^{-\,*}} = \frac{g^2}{4}v_d v_u + \frac{1}{\sqrt{2}}T^\lambda_i v_{iR} + \frac{1}{2}\lambda_k\kappa_{ijk}v_{iR}v_{jR} - \frac{1}{2}\lambda_i\lambda_i v_d v_u + \frac{1}{2}Y^\nu_{ij}\lambda_j v_u v_{iL} \, , \tag{A.37}$$

$$m^2_{\widetilde{e}_{iL} H_d^{-\,*}} = \frac{g^2}{4}v_d v_{iL} - \frac{1}{2}Y^\nu_{ij}\lambda_k v_{kR}v_{jR} - \frac{1}{2}Y^e_{ij}Y^e_{kj}v_d v_{kL} \, , \tag{A.38}$$

$$m^2_{\widetilde{e}_{iL} H_u^+} = \frac{g^2}{4}v_u v_{iL} - \frac{1}{\sqrt{2}}T^\nu_{ij}v_{jR} - \frac{1}{2}Y^\nu_{ij}\kappa_{ljk}v_{lR}v_{kR} + \frac{1}{2}Y^\nu_{ij}\lambda_j v_d v_u - \frac{1}{2}Y^\nu_{ik}Y^\nu_{kj}v_u v_{jL} \, , \tag{A.39}$$

$$m^2_{\widetilde{e}_{iR} H_d^{-\,*}} = -\frac{1}{\sqrt{2}}T^e_{ji}v_{jL} - \frac{1}{2}Y^e_{ki}Y^\nu_{kj}v_u v_{jR} \, , \tag{A.40}$$

$$m^2_{\widetilde{e}_{iR} H_u^+} = -\frac{1}{2}Y^e_{ki}(\lambda_j v_{kL}v_{jR} + Y^\nu_{kj}v_d v_{jR}) + \lambda_{lni}Y^\nu_{lk}v_{nL}v_{kR} \, , \tag{A.41}$$

$$m^2_{\widetilde{e}_{iL}\widetilde{e}^*_{jR}} = \frac{1}{\sqrt{2}}T^e_{ij}v_d - \frac{1}{2}Y^e_{ij}\lambda_k v_u v_{kR} + \frac{2}{\sqrt{2}}T^\lambda_{kij}v_{kL} \ , \tag{A.42}$$

$$m^2_{\widetilde{e}_{iR}\widetilde{e}^*_{jR}} = \left(m^2_{\widetilde{e}_R}\right)_{ij} + \frac{g'^2}{4}(v_u^2 - v_d^2 - v_{kL}v_{kL})\delta_{ij} + \frac{1}{2}Y^e_{ki}Y^e_{kj}v_d^2 + \frac{1}{2}Y^e_{li}Y^e_{kj}v_{kL}v_{lL} + 2\lambda_{mlj}\lambda_{nli}v_{mL}v_{nL} \ , \tag{A.43}$$

$$m^2_{\widetilde{e}_{iL}\widetilde{e}^*_{jL}} = m^2_{\widetilde{\nu}^{\mathcal{R}}_{iL}\widetilde{\nu}^{\mathcal{R}}_{jL}} - \frac{1}{4}(g^2+g'^2)v_{iL}v_{jL} + \frac{g^2}{4}(v_u^2 - v_d^2 - v_{kL}v_{kL})\delta_{ij} + \frac{g^2}{4}v_{iL}v_{jL} - \frac{1}{2}Y^\nu_{ik}Y^\nu_{jk}v_u^2 + \frac{1}{2}Y^e_{il}Y^e_{jl}v_d^2 + 2\lambda_{iml}\lambda_{jnl}v_{mL}v_{nL} \ , \tag{A.44}$$

and, in order to simplify some of these formulas, the entries of the mass matrix for Higgses are used when appropriate. Matrix of Eq. (A.34) is diagonalized by an orthogonal matrix Z^+:

$$Z^+ m^2_{H^+} \ {Z^+}^T = \left(m^2_{H^+}\right)^{\rm dia} \ , \tag{A.45}$$

with

$$C = {Z^+}^T H^+ \, , \tag{A.46}$$

where the 8 entries of the matrix H^+ are the 'charged Higgs' mass eigenstate fields. In particular,

$$H^-_d = Z^+_{b1}H^-_b \ , \quad H^+_u = Z^+_{b2}H^+_b \ , \quad \widetilde{e}_{iL} = Z^+_{bi}H^-_b \ , \quad \widetilde{e}_{jR} = Z^+_{bj}H^-_b \ . \tag{A.47}$$

Mass Matrix for Down-Squarks

Left and right down-squarks are mixed. In the basis $\tilde{d}^T = \left(\widetilde{d}_{iL}, \widetilde{d}_{jR}\right)$, one obtains the following mass terms in the Lagrangian:

$$-\tilde{d}^T m^2_{\tilde{d}} \, \widetilde{d}^* \, , \tag{A.48}$$

where $m^2_{\tilde{d}}$ is the 6×6 (symmetric) matrix

$$m^2_{\tilde{d}} = \begin{pmatrix} m^2_{\widetilde{d}_{iL}\widetilde{d}^*_{jL}} & m^2_{\widetilde{d}_{iL}\widetilde{d}^*_{jR}} \\ m^2_{\widetilde{d}_{iR}\widetilde{d}^*_{jL}} & m^2_{\widetilde{d}_{iR}\widetilde{d}^*_{jR}} \end{pmatrix} \ , \tag{A.49}$$

$$m^2_{\widetilde{d}_{iL}\widetilde{d}^*_{jL}} = \left(m^2_{\widetilde{Q}_L}\right)_{ij} - \frac{1}{24}\left(3g^2+g'^2\right)\left(v_d^2 - v_u^2 + v_{kL}v_{kL}\right) + \frac{1}{2}Y^d_{ik}Y^d_{jk}v_d^2 + \frac{1}{2}\lambda'_{nil}\lambda'_{mjl}v_{nL}v_{mL} + \frac{1}{2}\left(\lambda'_{nil}Y^d_{jl} + \lambda'_{njl}Y^d_{il}\right)v_{nL}v_d \ , \tag{A.50}$$

$$m^2_{\widetilde{d}_{iR}\widetilde{d}^*_{jR}} = \left(m^2_{\widetilde{d}_R}\right)_{ij} - \frac{g'^2}{12}\left(v_d^2 - v_u^2 + v_{kL}v_{kL}\right) + \frac{1}{2}Y^d_{ki}Y^d_{kj}v_d^2 + \frac{1}{2}\lambda'_{mli}\lambda'_{nlj}v_{mL}v_{nL} + \frac{1}{2}\left(\lambda'_{nli}Y^d_{lj} + \lambda'_{nlj}Y^d_{li}\right)v_{nL}v_d \ , \tag{A.51}$$

$$m^2_{\widetilde{d}_{iL}\widetilde{d}^*_{jR}} = m^2_{\widetilde{d}_{jR}\widetilde{d}^*_{iL}} = \frac{1}{\sqrt{2}}T^d_{ij}v_d - \frac{1}{2}Y^d_{ij}\lambda_k v_u v_{kR} + \frac{1}{\sqrt{2}}T^{\lambda'}_{kij}v_{kL} \ . \tag{A.52}$$

Matrix of Eq. (A.49) is diagonalized by an orthogonal matrix Z^D:

$$Z^D m_{\tilde{d}}^2 \, {Z^D}^T = \left(m_{\tilde{d}}^2\right)^{\rm dia} \ , \tag{A.53}$$

with

$$\tilde{d} = {Z^D}^T \tilde{D} \, , \tag{A.54}$$

where the 6 entries of the matrix $\tilde{D}$ are the down-squark mass eigenstate fields. In particular,

$$\tilde{d}_{iL} = Z^D_{bi} \tilde{D}_b \, , \quad \tilde{d}_{jR} = Z^D_{bj} \tilde{D}_b \, . \tag{A.55}$$

Mass Matrix for Up-Squarks

Left and right up-squarks are mixed. In the basis $\widetilde{u}^T = (\widetilde{u}_{iL}, \widetilde{u}_{jR})$, one obtains the following mass terms in the Lagrangian:

$$- \widetilde{u}^T m_{\widetilde{u}}^2 \, \widetilde{u}^* \, , \tag{A.56}$$

where $m_{\widetilde{u}}^2$ is the 6×6 (symmetric) matrix

$$m_{\widetilde{u}}^2 = \begin{pmatrix} m^2_{\widetilde{u}_{iL}\widetilde{u}^*_{jL}} & m^2_{\widetilde{u}_{iL}\widetilde{u}^*_{jR}} \\ m^2_{\widetilde{u}_{iR}\widetilde{u}^*_{jL}} & m^2_{\widetilde{u}_{iR}\widetilde{u}^*_{jR}} \end{pmatrix} \ , \tag{A.57}$$

$$m^2_{\widetilde{u}_{iL}\widetilde{u}^*_{jL}} = \left(m^2_{\widetilde{Q}_L}\right)_{ij} + \frac{1}{24}\left(3g^2 - g'^2\right)\left(v_d^2 - v_u^2 + v_{kL}v_{kL}\right) + \frac{1}{2} Y^u_{ik} Y^u_{jk} v_u^2 \ , \tag{A.58}$$

$$m^2_{\widetilde{u}_{iR}\widetilde{u}^*_{jR}} = \left(m^2_{\widetilde{u}_R}\right)_{ij} + \frac{g'^2}{6}\left(v_d^2 - v_u^2 + v_{kL}v_{kL}\right) + \frac{1}{2} Y^u_{ki} Y^u_{kj} v_u^2 \ , \tag{A.59}$$

$$m^2_{\widetilde{u}_{iL}\widetilde{u}^*_{jR}} = m^2_{\widetilde{u}_{jR}\widetilde{u}^*_{iL}} = \frac{1}{\sqrt{2}} T^u_{ij} v_u - \frac{1}{2} Y^u_{ij} \lambda_k v_d v_{kR} + \frac{1}{2} Y^u_{ij} Y^\nu_{lk} v_{lL} v_{kR} \ . \tag{A.60}$$

Matrix of Eq. (A.57) is diagonalized by an orthogonal matrix Z^U:

$$Z^U m_{\tilde{u}}^2 \, {Z^U}^T = \left(m_{\tilde{u}}^2\right)^{\rm dia} \ , \tag{A.61}$$

with

$$\tilde{u} = {Z^U}^T \tilde{U} \, , \tag{A.62}$$

where the 6 entries of the matrix $\tilde{U}$ are the up-squark mass eigenstate fields. In particular,

$$\tilde{u}_{iL} = Z^U_{bi} \tilde{U}_b \, , \quad \tilde{u}_{jR} = Z^U_{bj} \tilde{U}_b \, . \tag{A.63}$$

A.2 Fermion Mass Matrices

The neutrino and lepton mass matrices were computed in Appendix A.2 of Ref. [63] with the assumption of CP conservation. In this Appendix we write the general fermion mass matrices, including the quarks matrices, without assuming CP conservation. To obtain the

results, we apply the standard rotation in the gauge sector:

$$\begin{pmatrix} \widetilde{W}_1 \\ \widetilde{W}_2 \\ \widetilde{W}_3 \end{pmatrix} = Z^{\widetilde{W}} \begin{pmatrix} \widetilde{W}^- \\ \widetilde{W}^+ \\ \widetilde{W}^0 \end{pmatrix} ,$$

where the mixing matrix $Z^{\widetilde{W}}$ is parametrized by

$$Z^{\widetilde{W}} = \begin{pmatrix} \frac{1}{\sqrt{2}} & \frac{1}{\sqrt{2}} & 0 \\ \frac{-i}{\sqrt{2}} & \frac{i}{\sqrt{2}} & 0 \\ 0 & 0 & 1 \end{pmatrix} ,$$

and $\widetilde{W}_{1,2,3}$ are the 2–component wino fields in the soft Lagrangian of Eq. (3.4).

Mass Matrix for Neutrinos

The usual left-handed neutrinos of the SM mix with the right-handed neutrinos and the neutral gauginos and higgsinos. Working in the basis of 2–component spinors[1], $(\chi^0)^T = \left(\varphi_{\nu_i}, \widetilde{B}^0, \widetilde{W}^0, \widetilde{H}_d^0, \widetilde{H}_u^0, \eta_{\nu_j}\right)$, one obtains the following neutral fermion mass terms in the Lagrangian:

$$-\frac{1}{2}(\chi^0)^T m_\nu \chi^0 + \text{h.c.}\,, \tag{A.64}$$

where m_ν is the 10×10 (symmetric) matrix

$$m_\nu = \begin{pmatrix} 0_{3\times3} & -\frac{1}{\sqrt{2}}g'\langle\widetilde{\nu}_{iL}\rangle^* & \frac{1}{\sqrt{2}}g\langle\widetilde{\nu}_{iL}\rangle^* & 0_{3\times1} & Y^\nu_{ik}\langle\widetilde{\nu}_{kR}\rangle^* & \langle H_u^0\rangle Y^\nu_{ij} \\ -\frac{1}{\sqrt{2}}g'\langle\widetilde{\nu}_{jL}\rangle^* & M_1 & 0 & -\frac{1}{\sqrt{2}}g'\langle H_d^0\rangle^* & \frac{1}{\sqrt{2}}g'\langle H_u^0\rangle^* & 0_{1\times3} \\ \frac{1}{\sqrt{2}}g\langle\widetilde{\nu}_{jL}\rangle^* & 0 & M_2 & \frac{1}{\sqrt{2}}g\langle H_d^0\rangle^* & -\frac{1}{\sqrt{2}}g\langle H_u^0\rangle^* & 0_{1\times3} \\ 0_{1\times3} & -\frac{1}{\sqrt{2}}g'\langle H_d^0\rangle^* & \frac{1}{\sqrt{2}}g\langle H_d^0\rangle^* & 0 & -\lambda_k\langle\widetilde{\nu}_{kR}\rangle^* & -\lambda_j\langle H_u^0\rangle \\ Y^\nu_{jk}\langle\widetilde{\nu}_{kR}\rangle^* & \frac{1}{\sqrt{2}}g'\langle H_u^0\rangle^* & -\frac{1}{\sqrt{2}}g\langle H_u^0\rangle^* & -\lambda_k\langle\widetilde{\nu}_{kR}\rangle^* & 0 & -\lambda_j\langle H_d^0\rangle + Y^\nu_{kj}\langle\widetilde{\nu}_{kL}\rangle \\ \langle H_u^0\rangle(Y^\nu_{ij})^T & 0_{3\times1} & 0_{3\times1} & -\lambda_i\langle H_u^0\rangle & -\lambda_i\langle H_d^0\rangle + Y^\nu_{ki}\langle\widetilde{\nu}_{kL}\rangle & 2\kappa_{ijk}\langle\widetilde{\nu}_{kR}\rangle^* \end{pmatrix} . \tag{A.65}$$

This is diagonalized by an unitary matrix U^V:

$$U^{V^*} m_\nu \, U^{V^\dagger} = m_\nu^{\text{dia}}\,, \tag{A.66}$$

with

$$\chi^0 = U^{V^\dagger}\lambda^0\,, \tag{A.67}$$

where the 10 entries of the matrix λ^0 are the 2-component 'neutrino' mass eigenstate fields. In particular,

$$\begin{aligned} \nu_{iL} &= U^{V^*}_{bi}\lambda^0_b\,, \quad \widetilde{B}^0 = U^{V^*}_{b4}\lambda^0_b\,, \quad \widetilde{W}^0 = U^{V^*}_{b5}\lambda^0_b\,, \\ \widetilde{H}^0_d &= U^{V^*}_{b6}\lambda^0_b\,, \quad \widetilde{H}^0_u = U^{V^*}_{b7}\lambda^0_b\,, \quad (\nu_{jR})^{c^*} = U^V_{bj}\lambda^{0^*}_b\,. \end{aligned} \tag{A.68}$$

In the case of considering only one family of right-handed neutrinos as we do in Appendix B,

[1]Since both helicities are present for neutrinos, it is convenient to introduce here the notation where φ_α is a left-handed spinor and $\bar{\eta}^{\dot{\alpha}}$ a right-handed spinor. Thus we are using in $(\chi^0)^T$, $\varphi^\alpha_{\nu_i} \equiv (\nu_{iL})^{c^*}$ and $\eta^\alpha_{\nu_j} \equiv \nu^*_{jR}$, and in χ^0, $\varphi_{\nu_i\,\alpha} \equiv \nu_{iL}$ and $\eta_{\nu_j\,\alpha} \equiv (\nu_{jR})^c$.

the last equality can be written as

$$(\nu_R)^{c^*} = U^V_{b8}\lambda^{0^*}_b \ . \tag{A.69}$$

Mass Matrix for Leptons

The usual leptons of the SM mix with charged gauginos and higgsinos. In the basis of 2–component spinors[2], $(\chi^-)^T = \left(\varphi_{e_i}, \widetilde{W}^-, \widetilde{H}^-_d\right)$ and $(\chi^+)^T = \left(\eta_{e_j}, \widetilde{W}^+, \widetilde{H}^+_u\right)$, one obtains the following charged fermion mass terms in the Lagrangian:

$$-(\chi^-)^T m_e \chi^+ + \text{h.c.}\,, \tag{A.70}$$

where m_e is the 5×5 matrix

$$m_e = \begin{pmatrix} \langle H^0_d\rangle Y^e_{ij} + 2\langle\widetilde{\nu}_{lL}\rangle\lambda_{lij} & g\langle\widetilde{\nu}_{iL}\rangle^* & -Y^\nu_{ik}\langle\widetilde{\nu}_{kR}\rangle^* \\ 0_{1\times 3} & M_2 & g\langle H^0_u\rangle^* \\ -Y^e_{kj}\langle\widetilde{\nu}_{kL}\rangle & g\langle H^0_d\rangle^* & \lambda_k\langle\widetilde{\nu}_{kR}\rangle^* \end{pmatrix} . \tag{A.71}$$

This is diagonalized by two unitary matrices U^e_L and U^e_R:

$$U^{e^*}_R m_e U^{e\,\dagger}_L = m^{\text{dia}}_e\,, \tag{A.72}$$

with

$$\chi^+ = U^{e\,\dagger}_L \lambda^+\,, \tag{A.73}$$
$$\chi^- = U^{e\,\dagger}_R \lambda^-\,, \tag{A.74}$$

where the 5 entries of the matrices λ^+, λ^-, are the 2-component 'lepton' mass eigenstate fields. In particular,

$$\begin{aligned} (e_{jR})^{c^*} &= U^e_{Lb4}\lambda^{+*}_b\,, \quad \widetilde{W}^+ = U^{e*}_{Lb4}\lambda^+_b\,, \quad \widetilde{H}^+_u = U^{e*}_{Lb5}\lambda^+_b\,, \\ e_{iL} &= U^{e*}_{Rbi}\lambda^-_b\,, \quad \widetilde{W}^- = U^{e*}_{Rb4}\lambda^-_b\,, \quad \widetilde{H}^-_d = U^{e*}_{Rb5}\lambda^-_b\,. \end{aligned} \tag{A.75}$$

Mass Matrix for Down-Quarks

In the basis of 2–components spinors $(d^*_L)^T = (d^*_{iL})$, $(d_R)^T = (d_{jR})$, one obtains the following down-quark mass terms in the Lagrangian:

$$-(d^*_L)^T m_d d_R + \text{h.c.}\,, \tag{A.76}$$

where m_d is the 3×3 matrix

$$m_d = \left(\langle H^0_d\rangle^* Y^{d^*}_{ij} + \langle\widetilde{\nu}_{lL}\rangle^*\lambda'^*_{lij}\right) . \tag{A.77}$$

This is diagonalized by two unitary matrices U^d_L and U^d_R:

$$U^{d\,\dagger}_L m_d U^d_R = m^{\text{dia}}_d\,, \tag{A.78}$$

[2]Following the convention of the previous footnote, we have in this case $\varphi^\alpha_{e_i} \equiv (e_{iL})^{c^*}$ and $\eta_{e_j\,\alpha} \equiv (e_{jR})^c$.

with

$$d_R = U_R^d D_R \,, \tag{A.79}$$
$$d_L = U_L^d D_L \,. \tag{A.80}$$

where the 3 entries of the matrices D_L, D_R are the 2-component down-quark mass eigenstate fields. In particular,

$$\begin{aligned} d_{jR} &= U_{Rjb}^d D_{bR} \,, \\ d_{iL} &= U_{Rib}^d D_{bL} \,. \end{aligned} \tag{A.81}$$

Mass Matrix for Up-Quarks

In the basis of 2–components spinors $(u_L^*)^T = (u_{iL}^*)$, $(u_R)^T = (u_{jR})$, one obtains the following up-quark mass terms in the Lagrangian:

$$-(u_L^*)^T m_u u_R + \text{h.c.} \,, \tag{A.82}$$

where m_u is the 3×3 matrix

$$m_u = \left(\langle H_u^0 \rangle^* Y_{ij}^{u^*} \right) \,. \tag{A.83}$$

This is diagonalized by two unitary matrices U_L^u and U_R^u:

$$U_L^{u^\dagger} m_u U_R^u = m_u^{\text{dia}} \,, \tag{A.84}$$

with

$$u_R = U_R^u U_R \,, \tag{A.85}$$
$$u_L = U_L^u U_L \,. \tag{A.86}$$

where the 3 entries of the matrices U_L, U_R are the 2-component up-quark mass eigenstate fields. In particular,

$$\begin{aligned} u_{jR} &= U_{Rjb}^u U_{bR} \,, \\ u_{iL} &= U_{Rib}^u U_{bL} \,. \end{aligned} \tag{A.87}$$

Appendix B

Scalar-Two Fermion Interactions

One Scalar/Pseudoscalar Higgs-Two Fermion–Interactions

In this Appendix we write the relevant interactions for our computation of the decays of the left sneutrino. For consistency with the computation of Section 4 where the SARAH code was used, we follow its notation [108, 109, 110]. In particular, opposite to our convention in Appendix A, now $a, b = 1, 2, 3$ are family indexes, and i, j, k are the indexes for the physical states. Only one family of right-handed neutrinos ν_R, and the corresponding scalar and pseudoscalar sneutrino states $\tilde{\nu}_R^{\mathcal{R}}$, $\tilde{\nu}_R^{\mathcal{I}}$, are considered for the computation of the interactions below. Notice that the definitions of SARAH used in this Appendix for Yukawa, lepton and quark matrices are not the same as those in Appendix A. Taking all this into account, in the basis of 4–component spinors with the projectors $P_{L,R} = (1 \mp \gamma_5)/2$, the interactions for the mass eigenstates are as follows.

One Higgs-Two Up Quark–Interaction

$$-i\frac{1}{\sqrt{2}}\delta_{\alpha\beta}\sum_{a,b=1}^{3} Y^*_{u,ab}U^u_{R,ja}U^u_{L,ib}Z^H_{k2}P_R - i\frac{1}{\sqrt{2}}\delta_{\alpha\beta}\sum_{b=1}^{3} U^{u,*}_{L,jb}\sum_{a=1}^{3} U^{u,*}_{R,ia}Y_{u,ab}Z^H_{k2}P_L \ . \tag{B.1}$$

One Pseudoscalar Higgs-Two Up Quark–Interaction

$$-\frac{1}{\sqrt{2}}\delta_{\alpha\beta}\sum_{a,b=1}^{3} Y^*_{u,ab}U^u_{R,ja}U^u_{L,ib}Z^A_{k2}P_R + \frac{1}{\sqrt{2}}\delta_{\alpha\beta}\sum_{b=1}^{3} U^{u,*}_{L,jb}\sum_{a=1}^{3} U^{u,*}_{R,ia}Y_{u,ab}Z^A_{k2}P_L \ . \tag{B.2}$$

One Higgs-Two Down Quark–Interaction

$$-i\frac{1}{\sqrt{2}}\delta_{\alpha\beta}\sum_{a,b=1}^{3} Y^*_{d,ab}U^d_{R,ja}U^d_{L,ib}Z^H_{k1}P_R - i\frac{1}{\sqrt{2}}\delta_{\alpha\beta}\sum_{b=1}^{3} U^{d,*}_{L,jb}\sum_{a=1}^{3} U^{d,*}_{R,ia}Y_{d,ab}Z^H_{k1}P_L \ . \tag{B.3}$$

One Pseudoscalar Higgs-Two Down Quark–Interaction

$$-\frac{1}{\sqrt{2}}\delta_{\alpha\beta}\sum_{a,b=1}^{3} Y^*_{d,ab}U^d_{R,ja}U^d_{L,ib}Z^A_{k1}P_R + \frac{1}{\sqrt{2}}\delta_{\alpha\beta}\sum_{b=1}^{3} U^{d,*}_{L,jb}\sum_{a=1}^{3} U^{d,*}_{R,ia}Y_{d,ab}Z^A_{k1}P_L \ . \tag{B.4}$$

One Higgs-Two Lepton–Interaction

$$-i\frac{1}{\sqrt{2}}\Big\{ - U^{e,*}_{R,j5}\sum_{a,b=1}^{3} U^{e,*}_{L,ia}Y_{e,ab}Z^H_{k3+b} + g_2 U^{e,*}_{L,i4}\sum_{a=1}^{3} U^{e,*}_{R,ja}Z^H_{k3+a}$$

$$
\begin{aligned}
&+\sum_{a,b=1}^{3} U^{e,*}_{R,jb}U^{e,*}_{L,ia}Y_{e,ab}Z^H_{k1} + g_2 U^{e,*}_{L,i4}U^{e,*}_{R,j5}Z^H_{k1} + g_2 U^{e,*}_{R,j4}U^{e,*}_{L,i5}Z^H_{k2} \\
&+\lambda U^{e,*}_{R,j5}U^{e,*}_{L,i5}Z^H_{k3} - U^{e,*}_{L,i5}\sum_{a=1}^{3} U^{e,*}_{R,ja}Y_{\nu,a}Z^H_{k3}\Big\}P_L \\
&-i\frac{1}{\sqrt{2}}\Big\{-\sum_{a,b=1}^{3} Y^*_{e,ab}U^e_{L,ja}Z^H_{k3+b}U^e_{R,i5} + g_2\sum_{a=1}^{3} U^e_{R,ia}Z^H_{k3+a}U^e_{L,j4} \\
&+\sum_{a,b=1}^{3} Y^*_{e,ab}U^e_{L,ja}U^e_{R,ib}Z^H_{k1} + g_2 U^e_{R,i5}U^e_{L,j4}Z^H_{k1} + g_2 U^e_{R,i4}U^e_{L,j5}Z^H_{k2} \\
&+\lambda^* U^e_{R,i5}U^e_{L,j5}Z^H_{k3} - \sum_{a=1}^{3} Y^*_{\nu,a}U^e_{R,ia}U^e_{L,j5}Z^H_{k3}\Big\}P_R\ .
\end{aligned}
\tag{B.5}
$$

One Pseudoscalar Higgs-Two Lepton–Interaction

$$
\begin{aligned}
&\frac{1}{\sqrt{2}}\Big\{-U^{e,*}_{R,j5}\sum_{a,b=1}^{3} U^{e,*}_{L,ia}Y_{e,ab}Z^A_{k3+b} - g_2 U^{e,*}_{L,i4}\sum_{a=1}^{3} U^{e,*}_{R,ja}Z^A_{k3+a} \\
&+\sum_{a,b=1}^{3} U^{e,*}_{R,jb}U^{e,*}_{L,ia}Y_{e,ab}Z^A_{k1} - g_2 U^{e,*}_{L,i4}U^{e,*}_{R,j5}Z^A_{k1} - g_2 U^{e,*}_{R,j4}U^{e,*}_{L,i5}Z^A_{k2} \\
&-\lambda U^{e,*}_{R,j5}U^{e,*}_{L,i5}Z^A_{k3} + U^{e,*}_{L,i5}\sum_{a=1}^{3} U^{e,*}_{R,ja}Y_{\nu,a}Z^A_{k3}\Big\}P_L \\
&-\frac{1}{\sqrt{2}}\Big\{-\sum_{a,b=1}^{3} Y^*_{e,ab}U^e_{L,ja}Z^A_{k3+b}U^e_{R,i5} - g_2\sum_{a=1}^{3} U^e_{R,ia}Z^A_{k3+a}U^e_{L,j4} \\
&+\sum_{a,b=1}^{3} Y^*_{e,ab}U^e_{L,ja}U^e_{R,ib}Z^A_{k1} - g_2 U^e_{R,i5}U^e_{L,j4}Z^A_{k1} - g_2 U^e_{R,i4}U^e_{L,j5}Z^A_{k2} \\
&-\lambda^* U^e_{R,i5}U^e_{L,j5}Z^A_{k3} + \sum_{a=1}^{3} Y^*_{\nu,a}U^e_{R,ia}U^e_{L,j5}Z^A_{k3}\Big\}P_R\ .
\end{aligned}
\tag{B.6}
$$

One Higgs-Two Neutrino-Interaction

$$
\begin{aligned}
&\frac{i}{2}\Big\{g_1(U^{V,*}_{i4}\sum_{a=1}^{3} U^{V,*}_{ja} + U^{V,*}_{j4}\sum_{a=1}^{3} U^{V,*}_{ia})Z^H_{k3+a} - g_2(U^{V,*}_{i5}\sum_{a=1}^{3} U^{V,*}_{ja} + U^{V,*}_{j5}\sum_{a=1}^{3} U^{V,*}_{ia})Z^H_{k3+a} \\
&-\sqrt{2}(U^{V,*}_{i8}U^{V,*}_{j7} + U^{V,*}_{i7}U^{V,*}_{j8})\sum_{a=1}^{3} Y_{\nu,a}Z^H_{k3+a} + \sqrt{2}\lambda(U^{V,*}_{i8}U^{V,*}_{j7} + U^{V,*}_{i7}U^{V,*}_{j8})Z^H_{k1} \\
&+g_1(U^{V,*}_{j4}U^{V,*}_{i6} + U^{V,*}_{i4}U^{V,*}_{j6})Z^H_{k1} - g_2(U^{V,*}_{i5}U^{V,*}_{j6} + U^{V,*}_{j5}U^{V,*}_{i6})Z^H_{k1} \\
&-g_1(U^{V,*}_{j4}U^{V,*}_{i7} + U^{V,*}_{i4}U^{V,*}_{j7})Z^H_{k2} + g_2(U^{V,*}_{i5}U^{V,*}_{j7} + U^{V,*}_{j5}U^{V,*}_{i7})Z^H_{k2} \\
&-\sqrt{2}(U^{V,*}_{j8}\sum_{a=1}^{3} U^{V,*}_{ia} + U^{V,*}_{i8}\sum_{a=1}^{3} U^{V,*}_{ja})Y_{\nu,a}Z^H_{k2} + \sqrt{2}\lambda(U^{V,*}_{i8}U^{V,*}_{j6} + U^{V,*}_{i6}U^{V,*}_{j8})Z^H_{k2} \\
&-2\sqrt{2}\kappa U^{V,*}_{i8}U^{V,*}_{j8}Z^H_{k3} + \sqrt{2}\lambda(U^{V,*}_{i7}U^{V,*}_{j6}Z^H_{k3} + U^{V,*}_{i6}U^{V,*}_{j7})Z^H_{k3} \\
&-\sqrt{2}(U^{V,*}_{j7}\sum_{a=1}^{3} U^{V,*}_{ia}Y_{\nu,a} + U^{V,*}_{i7}\sum_{a=1}^{3} U^{V,*}_{ja}Y_{\nu,a})Z^H_{k3}\Big\}P_L
\end{aligned}
$$

$$
\begin{aligned}
&+\frac{i}{2}\Big\{g_1\sum_{a=1}^{3}Z^H_{k3+a}(U^V_{ja}U^V_{i4}+U^V_{ia}U^V_{j4})-g_2\sum_{a=1}^{3}Z^H_{k3+a}(U^V_{ja}U^V_{i5}+U^V_{ia}U^V_{j5})\\
&-\sqrt{2}\sum_{a=1}^{3}Y^*_{\nu,a}Z^H_{k3+a}(U^V_{i8}U^V_{j7}+U^V_{i7}U^V_{j8})+\sqrt{2}\lambda^*Z^H_{k1}(U^V_{i8}U^V_{j7}+U^V_{i7}U^V_{j8})\\
&+g_1Z^H_{k1}(U^V_{i6}U^V_{j4}+U^V_{i4}U^V_{j6})-g_2Z^H_{k1}(U^V_{i5}U^V_{j6}+U^V_{i6}U^V_{j5})\\
&-g_1Z^H_{k2}(U^V_{i7}U^V_{j4}+U^V_{i4}U^V_{j7})+g_2Z^H_{k2}(U^V_{i5}U^V_{j7}+U^V_{i7}U^V_{j5})\\
&-\sqrt{2}\sum_{a=1}^{3}Y^*_{\nu,a}(U^V_{ja}Z^H_{k2}U^V_{i8}+U^V_{ia}Z^H_{k2}U^V_{j8})+\sqrt{2}\lambda^*Z^H_{k2}(U^V_{i8}U^V_{j6}+Z^H_{k2}U^V_{i6}U^V_{j8})\\
&-2\sqrt{2}\kappa^*Z^H_{k3}U^V_{i8}U^V_{j8}+\sqrt{2}\lambda^*Z^H_{k3}(U^V_{i7}U^V_{j6}+Z^H_{k3}U^V_{i6}U^V_{j7})\\
&-\sqrt{2}\sum_{a=1}^{3}Y^*_{\nu,a}(U^V_{ja}Z^H_{k3}U^V_{i7}+U^V_{ia}Z^H_{k3}U^V_{j7})\Big\}P_R\ .
\end{aligned}
\tag{B.7}
$$

One Pseudoscalar Higgs-Two Neutrino–Interaction

$$
\begin{aligned}
&\frac{1}{2}\Big\{g_1(U^{V,*}_{i4}\sum_{a=1}^{3}U^{V,*}_{ja}+U^{V,*}_{j4}\sum_{a=1}^{3}U^{V,*}_{ia})Z^A_{k3+a}-g_2(U^{V,*}_{i5}\sum_{a=1}^{3}U^{V,*}_{ja}+U^{V,*}_{j5}\sum_{a=1}^{3}U^{V,*}_{ia})Z^A_{k3+a}\\
&+\sqrt{2}(U^{V,*}_{i8}U^{V,*}_{j7}+U^{V,*}_{i7}U^{V,*}_{j8})\sum_{a=1}^{3}Y_{\nu,a}Z^A_{k3+a}-\sqrt{2}\lambda(U^{V,*}_{i8}U^{V,*}_{j7}+U^{V,*}_{i7}U^{V,*}_{j8})Z^A_{k1}\\
&+g_1(U^{V,*}_{i4}U^{V,*}_{j6}+U^{V,*}_{j4}U^{V,*}_{i6})Z^A_{k1}-g_2(U^{V,*}_{i5}U^{V,*}_{j6}+U^{V,*}_{j5}U^{V,*}_{i6})Z^A_{k1}\\
&-g_1(U^{V,*}_{i4}U^{V,*}_{j7}+U^{V,*}_{j4}U^{V,*}_{i7})Z^A_{k2}+g_2(U^{V,*}_{i5}U^{V,*}_{j7}+U^{V,*}_{j5}U^{V,*}_{i7})Z^A_{k2}\\
&+\sqrt{2}(U^{V,*}_{j8}\sum_{a=1}^{3}U^{V,*}_{ia}+U^{V,*}_{i8}\sum_{a=1}^{3}U^{V,*}_{ja})Y_{\nu,a}Z^A_{k2}-\sqrt{2}\lambda(U^{V,*}_{i8}U^{V,*}_{j6}+U^{V,*}_{i6}U^{V,*}_{j8})Z^A_{k2}\\
&-2\sqrt{2}\kappa U^{V,*}_{i8}U^{V,*}_{j8}Z^A_{k3}+\sqrt{2}\lambda(U^{V,*}_{i7}U^{V,*}_{j6}+U^{V,*}_{i6}U^{V,*}_{j7})Z^A_{k3}\\
&-\sqrt{2}(U^{V,*}_{j7}\sum_{a=1}^{3}U^{V,*}_{ia}Y_{\nu,a}+U^{V,*}_{i7}\sum_{a=1}^{3}U^{V,*}_{ja}Y_{\nu,a})Z^A_{k3}\Big\}P_L\\
&-\frac{1}{2}\Big\{g_1\sum_{a=1}^{3}Z^A_{k3+a}(U^V_{ja}U^V_{i4}+U^V_{ia}U^V_{j4})-g_2\sum_{a=1}^{3}Z^A_{k3+a}(U^V_{ja}U^V_{i5}+U^V_{ia}U^V_{j5})\\
&+\sqrt{2}\sum_{a=1}^{3}Y^*_{\nu,a}Z^A_{k3+a}(U^V_{i8}U^V_{j7}+U^V_{i7}U^V_{j8})-\sqrt{2}\lambda^*Z^A_{k1}(U^V_{i8}U^V_{j7}+U^V_{i7}U^V_{j8})\\
&+g_1Z^A_{k1}(+U^V_{i4}U^V_{j6}+U^V_{i6}U^V_{j4})-g_2Z^A_{k1}(U^V_{i5}U^V_{j6}+U^V_{i6}U^V_{j5})\\
&-g_1Z^A_{k2}(U^V_{i4}U^V_{j7}+U^V_{i7}U^V_{j4})+g_2Z^A_{k2}(U^V_{i5}U^V_{j7}+U^V_{i7}U^V_{j5})\\
&+\sqrt{2}\sum_{a=1}^{3}Y^*_{\nu,a}(U^V_{ia}Z^A_{k2}U^V_{j8}+U^V_{ja}Z^A_{k2}U^V_{i8})-\sqrt{2}\lambda^*Z^A_{k2}(U^V_{i8}U^V_{j6}+U^V_{i6}U^V_{j8})\\
&-2\sqrt{2}\kappa^*Z^A_{k3}U^V_{i8}U^V_{j8}+\sqrt{2}\lambda^*Z^A_{k3}(U^V_{i7}U^V_{j6}+U^V_{i6}U^V_{j7})\\
&-\sqrt{2}\sum_{a=1}^{3}Y^*_{\nu,a}(U^V_{ia}Z^A_{k3}U^V_{j7}+U^V_{ja}Z^A_{k3}U^V_{i7})\Big\}P_R\ .
\end{aligned}
\tag{B.8}
$$

Appendix C

Three Scalar Higgs Interactions

In this Appendix we write the relevant interactions for our computation of the decays of the left sneutrino to two scalars.

$$
\begin{aligned}
&-\frac{i}{8}\Big(g_1^2\sum_{a=1}^{3}v_{L,a}Z^H_{k5+a}\sum_{b=1}^{3}Z^H_{i5+b}Z^H_{j5+b}+g_2^2\sum_{a=1}^{3}v_{L,a}Z^H_{k5+a}\sum_{b=1}^{3}Z^H_{i5+b}Z^H_{j5+b}\\
&+g_1^2\sum_{a=1}^{3}Z^H_{i5+a}Z^H_{j5+a}\sum_{b=1}^{3}v_{L,b}Z^H_{k5+b}+g_2^2\sum_{a=1}^{3}Z^H_{i5+a}Z^H_{j5+a}\sum_{b=1}^{3}v_{L,b}Z^H_{k5+b}\\
&+g_1^2\sum_{a=1}^{3}v_{L,a}Z^H_{j5+a}\sum_{b=1}^{3}Z^H_{i5+b}Z^H_{k5+b}+g_2^2\sum_{a=1}^{3}v_{L,a}Z^H_{j5+a}\sum_{b=1}^{3}Z^H_{i5+b}Z^H_{k5+b}\\
&+g_1^2\sum_{a=1}^{3}v_{L,a}Z^H_{i5+a}\sum_{b=1}^{3}Z^H_{j5+b}Z^H_{k5+b}+g_2^2\sum_{a=1}^{3}v_{L,a}Z^H_{i5+a}\sum_{b=1}^{3}Z^H_{j5+b}Z^H_{k5+b}\\
&+4v_u\sum_{l=1}^{3}\sum_{a=1}^{3}Y_{\nu,al}Z^H_{k5+a}\sum_{b=1}^{3}Y^*_{\nu,bl}Z^H_{j5+b}Z^H_{i2}+4v_u\sum_{l=1}^{3}\sum_{a=1}^{3}Y_{\nu,a1}Z^H_{j5+a}\sum_{b=1}^{3}Y^*_{\nu,b1}Z^H_{k5+b}Z^H_{i2}\\
&+\Big(g_1^2+g_2^2\Big)\sum_{a=1}^{3}Z^H_{j5+a}Z^H_{k5+a}\Big(2v_dZ^H_{i1}-2v_uZ^H_{i2}+\sum_{b=1}^{3}v_{L,b}Z^H_{i5+b}\Big)\\
&+4v_R\sum_{a=1}^{3}Y_{\nu,a1}Z^H_{k5+a}\sum_{b=1}^{3}Y^*_{\nu,b1}Z^H_{j5+b}Z^H_{i3}+4v_R\sum_{a=1}^{3}Y_{\nu,a1}Z^H_{j5+a}\sum_{b=1}^{3}Y^*_{\nu,b1}Z^H_{k5+b}Z^H_{i3}\\
&+2g_1^2\sum_{a=1}^{3}v_{L,a}Z^H_{k5+a}Z^H_{i1}Z^H_{j1}+2g_2^2\sum_{a=1}^{3}v_{L,a}Z^H_{k5+a}Z^H_{i1}Z^H_{j1}\\
&-4v_u\sum_{l=1}^{3}\lambda^*_l\sum_{a=l}^{3}Y_{\nu,a1}Z^H_{k5+a}Z^H_{i2}Z^H_{j1}-4\sum_{l=1}^{3}v_{Rl}\lambda^*_l\sum_{m=1}^{3}\sum_{a=1}^{3}Y_{\nu,am}Z^H_{k5+a}Z^H_{i2+m}Z^H_{j1}\\
&+4v_u\sum_{l=1}^{3}\sum_{a=1}^{3}Y_{\nu,al}Z^H_{k5+a}\sum_{b=1}^{3}Y^*_{\nu,bl}Z^H_{i5+b}Z^H_{j2}+4v_u\sum_{l=1}^{3}\sum_{a=1}^{3}Y_{\nu,al}Z^H_{i5+a}\sum_{b=1}^{3}Y^*_{\nu,bl}Z^H_{k5+b}Z^H_{j2}\\
&-4\sum_{l=1}^{3}v_u\lambda^*_l\sum_{a=1}^{3}Y_{\nu,al}Z^H_{k5+a}Z^H_{i1}Z^H_{j2}-2g_1^2\sum_{a=1}^{3}v_{L,a}Z^H_{k5+a}Z^H_{i2}Z^H_{j2}\\
&-2g_2^2\sum_{a=1}^{3}v_{L,a}Z^H_{k5+a}Z^H_{i2}Z^H_{j2}-4v_d\sum_{l=1}^{3}\lambda^*_l\sum_{a=1}^{3}Y_{\nu,al}Z^H_{k5+a}Z^H_{i2}Z^H_{j2}\\
&+4\sum_{l=1}^{3}\sum_{a=1}^{3}v_{L,a}Y_{\nu,al}\sum_{b=1}^{3}Y^*_{\nu,bl}Z^H_{k5+b}Z^H_{i2}Z^H_{j2}+4\sum_{l=1}^{3}\sum_{a=1}^{3}Y^*_{\nu,al}v_{L,a}\sum_{b=1}^{3}Y_{\nu,bl}Z^H_{k5+b}Z^H_{i2}Z^H_{j2}\\
&+2\sqrt{2}\sum_{l=1}^{3}\sum_{a=1}^{3}T^*_{\nu,al}Z^H_{k5+a}Z^H_{i2+l}Z^H_{j2}+4\sum_{l=1}^{3}\sum_{m=1}^{3}\sum_{n=1}^{3}v_{Rl}\kappa^*_{lmn}\sum_{a=1}^{3}Y_{\nu,am}Z^H_{k5+a}Z^H_{i2+n}Z^H_{j2}
\end{aligned}
$$

$$+2\sqrt{2}\sum_{l=1}^{3}\sum_{a=1}^{3}Z^H_{k5+a}T_{\nu,al}Z^H_{i2+l}Z^H_{j2}+\left(g_1^2+g_2^2\right)\sum_{a=1}^{3}Z^H_{i5+a}Z^H_{k5+a}\left(2v_dZ^H_{j1}-2v_uZ^H_{j2}+\sum_{b=1}^{3}v_{L,b}Z^H_{j5+b}\right)$$
$$+4\sum_{l=1}^{3}v_{Rl}\sum_{a=1}^{3}Y_{\nu,al}Z^H_{k5+a}\sum_{m=1}^{3}\sum_{b=1}^{3}Y^*_{\nu,bm}Z^H_{i5+b}Z^H_{j2+m}+4\sum_{l=1}^{3}v_{Rl}\sum_{a=1}^{3}Y_{\nu,al}Z^H_{i5+a}\sum_{m=1}^{3}\sum_{b=1}^{3}Y^*_{\nu,bm}Z^H_{k5+b}Z^H_{j2+m}$$
$$-4\sum_{l=1}^{3}v_{Rl}\lambda^*_l\sum_{m=1}^{3}\sum_{a=1}^{3}Y_{\nu,am}Z^H_{k5+a}Z^H_{i1}Z^H_{j2+m}+2\sqrt{2}\sum_{l=1}^{3}\sum_{a=1}^{3}T^*_{\nu,al}Z^H_{k5+a}Z^H_{i2}Z^H_{j2+l}$$
$$+4\sum_{l=1}^{3}\sum_{m=1}^{3}\sum_{n=1}^{3}v_{Rl}\kappa^*_{lmn}\sum_{a=1}^{3}Y_{\nu,am}Z^H_{k5+a}Z^H_{i2}Z^H_{j2+n}+2\sqrt{2}\sum_{l=1}^{3}\sum_{a=1}^{3}Z^H_{k5+a}T_{\nu,al}Z^H_{i2}Z^H_{j2+l}$$
$$+4v_u\sum_{l=1}^{3}\sum_{m=1}^{3}\sum_{n=1}^{3}\kappa^*_{lmn}\sum_{a=1}^{3}Y_{\nu,al}Z^H_{k5+a}Z^H_{i2+n}Z^H_{j2+n}-4v_d\sum_{l=1}^{3}\sum_{m=1}^{3}\lambda^*_l\sum_{a=1}^{3}Y_{\nu,am}Z^H_{k5+a}Z^H_{i2+l}Z^H_{j2+n}$$
$$+4\sum_{l=1}^{3}\sum_{m=1}^{3}\sum_{a=1}^{3}v_{L,a}Y_{\nu,al}\sum_{b=1}^{3}Y^*_{\nu,bm}Z^H_{k5+b}Z^H_{i2+l}Z^H_{j2+m}+4\sum_{l=1}^{3}\sum_{m=1}^{3}\sum_{a=1}^{3}Y^*_{\nu,al}v_{L,a}\sum_{b=1}^{3}Y_{\nu,bm}Z^H_{k5+b}Z^H_{i2+l}Z^H_{j2+m}$$
$$+2g_1^2v_d\sum_{a=1}^{3}Z^H_{i5+a}Z^H_{j5+a}Z^H_{k1}+2g_2^2v_d\sum_{a=1}^{3}Z^H_{i5+a}Z^H_{j5+a}Z^H_{k1}$$
$$+2g_1^2\sum_{a=1}^{3}v_{L,a}Z^H_{j5+a}Z^H_{i1}Z^H_{k1}+2g_2^2\sum_{a=1}^{3}v_{L,a}Z^H_{j5+a}Z^H_{i1}Z^H_{k1}$$
$$-4v_u\sum_{l=1}^{3}\lambda^*_l\sum_{a=1}^{3}Y_{\nu,al}Z^H_{j5+a}Z^H_{i2}Z^H_{k1}-4\sum_{l=1}^{3}\sum_{m=1}^{3}v_{Rl}\lambda^*_l\sum_{a=1}^{3}Y_{\nu,am}Z^H_{j5+a}Z^H_{i2+m}Z^H_{k1}$$
$$+2g_1^2\sum_{a=1}^{3}v_{L,a}Z^H_{i5+a}Z^H_{j1}Z^H_{k1}+2g_2^2\sum_{a=1}^{3}v_{L,a}Z^H_{i5+a}Z^H_{j1}Z^H_{k1}+6g_1^2v_dZ^H_{i1}Z^H_{j1}Z^H_{k1}$$
$$+6g_2^2v_dZ^H_{i1}Z^H_{j1}Z^H_{k1}-2g_1^2v_uZ^H_{i2}Z^H_{j1}Z^H_{k1}-2g_2^2v_uZ^H_{i2}Z^H_{j1}Z^H_{k1}$$
$$+8v_u|\sum_{l=1}^{3}\lambda_l|^2Z^H_{i2}Z^H_{j1}Z^H_{k1}+8\sum_{l=1}^{3}\sum_{m=1}^{3}v_{lR}\lambda_l\lambda^*_mZ^H_{i2+m}Z^H_{j1}Z^H_{k1}-4\sum_{l=1}^{3}v_u\lambda^*_l\sum_{a=1}^{3}Y_{\nu,al}Z^H_{i5+a}Z^H_{j2}Z^H_{k1}$$
$$-2g_1^2v_uZ^H_{i1}Z^H_{j2}Z^H_{k1}-2g_2^2v_uZ^H_{i1}Z^H_{j2}Z^H_{k1}+8v_u|\sum_{l=1}^{3}\lambda_l|^2Z^H_{i1}Z^H_{j2}Z^H_{k1}$$
$$-2g_1^2v_dZ^H_{i2}Z^H_{j2}Z^H_{k1}-2g_2^2v_dZ^H_{i2}Z^H_{j2}Z^H_{k1}+8v_d|\sum_{l=1}^{3}\lambda_l|^2Z^H_{i2}Z^H_{j2}Z^H_{k1}$$
$$-4\sum_{l=1}^{3}\lambda^*_l\sum_{a=1}^{3}v_{L,a}Y_{\nu,al}Z^H_{i2}Z^H_{j2}Z^H_{k1}-2\sqrt{2}\sum_{l=1}^{3}T^*_{\lambda,l}Z^H_{i2+l}Z^H_{j2}Z^H_{k1}$$
$$-4\sum_{l=1}^{3}\sum_{m=1}^{3}v_{Rl}\lambda^*_l\sum_{a=1}^{3}Y_{\nu,am}Z^H_{i5+a}Z^H_{j2+m}Z^H_{k1}+8\sum_{l=1}^{3}\sum_{m=1}^{3}v_{Rl}\lambda_l\lambda_mZ^H_{i1}Z^H_{j2+m}Z^H_{k1}-2\sum_{l=1}^{3}\sqrt{2}T^*_{\lambda,l}Z^H_{i2}Z^H_{j2+l}Z^H_{k1}$$
$$+8v_d\sum_{l=1}^{3}\sum_{m=1}^{3}\lambda_l\lambda^*_mZ^H_{i2+l}Z^H_{j2+m}Z^H_{k1}-4\sum_{l=1}^{3}\sum_{m=1}^{3}\lambda^*_l\sum_{a=1}^{3}v_{L,a}Y_{\nu,al}Z^H_{i2+l}Z^H_{j2+m}Z^H_{k1}$$
$$-2g_1^2v_u\sum_{a=1}^{3}Z^H_{i5+a}Z^H_{j5+a}Z^H_{k2}-2g_2^2v_u\sum_{a=1}^{3}Z^H_{i5+a}Z^H_{j5+a}Z^H_{k2}$$
$$+4v_u\sum_{l=1}^{3}\sum_{a=1}^{3}Y_{\nu,al}Z^H_{j5+a}\sum_{b=1}^{3}Y^*_{\nu,bl}Z^H_{i5+b}Z^H_{k2}+4v_u\sum_{l=1}^{3}\sum_{a=1}^{3}Y_{\nu,al}Z^H_{i5+a}\sum_{b=1}^{3}Y^*_{\nu,bl}Z^H_{j5+b}Z^H_{k2}$$
$$-4v_u\sum_{l=1}^{3}\lambda^*_l\sum_{a=1}^{3}Y_{\nu,al}Z^H_{j5+a}Z^H_{i1}Z^H_{k2}-2g_1^2\sum_{a=1}^{3}v_{L,a}Z^H_{j5+a}Z^H_{i2}Z^H_{k2}$$
$$-2g_2^2\sum_{a=1}^{3}v_{L,a}Z^H_{j5+a}Z^H_{i2}Z^H_{k2}-4v_d\sum_{l=1}^{3}\lambda^*_l\sum_{a=1}^{3}Y_{\nu,al}Z^H_{j5+a}Z^H_{i2}Z^H_{k2}$$

$$+4\sum_{l=1}^{3}\sum_{a=1}^{3}v_{L,a}Y_{\nu,al}\sum_{b=1}^{3}Y^{*}_{\nu,bl}Z^{H}_{j5+b}Z^{H}_{i2}Z^{H}_{k2}+4\sum_{l=1}^{3}\sum_{a=1}^{3}Y^{*}_{\nu,al}v_{L,a}\sum_{b=1}^{3}Y_{\nu,bl}Z^{H}_{j5+b}Z^{H}_{i2}Z^{H}_{k2}$$

$$+2\sqrt{2}\sum_{l=1}^{3}\sum_{a=1}^{3}T^{*}_{\nu,al}Z^{H}_{j5+a}Z^{H}_{i2+l}Z^{H}_{k2}+4\sum_{l=1}^{3}\sum_{m=1}^{3}\sum_{n=1}^{3}v_{lR}\kappa^{*}_{lmn}\sum_{a=1}^{3}Y_{\nu,am}Z^{H}_{j5+a}Z^{H}_{i2+n}Z^{H}_{k2}$$

$$+2\sqrt{2}\sum_{l=1}^{3}\sum_{a=1}^{3}Z^{H}_{j5+a}T_{\nu,al}Z^{H}_{i2+l}Z^{H}_{k2}-4v_{u}\sum_{l=1}^{3}\lambda^{*}_{l}\sum_{a=1}^{3}Y_{\nu,al}Z^{H}_{i5+a}Z^{H}_{j1}Z^{H}_{k2}-2g_{1}^{2}v_{u}Z^{H}_{i1}Z^{H}_{j1}Z^{H}_{k2}$$

$$-2g_{2}^{2}v_{u}Z^{H}_{i1}Z^{H}_{j1}Z^{H}_{k2}+8v_{u}|\sum_{l=1}^{3}\lambda_{l}|^{2}Z^{H}_{i1}Z^{H}_{j1}Z^{H}_{k2}-2g_{1}^{2}v_{d}Z^{H}_{i2}Z^{H}_{j1}Z^{H}_{k2}$$

$$-2g_{2}^{2}v_{d}Z^{H}_{i2}Z^{H}_{j1}Z^{H}_{k2}+8v_{d}|\sum_{l=1}^{3}\lambda_{l}|^{2}Z^{H}_{i2}Z^{H}_{j1}Z^{H}_{k2}-4\sum_{l=1}^{3}\lambda^{*}_{l}\sum_{a=1}^{3}v_{L,a}Y_{\nu,al}Z^{H}_{i2}Z^{H}_{j1}Z^{H}_{k2}$$

$$-2\sqrt{2}\sum_{l=1}^{3}T^{*}_{\lambda,l}Z^{H}_{i2+l}Z^{H}_{j1}Z^{H}_{k2}-2g_{1}^{2}\sum_{a=1}^{3}v_{L,a}Z^{H}_{i5+a}Z^{H}_{j2}Z^{H}_{k2}-2g_{2}^{2}\sum_{a=1}^{3}v_{L,a}Z^{H}_{i5+a}Z^{H}_{j2}Z^{H}_{k2}$$

$$-4v_{d}\sum_{l=1}^{3}\lambda^{*}_{l}\sum_{a=1}^{3}Y_{\nu,al}Z^{H}_{i5+a}Z^{H}_{j2}Z^{H}_{k2}+4\sum_{l=1}^{3}\sum_{a=1}^{3}v_{L,a}Y_{\nu,al}\sum_{b=1}^{3}Y^{*}_{\nu,bl}Z^{H}_{i5+b}Z^{H}_{j2}Z^{H}_{k2}$$

$$+4\sum_{l=1}^{3}\sum_{a=1}^{3}Y^{*}_{\nu,al}v_{L,a}\sum_{b=1}^{3}Y_{\nu,bl}Z^{H}_{i5+b}Z^{H}_{j2}Z^{H}_{k2}-2g_{1}^{2}v_{d}Z^{H}_{i1}Z^{H}_{j2}Z^{H}_{k2}$$

$$-2g_{2}^{2}v_{d}Z^{H}_{i1}Z^{H}_{j2}Z^{H}_{k2}+8v_{d}|\sum_{l=1}^{3}\lambda_{l}|^{2}Z^{H}_{i1}Z^{H}_{j2}Z^{H}_{k2}-4\sum_{l=1}^{3}\lambda^{*}_{l}\sum_{a=1}^{3}v_{L,a}Y_{\nu,al}Z^{H}_{i1}Z^{H}_{j2}Z^{H}_{k2}$$

$$+6g_{1}^{2}v_{u}Z^{H}_{i2}Z^{H}_{j2}Z^{H}_{k2}+6g_{2}^{2}v_{u}Z^{H}_{i2}Z^{H}_{j2}Z^{H}_{k2}+8\sum_{l=1}^{3}\sum_{m=1}^{3}v_{lR}\lambda_{l}\lambda^{*}_{m}Z^{H}_{i2+m}Z^{H}_{j2}Z^{H}_{k2}$$

$$+8\sum_{l=1}^{3}\sum_{m=1}^{3}v_{Rl}\sum_{a=1}^{3}Y_{\nu,al}Y^{*}_{\nu,am}Z^{H}_{i2+m}Z^{H}_{j2}Z^{H}_{k2}+2\sqrt{2}\sum_{l=1}^{3}\sum_{a=1}^{3}T^{*}_{\nu,al}Z^{H}_{i5+a}Z^{H}_{j2+l}Z^{H}_{k2}$$

$$+4\sum_{l=1}^{3}\sum_{m=1}^{3}\sum_{n=1}^{3}v_{lR}\kappa^{*}_{lmn}\sum_{a=1}^{3}Y_{\nu,am}Z^{H}_{i5+a}Z^{H}_{j2+n}Z^{H}_{k2}+2\sqrt{2}\sum_{l=1}^{3}\sum_{a=1}^{3}Z^{H}_{i5+a}T_{\nu,al}Z^{H}_{j2+l}Z^{H}_{k2}$$

$$-2\sqrt{2}\sum_{l=1}^{3}T^{*}_{\lambda,l}Z^{H}_{i1}Z^{H}_{j2+l}Z^{H}_{k2}+8\sum_{l=1}^{3}\sum_{m=1}^{3}v_{Rl}\lambda_{l}\lambda^{*}_{m}Z^{H}_{i2}Z^{H}_{j2+m}Z^{H}_{k2}+8\sum_{l=1}^{3}\sum_{m=1}^{3}v_{Rl}\sum_{a=1}^{3}Y_{\nu,al}Y_{\nu,am}Z^{H}_{i2}Z^{H}_{j2+m}Z^{H}_{k2}$$

$$+8v_{u}\sum_{l=1}^{3}\sum_{m=1}^{3}\lambda_{l}\lambda^{*}_{m}Z^{H}_{i2+l}Z^{H}_{j2+m}Z^{H}_{k2}+8v_{u}\sum_{l=1}^{3}\sum_{m=1}^{3}\sum_{a=1}^{3}Y_{\nu,al}Y_{\nu,a,m}Z^{H}_{i2+l}Z^{H}_{j2+l}Z^{H}_{k2}$$

$$+4\sum_{l=1}^{3}\sum_{m=1}^{3}\sum_{n=1}^{3}\kappa^{*}_{lmn}\sum_{a=1}^{3}v_{L,a}Y_{\nu,al}Z^{H}_{i2+m}Z^{H}_{j2+n}Z^{H}_{k2}+4\sum_{l=1}^{3}\sum_{m=1}^{3}v_{Rl}\sum_{a=1}^{3}Y_{\nu,al}Z^{H}_{j5+a}\sum_{b=1}^{3}Y^{*}_{\nu,bm}Z^{H}_{i5+b}Z^{H}_{k2+m}$$

$$+4\sum_{l=1}^{3}\sum_{m=1}^{3}v_{Rl}\sum_{a=1}^{3}Y_{\nu,al}Z^{H}_{i5+a}\sum_{b=1}^{3}Y^{*}_{\nu,bm}Z^{H}_{j5+b}Z^{H}_{k2+m}-4\sum_{l=1}^{3}\sum_{m=1}^{3}v_{Rl}\lambda^{*}_{l}\sum_{a=1}^{3}Y_{\nu,am}Z^{H}_{j5+a}Z^{H}_{i1}Z^{H}_{k2+m}$$

$$+2\sqrt{2}\sum_{l=1}^{3}\sum_{a=1}^{3}T^{*}_{\nu,al}Z^{H}_{j5+a}Z^{H}_{i2}Z^{H}_{k2+l}+4\sum_{l=1}^{3}\sum_{m=1}^{3}\sum_{n=1}^{3}v_{Rl}\kappa^{*}_{lmn}\sum_{a=1}^{3}Y_{\nu,am}Z^{H}_{j5+a}Z^{H}_{i2}Z^{H}_{k2+n}$$

$$+2\sqrt{2}\sum_{l=1}^{3}\sum_{a=1}^{3}Z^{H}_{j5+a}T_{\nu,al}Z^{H}_{i2}Z^{H}_{k2+l}+4v_{u}\sum_{l=1}^{3}\sum_{m=1}^{3}\sum_{n=1}^{3}\kappa^{*}_{lmn}\sum_{a=1}^{3}Y_{\nu,al}Z^{H}_{j5+a}Z^{H}_{i2+m}Z^{H}_{k2+n}$$

$$-4v_{d}\sum_{l=1}^{3}\sum_{m=1}^{3}\lambda^{*}_{l}\sum_{a=1}^{3}Y_{\nu,am}Z^{H}_{j5+a}Z^{H}_{i2+l}Z^{H}_{k2+n}+4\sum_{l=1}^{3}\sum_{m=1}^{3}\sum_{a=1}^{3}v_{L,a}Y_{\nu,al}\sum_{b=1}^{3}Y^{*}_{\nu,bm}Z^{H}_{j5+b}Z^{H}_{i2+l}Z^{H}_{k2+m}$$

$$+4\sum_{l=1}^{3}\sum_{m=1}^{3}\sum_{a=1}^{3}Y^{*}_{\nu,al}v_{L,a}\sum_{b=1}^{3}Y_{\nu,bm}Z^{H}_{j5+b}Z^{H}_{i2+l}Z^{H}_{k2+m}-4\sum_{l=1}^{3}\sum_{m=1}^{3}v_{Rl}\lambda^{*}_{l}\sum_{a=1}^{3}Y_{\nu,am}Z^{H}_{i5+a}Z^{H}_{j1}Z^{H}_{k2+m}$$

$$
+ 8\sum_{l=1}^{3}\sum_{m=1}^{3} v_{Rl}\lambda_l\lambda_m^* Z_{i1}^H Z_{j1}^H Z_{k2+m}^H - 2\sqrt{2}\sum_{l=1}^{3} T_{\lambda,l}^* Z_{i2}^H Z_{j1}^H Z_{k2+l}^H
$$

$$
+ 8v_d\sum_{l=1}^{3}\sum_{m=1}^{3} \lambda_l\lambda_m^* Z_{i2+l}^H Z_{j1}^H Z_{k2+m}^H - 4\sum_{l=1}^{3}\sum_{m=1}^{3}\lambda_l^*\sum_{a=1}^{3} v_{L,a}Y_{\nu,am} Z_{i2+l}^H Z_{j1}^H Z_{k2+m}^H
$$

$$
+ 2\sqrt{2}\sum_{l=1}^{3}\sum_{a=1}^{3} T_{\nu,al}^* Z_{i5+a}^H Z_{j2}^H Z_{k2+l}^H + 4\sum_{l=1}^{3}\sum_{m=1}^{3}\sum_{n=1}^{3} v_{Rl}\kappa_{lmn}^*\sum_{a=1}^{3} Y_{\nu,am} Z_{i5+a}^H Z_{j2}^H Z_{k2+n}^H
$$

$$
+ 2\sqrt{2}\sum_{l=1}^{3}\sum_{a=1}^{3} Z_{i5+a}^H T_{\nu,al} Z_{j2}^H Z_{k2+l}^H - 2\sqrt{2}\sum_{l=1}^{3} T_{\lambda,l}^* Z_{i1}^H Z_{j2}^H Z_{k2+l}^H + 8\sum_{l=1}^{3}\sum_{m=1}^{3} v_{Rl}\lambda_l\lambda_m^* Z_{i2}^H Z_{j2}^H Z_{k2+m}^H
$$

$$
+ 8\sum_{l=1}^{3} v_{Rl}\sum_{a=1}^{3} Y_{\nu,al}Y_{\nu,am}^* Z_{i2}^H Z_{j2}^H Z_{k2+m}^H + 8v_u\sum_{l=1}^{3}\sum_{m=1}^{3}\lambda_l\lambda_m^* Z_{i2+l}^H Z_{j2}^H Z_{k2+m}^H
$$

$$
+ 8\sum_{l=1}^{3}\sum_{m=1}^{3} v_u\sum_{a=1}^{3} Y_{\nu,a1}Y_{\nu,am}^* Z_{i2+l}^H Z_{j2}^H Z_{k2+m}^H + 4\sum_{l=1}^{3}\sum_{m=1}^{3}\sum_{n=1}^{3}\kappa_{lmn}^*\sum_{a=1}^{3} v_{L,a}Y_{\nu,al} Z_{i2+m}^H Z_{j2}^H Z_{k2+n}^H
$$

$$
+ 4v_u\sum_{l=1}^{3}\sum_{m=1}^{3}\sum_{n=1}^{3}\kappa_{lmn}^*\sum_{a=1}^{3} Y_{\nu,al} Z_{i5+a}^H Z_{j2+m}^H Z_{k2+n}^H - 4v_d\sum_{l=1}^{3}\sum_{m=1}^{3}\lambda_l^*\sum_{a=1}^{3} Y_{\nu,am} Z_{i5+a}^H Z_{j2+l}^H Z_{k2+m}^H
$$

$$
+ 4\sum_{l=1}^{3}\sum_{m=1}^{3}\sum_{a=1}^{3} v_{L,a}Y_{\nu,al}\sum_{b=1}^{3} Y_{\nu,bm}^* Z_{i5+b}^H Z_{j2+l}^H Z_{k2+m}^H + 4\sum_{l=1}^{3}\sum_{m=1}^{3}\sum_{a=1}^{3} Y_{\nu,al}^* v_{L,a}\sum_{b=1}^{3} Y_{\nu,bm} Z_{i5+b}^H Z_{j2+l}^H Z_{k2+m}^H
$$

$$
+ 8v_d\sum_{l=1}^{3}\sum_{m=1}^{3}\lambda_l\lambda_m^* Z_{i1}^H Z_{j2+l}^H Z_{k2+m}^H - 4\sum_{l=1}^{3}\sum_{m=1}^{3}\lambda_l^*\sum_{a=1}^{3} v_{L,a}Y_{\nu,am} Z_{i1}^H Z_{j2+l}^H Z_{k2+m}^H
$$

$$
+ 8v_u\sum_{l=1}^{3}\sum_{m=1}^{3}\lambda_1\lambda_m^* Z_{i2}^H Z_{j2+l}^H Z_{k2+m}^H
$$

$$
+ 8v_u\sum_{l=1}^{3}\sum_{m=1}^{3}\sum_{a=1}^{3} Y_{\nu,al}Y_{\nu,am}^* Z_{i2}^H Z_{j2+l}^H Z_{k2+m}^H + 4\sum_{l=1}^{3}\sum_{m=1}^{3}\sum_{n=1}^{3}\kappa_{lmn}^*\sum_{a=1}^{3} v_{L,a}Y_{\nu,al} Z_{i2}^H Z_{j2+m}^H Z_{k2+n}^H
$$

$$
+ 48\sum_{l=1}^{3}\sum_{m=1}^{3}\sum_{n=1}^{3}\sum_{q=1}^{3} v_{Rl}\sum_{o=1}^{3}\kappa_{lmq}\kappa_{qno}^* Z_{i2+m}^H Z_{j2+n}^H Z_{k2+o}^H + 4\sum_{l=1}^{3}\sum_{m=1}^{3}\sum_{n=1}^{3}\sqrt{2}T_{\kappa,lmn}^* Z_{i2+l}^H Z_{j2+m}^H Z_{k2+n}^H
$$

$$
+ 4\sum_{l=1}^{3}\sum_{m=1}^{3}\sum_{n=1}^{3} v_{Rl}\sum_{a=1}^{3} Y_{\nu,am}^* Z_{k5+a}^H Z_{i2+n}^H Z_{j2}^H\kappa_{lmn}
$$

$$
+ 4\sum_{l=1}^{3}\sum_{m=1}^{3}\sum_{n=1}^{3} v_{Rl}\sum_{a=1}^{3} Y_{\nu,am}^* Z_{k5+a}^H Z_{i2}^H Z_{j2+n}^H\kappa_{lmn} + 4v_u\sum_{l=1}^{3}\sum_{m=1}^{3}\sum_{n=1}^{3}\sum_{a=1}^{3} Y_{\nu,al}^* Z_{k5+a}^H Z_{i2+m}^H Z_{j2+n}^H\kappa_{lmn}
$$

$$
- 4\sum_{l=1}^{3}\sum_{m=1}^{3}\sum_{n=1}^{3} v_{Rl}\lambda_m^* Z_{i2+n}^H Z_{j2}^H Z_{k1}^H\kappa_{lmn} - 4\sum_{l=1}^{3}\sum_{m=1}^{3}\sum_{n=1}^{3} v_{Rl}\lambda_m^* Z_{i2}^H Z_{j2+n}^H Z_{k1}^H\kappa_{lmn}
$$

$$
- 4v_u\sum_{l=1}^{3}\sum_{m=1}^{3}\sum_{n=1}^{3}\lambda_l^* Z_{i2+m}^H Z_{j2+n}^H Z_{k1}^H\kappa_{lmn}
$$

$$
+ 4\sum_{l=1}^{3}\sum_{m=1}^{3}\sum_{n=1}^{3} v_{Rl}\sum_{a=1}^{3} Y_{\nu,am}^* Z_{j5+a}^H Z_{i2+n}^H Z_{k2}^H\kappa_{lmn} - 4\sum_{l=1}^{3}\sum_{m=1}^{3}\sum_{n=1}^{3} v_{Rl}\lambda_m^* Z_{i2+n}^H Z_{j1}^H Z_{k2}^H\kappa_{lmn}
$$

$$
+ 4\sum_{l=1}^{3}\sum_{m=1}^{3}\sum_{n=1}^{3} v_{Rl}\sum_{a=1}^{3} Y_{\nu,am}^* Z_{i5+a}^H Z_{j2+n}^H Z_{k2}^H\kappa_{lmn} - 4\sum_{l=1}^{3}\sum_{m=1}^{3}\sum_{n=1}^{3} v_{Rl}\lambda_m^* Z_{i1}^H Z_{j2+n}^H Z_{k2}^H\kappa_{lmn}
$$

$$
- 4v_d\sum_{l=1}^{3}\sum_{m=1}^{3}\sum_{n=1}^{3}\lambda_l^* Z_{i2+m}^H Z_{j2+n}^H Z_{k2}^H\kappa_{lmn}
$$

$$
+ 4\sum_{l=1}^{3}\sum_{m=1}^{3}\sum_{n=1}^{3}\sum_{a=1}^{3} Y_{\nu,al}^* v_{L,a} Z_{i2+m}^H Z_{j2+n}^H Z_{k2}^H\kappa_{lmn} + 4\sum_{l=1}^{3}\sum_{m=1}^{3}\sum_{n=1}^{3} v_{Rl}\sum_{a=1}^{3} Y_{\nu,am}^* Z_{j5+a}^H Z_{i2}^H Z_{k2+n}^H\kappa_{lmn}
$$

$$+4v_u\sum_{l=1}^{3}\sum_{m=1}^{3}\sum_{n=1}^{3}\sum_{a=1}^{3}Y^*_{\nu,al}Z^H_{j5+a}Z^H_{i2+m}Z^H_{k2+n}\kappa_{lmn}-4\sum_{l=1}^{3}\sum_{m=1}^{3}\sum_{n=1}^{3}v_{Rl}\lambda^*_m Z^H_{i2}Z^H_{j1}Z^H_{k2+n}\kappa_{lmn}$$
$$-4v_u\sum_{l=1}^{3}\sum_{m=1}^{3}\sum_{n=1}^{3}\lambda^*_l Z^H_{i2+m}Z^H_{j1}Z^H_{k2+n}\kappa_{lmn}$$
$$+4\sum_{l=1}^{3}\sum_{m=1}^{3}\sum_{n=1}^{3}v_{Rl}\sum_{a=1}^{3}Y^*_{\nu,am}Z^H_{i5+a}Z^H_{j2}Z^H_{k2+n}\kappa_{lmn}-4\sum_{l=1}^{3}\sum_{m=1}^{3}\sum_{n=1}^{3}v_{Rl}\lambda^*_m Z^H_{i1}Z^H_{j2}Z^H_{k2+n}\kappa_{lmn}$$
$$-4v_d\sum_{l=1}^{3}\sum_{m=1}^{3}\sum_{n=1}^{3}\lambda^*_l Z^H_{i2+m}Z^H_{j2}Z^H_{k2+n}\kappa_{lmn}$$
$$+4\sum_{l=1}^{3}\sum_{m=1}^{3}\sum_{n=1}^{3}\sum_{a=1}^{3}Y^*_{\nu,al}v_{L,a}Z^H_{i2+m}Z^H_{j2}Z^H_{k2+n}\kappa_{lmn}+4v_u\sum_{l=1}^{3}\sum_{m=1}^{3}\sum_{n=1}^{3}\sum_{a=1}^{3}Y^*_{\nu,al}Z^H_{i5+a}Z^H_{j2+m}Z^H_{k2+n}\kappa_{lmn}$$
$$-4v_u\sum_{l=1}^{3}\sum_{m=1}^{3}\sum_{n=1}^{3}\lambda^*_l Z^H_{i1}Z^H_{j2+m}Z^H_{k2+n}\kappa_{lmn}-4v_d\sum_{l=1}^{3}\sum_{m=1}^{3}\sum_{n=1}^{3}\lambda^*_l Z^H_{i2}Z^H_{j2+m}Z^H_{k2+n}\kappa_{lmn}$$
$$+4\sum_{l=1}^{3}\sum_{m=1}^{3}\sum_{n=1}^{3}\sum_{a=1}^{3}Y^*_{\nu,al}v_{L,a}Z^H_{i2}Z^H_{j2+m}Z^H_{k2+n}\kappa_{lmn}$$
$$-4v_u\sum_{l=1}^{3}\sum_{a=1}^{3}Y^*_{\nu,al}Z^H_{k5+a}Z^H_{i2}Z^H_{j1}\lambda_l-4\sum_{l=1}^{3}\sum_{m=1}^{3}v_{Rl}\sum_{a=1}^{3}Y^*_{\nu,al}Z^H_{k5+a}Z^H_{i2+m}Z^H_{j1}\lambda_m$$
$$-4v_u\sum_{l=1}^{3}\sum_{a=1}^{3}Y^*_{\nu,al}Z^H_{k5+a}Z^H_{i1}Z^H_{j2}\lambda_l-4v_d\sum_{l=1}^{3}\sum_{a=1}^{3}Y^*_{\nu,al}Z^H_{k5+a}Z^H_{i2}Z^H_{j2}\lambda_l$$
$$-4\sum_{l=1}^{3}\sum_{m=1}^{3}v_{Rl}\sum_{a=1}^{3}Y^*_{\nu,al}Z^H_{k5+a}Z^H_{i1}Z^H_{j2+m}\lambda_m-4v_d\sum_{l=1}^{3}\sum_{m=1}^{3}\sum_{a=1}^{3}Y^*_{\nu,al}Z^H_{k5+a}Z^H_{i2+l}Z^H_{j2+m}\lambda_m$$
$$-4v_u\sum_{l=1}^{3}\sum_{a=1}^{3}Y^*_{\nu,al}Z^H_{j5+a}Z^H_{i2}Z^H_{k1}\lambda_l-4\sum_{l=1}^{3}\sum_{m=1}^{3}v_{Rl}\sum_{a=1}^{3}Y^*_{\nu,am}Z^H_{j5+a}Z^H_{i2+l}Z^H_{k1}\lambda_m$$
$$-4\sum_{l=1}^{3}v_u\sum_{a=1}^{3}Y^*_{\nu,al}Z^H_{i5+a}Z^H_{j2}Z^H_{k1}\lambda_l-4\sum_{l=1}^{3}\sum_{a=1}^{3}Y^*_{\nu,al}v_{L,a}Z^H_{i2}Z^H_{j2}Z^H_{k1}\lambda_l$$
$$-4\sum_{l=1}^{3}\sum_{m=1}^{3}\sum_{n=1}^{3}v_{Rl}\kappa^*_{lmn}Z^H_{i2+m}Z^H_{j2}Z^H_{k1}\lambda_n-4\sum_{l=1}^{3}\sum_{m=1}^{3}v_{Rl}\sum_{a=1}^{3}Y^*_{\nu,al}Z^H_{i5+a}Z^H_{j2+m}Z^H_{k1}\lambda_m$$
$$-4\sum_{l=1}^{3}\sum_{m=1}^{3}\sum_{n=1}^{3}v_{Rl}\kappa^*_{lmn}Z^H_{i2}Z^H_{j2+m}Z^H_{k1}\lambda_n$$
$$-4v_u\sum_{l=1}^{3}\sum_{m=1}^{3}\sum_{n=1}^{3}\kappa^*_{lmn}Z^H_{i2+l}Z^H_{j2+m}Z^H_{k1}\lambda_n-4\sum_{l=1}^{3}\sum_{m=1}^{3}\sum_{a=1}^{3}Y^*_{\nu,al}v_{L,a}Z^H_{i2+l}Z^H_{j2+m}Z^H_{k1}\lambda_m$$
$$-4\sum_{l=1}^{3}v_u\sum_{a=1}^{3}Y^*_{\nu,al}Z^H_{j5+a}Z^H_{i1}Z^H_{k2}\lambda_l-4v_d\sum_{l=1}^{3}\sum_{a=1}^{3}Y^*_{\nu,al}Z^H_{j5+a}Z^H_{i2}Z^H_{k2}\lambda_l$$
$$-4v_u\sum_{l=1}^{3}\sum_{a=1}^{3}Y^*_{\nu,al}Z^H_{i5+a}Z^H_{j1}Z^H_{k2}\lambda_l-4\sum_{l=1}^{3}\sum_{a=1}^{3}Y^*_{\nu,al}v_{L,a}Z^H_{i2}Z^H_{j1}Z^H_{k2}\lambda_l$$
$$-4\sum_{l=1}^{3}\sum_{m=1}^{3}\sum_{n=1}^{3}v_{Rl}\kappa^*_{lmn}Z^H_{i2+m}Z^H_{j1}Z^H_{k2}\lambda_n-4v_d\sum_{l=1}^{3}\sum_{a=1}^{3}Y^*_{\nu,al}Z^H_{i5+a}Z^H_{j2}Z^H_{k2}\lambda_l$$
$$-4\sum_{l=1}^{3}\sum_{a=1}^{3}Y^*_{\nu,al}v_{L,a}Z^H_{i1}Z^H_{j2}Z^H_{k2}\lambda_l-4\sum_{l=1}^{3}\sum_{m=1}^{3}\sum_{n=1}^{3}v_{Rl}\kappa^*_{lmn}Z^H_{i1}Z^H_{j2+m}Z^H_{k2}\lambda_n$$
$$-4v_d\sum_{l=1}^{3}\sum_{m=1}^{3}\sum_{n=1}^{3}\kappa^*_{lmn}Z^H_{i2+l}Z^H_{j2+m}Z^H_{k2}\lambda_n$$

$$
\begin{aligned}
&- 4\sum_{l=1}^{3}\sum_{m=1}^{3} v_{Rl}\sum_{a=1}^{3} Y^{*}_{\nu,am} Z^{H}_{j5+a} Z^{H}_{i1} Z^{H}_{km}\lambda_l - 4v_d\sum_{l=1}^{3}\sum_{l=1}^{3}\sum_{a=1}^{3} Y^{*}_{\nu,al} Z^{H}_{j5+a} Z^{H}_{i2+l} Z^{H}_{k2+m}\lambda_m \\
&- 4\sum_{l=1}^{3}\sum_{m=1}^{3} v_{Rl}\sum_{a=1}^{3} Y^{*}_{\nu,al} Z^{H}_{i5+a} Z^{H}_{j1} Z^{H}_{k2+m}\lambda_m - 4\sum_{l=1}^{3}\sum_{l=1}^{3}\sum_{l=1}^{3} v_{Rl}\kappa^{*}_{lmn} Z^{H}_{i2} Z^{H}_{j1} Z^{H}_{k2+m}\lambda_n \\
&- 4\sum_{l=1}^{3}\sum_{m=1}^{3}\sum_{n=1}^{3} v_u\kappa^{*}_{lmn} Z^{H}_{i2+l} Z^{H}_{j1} Z^{H}_{k2+m}\lambda_n \\
&- 4\sum_{l=1}^{3}\sum_{m=1}^{3}\sum_{a=1}^{3} Y^{*}_{\nu,al} v_{L,a} Z^{H}_{i2+l} Z^{H}_{j1} Z^{H}_{k2+m}\lambda_m - 4\sum_{l=1}^{3}\sum_{l=1}^{3}\sum_{l=1}^{3} v_{Rl}\kappa^{*}_{lmn} Z^{H}_{i1} Z^{H}_{j2} Z^{H}_{k2+m}\lambda_n \\
&- 4v_d\sum_{l=1}^{3}\sum_{m=1}^{3}\sum_{n=1}^{3} \kappa^{*}_{lmn} Z^{H}_{i2+l} Z^{H}_{j2} Z^{H}_{k2+m}\lambda_n \\
&- 4v_d\sum_{l=1}^{3}\sum_{m=1}^{3}\sum_{a=1}^{3} Y^{*}_{\nu,al} Z^{H}_{i5+a} Z^{H}_{j2+l} Z^{H}_{k2+n}\lambda_n - 4v_u\sum_{l=1}^{3}\sum_{n=1}^{3}\sum_{m=1}^{3} \kappa^{*}_{lmn} Z^{H}_{i1} Z^{H}_{j2+l} Z^{H}_{k2+m}\lambda_n \\
&- 4\sum_{l=1}^{3}\sum_{m=1}^{3}\sum_{a=1}^{3} Y^{*}_{\nu,al} v_{L,a} Z^{H}_{i1} Z^{H}_{j2+l} Z^{H}_{k2+m}\lambda_m - 4v_d\sum_{l=1}^{3}\sum_{m=1}^{3}\sum_{n=1}^{3} \kappa^{*}_{lmn} Z^{H}_{i2} Z^{H}_{j2+l} Z^{H}_{k2+m}\lambda_n \\
&+ 4\sqrt{2}\sum_{l=1}^{3}\sum_{m=1}^{3}\sum_{n=1}^{3} Z^{H}_{i2+l} Z^{H}_{j2+m} Z^{H}_{k2+n} T_{\kappa,lmn} \\
&- 2\sqrt{2}\sum_{l=1}^{3} Z^{H}_{i2+l} Z^{H}_{j2} Z^{H}_{k1} T_{\lambda,l} - 2\sqrt{2}\sum_{l=1}^{3} Z^{H}_{i2} Z^{H}_{j2+l} Z^{H}_{k1} T_{\lambda,l} - 2\sqrt{2}\sum_{l=1}^{3} Z^{H}_{i2+l} Z^{H}_{j1} Z^{H}_{k2} T_{\lambda,l} \\
&- 2\sqrt{2}\sum_{l=1}^{3} Z^{H}_{i1} Z^{H}_{j2+l} Z^{H}_{k2} T_{\lambda,l} - 2\sqrt{2}\sum_{l=1}^{3} Z^{H}_{i2} Z^{H}_{j1} Z^{H}_{k2+l} T_{\lambda,l} - 2\sqrt{2}\sum_{l=1}^{3} Z^{H}_{i1} Z^{H}_{j2} Z^{H}_{k2+l} T_{\lambda,1}\Big)
\end{aligned}
\tag{C.1}
$$

Bibliography

[1] **ATLAS** Collaboration, G. Aad *et al.*, "Observation of a new particle in the search for the Standard Model Higgs boson with the ATLAS detector at the LHC," *Phys. Lett.* **B716** (2012) 1–29, arXiv:1207.7214 [hep-ex].

[2] **CMS** Collaboration, S. Chatrchyan *et al.*, "Observation of a new boson at a mass of 125 GeV with the CMS experiment at the LHC," *Phys. Lett.* **B716** (2012) 30, arXiv:1207.7235 [hep-ex].

[3] J. Wess and J. A. Bagger, *Supersymmetry and supergravity; 2nd ed.* Princeton Series in Physics. Princeton Univ. Press, Princeton, NJ, 1992. https://cds.cern.ch/record/320631.

[4] M. Drees, R. Godbole, and P. Roy, *Theory and phenomenology of Sparticles: an account of four-dimensional N=1 supersymmetry in high-energy physics.* World Scientific, Singapore, 2004. https://cds.cern.ch/record/873465.

[5] H. Müller-Kirsten, *Introduction to supersymmetry.* World scientific lecture notes in physics. World Scientific, New Jersey [etc., 2nd ed. ed., 2010.

[6] S. P. Martin, "A Supersymmetry primer," *Adv. Ser. Direct. High Energy Phys. 18 (1998) 1* (1997) , arXiv:hep-ph/9709356 [hep-ph].

[7] **BaBar** Collaboration, J. P. Lees *et al.*, "Measurement of an Excess of $\bar{B} \to D^{(*)}\tau^-\bar{\nu}_\tau$ Decays and Implications for Charged Higgs Bosons," *Phys. Rev.* **D88** no. 7, (2013) 072012, arXiv:1303.0571 [hep-ex].

[8] **LHCb** Collaboration, R. Aaij *et al.*, "Test of lepton universality using $B^+ \to K^+\ell^+\ell^-$ decays," *Phys. Rev. Lett.* **113** (2014) 151601, arXiv:1406.6482 [hep-ex].

[9] **Belle** Collaboration, S. Hirose, "Measurement of $\bar{B} \to D^{(*)}\tau^-\bar{\nu}_\tau$ at Belle," *Nucl. Part. Phys. Proc.* **287-288** (2017) 185–188.

[10] **LHCb** Collaboration, R. Aaij *et al.*, "Measurement of the ratio of branching fractions $\mathcal{B}(\bar{B}^0 \to D^{*+}\tau^-\bar{\nu}_\tau)/\mathcal{B}(\bar{B}^0 \to D^{*+}\mu^-\bar{\nu}_\mu)$," *Phys. Rev. Lett.* **115** no. 11, (2015) 111803, arXiv:1506.08614 [hep-ex]. [Erratum: Phys. Rev. Lett.115,no.15,159901(2015)].

[11] **Belle** Collaboration, S. Hirose *et al.*, "Measurement of the τ lepton polarization and $R(D^*)$ in the decay $\bar{B} \to D^*\tau^-\bar{\nu}_\tau$," *Phys. Rev. Lett.* **118** no. 21, (2017) 211801, arXiv:1612.00529 [hep-ex].

[12] **LHCb** Collaboration, R. Aaij *et al.*, "Test of Lepton Flavor Universality by the measurement of the $B^0 \to D^{*-}\tau^+\nu_\tau$ branching fraction using three-prong τ decays," *Phys. Rev.* **D97** no. 7, (2018) 072013, arXiv:1711.02505 [hep-ex].

[13] **LHCb** Collaboration, R. Aaij *et al.*, "Test of lepton universality with $B^0 \to K^{*0}\ell^+\ell^-$ decays," *JHEP* **08** (2017) 055, arXiv:1705.05802 [hep-ex].

[14] **LHCb** Collaboration, R. Aaij *et al.*, "Measurement of the ratio of branching fractions $\mathcal{B}(B_c^+ \to J/\psi\tau^+\nu_\tau)/\mathcal{B}(B_c^+ \to J/\psi\mu^+\nu_\mu)$," *Phys. Rev. Lett.* **120** no. 12, (2018) 121801, arXiv:1711.05623 [hep-ex].

[15] **Muon g-2 Collaboration** Collaboration, G. W. Bennett, B. Bousquet, H. N. Brown, *et al.*, "Final report of the e821 muon anomalous magnetic moment measurement at bnl," *Phys. Rev. D* **73** (Apr, 2006) 072003. https://link.aps.org/doi/10.1103/PhysRevD.73.072003.

[16] S. Weinberg, "Implications of dynamical symmetry breaking," *Phys. Rev. D* **13** (Feb, 1976) 974–996. http://link.aps.org/doi/10.1103/PhysRevD.13.974.

[17] S. Weinberg, "Implications of dynamical symmetry breaking: An addendum," *Phys. Rev. D* **19** (Feb, 1979) 1277–1280. http://link.aps.org/doi/10.1103/PhysRevD.19.1277.

[18] E. Gildener, "Gauge-symmetry hierarchies," *Phys. Rev. D* **14** (Sep, 1976) 1667–1672. http://link.aps.org/doi/10.1103/PhysRevD.14.1667.

[19] L. Susskind, "Dynamics of spontaneous symmetry breaking in the weinberg-salam theory," *Phys. Rev. D* **20** (Nov, 1979) 2619–2625. http://link.aps.org/doi/10.1103/PhysRevD.20.2619.

[20] M. Schmaltz and D. Tucker-Smith, "Little Higgs review," *Ann. Rev. Nucl. Part. Sci.* **55** (2005) 229–270, arXiv:hep-ph/0502182 [hep-ph].

[21] D. B. Kaplan, H. Georgi, and S. Dimopoulos, "Composite higgs scalars," *Physics Letters B* **136** no. 3, (1984) 187 – 190. http://www.sciencedirect.com/science/article/pii/037026938491178X.

[22] H. Georgi and D. B. Kaplan, "Composite higgs and custodial su(2)," *Physics Letters B* **145** no. 3, (1984) 216 – 220. http://www.sciencedirect.com/science/article/pii/0370269384903411.

[23] M. J. Dugan, H. Georgi, and D. B. Kaplan, "Anatomy of a composite higgs model," *Nuclear Physics B* **254** (1985) 299 – 326. http://www.sciencedirect.com/science/article/pii/0550321385902214.

[24] N. Arkani-Hamed, S. Dimopoulos, and G. R. Dvali, "The Hierarchy problem and new dimensions at a millimeter," *Phys. Lett.* **B429** (1998) 263–272, arXiv:hep-ph/9803315 [hep-ph].

[25] N. Arkani-Hamed, S. Dimopoulos, and G. R. Dvali, "Phenomenology, astrophysics and cosmology of theories with submillimeter dimensions and TeV scale quantum gravity," *Phys. Rev.* **D59** (1999) 086004, arXiv:hep-ph/9807344 [hep-ph].

[26] L. Randall and R. Sundrum, "A Large mass hierarchy from a small extra dimension," *Phys. Rev. Lett.* **83** (1999) 3370–3373, arXiv:hep-ph/9905221 [hep-ph].

[27] S. Coleman and J. Mandula, "All possible symmetries of the s matrix," *Phys. Rev.* **159** (Jul, 1967) 1251–1256. https://link.aps.org/doi/10.1103/PhysRev.159.1251.

[28] R. Haag, J. T. Łopuszański, and M. Sohnius, "All possible generators of supersymmetries of the s-matrix," *Nuclear Physics B* **88** no. 2, (1975) 257 – 274. http://www.sciencedirect.com/science/article/pii/0550321375902795.

[29] A. H. Chamseddine, R. Arnowitt, and P. Nath, "Locally supersymmetric grand unification," *Phys. Rev. Lett.* **49** (Oct, 1982) 970–974. https://link.aps.org/doi/10.1103/PhysRevLett.49.970.

[30] R. Barbieri, S. Ferrara, and C. Savoy, "Gauge models with spontaneously broken local supersymmetry," *Physics Letters B* **119** no. 4, (1982) 343 – 347. http://www.sciencedirect.com/science/article/pii/0370269382906852.

[31] L. Ibáñez, "Locally supersymmetric su(5) grand unification," *Physics Letters B* **118** no. 1, (1982) 73 – 78. http://www.sciencedirect.com/science/article/pii/0370269382906049.

[32] L. Hall, J. Lykken, and S. Weinberg, "Supergravity as the messenger of supersymmetry breaking," *Phys. Rev. D* **27** (May, 1983) 2359–2378. https://link.aps.org/doi/10.1103/PhysRevD.27.2359.

[33] N. Ohta, "Grand unified theories based on local supersymmetry," *Progress of Theoretical Physics* **70** no. 2, (1983) 542–549. http://dx.doi.org/10.1143/PTP.70.542.

[34] J. Ellis, D. Nanopoulos, and K. Tamvakis, "Grand unification in simple supergravity," *Physics Letters B* **121** no. 2, (1983) 123 – 129. http://www.sciencedirect.com/science/article/pii/0370269383909000.

[35] L. Alvarez-Gaumé, J. Polchinski, and M. B. Wise, "Minimal low-energy supergravity," *Nuclear Physics B* **221** no. 2, (1983) 495 – 523. http://www.sciencedirect.com/science/article/pii/0550321383905916.

[36] "Supersymmetric extension of the $su(3) \times su(2) \times u(1)$ model,".

[37] M. Dine and W. Fischler, "A phenomenological model of particle physics based on supersymmetry," *Physics Letters B* **110** no. 3, (1982) 227 – 231. http://www.sciencedirect.com/science/article/pii/0370269382912412.

[38] L. Alvarez-Gaumé, M. Claudson, and M. B. Wise, "Low-energy supersymmetry," *Nuclear Physics B* **207** no. 1, (1982) 96 – 110. http://www.sciencedirect.com/science/article/pii/0550321382901389.

[39] M. Dine and A. E. Nelson, "Dynamical supersymmetry breaking at low-energies," *Phys. Rev.* **D48** (1993) 1277–1287, arXiv:hep-ph/9303230 [hep-ph].

[40] M. Dine, A. E. Nelson, and Y. Shirman, "Low-energy dynamical supersymmetry breaking simplified," *Phys. Rev.* **D51** (1995) 1362–1370, arXiv:hep-ph/9408384 [hep-ph].

[41] M. Dine, A. E. Nelson, Y. Nir, and Y. Shirman, "New tools for low-energy dynamical supersymmetry breaking," *Phys. Rev.* **D53** (1996) 2658–2669, arXiv:hep-ph/9507378 [hep-ph].

[42] V. Rubakov and M. Shaposhnikov, "Do we live inside a domain wall?," *Physics Letters B* **125** no. 2, (1983) 136 – 138. http://www.sciencedirect.com/science/article/pii/0370269383912534.

[43] V. Rubakov and M. Shaposhnikov, "Extra space-time dimensions: Towards a solution to the cosmological constant problem," *Physics Letters B* **125** no. 2, (1983) 139 – 143. http://www.sciencedirect.com/science/article/pii/0370269383912546.

[44] L. Randall and R. Sundrum, "An Alternative to compactification," *Phys. Rev. Lett.* **83** (1999) 4690–4693, arXiv:hep-th/9906064 [hep-th].

[45] E. A. Mirabelli and M. E. Peskin, "Transmission of supersymmetry breaking from a four-dimensional boundary," *Phys. Rev.* **D58** (1998) 065002, arXiv:hep-th/9712214 [hep-th].

[46] D. E. Kaplan, G. D. Kribs, and M. Schmaltz, "Supersymmetry breaking through transparent extra dimensions," *Phys. Rev.* **D62** (2000) 035010, arXiv:hep-ph/9911293 [hep-ph].

[47] Z. Chacko, M. A. Luty, A. E. Nelson, and E. Ponton, "Gaugino mediated supersymmetry breaking," *JHEP* **01** (2000) 003, arXiv:hep-ph/9911323 [hep-ph].

[48] M. Schmaltz and W. Skiba, "Minimal gaugino mediation," *Phys. Rev.* **D62** (2000) 095005, arXiv:hep-ph/0001172 [hep-ph].

[49] M. Schmaltz and W. Skiba, "The Superpartner spectrum of gaugino mediation," *Phys. Rev.* **D62** (2000) 095004, arXiv:hep-ph/0004210 [hep-ph].

[50] L. Randall and R. Sundrum, "Out of this world supersymmetry breaking," *Nucl. Phys.* **B557** (1999) 79–118, arXiv:hep-th/9810155 [hep-th].

[51] G. F. Giudice, M. A. Luty, H. Murayama, and R. Rattazzi, "Gaugino mass without singlets," *JHEP* **12** (1998) 027, arXiv:hep-ph/9810442 [hep-ph].

[52] "Renormalization and symmetry: a review for non-specialists," pp. 99–112.

[53] L. Girardello and M. Grisaru, "Soft breaking of supersymmetry," *Nuclear Physics B* **194** no. 1, (1982) 65 – 76. http://www.sciencedirect.com/science/article/pii/0550321382905120.

[54] G. 't Hooft, "Symmetry breaking through bell-jackiw anomalies," *Phys. Rev. Lett.* **37** (Jul, 1976) 8–11. http://link.aps.org/doi/10.1103/PhysRevLett.37.8.

[55] L. E. Ibáñez and G. G. Ross, "Discrete gauge symmetries and the origin of baryon and lepton number conservation in supersymmetric versions of the standard model," *Nuclear Physics B* **368** no. 1, (1992) 3 – 37. http://www.sciencedirect.com/science/article/pii/055032139290195H.

[56] H. K. Dreiner, C. Luhn, and M. Thormeier, "What is the discrete gauge symmetry of the minimal supersymmetric standard model," *Phys. Rev. D* **73** (Apr, 2006) 075007. http://link.aps.org/doi/10.1103/PhysRevD.73.075007.

[57] A. Kundu and J. P. Saha, "Constraints on R-parity violating supersymmetry from neutral meson mixing," *Phys. Rev.* **D70** (2004) 096002, arXiv:hep-ph/0403154 [hep-ph].

[58] R. Barbier *et al.*, "R-parity violating supersymmetry," *Phys. Rept.* **420** (2005) 1, arXiv:hep-ph/0406039 [hep-ph].

[59] **HFLAV** Collaboration, Y. Amhis *et al.*, "Averages of b-hadron, c-hadron, and τ-lepton properties as of summer 2016," *Eur. Phys. J.* **C77** no. 12, (2017) 895, arXiv:1612.07233 [hep-ex].

[60] **MEG** Collaboration, J. Adam *et al.*, "New limit on the lepton-flavour violating decay $\mu^+ \to e^+\gamma$," *Phys. Rev. Lett.* **107** (2011) 171801, arXiv:1107.5547 [hep-ex].

[61] U. Ellwanger, C. Hugonie, and A. M. Teixeira, "The next-to-minimal supersymmetric standard model," *Phys. Rept.* **496** (2010) 1, arXiv:0910.1785 [hep-ph].

[62] D. E. López-Fogliani and C. Muñoz, "Proposal for a supersymmetric standard model," *Phys. Rev. Lett.* **97** (2006) 041801, arXiv:hep-ph/0508297 [hep-ph].

[63] N. Escudero, D. E. López-Fogliani, C. Muñoz, and R. R. de Austri, "Analysis of the parameter space and spectrum of the $\mu\nu$SSM," *JHEP* **12** (2008) 099, arXiv:0810.1507 [hep-ph].

[64] D. E. López-Fogliani and C. Muñoz, "On a reinterpretation of the Higgs field in supersymmetry and a proposal for new quarks," *Phys. Lett.* **B771** (2017) 136, arXiv:1701.02652 [hep-ph].

[65] J. A. Aguilar-Saavedra, D. E. López-Fogliani, and C. Muñoz, "Novel signatures for vector-like quarks," arXiv:1705.02526 [hep-ph].

[66] N. Escudero, C. Muñoz, and A. M. Teixeira, "FCNCs in supersymmetric multi-Higgs doublet models," *Phys. Rev.* **D73** (2006) 055015, arXiv:hep-ph/0512046 [hep-ph].

[67] N. Escudero, C. Muñoz, and A. M. Teixeira, "Phenomenological viability of orbifold models with three Higgs families," *JHEP* **07** (2006) 041, arXiv:hep-ph/0512301 [hep-ph].

[68] N. Escudero, C. Muñoz, and A. M. Teixeira, "Lepton masses and mixings in orbifold models with three Higgs families," *JHEP* **12** (2007) 080, arXiv:0710.3672 [hep-ph].

[69] M. Chemtob, "Phenomenological constraints on broken R parity symmetry in supersymmetry models," *Prog. Part. Nucl. Phys.* **54** (2005) 71–191, arXiv:hep-ph/0406029 [hep-ph].

[70] H. K. Dreiner, K. Nickel, F. Staub, and A. Vicente, "New bounds on trilinear R-parity violation from lepton flavor violating observables," *Phys. Rev.* **D86** (2012) 015003, arXiv:1204.5925 [hep-ph].

[71] B. de Carlos and P. L. White, "R-parity violation effects through soft supersymmetry breaking terms and the renormalization group," *Phys. Rev.* **D54** (1996) 3427, arXiv:hep-ph/9602381 [hep-ph].

[72] F. Gabbiani, E. Gabrielli, A. Masiero, and L. Silvestrini, "A Complete analysis of FCNC and CP constraints in general SUSY extensions of the standard model," *Nucl. Phys.* **B477** (1996) 321, arXiv:hep-ph/9604387 [hep-ph].

[73] A. Brignole, L. E. Ibanez, and C. Munoz, "Soft supersymmetry breaking terms from supergravity and superstring models," *Adv. Ser. Direct. High Energy Phys.* **21** (2010) 244, arXiv:hep-ph/9707209 [hep-ph].

[74] J. Fidalgo, D. E. López-Fogliani, C. Muñoz, and R. Ruiz de Austri, "Neutrino physics and spontaneous CP violation in the $\mu\nu$SSM," *JHEP* **08** (2009) 105, arXiv:0904.3112 [hep-ph].

[75] J. E. Kim and H. P. Nilles, "The μ problem and the strong CP Problem," *Phys. Lett.* **B138** (1984) 150.

[76] P. Ghosh and S. Roy, "Neutrino masses and mixing, lightest neutralino decays and a solution to the μ problem in supersymmetry," *JHEP* **04** (2009) 069, arXiv:0812.0084 [hep-ph].

[77] A. Bartl, M. Hirsch, A. Vicente, S. Liebler, and W. Porod, "LHC phenomenology of the $\mu\nu$SSM," *JHEP* **05** (2009) 120, arXiv:0903.3596 [hep-ph].

[78] P. Ghosh, P. Dey, B. Mukhopadhyaya, and S. Roy, "Radiative contribution to neutrino masses and mixing in $\mu\nu$SSM," *JHEP* **05** (2010) 087, arXiv:1002.2705 [hep-ph].

[79] J. Fidalgo, D. E. López-Fogliani, C. Muñoz, and R. Ruiz de Austri, "The Higgs sector of the $\mu\nu$SSM and collider physics," *JHEP* **10** (2011) 020, arXiv:1107.4614 [hep-ph].

[80] P. Ghosh, D. E. López-Fogliani, V. A. Mitsou, C. Muñoz, and R. Ruiz de Austri, "Probing the $\mu\nu$SSM with light scalars, pseudoscalars and neutralinos from the decay of a SM-like Higgs boson at the LHC," *JHEP* **11** (2014) 102, arXiv:1410.2070 [hep-ph].

[81] P. Ghosh, D. E. López-Fogliani, V. A. Mitsou, C. Muñoz, and R. Ruiz de Austri, "Probing the μ-from-ν supersymmetric standard model with displaced multileptons from the decay of a Higgs boson at the LHC," *Phys. Rev.* **D88** (2013) 015009, arXiv:1211.3177 [hep-ph].

[82] M. C. Gonzalez-Garcia, M. Maltoni, and T. Schwetz, "Global Analyses of Neutrino Oscillation Experiments," *Nucl. Phys.* **B908** (2016) 199–217, arXiv:1512.06856 [hep-ph].

[83] D. V. Forero, M. Tortola, and J. W. F. Valle, "Neutrino oscillations refitted," *Phys. Rev.* **D90** no. 9, (2014) 093006, arXiv:1405.7540 [hep-ph].

[84] F. Capozzi, G. L. Fogli, E. Lisi, *et al.*, "Status of three-neutrino oscillation parameters, circa 2013," *Phys. Rev.* **D89** (2014) 093018, arXiv:1312.2878 [hep-ph].

[85] S. Borgani, A. Masiero, and M. Yamaguchi, "Light gravitinos as mixed dark matter," *Phys. Lett.* **B386** (1996) 189, arXiv:hep-ph/9605222 [hep-ph].

[86] F. Takayama and M. Yamaguchi, "Gravitino dark matter without R-parity," *Phys. Lett.* **B485** (2000) 388, arXiv:hep-ph/0005214 [hep-ph].

[87] K.-Y. Choi, D. E. López-Fogliani, C. Muñoz, and R. R. de Austri, "Gamma-ray detection from gravitino dark matter decay in the $\mu\nu$SSM," *JCAP* **03** (2010) 028, arXiv:0906.3681 [hep-ph].

[88] G. A. Gómez-Vargas, M. Fornasa, F. Zandanel, *et al.*, "CLUES on Fermi-LAT prospects for the extragalactic detection of $\mu\nu$SSM gravitino dark matter," *JCAP* **02** (2012) 001, arXiv:1110.3305 [astro-ph.HE].

[89] A. Albert, G. A. Gómez-Vargas, M. Grefe, *et al.*, "Search for 100 MeV to 10 GeV γ-ray lines in the Fermi-LAT data and implications for gravitino dark matter in $\mu\nu$SSM," *JCAP* **10** (2014) 023, arXiv:1406.3430 [astro-ph.HE].

[90] G. A. Gómez-Vargas, D. E. López-Fogliani, C. Muñoz, A. D. Perez, and R. Ruiz de Austri, "Search for sharp and smooth spectral signatures of $\mu\nu$SSM gravitino dark matter with Fermi-LAT," *JCAP* **1703** no. 03, (2017) 047, arXiv:1608.08640 [hep-ph].

[91] D. J. H. Chung and A. J. Long, "Electroweak Phase Transition in the $\mu\nu$SSM," *Phys. Rev.* **D81** (2010) 123531, arXiv:1004.0942 [hep-ph].

[92] I. Lara, D. E. López-Fogliani, C. Muñoz, *et al.*, "Looking for the left sneutrino LSP with displaced-vertex searches," *Phys. Rev.* **D98** no. 7, (2018) 075004, arXiv:1804.00067 [hep-ph].

[93] P. Ghosh, D. E. López-Fogliani, V. A. Mitsou, C. Muñoz, and R. R. de Austri, "Hunting physics beyond the standard model with unusual $W^{\pm}$ and Z decays," *Phys. Rev.* **D91** no. 3, (2015) 035020, arXiv:1403.3675 [hep-ph].

[94] P. Ghosh, I. Lara, D. E. Lopez-Fogliani, C. Munoz, and R. Ruiz de Austri, "Searching for left sneutrino LSP at the LHC," *Int. J. Mod. Phys.* **A33** no. 18n19, (2018) 1850110, arXiv:1707.02471 [hep-ph].

[95] D. O. Caldwell, R. M. Eisberg, D. M. Grumm, *et al.*, "Laboratory limits on galactic cold dark matter," *Phys. Rev. Lett.* **61** (Aug, 1988) 510–513. https://link.aps.org/doi/10.1103/PhysRevLett.61.510.

[96] D. O. Caldwell, B. Magnusson, M. S. Witherell, *et al.*, "Searching for the cosmion by scattering in si detectors," *Phys. Rev. Lett.* **65** (Sep, 1990) 1305–1308. https://link.aps.org/doi/10.1103/PhysRevLett.65.1305.

[97] D. Reusser, M. Treichel, F. Boehm, *et al.*, "Limits on cold dark matter from the gotthard ge experiment," *Physics Letters B* **255** no. 1, (1991) 143 – 145. http://www.sciencedirect.com/science/article/pii/037026939191155O.

[98] M. Mori, M. M. Nojiri, K. S. Hirata, *et al.*, "Search for neutralino dark matter heavier than the w boson at kamiokande," *Phys. Rev. D* **48** (Dec, 1993) 5505–5518. https://link.aps.org/doi/10.1103/PhysRevD.48.5505.

[99] S. Dawson, E. Eichten, and C. Quigg, "Search for Supersymmetric Particles in Hadron - Hadron Collisions," *Phys. Rev.* **D31** (1985) 1581.

[100] E. Eichten, I. Hinchliffe, K. D. Lane, and C. Quigg, "Super Collider Physics," *Rev. Mod. Phys.* **56** (1984) 579. [Addendum: Rev. Mod. Phys.58,1065(1986)].

[101] F. del Aguila and L. Ametller, "On the detectability of sleptons at large hadron colliders," *Phys. Lett.* **B261** (1991) 326.

[102] H. Baer, C.-h. Chen, F. Paige, and X. Tata, "Detecting Sleptons at Hadron Colliders and Supercolliders," *Phys. Rev.* **D49** (1994) 3283, arXiv:hep-ph/9311248 [hep-ph].

[103] H. Baer, B. W. Harris, and M. H. Reno, "Next-to-leading order slepton pair production at hadron colliders," *Phys. Rev.* **D57** (1998) 5871, arXiv:hep-ph/9712315 [hep-ph].

[104] G. Bozzi, B. Fuks, and M. Klasen, "Slepton production in polarized hadron collisions," *Phys. Lett.* **B609** (2005) 339–350, arXiv:hep-ph/0411318 [hep-ph].

[105] **ATLAS** Collaboration, M. Aaboud *et al.*, "Search for electroweak production of supersymmetric particles in final states with two or three leptons at $\sqrt{s} = 13\,\text{TeV}$ with the ATLAS detector," arXiv:1803.02762 [hep-ex].

[106] **CMS** Collaboration, A. M. Sirunyan *et al.*, "Search for supersymmetric partners of electrons and muons in proton-proton collisions at $\sqrt{s} = 13$ TeV," *Submitted to: Phys. Lett.* (2018) , arXiv:1806.05264 [hep-ex].

[107] **ATLAS** Collaboration, M. Aaboud *et al.*, "Search for supersymmetry in events with four or more leptons in $\sqrt{s} = 13$ TeV pp collisions with ATLAS," *Phys. Rev.* **D98** no. 3, (2018) 032009, arXiv:1804.03602 [hep-ex].

[108] F. Staub, "SARAH," arXiv:0806.0538 [hep-ph].

[109] F. Staub, T. Ohl, W. Porod, and C. Speckner, "A Tool Box for Implementing Supersymmetric Models," *Comput. Phys. Commun.* **183** (2012) 2165–2206, arXiv:1109.5147 [hep-ph].

[110] F. Staub, "SARAH 4 : A tool for (not only SUSY) model builders," *Comput. Phys. Commun.* **185** (2014) 1773–1790, arXiv:1309.7223 [hep-ph].

[111] W. Porod, "SPheno, a program for calculating supersymmetric spectra, SUSY particle decays and SUSY particle production at e+ e- colliders," *Comput. Phys. Commun.* **153** (2003) 275, arXiv:hep-ph/0301101 [hep-ph].

[112] W. Porod and F. Staub, "SPheno 3.1: Extensions including flavour, CP-phases and models beyond the MSSM," *Comput. Phys. Commun.* **183** (2012) 2458, arXiv:1104.1573 [hep-ph].

[113] J. Alwall, R. Frederix, S. Frixione, *et al.*, "The automated computation of tree-level and next-to-leading order differential cross sections, and their matching to parton shower simulations," *JHEP* **07** (2014) 079, arXiv:1405.0301 [hep-ph].

[114] T. Sjostrand, S. Mrenna, and P. Z. Skands, "PYTHIA 6.4 physics and manual," *JHEP* **05** (2006) 026, arXiv:hep-ph/0603175 [hep-ph].

[115] P. Ghosh, E. Kaptcha, D. E. López-Fogliani, C. Muñoz, and R. Ruiz de Austri in preparation.

[116] J. E. Camargo-Molina, B. O'Leary, W. Porod, and F. Staub, "Stability of the cmssm against sfermion vevs," *Journal of High Energy Physics* **2013** no. 12, (Dec, 2013) 103. https://doi.org/10.1007/JHEP12(2013)103.

[117] N. Blinov and D. E. Morrissey, "Vacuum Stability and the MSSM Higgs Mass," *JHEP* **03** (2014) 106, arXiv:1310.4174 [hep-ph].

[118] J. E. Camargo-Molina, B. Garbrecht, B. O'Leary, W. Porod, and F. Staub, "Constraining the Natural MSSM through tunneling to color-breaking vacua at zero and non-zero temperature," *Phys. Lett.* **B737** (2014) 156–161, arXiv:1405.7376 [hep-ph].

[119] M. Bobrowski, G. Chalons, W. G. Hollik, and U. Nierste, "Vacuum stability of the effective Higgs potential in the Minimal Supersymmetric Standard Model," *Phys. Rev.* **D90** no. 3, (2014) 035025, arXiv:1407.2814 [hep-ph]. [Erratum: Phys. Rev.D92,no.5,059901(2015)].

[120] U. Chattopadhyay and A. Dey, "Exploring MSSM for Charge and Color Breaking and Other Constraints in the Context of Higgs@125 GeV," *JHEP* **11** (2014) 161, arXiv:1409.0611 [hep-ph].

[121] W. G. Hollik, "A new view on vacuum stability in the MSSM," *JHEP* **08** (2016) 126, arXiv:1606.08356 [hep-ph].

[122] J. Beuria, U. Chattopadhyay, A. Datta, and A. Dey, "Exploring viable vacua of the Z_3-symmetric NMSSM," *JHEP* **04** (2017) 024, arXiv:1612.06803 [hep-ph].

[123] J. A. Casas, A. Lleyda, and C. Munoz, "Strong constraints on the parameter space of the MSSM from charge and color breaking minima," *Nucl. Phys.* **B471** (1996) 3–58, arXiv:hep-ph/9507294 [hep-ph].

[124] **Planck** Collaboration, P. A. R. Ade *et al.*, "Planck 2015 results. XIII. Cosmological parameters," *Astron. Astrophys.* **594** (2016) A13, arXiv:1502.01589 [astro-ph.CO].

[125] **Daya Bay** Collaboration, F. P. An *et al.*, "New measurement of antineutrino oscillation with the full detector configuration at Daya Bay," *Phys. Rev. Lett.* **115** no. 11, (2015) 111802, arXiv:1505.03456 [hep-ex].

[126] S. Bar-Shalom, G. Eilam, J. Wudka, and A. Soni, "R-parity violation and uses of the rare decay $\widetilde{\nu} \to \gamma\gamma$ in hadron and photon colliders," *Phys. Rev.* **D59** (1999) 035010, arXiv:hep-ph/9809253 [hep-ph].

[127] **ATLAS** Collaboration, M. Aaboud *et al.*, "Search for supersymmetry in a final state containing two photons and missing transverse momentum in $\sqrt{s} = 13\ TeV$ pp collisions at the LHC using the ATLAS detector," *Eur. Phys. J.* **C76** no. 9, (2016) 517, 1606.09150.

[128] **ATLAS** Collaboration, G. Aad *et al.*, "Search for supersymmetry at $\sqrt{s} = 13$ TeV in final states with jets and two same-sign leptons or three leptons with the ATLAS detector," *Eur. Phys. J.* **C76** no. 5, (2016) 259, arXiv:1602.09058 [hep-ex].

[129] **CMS** Collaboration, V. Khachatryan *et al.*, "Search for supersymmetry with multiple charged leptons in proton-proton collisions at $\sqrt{s} = 13$ TeV," arXiv:1701.06940 [hep-ex].

[130] **CMS** Collaboration, V. Khachatryan *et al.*, "Searches for R-parity-violating supersymmetry in pp collisions at $\sqrt{s} = 8$ TeV in final states with 0-4 leptons," *Phys. Rev.* **D94** no. 11, (2016) 112009, arXiv:1606.08076 [hep-ex].

[131] **CMS** Collaboration, V. Khachatryan *et al.*, "Search for supersymmetry in events with photons and missing transverse energy in pp collisions at 13 TeV," *Phys. Lett.* **B769** (2017) 391–412, arXiv:1611.06604 [hep-ex].

[132] **ATLAS** Collaboration, "Search for supersymmetry with two and three leptons and missing transverse momentum in the final state at $\sqrt{s} = 13$ TeV with the ATLAS detector," Tech. Rep. ATLAS-CONF-2016-096, CERN, Geneva, Sep, 2016. http://cds.cern.ch/record/2212162.

[133] **ATLAS** Collaboration, M. Aaboud *et al.*, "Search for new phenomena in events with a photon and missing transverse momentum in pp collisions at $\sqrt{s} = 13$ TeV with the ATLAS detector," *JHEP* **06** (2016) 059, arXiv:1604.01306 [hep-ex].

[134] **ATLAS** Collaboration, M. Aaboud *et al.*, "Search for new phenomena in final states with an energetic jet and large missing transverse momentum in pp collisions at $\sqrt{s} = 13$ TeV using the ATLAS detector," *Phys. Rev.* **D94** no. 3, (2016) 032005, arXiv:1604.07773 [hep-ex].

[135] **ATLAS** Collaboration, M. Aaboud *et al.*, "Search for squarks and gluinos in final states with jets and missing transverse momentum at $\sqrt{s} = 13$ TeV with the ATLAS detector," *Eur. Phys. J.* **C76** no. 7, (2016) 392, arXiv:1605.03814 [hep-ex].

[136] **ATLAS** Collaboration, G. Aad *et al.*, "Search for gluinos in events with an isolated lepton, jets and missing transverse momentum at $\sqrt{s} = 13$ Te V with the ATLAS detector," *Eur. Phys. J.* **C76** no. 10, (2016) 565, arXiv:1605.04285 [hep-ex].

[137] **ATLAS** Collaboration, G. Aad *et al.*, "Search for pair production of gluinos decaying via stop and sbottom in events with b-jets and large missing transverse momentum in pp collisions at $\sqrt{s} = 13$ TeV with the ATLAS detector," *Phys. Rev.* **D94** no. 3, (2016) 032003, arXiv:1605.09318 [hep-ex].

[138] **ATLAS** Collaboration, M. Aaboud *et al.*, "Search for top squarks in final states with one isolated lepton, jets, and missing transverse momentum in $\sqrt{s} = 13$ TeV pp collisions with the ATLAS detector," *Phys. Rev.* **D94** no. 5, (2016) 052009, arXiv:1606.03903 [hep-ex].

[139] "A search for Supersymmetry in events containing a leptonically decaying Z boson, jets and missing transverse momentum in $\sqrt{s} = 13$ TeV pp collisions with the ATLAS detector," Tech. Rep. ATLAS-CONF-2015-082, CERN, Geneva, Dec, 2015. http://cds.cern.ch/record/2114854.

[140] "Search for production of vector-like top quark pairs and of four top quarks in the lepton-plus-jets final state in pp collisions at $\sqrt{s} = 13$ TeV with the ATLAS detector," Tech. Rep. ATLAS-CONF-2016-013, CERN, Geneva, Mar, 2016. http://cds.cern.ch/record/2140998.

[141] **ATLAS** Collaboration, "Search for top squarks in final states with one isolated lepton, jets, and missing transverse momentum in $\sqrt{s} = 13$ TeV pp collisions with the ATLAS detector," Tech. Rep. ATLAS-CONF-2016-050, CERN, Geneva, Aug, 2016. https://cds.cern.ch/record/2206132.

[142] **ATLAS** Collaboration, "Search for direct top squark pair production and dark matter production in final states with two leptons in $\sqrt{s} = 13$ TeV pp collisions using 13.3 fb^{-1} of ATLAS data," Tech. Rep. ATLAS-CONF-2016-076, CERN, Geneva, Aug, 2016. http://cds.cern.ch/record/2206249.

[143] D. Dercks, N. Desai, J. S. Kim, *et al.*, "CheckMATE 2: From the model to the limit," *Comput. Phys. Commun.* **221** (2017) 383, arXiv:1611.09856 [hep-ph].

[144] **DELPHES 3** Collaboration, J. de Favereau, C. Delaere, P. Demin, *et al.*, "DELPHES 3, A modular framework for fast simulation of a generic collider experiment," *JHEP* **02** (2014) 057, arXiv:1307.6346 [hep-ex].

[145] M. Cacciari, G. P. Salam, and G. Soyez, "FastJet User Manual," *Eur. Phys. J.* **C72** (2012) 1896, arXiv:1111.6097 [hep-ph].

[146] M. Cacciari and G. P. Salam, "Dispelling the N^3 myth for the k_t jet-finder," *Phys. Lett.* **B641** (2006) 57, arXiv:hep-ph/0512210 [hep-ph].

[147] M. Cacciari, G. P. Salam, and G. Soyez, "The Anti-k(t) jet clustering algorithm," *JHEP* **04** (2008) 063, arXiv:0802.1189 [hep-ph].

[148] A. L. Read, "Presentation of search results: The CL(s) technique," *J. Phys.* **G28** (2002) 2693. [,11(2002)].

[149] P. Bechtle, O. Brein, S. Heinemeyer, G. Weiglein, and K. E. Williams, "HiggsBounds: Confronting Arbitrary Higgs Sectors with Exclusion Bounds from LEP and the Tevatron," *Comput. Phys. Commun.* **181** (2010) 138, arXiv:0811.4169 [hep-ph].

[150] P. Bechtle, O. Brein, S. Heinemeyer, G. Weiglein, and K. E. Williams, "HiggsBounds 2.0.0: Confronting Neutral and Charged Higgs Sector Predictions with Exclusion Bounds from LEP and the Tevatron," *Comput. Phys. Commun.* **182** (2011) 2605, arXiv:1102.1898 [hep-ph].

[151] P. Bechtle, O. Brein, S. Heinemeyer, *et al.*, "Recent Developments in HiggsBounds and a Preview of HiggsSignals," *PoS* **CHARGED2012** (2012) 024, arXiv:1301.2345 [hep-ph].

[152] P. Bechtle, O. Brein, S. Heinemeyer, *et al.*, "HiggsBounds – 4: Improved Tests of Extended Higgs Sectors against Exclusion Bounds from LEP, the Tevatron and the LHC," *Eur. Phys. J.* **C74** no. 3, (2014) 2693, arXiv:1311.0055 [hep-ph].

[153] P. Bechtle, S. Heinemeyer, O. Stal, T. Stefaniak, and G. Weiglein, "Applying Exclusion Likelihoods from LHC Searches to Extended Higgs Sectors," *Eur. Phys. J.* **C75** no. 9, (2015) 421, arXiv:1507.06706 [hep-ph].

[154] **CMS** Collaboration, S. Chatrchyan *et al.*, "Search for anomalous production of multilepton events in pp collisions at $\sqrt{s} = 7$ TeV," *JHEP* **06** (2012) 169, arXiv:1204.5341 [hep-ex].

[155] **CMS** Collaboration, S. Chatrchyan *et al.*, "Search for anomalous production of events with three or more leptons in pp collisions at $\sqrt{s} = 8$ TeV," *Phys. Rev.* **D90** (2014) 032006, arXiv:1404.5801 [hep-ex].

[156] **CDF** Collaboration, T. Aaltonen *et al.*, "Search for R-parity Violating Decays of τ sneutrinos to $e\mu$, $\mu\tau$, and $e\tau$ pairs in $p\bar{p}$ Collisions at $\sqrt{s} = 1.96$ TeV," *Phys. Rev. Lett.* **105** (2010) 191801, arXiv:1004.3042 [hep-ex].

[157] **D0** Collaboration, V. M. Abazov *et al.*, "Search for sneutrino production in emu final states in 5.3 fb^{-1} of $p\bar{p}$ collisions at sqrt(s) =1.96 TeV," *Phys. Rev. Lett.* **105** (2010) 191802, arXiv:1007.4835 [hep-ex].

[158] **L3** Collaboration, P. Achard *et al.*, "Search for R parity violating decays of supersymmetric particles in e^+e^- collisions at LEP," *Phys. Lett.* **B524** (2002) 65–80, arXiv:hep-ex/0110057 [hep-ex].

[159] **ALEPH** Collaboration, A. Heister *et al.*, "Search for R-parity violating production of single sneutrinos in e^+e^- collisions at $\sqrt{s} = 189$ GeV to 209 GeV," *Eur. Phys. J.* **C25** (2002) 1–12, arXiv:hep-ex/0201013 [hep-ex].

[160] **ALEPH** Collaboration, A. Heister *et al.*, "Search for supersymmetric particles with R parity violating decays in e^+e^- collisions at $\sqrt{s}$ up to 209 GeV," *Eur. Phys. J.* **C31** (2003) 1–16, arXiv:hep-ex/0210014 [hep-ex].

[161] **OPAL** Collaboration, G. Abbiendi *et al.*, "Search for R parity violating decays of scalar fermions at LEP," *Eur. Phys. J.* **C33** (2004) 149–172, arXiv:hep-ex/0310054 [hep-ex].

[162] **DELPHI** Collaboration, J. Abdallah *et al.*, "Search for supersymmetric particles assuming R-parity nonconservation in e^+e^- collisions at $\sqrt{s} = 192$ GeV to 208 GeV," *Eur. Phys. J.* **C36** no. 1, (2004) 1–23, arXiv:hep-ex/0406009 [hep-ex]. [Erratum: Eur. Phys. J.C37,no.1,129(2004)].

[163] **CMS** Collaboration, "Search for Resonances Decaying to Dijet Final States at $\sqrt{s} = 8$ TeV with Scouting Data," *CMS-PAS-EXO-14-005* (2015) .

[164] **ATLAS** Collaboration, G. Aad *et al.*, "Search for new phenomena in the dijet mass distribution using $p - p$ collision data at $\sqrt{s} = 8$ TeV with the ATLAS detector," *Phys. Rev.* **D91** (2015) 052007, arXiv:1407.1376 [hep-ex].

[165] **CMS** Collaboration, V. Khachatryan *et al.*, "Search for narrow resonances decaying to dijets in proton-proton collisions at $\sqrt(s) = 13$ TeV," *Phys. Rev. Lett.* **116** no. 7, (2016) 071801, arXiv:1512.01224 [hep-ex].

[166] **ATLAS** Collaboration, G. Aad *et al.*, "Search for new phenomena in dijet mass and angular distributions from pp collisions at $\sqrt{s} = 13$ TeV with the ATLAS detector," *Phys. Lett.* **B754** (2016) 302–322, arXiv:1512.01530 [hep-ex].

[167] **ATLAS** Collaboration, G. Aad *et al.*, "Search for a Heavy Neutral Particle Decaying to $e\mu$, $e\tau$, or $\mu\tau$ in pp Collisions at $\sqrt{s} = 8$ TeV with the ATLAS Detector," *Phys. Rev. Lett.* **115** no. 3, (2015) 031801, arXiv:1503.04430 [hep-ex].

[168] **CMS** Collaboration, V. Khachatryan *et al.*, "Search for lepton flavour violating decays of heavy resonances and quantum black holes to an eμ pair in proton-proton collisions at $\sqrt{s} = 8$ TeV," *Eur. Phys. J.* **C76** no. 6, (2016) 317, arXiv:1604.05239 [hep-ex].

[169] B. Fuks, M. Klasen, D. R. Lamprea, and M. Rothering, "Revisiting slepton pair production at the Large Hadron Collider," *JHEP* **01** (2014) 168, arXiv:1310.2621.

[170] PGS, "http://conway.physics.ucdavis.edu/research/software/pgs/pgs4-general.htm,".

[171] S. Jadach, J. H. Kuhn, and Z. Was, "TAUOLA: A Library of Monte Carlo programs to simulate decays of polarized tau leptons," *Comput. Phys. Commun.* **64** (1990) 275–299.

[172] S. Jadach, Z. Was, R. Decker, and J. H. Kuhn, "The tau decay library TAUOLA: Version 2.4," *Comput. Phys. Commun.* **76** (1993) 361–380.

[173] **ATLAS** Collaboration, G. Aad *et al.*, "Search for supersymmetry in events with four or more leptons in $\sqrt{s} = 8$ TeV pp collisions with the ATLAS detector," *Phys. Rev.* **D90** no. 5, (2014) 052001, arXiv:1405.5086 [hep-ex].

[174] **ATLAS** Collaboration, G. Aad *et al.*, "Search for photonic signatures of gauge-mediated supersymmetry in 8 TeV pp collisions with the ATLAS detector," *Phys. Rev.* **D92** no. 7, (2015) 072001, arXiv:1507.05493 [hep-ex].

[175] I. Lara, D. E. López-Fogliani, C. Muñoz, *et al.* in preparation.

[176] **ATLAS** Collaboration, G. Aad *et al.*, "Search for massive, long-lived particles using multitrack displaced vertices or displaced lepton pairs in pp collisions at $\sqrt{s} = 8$ TeV with the ATLAS detector," *Phys. Rev.* **D92** no. 7, (2015) 072004, arXiv:1504.05162 [hep-ex].

[177] **CMS** Collaboration, V. Khachatryan *et al.*, "Search for long-lived particles that decay into final states containing two electrons or two muons in proton-proton collisions at $\sqrt{s} = 8$ TeV," *Phys. Rev.* **D91** no. 5, (2015) 052012, arXiv:1411.6977 [hep-ex].

[178] **DELPHI** Collaboration, N. Benekos, C. Berat, F. Ledroit, R. Lopez-Fernandez, and T. Papadopoulou, "Search for SUSY with R-parity violating L L anti-E couplings at s**(1/2) = 189-GeV," in *Proceedings, International Europhysics Conference on High energy physics (EPS-HEP 1999): Tampere, Finland, July 15-21, 1999*. 1999. http://cdsweb.cern.ch/search.py?sysno=000339327cer.

[179] **ALEPH** Collaboration, O. Awunor, "LSP mass limit with a dominant R-parity violating L L anti-E coupling in e+ e- collisions at centre-of-mass energies between s**(1/2) = 189-GeV - 209-GeV," in *Lepton and photon interactions at high energies. Proceedings, 20th International Symposium, LP 2001, Rome, Italy, July 23-28, 2001*. 2001.

[180] P. Achard, O. Adriani, M. Aguilar-Benitez, *et al.*, "Search for r-parity violating decays of supersymmetric particles in e+e- collisions at lep," *Physics Letters B* **524** no. 1, (2002) 65 – 80. http://www.sciencedirect.com/science/article/pii/S0370269301013673.

[181] R. Barate, D. Buskulic, D. Décamp, *et al.*, "Single- and multi-photon production in e^+e^- collisions at a centre-of-mass energy of 183 gev,".

[182] **DELPHI** Collaboration, J. Abdallah *et al.*, "Photon events with missing energy in e+ e- collisions at s**(1/2) = 130-GeV to 209-GeV," *Eur. Phys. J.* **C38** (2005) 395–411, arXiv:hep-ex/0406019 [hep-ex].

[183] **ATLAS** Collaboration, M. Aaboud *et al.*, "Search for long-lived, massive particles in events with displaced vertices and missing transverse momentum in $\sqrt{s} = 13$ TeV pp collisions with the ATLAS detector," arXiv:1710.04901 [hep-ex].

[184] T. Sjostrand, S. Mrenna, and P. Z. Skands, "A Brief Introduction to PYTHIA 8.1," *Comput. Phys. Commun.* **178** (2008) 852, arXiv:0710.3820 [hep-ph].

[185] **ATLAS** Collaboration, G. Aad *et al.*, "Performance of the ATLAS muon trigger in pp collisions at $\sqrt{s} = 8$ TeV," *Eur. Phys. J.* **C75** (2015) 120, arXiv:1408.3179 [hep-ex].

[186] **ATLAS** Collaboration, G. Aad *et al.*, "Performance of the ATLAS Trigger System in 2010," *Eur. Phys. J.* **C72** (2012) 1849, arXiv:1110.1530 [hep-ex].

[187] **ATLAS** Collaboration, G. Aad *et al.*, "The ATLAS Experiment at the CERN Large Hadron Collider," *JINST* **3** (2008) S08003.

[188] ATLAS. https://twiki.cern.ch/twiki/pub/AtlasPublic/EgammaTriggerPublicResults/Plots2014ICHEP_Fig2a.pdf.

[189] **ATLAS** Collaboration, M. Aaboud *et al.*, "Performance of the ATLAS Trigger System in 2015," *Eur. Phys. J.* **C77** no. 5, (2017) 317, arXiv:1611.09661 [hep-ex].

[190] ATLAS. https://twiki.cern.ch/twiki/bin/view/AtlasPublic/MuonTriggerPublicResults#Plots_for_2017_data_13_TeV.

[191] ATLAS. https://twiki.cern.ch/twiki/bin/view/AtlasPublic/EgammaTriggerPublicResults#2017_Data_13_TeV.

[192] "Track Reconstruction Performance of the ATLAS Inner Detector at $\sqrt{s} = 13$ TeV," Tech. Rep. ATL-PHYS-PUB-2015-018, CERN, Geneva, Jul, 2015. https://cds.cern.ch/record/2037683.

[193] H. Ito, O. Jinnouchi, T. Moroi, N. Nagata, and H. Otono, "Extending the LHC Reach for New Physics with Sub-Millimeter Displaced Vertices," *Phys. Lett.* **B771** (2017) 568, arXiv:1702.08613 [hep-ph].

[194] H. Ito, O. Jinnouchi, T. Moroi, N. Nagata, and H. Otono, "Searching for Metastable Particles with Sub-Millimeter Displaced Vertices at Hadron Colliders," arXiv:1803.00234 [hep-ph].

[195] **CMS** Collaboration, V. Khachatryan *et al.*, "Search for Displaced Supersymmetry in events with an electron and a muon with large impact parameters," *Phys. Rev. Lett.* **114** no. 6, (2015) 061801, arXiv:1409.4789 [hep-ex].

[196] **CMS** Collaboration, V. Khachatryan *et al.*, "Search for R-parity violating supersymmetry with displaced vertices in proton-proton collisions at $\sqrt{s} = 8$ TeV," *Phys. Rev.* **D95** no. 1, (2017) 012009, arXiv:1610.05133 [hep-ex].

[197] **CMS** Collaboration, "Search for displaced leptons in the e-μ channel," Tech. Rep. CMS-PAS-EXO-16-022, CERN, Geneva, 2016. http://cds.cern.ch/record/2205146.

[198] I. Lara, D. E. Lopez-Fogliani, and C. Munoz, "Electroweak superpartners scrutinized at the LHC in events with multi-leptons," *To be published in Phys. Lett. B* , arXiv:1810.12455 [hep-ph].

[199] **ATLAS** Collaboration, M. Aaboud *et al.*, "Search for chargino-neutralino production using recursive jigsaw reconstruction in final states with two or three charged leptons in proton-proton collisions at $\sqrt{s} = 13$ TeV with the ATLAS detector," arXiv:1806.02293 [hep-ex].

[200] M. Carena, J. Osborne, N. R. Shah, and C. E. M. Wagner, "Supersymmetry and LHC Missing Energy Signals," arXiv:1809.11082 [hep-ph].

[201] B. Fuks, M. Klasen, D. R. Lamprea, and M. Rothering, "Gaugino production in proton-proton collisions at a center-of-mass energy of 8 TeV," *JHEP* **10** (2012) 081, arXiv:1207.2159 [hep-ph].

[202] B. Fuks, M. Klasen, D. R. Lamprea, and M. Rothering, "Precision predictions for electroweak superpartner production at hadron colliders with Resummino," *Eur. Phys. J. C* **73** (2013) 2480, arXiv:1304.0790 [hep-ph].

[203] P. Jackson, C. Rogan, and M. Santoni, "Sparticles in motion: Analyzing compressed SUSY scenarios with a new method of event reconstruction," *Phys. Rev.* **D95** no. 3, (2017) 035031, arXiv:1607.08307 [hep-ph].

[204] P. Jackson and C. Rogan, "Recursive Jigsaw Reconstruction: HEP event analysis in the presence of kinematic and combinatoric ambiguities," *Phys. Rev.* **D96** no. 11, (2017) 112007, arXiv:1705.10733 [hep-ph].

[205] E. Conte, B. Fuks, and G. Serret, "MadAnalysis 5, A User-Friendly Framework for Collider Phenomenology," *Comput. Phys. Commun.* **184** (2013) 222–256, arXiv:1206.1599 [hep-ph].

[206] E. Conte, B. Dumont, B. Fuks, and C. Wymant, "Designing and recasting LHC analyses with MadAnalysis 5," *Eur. Phys. J.* **C74** no. 10, (2014) 3103, arXiv:1405.3982 [hep-ph].

[207] B. Dumont, B. Fuks, S. Kraml, *et al.*, "Toward a public analysis database for LHC new physics searches using MADANALYSIS 5," *Eur. Phys. J.* **C75** no. 2, (2015) 56, arXiv:1407.3278 [hep-ph].

[208] "ATLAS Run 1 Pythia8 tunes," Tech. Rep. ATL-PHYS-PUB-2014-021, CERN, Geneva, Nov, 2014. https://cds.cern.ch/record/1966419.

[209] A. Buckley, J. Ferrando, S. Lloyd, *et al.*, "LHAPDF6: parton density access in the LHC precision era," *Eur. Phys. J.* **C75** (2015) 132, arXiv:1412.7420 [hep-ph].

[210] G. Bozzi, B. Fuks, and M. Klasen, "Transverse-momentum resummation for slepton-pair production at the CERN LHC," *Phys. Rev.* **D74** (2006) 015001, arXiv:hep-ph/0603074 [hep-ph].

[211] G. Bozzi, B. Fuks, and M. Klasen, "Threshold Resummation for Slepton-Pair Production at Hadron Colliders," *Nucl. Phys.* **B777** (2007) 157–181, arXiv:hep-ph/0701202 [hep-ph].

[212] G. Bozzi, B. Fuks, and M. Klasen, "Joint resummation for slepton pair production at hadron colliders," *Nucl. Phys.* **B794** (2008) 46–60, arXiv:0709.3057 [hep-ph].

[213] I. Lara, D. E. López-Fogliani, and C. Muñoz in preparation.